Understanding molecular mechanisms of microRNA-mediated gene silencing

Vinay K. Mayya

Department of Biochemistry

McGill University

Montreal, Quebec, Canada

April 2021

A thesis submitted to McGill University in partial fulfillment of the requirements for the degree of Doctor of Philosophy

Abstract

This thesis explores the mechanisms underlying the functions of microRNAs (miRNAs) across multiple model systems and physiological contexts. miRNAs are ~ 22 nucleotide (nt) long RNA molecules that regulate gene expression in an important diversity of biological processes. To control gene expression, miRNAs associate with Argonaute proteins to form the miRNA-induced silencing complex (miRISC), which uses the miRNA as a guide to pair with messenger RNA (mRNAs) targets and directs their silencing. For this silencing to occur, the miRISC recruits effector proteins and complexes that enact a series of events leading to translation repression, mRNA deadenylation, and decay. Much has been learned from the important functions of miRNAs across biological cascades, but fundamental determinants such as kinetic and stoichiometric properties of the miRISC with its targets, and the details of effector protein activities and regulation remain elusive. Furthermore, the interplay between functional elements embedded within native mRNA sequences and miRISC and its associated effector proteins in specific cell fates or states is poorly understood in the physiological context of a live animal.

To understand how stoichiometry of miRISC and its targets affect miRNA-mediated gene silencing, in Chapter 2, we developed a quantitative target analog-based miRISC capture method. This enabled the measurement of *the available* fraction of miRISC for a set of cancer-related miRNAs expressed at different levels in HEK 293T cells. By experimentally altering the stoichiometry and availability of miRISC for those miRNAs and following their activity using reporters, we observed that the available fraction of miRISC greatly varies among miRNAs and is quite distinct from their expression. With this work we show that the stoichiometric relationship between miRISC and target abundance deeply influences the silencing activity of miRNAs.

In Chapters 3 and 4, we leveraged the genetic and molecular tools uniquely available in *C. elegans* to elucidate the implications of biological context to miRNA-mediated gene silencing. In Chapter 3, through concerted proteomic surveys, we identified the GYF domain-containing protein GYF-1 and its direct interacting partner IFE-4 (an ortholog of the mammalian 4EHP) as key effectors of miRNA-mediated translational repression. Loss of *gyf-1* or CRISPR-engineered mutations in *gyf-1* that abolish interactions with IFE-4 severely exacerbates the developmental defects associated with alleles of *miR-35* and *let-7* miRNAs. Strikingly, GYF-1 is dispensable for the activity of other miRNAs such as *lin-4* and *lsy-6*. This chapter revealed the physiological importance of miRNA-mediated translation repression for *C. elegans* development and showed that miRNAs could exert their silencing functions quite differently on different target mRNAs and in different cell types.

miRNAs and RNA-binding proteins (RBP) can control gene expression using related molecular mechanisms, but their functional interplay on nearby target sequences is poorly understood. In Chapter 4, using a cell-free embryonic extract derived from *C. elegans,* we investigate the mechanism and functions of the TRIM-NHL RBP NHL-2, and its cooperation with miRNA-mediated silencing. We found that NHL-2 and its interacting partner CGH-1 cooperate with miRNAs and strongly potentiate the deadenylation of target mRNAs. Several lines of evidence support a model wherein this synergy occurs through the reorganization of the liquid-liquid phase separated mRNP assembled on miRNA targets.

This thesis work, pursued both in *C. elegans* and mammalian cell culture, revealed key parameters that contribute to miRNA-mediated gene silencing and the function of RBPs. It lays new ground upon which we may now reinterpret the functions of miRNAs in their biological and pathological processes.

Résumé

Les microARNs (miARNs) sont de petits ARN non-codants de longueurs pouvant varier de 18 à 22 nucléotides (nt) qui régulent l'expression génique en s'appariant aux séquences 3'non-traduites (3'UTR) des ARNm et jouent ainsi un rôle important dans une diversité de processus biologiques. Les miARNs fonctionnent en association avec les protéines Argonaute, et forment ainsi le complexe de silencing induit par les miRNA (miRISC), et dirigent l'extinction post-transcriptionnelle de gènes, en contrôlant l'expression des ARN messagers (ARNm). Une diversité de protéines effectrices associées au miRISC portent des activités moléculaires qui se somment par la répression de la traduction, la deadénylation et la déstabilisation des ARNm ciblés. Les fonctions régulatrices des miARNs sont relativement bien connues, mais les mécanismes, activités moléculaires et les paramètres stoechiométriques fondamentaux qui contribuent à l'efficacité de l'extinction génique par les miARNs demeurent moins bien caractérisés. De plus, les interactions fonctionnelles entre les miARNs et les autres protéines associées aux ARNm dans ses séquences 3'UTR demeurent moins bien définies, surtout dans leur contexte physiologique.

Pour comprendre les aspects stoichiométriques de l'extinction génique par les miARNs, nous avons développé une méthode quantitative de capture du miRISC à base d'analogue de séquences-cible. Cette approche nous a permis de mesurer la fraction de miRISC disponible pour plusieurs des familles de miRNAs. Dans le Chapitre 2, nous avons examiné la disponibilité fonctionnelle de miARNs liées à des maladies qui sont exprimés à différents niveaux dans les cellules HEK 293T. En modifiant expérimentalement la disponibilité du miRISC pour chaque famille et en suivant son impact sur l'extinction génique de constructions témoins (rapporteurs), nous avons révélé que la fraction disponible de miRISC varie grandement entre les familles de miARNs et est distincte de leur expression, et selon les cellules. La disponibilité du miRISC, modulée selon la stoichiométrie

des miARNs et l'abondance des sites-cibles propre à chaque transcriptome module grandement l'activité des miARNs.

Dans les chapîtres 3 et 4, nous avons tiré parti d'outils génétiques et moléculaires disponibles chez C. elegans, afin d'élucider davantage les implications du contexte biologique sur l'extinction génique par les miARNs. Avec le chapître 3, grâce à une approche de protéomique concertée, nous avons identifié la protéine contenant le domaine GYF, GYF-1 et son partenaire IFE-4, comme effecteurs clés de la répression traductionnelle médiée par certains miARNs. La perte de gyf-1 ou des mutations ponctuelles dans gyf-1 qui abolissent son interaction avec IFE-4 ont sévèrement empiré les défauts développementaux associés avec des mutants hypomorphes des familles de miRNAs miR-35 et let-7. Pour d'autres miARNs tels que lin-4 et lsy-6, GYF-1 ne semble pas impliqué, et d'autres mécanismes semblent mis en action.

Dans le chapître 4, j'explore les interactions fonctionnelles coopératives entre les miARNs et les protéines de liaison à l'ARN (RBP) dans l'extinction génique par les miARNs. En utilisant un extrait embryonnaire dérivé de C. elegans et au travers l'édition génomique par CRISPR-Cas9, nous avons étudié les détails moléculaires de l'interaction fonctionnelle entre la RBP TRIM-NHL NHL-2 et les miARNs. Nous avons aussi découvert que NHL-2 et un autre partenaire d'interaction, l'hélicase d'ARN CGH-1, coopèrent avec les miARNs pour promouvoir la deadénylation de l'ARNm cible.

Les résultats présentés dans ma thèse, dans des modèles biologiques aussi distincts que les cellules mammifères en culture et dans l'animal C. elegans, mettent en évidence les interactions et paramètres qui contribuent à l'efficacité de l'extinction génique médié par les miARNs. Mes travaux ont élucidé des fondements mécanistiques sous-jacents aux fonctions biologiques et pathologiques divers des miARNs.

Table of Contents

List of Figures

List of Tables

List of abbreviations

3′ Rapid amplification of cDNA end ..... 3′RACE
7-methylguanylate..... m7G
ALG-1 interacting protein ..... AIN
alternative polyadenylation ..... APA
Amphid neuron, single ciliated ending left/right ..... ASEL/ASER
ARE-binding protein ..... ARE-BP
Argonaute .....Ago
Argonaute-like gene .....alg
AU-rich element ..... ARE
B-Box-type zinc fingers ..... BB
Brain tumor .....Brat
Caenorhabditis elegans .....*C. elegans*
Clustered regularly interspaced short palindromic repeats ..... *CRISPR*
coding sequence .....CDS
Coiled-coil CC
Crosslinking immunoprecipitation .....CLIP
cytoplasmic polyadenylation binding elements ..... CPEB
Danio rerio .....*D. rerio*
Deoxyribonucleic acid .....DNA
Dimethyl sulfide .....DMS
Dual-specificity phosphatase 6……..……. DUSP6
Egg laying defective .....*egl*
Enhancer of decapping ..... Edc
eIF4E-homologous protein……..……...4EHP
Eukaryotic translation initiation factor 4E…….……eIF4E
Eukaryotic translation initiation factor 4E transporter…….……...4E-T
Exoribonuclease-1 .....Xrn-1
Exportin-5 ..... Xpo-5

Extracellular signal-related kinases……..……ERK

Gain of function ..... gf

Gene Ontology ..... *GO*

Glycine tryptophan diresidue .....GW

Green fluorescent protein ..... GFP

Human embryonic kidney ..... HEK

Human antigen R .....HuR

hunchback ..... hb

hunchback like-1 ..... *hbl-1*

Immunoprecipitation .....IP

Internal ribosome entry site .....IRES

Iron response element .....IRE

K-homology…….……..KH

KiloDalton .....kDa

Long non-coding RNA ..... lncRNA

Maternal-to-zygotic transition .....MZT

messenger ribonucleoprotein .....mRNP

Messenger RNA .....mRNA

Micrococcal nuclease ..... *MNase*

microRNA .....miRNA

miRNA-induced silencing complex ..... miRISC

mRNA nucleoprotein complex .....mRNP

mitogen-activated protein kinase……..MAPK

Multidimensional protein identification technology .....MudPIT

nanos .....nos

nanos response elements ..... NRE

Noncoding RNA activated by DNA damage……..NORAD

Ncl-1, HT2A and Lin-41 ..... NHL

Nuclear factor- κB…….NF-κB

Nucleotide ..... nt

open reading frame ..... ORF

P-element-induced wimpy testes ..... PIWI

Phosphoinositide 3-kinase..... PI3K

piwiRNA ..... piRNA

Poly(A) binding protein ..... PABP

Poly(A) nuclease ..... PAN

Polymerase chain reaction ..... PCR

Precursor miRNA ..... pre-miRNA

precursor mRNA ..... pre-mRNA

Processing-body ..... P-body

Pumilio ..... pum

Pumilio and FBF ..... PUF

Quantitative PCR ..... qPCR

Really interesting new gene ..... RING

Renilla luciferase ..... RL

Ribonucleic acid ..... RNA

RNA binding domain ..... RBD

RNA immunoprecipitation ..... RIP

RNA interference ..... RNAi

RNA-induced silencing complex ..... RISC

RNA recognition motif ..... RRM

Sequencing ..... Seq

Silencing domain ..... SD

Suppressor/enhancer of lin-12 – 1 ..... *sel-1*

Terminal uridine transferase 4 ..... Tut-4

Tripartite motif ..... TRIM

Tristetraprolin ..... TTP

Ultraviolet ..... UV

untranslated regions ..... UTR

Wild-type ..... WT

Preface

In compliance with the guidelines for preparing a doctoral thesis at McGill University, this thesis is manuscript-based. It consists of three published articles and one manuscript in preparation.

Chapter 1: General introduction and literature review

Mayya V.K. & Duchaine T.F. Ciphers and Executioners: How 3`-Untranslated Regions Determine the Fate of Messenger RNAs (2019). *Frontiers in Genetics*, doi: 10.3389/fgene.2019.00006

Chapter 2: Manuscript published

Mayya V.K. & Duchaine T.F. On the availability of microRNA-induced silencing complexes, saturation of microRNA-binding sites and stoichiometry. *Nucleic Acids Res*. 2015 Sep 3;43(15):7556-65. doi: 10.1093/nar/gkv720.

Chapter 3: Manuscript published

Mayya V.K., Flamand M.N., Lambert A.M., Jafarnejad S.M., Wohlschlegel J.A., Sonenberg N, Duchaine T.F. microRNA-mediated translation repression through GYF-1/IFE-4 in *C. elegans* development. *Nucleic Acids Res. Breakthrough article, 2021 doi: 10.1093/nar/gkab162*

Chapter 4: Manuscript in preparation

Mayya V.K., Flamand M.N., Vidya E, Sonenberg N., Wohlschlegel J.A., Hammell C.M., Duchaine T.F. Enhancement of microRNA-mediated deadenylation by the TRIM-NHL protein NHL-2 and DEAD-box protein CGH-1

Chapter 5: General discussion

Contribution of authors

Chapter 2. I performed all the experiments.

Chapter 3. I performed all the experiments except; the generation of *gyf-1* null allele, experiments in Figure 3-1A, Figure A2-2A, and Figure A2-2C was performed by Dr. Mathieu Flamand, Alice Lambert performed experiments in Figure 3-1E, Dr. James Wohlschlegel performed the MuDPIT analysis on the GYF-1 IPs I performed.

Chapter 4. I performed all the experiments except; 3x-FLAG tagging of NHL-2 and RNase untreated IPs for MuDPIT analysis was performed by Dr. Mathieu Flamand. The group of James Wohlschlegel performed MuDPIT analysis, Elva Vidya performed experiments in Figure 4-1C and Figure 4-1D, Dr. Christopher Hammell performed experiments in Figure A3-1.

Contribution to knowledge

Chapter 2: On the availability of microRNA-induced silencing complexes, saturation of microRNA-binding sites and stoichiometry.

- Challenged common assumptions related to miRNA expression levels and their impact on gene silencing.
- Quantified the fraction of miRISC available for silencing across several families of miRNAs.
- Provided direct experimental evidence that only a subset of miRNAs whose concentrations lie in a dynamic range with respect to target site abundance are subjected to competitive effects through miRNA-binding sites.

Chapter 3: microRNA-mediated translation repression through GYF-1/IFE-4 in *C. elegans* development.

- Identified GYF-1/IFE-4 as a direct effector of microRNA-mediated translation repression in *C. elegans*
- Loss of *gyf-1* or mutations affecting the interaction between GYF-1 and IFE-4 impacts the functions of specific miRNAs (*let-7* and *miR-35*)
- Developed *in vitro* and *in vivo* tethering assays to monitor the molecular function of GYF-1/IFE-4 complex

Chapter 4: Enhancement of microRNA-mediated deadenylation by the TRIM-NHL protein NHL-2 and DEAD-box protein CGH-1

- Surveyed proteomic interactions of NHL-2 through MuDPIT.
- NHL-2 cooperates with miRNAs.
- NHL-2/CGH-1 interaction reorganizes the RNP to promote miRNA-mediated deadenylation.

Acknowledgements

To my supervisor, Thomas Duchaine- I am so grateful to have worked with you for the past seven years. You are a fantastic mentor, scientist, and above all, a great human being. I am thankful for your constant support, motivation, and kindness. I also thank you for all the time and effort you gave to me.

To all the past and present members of the lab, I thank you for making the lab a fun place to work. Carine Lussier, thank you for showing me the ropes. Ahilya, Edlyn, and Mathieu- I thank you all for the love you have given me. You always made me feel welcome. Caroline, Alexandra, Rania, Elva, Cynthia, Chehrona, and Alice, I thank you for all the fond memories. I shall always cherish them.

I am grateful to have had the opportunity to collaborate with Dr. Nahum Sonenberg and Dr. Mehdi Jafarnejad. I thank you for your mentorship and guidance. I will greatly miss the weekly Thursday afternoon meetings.

To my thesis committee members: Dr. Pascal Chartrand and Dr. Kalle Gehring, I thank you for your continuous support throughout these years.

I would like to express my sincere thanks to Dr. Gerhart Wagner (Uppsala University) and Dr. Elisa Izaurralde (Max Planck Institute for developmental biology). Your guidance and support inspired me to pursue a Ph.D. in basic science research.

To all my other dear friends, outside of the lab, thank you for being so ever supportive and understanding. Now, I hope to see you more and make up for lost time.

Finally, none of this would have been possible without the sacrifice, love, and support from my parents Shashikala and Vasantha Kumar, my uncle Nataraj Sarjapur, and my sisters Shubha and Shyla. I dedicate this thesis to you.

Chapter 1: Introduction

1.1 Post-transcriptional regulation

Precise spatial and temporal regulation of gene expression is necessary for the proper development and homeostasis of organisms. Systems approaches indicate that post-transcriptional mechanism, and in particular translational repression, make the determining contribution in establishing a gene's expression in mammalian cells (Schwanhausser et al., 2011). Post-transcriptional regulation is instated by mechanisms that control translation, stability, and localization of mRNAs. Such mechanisms converge on one or several of the distinctive features of mRNAs (Figure 1-1).

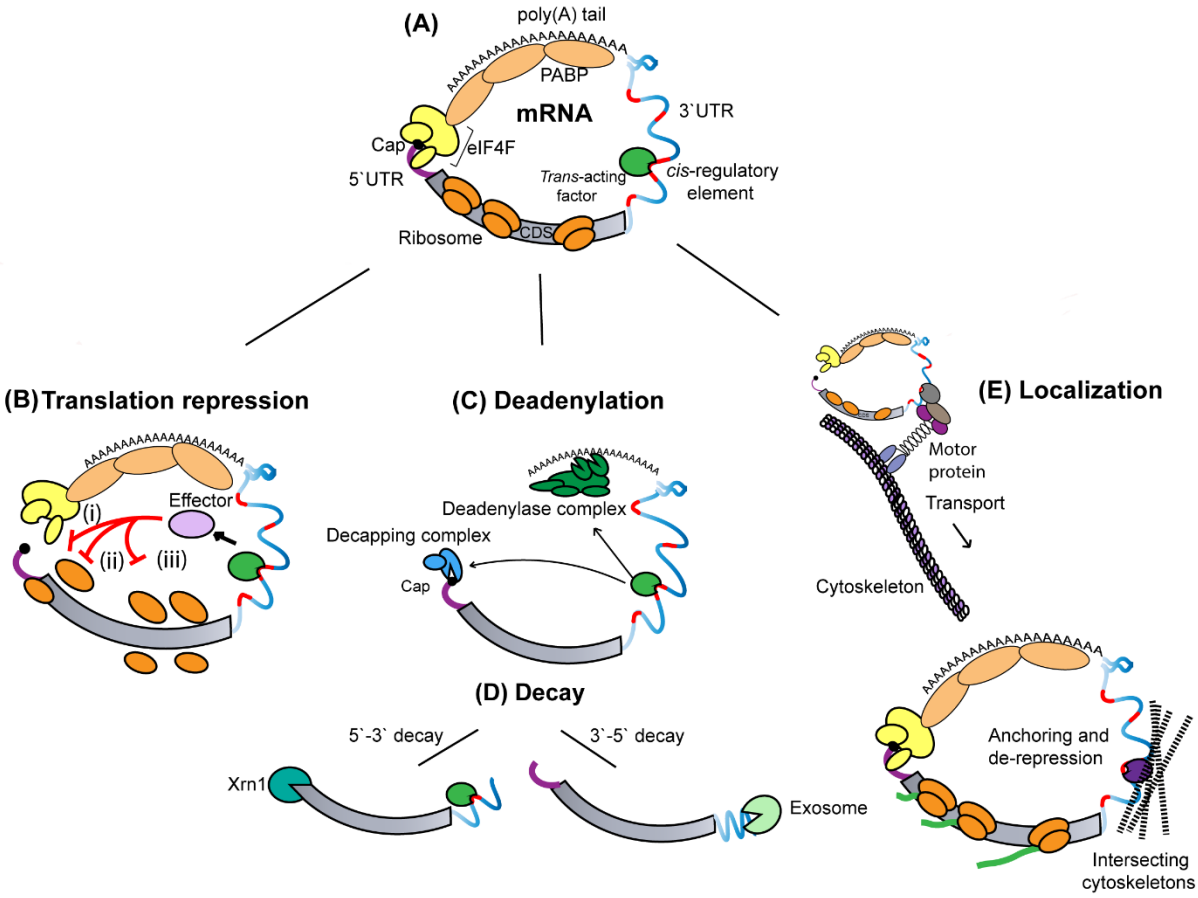

Figure 1-1. General modes and determinants of 3`UTR in post-transcriptional regulation.

(A) Schematic illustration of the distinctive features of an eukaryotic mRNA. The 5'-terminal cap structure interacts with the 3'-terminal poly(A) tail of an mRNA through associated eIF4F and PABP. The coding sequence (CDS) is flanked by 5'- and 3`UTR, which harbors *cis*-regulatory

sequences (marked in red) and provides a binding platform for *trans*-acting factors (green). **(B)** Translational repression mechanisms. (i) Competition/interference with cap-binding complex, eIF4F (ii) Inhibition of ribosomal subunit joining (iii) Inhibition of translation elongation. **(C)** Deadenylation and decapping. Recruitment of the CCR4-NOT deadenylase complex by *trans*-acting factors catalyzes the deadenylation of the mRNA target. This is often followed by the removal of the 5'-terminal cap structure by the decapping factors (DCP1-DCP2), and the associated co-factors. **(D)** mRNA decay. mRNAs that are deadenylated and decapped are rapidly degraded by either 5'->3' exonuclease (XRN1) or 3'->5' exonuclease (exosome). **(E)** RNA localization. Translationally repressed mRNAs are transported along the cytoskeleton to which it is tethered by RBPs and motor proteins. Upon reaching its destination, the mRNA is anchored, and its translation is de-repressed.

The coding sequence (CDS) of an mRNA is flanked by 5'- and 3'-untranslated regions (UTR). These sequences encode regulatory structures and sequences often referred to as *cis*-regulatory or *cis*-acting. When unrepressed, interactions between the 5'-terminal cap, the eIF4F cap-binding complex (an assembly of eIF4E, eIF4A, and eIF4G), the 3'-terminal poly(A) tail, and the associated poly(A) binding proteins (PABPs) lead to circularization of an mRNA (Gallie, 1991; Wells et al., 1998). mRNA circularization is thought to allow the synergy of the 5'-cap and poly(A) tail in potentiating translation initiation and possibly also in stabilizing the mRNA (Sachs et al., 1997; Schwartz and Parker, 1999). Circularization brings 3`UTR *cis*-acting elements closer to the translation initiation machinery. Perhaps not surprisingly then, 3`UTR-driven mechanisms determine the expression and fate of mRNAs by targeting the 5'-cap and 3'-poly(A) tail moieties and/or the associated cofactors.

The functional information encoded in the sequence and structure of 3`UTRs is decrypted and acted upon by an array of cellular regulatory factors (often referred to as *trans*-acting factors). Regulatory factors can be broken down into two distinct categories based on their direct molecular

implication in *i- specific recognition* of the 3`UTR sequence and structure, and *ii- execution* of consequent activities. Factors involved in specific recognition include a variety of non-coding RNAs, such as microRNAs (miRNAs), and RNA-binding proteins (RBPs) to match the sequences and structural determinants encoded in 3`UTRs. More limited diversity of effector machinery can be grouped in three effector activities: i- translational control (Figure 1-1B), most often acting on translation initiation (Chendrimada et al., 2007; Humphreys et al., 2005; Mathonnet et al., 2007; Nelson et al., 2004; Zdanowicz et al., 2009), but also in some cases on translation elongation (Gu et al., 2009; Petersen et al., 2006), ii- deadenylation and decay (Figure 1-1C-D), whereby deadenylation of an mRNA can be coupled to some degree to its decapping and decay, and iii- localization (Figure 1-1E), which can be established through active RNA transport along the cytoskeleton and/or asymmetric anchoring of an mRNA in a cellular domain.

In many cases, including the examples presented below, more than one effector activity can be mobilized by a 3`UTR. Recognition and effector activities can involve synergistic, cooperative, or coordinated interactions dictated by the 3`UTR regulatory sequences themselves, but also by the cellular, sub-cellular, and biochemical context wherein the mRNA is found. mRNAs and the regulatory machinery are deeply affected by concentration, stoichiometry, affinities, RNA editing, protein post-translational modifications, and physical seclusion, all of which can change with cell identity or adaptation to environmental cues. Directly speaking to both cellular and biochemical contexts and re-emerging with the refining of different classes of RNA-protein condensates (referred to as mRNP granules) is the concept of phase transition. It remains less than clear how phase transition functionally intersects with 3`UTR regulatory mechanisms. Several hypotheses have recently been substantiated and will be discussed later in this section.

1.2 microRNAs (miRNAs)

miRNAs are genome-encoded, ~22-nucleotide (nt)-long RNA molecules that guide the associated proteins towards binding sites located in the 3`UTRs of mRNAs to repress their expression. miRNAs were first discovered in *C. elegans* where they regulate the heterochronic genes that pre-determines cell fate and developmental transitions (the *lin-4* and *let-7* miRNAs) (Lee et al., 1993; Reinhart et al., 2000; Wightman et al., 1993). A turning point for the fields of miRNAs and 3`UTRs was the identification of several *let-7* homologs in other species including humans (Pasquinelli et al., 2000). This discovery coincided with important advances in sequencing technologies and sparked a concerted effort of miRNA sequencing and prediction, leading to the identification of thousands of new miRNAs (Friedman et al., 2009; Lagos-Quintana et al., 2001; Lau et al., 2001; Lee and Ambros, 2001). Currently, more than two thousand miRNAs have been identified in the human genome, and the miRbase database contains 48,885 mature miRNAs from a total of 271 species (Kozomara et al., 2018). Since their conservation across species has been shown, miRNAs have been implicated in a myriad of functional processes across metazoans, including development, signaling, immune system, and metabolism (Ameres and Zamore, 2013). Conversely, their misexpression or misregulation contributes to or plays instrumental roles in a variety of diseases ranging from heart disease to diabetes to cancer (Hesse and Arenz, 2014).

1.2.1 miRNA biogenesis

miRNA genes located in intergenic (forming independent transcription units) and intragenic regions found in introns or exons of host genes) are predominantly transcribed by RNA polymerase II in long (> 1kb) polyadenylated transcript called the primary miRNA (pri-miRNA)(Lagos-Quintana et al., 2001; Lau et al., 2001; Lee et al., 2002; Lee et al., 2004; Mourelatos et al., 2002; Ozsolak et al., 2008; Rodriguez et al., 2004; Saini et al., 2007) (Figure 1-2). Some exceptions, such

as miRNA sequences embedded within *Alu* repetitive elements, are transcribed by RNA Pol III (Borchert et al., 2006). These pri-miRNAs often encode multiple clustered miRNAs derived from the same transcriptional unit (Altuvia et al., 2005; Bentwich et al., 2005), termed polycistronic. Structural elements in pri-miRNAs are recognized and then processed by the conserved nuclear Microprocessor complex comprising of the RNase III endonuclease DROSHA and its cofactor DGCR8 to generate a ~65 nt intermediate RNA called the precursor miRNA (pre-miRNA) (Lee et al., 2003; Lee et al., 2002; Zeng et al., 2005). Diverse RBPs have been shown to affect processing by the microprocessor. For instance, the binding of RNA-binding protein hnRNP A1 to pri-miR-18a is required for Drosha processing (Guil and Cáceres, 2007). In contrast, the nuclear Lin28B binds to the loop region of pri-let-7g with nanomolar affinity to hinder processing by Drosha (Newman et al., 2008; Piskounova et al., 2011).

Following the export of the pre-miRNA to the cytoplasm by Exportin 5 (or XPO-1 in *C. elegans)*, another evolutionarily conserved RNaseIII enzyme DICER binds to the two-nucleotide long 3' overhang generated by DROSHA, and cleaves near the terminal loop to generate ~22 nt long small RNA duplex (Bernstein et al., 2001; Bohnsack et al., 2004; Grishok et al., 2001; Hutvagner et al., 2001; Ketting et al., 2001; Knight and Bass, 2001; Lund et al., 2004; Yi et al., 2003; Zhang et al., 2004). For pri-miRNA processing, the action of DICER is highly regulated by the intrinsic properties of the RNA stem loop and trans-acting RBPs that can alter kinetics of processing and precursor stability. For example, Processing by DICER can be regulated by the interaction between Lin28A and pre-let-7 (Lin28A binds to a tetra-nucleotide motif GGAG of the terminal loop). This interaction leads to the uridylation of the 3`end of pre-miRNA by TUT4 (terminal uridylyl transferase-4), which blocks processing by Dicer, leading to the rapid decay of the miRNA (Hagan et al., 2009; Heo et al., 2009; Piskounova et al., 2011; Viswanathan et al., 2008).

The RNA duplex processed by Dicer is then loaded on to distinct Argonaute proteins (AGO1 in *D. melanogaster*, ALG-1/ALG-2 in *C.elegans*, AGO1-4 in mammals) in the presence of ATP to form the miRNA-Induced silencing complex (miRISC). Depending on the thermodynamic stability of the two strands of the duplex, one with a relatively unstable 5' terminus is retained (guide strand) while the other passenger strand is released and degraded (Khvorova et al., 2003). The miRISC is now ready to scan and bind to complementary regions located in the 3` UTR of target mRNAs.

Although most miRNAs use the aforementioned pathways, some are processed using alternative biogenesis pathways. They are broadly classified into DROSHA/DGCR8 independent and Dicer-independent. For example, Mirtrons are a class of miRNAs that arise from processed introns resembling pre-miRNAs and are substrates for Dicer without the need for microprocessor processing (Babiarz et al., 2008; Ruby et al., 2007). Similarly, pre-miRNAs containing an m7G cap at the 5`end (generated directly by transcription initiation), also bypass the microprocessor processing and are exported to the cytoplasm for Dicer processing (Xie et al., 2013). A highly conserved vertebrate miRNA, *miR-451,* is currently the only example for miRNA biogenesis independent of Dicer. Following processing by Drosha, *pre-miR-451* bypasses Dicer, and instead directly cleaved by Argonaute protein due to an unusual structure of the RNA(Cheloufi et al., 2010; Yang et al., 2010).

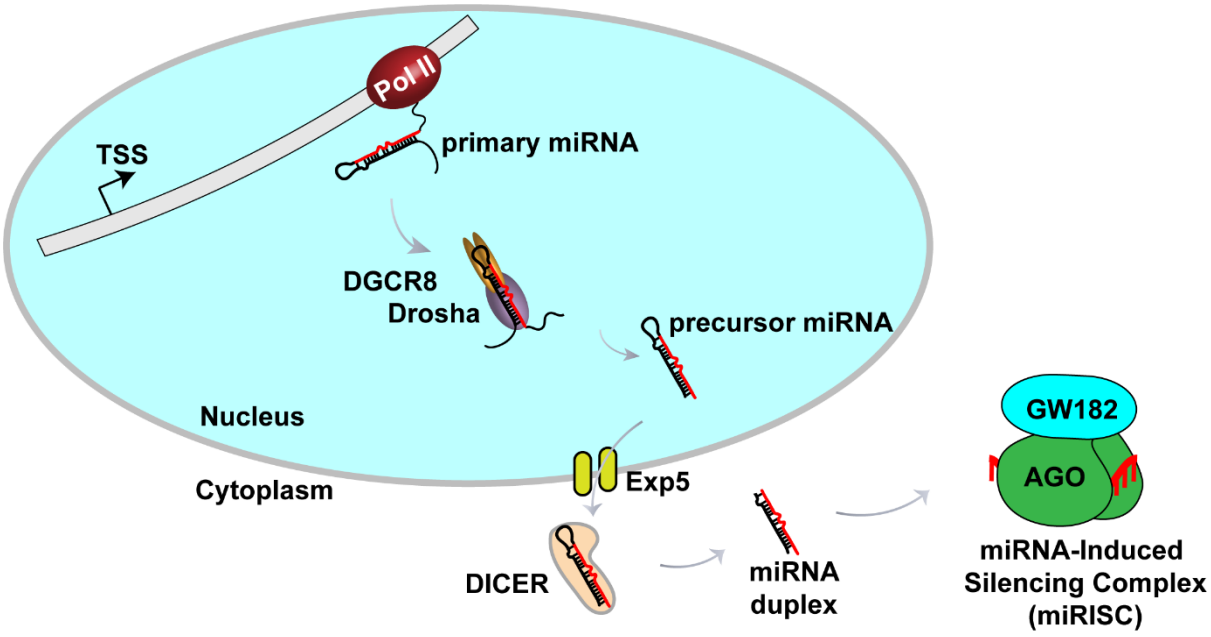

Figure 1-2. Biogenesis of miRNAs.
miRNAs are transcribed as primary miRNA predominantly by RNA pol II. The pri-miRNA transcript is then processed by the microprocessor (DROSHA/DGCR8) and DICER to form a miRNA: miRNA* duplex of ~22 nt in length. One of the duplex strands is loaded on to an Argonaute protein, and together with GW182 protein, form the miRNA-Induced Silencing Complex (miRISC).

1.2.2 Target recognition by miRNAs

Given that miRNAs do not code for proteins, understanding their regulatory functions rely on the identification of their respective miRNA targets. The Ambros and Ruvkun labs had noticed that *lin-4* and *let-7* miRNAs had antisense complementarity to sequences located in the 3`UTR of the *lin-14* and *lin-41* genes, respectively (Lee et al., 1993; Slack et al., 2000; Wightman et al., 1993). These miRNA-target duplexes contained mismatches, G:U base-pairs, and gaps at different positions. Unlike in plants, where miRNA targets base-pair extensively with miRNAs (Reinhart et al., 2002; Rhoades et al., 2002), computational and experimental evidence show that pairing to the 5`portion of the miRNA, especially nucleotides 2-8 (termed as the “seed” sequence) , is the most

important for metazoan target recognition (Brennecke et al., 2005; Doench and Sharp, 2004; Lai et al., 2005; Lewis et al., 2003). miRNAs that share the same seed are grouped into families, and are presumed to target the same genes.

While the seed is generally a good predictor of miRNA targets, multiple genomic studies and individual assessment of miRNA-binding sites have indicated that alternate, non-canonical routes of target recognition may be prevalent. Some miRNAs further use the 3`end of the miRNA in target recognition (Brancati and Großhans, 2018; Broughton et al., 2016; Chi et al., 2009; Hafner et al., 2010; Leung et al., 2011; Loeb et al., 2012; Zisoulis et al., 2010). Such alternate modes of target recognition likely involve dynamic interactions with the N-PAZ pair of Argonaute domains (discussed in the next section). A classic example is the regulation of *lin-41* gene by *let-7* miRNA in *C. elegans. let-7* family members *miR-48*, *miR-84*, and *miR-241* have overlapping expression patterns, but fail to target *lin-41*. 3`-end base-pairing between *let-7* miRNA to the two complementary sites in *lin-41* 3`UTR ensures *let-7* specific silencing of *lin-41* (Abbott et al., 2005; Brancati and Großhans, 2018; Ecsedi et al., 2015; Lim et al., 2003; Vella et al., 2004).

1.2.3 Argonautes

The base-pairing of miRNAs with 3`UTR sequences is quite distinct from what is to be expected from a 'free' single-stranded RNA of the same length. A miRNA's target recognition kinetics and specificity are largely dictated by its interactions with the Argonaute protein within which it is bound in the cell (for a review, see (Duchaine and Fabian, 2019)).

The Argonaute (AGO) protein was first identified in *A. thaliana* through a forward genetic screen for genetic loci involved in leaf development (Bohmert et al., 1998). Mutants of Argonaute displayed narrow rosette leaves resembling the Argonaute squid thus naming the gene. Subsequently, AGO proteins were identified in other organisms and have since then been

implicated in all forms of small-RNA mediated gene silencing (Cogoni and Macino, 1999; Tabara et al., 1999).

The Argonaute proteins are evolutionarily conserved and are phylogenetically subdivided into three clades: AGO-like proteins (similar to AGO1 of *A. thaliana*), PIWI-like proteins (similar to *D. melanogaster* P-element induced wimpy testis), and a *C. elegans*-specific clade called WAGO proteins (Worm AGO) (Hutvagner and Simard, 2008). Members of the AGO family mainly interact with short interfering RNAs (siRNAs) and miRNAs, while members of the PIWI family are predominantly expressed in the germline cells that associate with another class of small RNAs known as Piwi-interacting RNAs (piRNAs) to suppress expression of transposable genetic elements in germ cells (Siomi et al., 2011). In contrast, WAGO proteins are loaded with small RNAs generated by primary Argonautes' action and serve as secondary Argonautes for both mRNA target destabilization and transcriptional silencing (Guang et al., 2010; Yigit et al., 2006). While both AGO-like and PIWI-like proteins are present in bacteria, archaea, and eukaryotes, the number of Argonaute genes varies between species. For example, there are only 5 Argonautes in flies (2 AGO-like and 3 Piwi-like proteins), most mammals possess 8 (in humans; AGO1-4 that bind miRNAs, and 4 PIWI-like proteins), and there are 27 Argonautes in *C. elegans* (5 Argonaute-like genes (ALG), 3 PIWI, and the remaining are WAGO proteins). Within the AGO protein family, individual Argonaute proteins can be functionally specialized and can embed distinct small RNA populations. In mammals, miRNAs appear to be randomly sorted into the four AGO proteins (Wang et al., 2012) while in flies, siRNAs are loaded into Ago2, and miRNAs are exclusively loaded into Ago1, with exceptions such as the miRNA miR-277 that is loaded into Ago2 (Förstemann et al., 2007; Tomari et al., 2007). In *C. elegans*, the broadly expressed ALG-1 and

ALG-2 bind most miRNAs, whereas ALG-5 binds to a subset of miRNAs expressed in the germline (Brown et al., 2017; Vasquez-Rifo et al., 2012).

Structural analyses of Argonaute proteins have identified four functional domains: The N-terminal, PAZ (PIWI-ARGONAUTE-ZWILLE), Mid, and PIWI domains (Duchaine and Fabian, 2019). The miRNA strand is stretched across Argonaute's croissant-shaped structure by interactions with its four domains (Figure 1-3). On its 5`end, the miRNA interacts with the Mid and PIWI domains. Across a central cleft, the 3`end of the miRNA is bound to the PAZ domain, which closely interacts with the N-domain. Extensive interactions pre-orients the 5`-most bases of the miRNA (seed) into a favorable conformation for pairing with target sequences. Target recognition through the seed is a two-step process wherein the rate-limiting step is the pairing of nts 2-5 and the dissociation rate is largely determined by the pairing of nts 6-8 (Chandradoss et al., 2015; Salomon et al., 2015; Schirle et al., 2014; Wee et al., 2012).

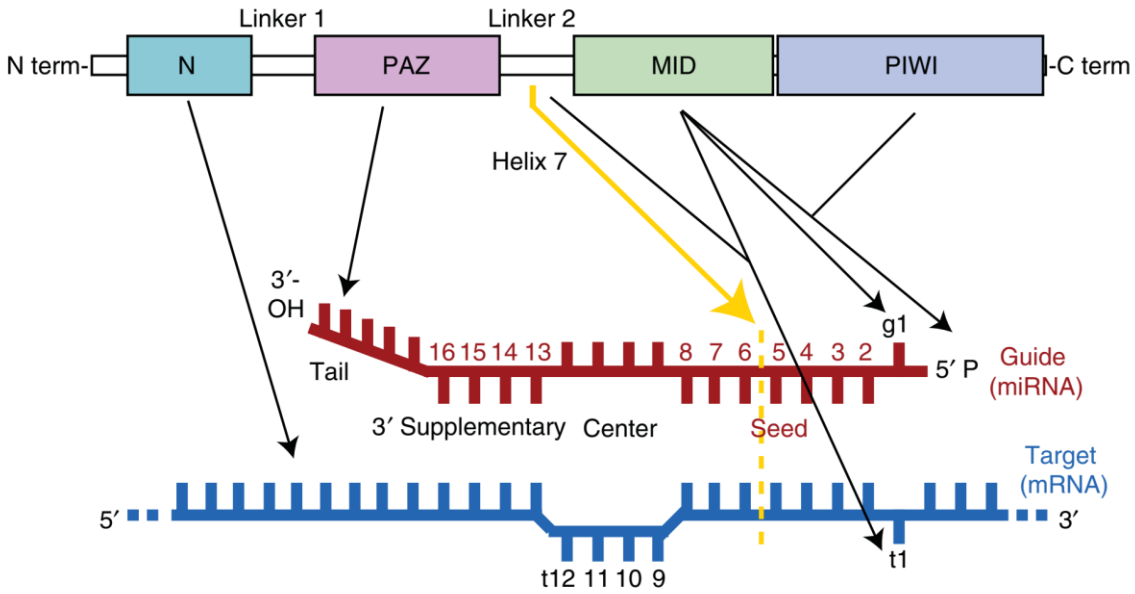

Figure 1-3. Schematic representation of the domains of Argonaute protein and their interaction with RNA.
Interactions of the human Argonaute 2 protein (AGO2) with the guide (miRNA) and target mRNA are indicated via the arrowheads. Connected lines indicate interactions occurring at the interface between two domains. Upon pairing of nts 2-5, Helix 7 (encoded in Linker 2, yellow line) of Argonaute is docked away from the miRNA, allowing pairing of nts 6-8 (Klum et al., 2018). Image obtained from (Duchaine and Fabian, 2019)

The importance of the interactions and molecular mechanics of the Argonaute scaffold in dictating miRNA targeting kinetics recently led the Zamore group to suggest that the miRNA/Argonaute (a minimal assembly referred to as RISC) behaves as a 'programmable RNA-binding protein' (Salomon et al., 2015). Incidentally, this analogy further extends to the effector activities that are mobilized by miRNAs, which largely overlap with effectors and mechanisms mobilized by RBPs.

1.3 GW182 proteins

Metazoan Argonautes programmed by miRNAs also stably interact with the TNRC6 or GW182 family of proteins to form a core complex, referred to as miRNA Induced Silencing Complex or miRISC (Jonas and Izaurralde, 2015). In essence, GW182 proteins bridge interactions between Argonaute proteins and effector complexes, including mRNA deadenylation, decapping, and decay machinery (Duchaine and Fabian, 2019).

Named after the presence of multiple Glycine-Tryptophan (GW) repeats and the molecular weight, GW182 was initially identified in human cells as proteins that localized to distinct cytoplasmic aggregates called GW bodies or P-bodies (Eystathioy et al., 2002; Eystathioy et al., 2003) (P-bodies are discussed later in a separate section) and subsequent studies identified GW182 as Argonaute-interacting proteins involved in miRNA-mediated gene silencing (reviewed in (Eulalio et al., 2009b)).

While GW182 orthologs are not identified in fungi or plants, there exist three GW182 paralogs in vertebrates termed as Tri-nucleotide repeat-containing 6 (TNRC6A, TNRC6B, TNRC6C), one ortholog (GW182) in *D. melanogaster* and two functional analogs AIN-1 and AIN-2 (ALG-interacting protein) that might have evolved independently in *C. elegans* (Zielezinski and Karlowski, 2015). Vertebrate and insect GW182 proteins share common domains: a central ubiquitin associated-like (UBA) domain and a C-terminal RNA recognition motif (RRM), both of which are surrounded by regions that are predicted to be unstructured. These unstructured regions include N-terminal, Middle, and C-terminal sequences that contain a varying number of GW-repeats. Based on biochemical experiments, vertebrate and insect GW182 can be functionally divided into two domains: Argonaute-binding domain (ABD) in the N-terminal region of GW182 that contain at least 30 GW repeats of which only three GW-motifs can bind to Argonaute proteins (Elkayam et al., 2017; Lazzaretti et al., 2009; Takimoto et al., 2009), and Silencing domain (SD) that includes both middle and C-terminal regions of GW182 that mediates interactions with other effector proteins such as the CCR4-NOT complex, and DDX6 to elicit miRNA-mediated gene repression (Braun et al., 2011; Braun et al., 2013; Huntzinger et al., 2013). Such interactions along with other intrinsically-disordered region (IDR)-encoding proteins could also trigger phase transition to larger RNP granules and provide an environment for mRNA storage or decay (Wu et al., 2017) (Figure 1-4E) (discussed later).

1.4 The CCR4-NOT complex: A hub for 3`UTR effector activities

The CCR4-NOT (Carbon Catabolite Repressor-Negative on TATA) complex plays a central role in the fate of an important diversity of mRNAs (Braun et al., 2013; Fabian et al., 2011; Jonas and Izaurralde, 2015). Other deadenylases such as the PAN2/3 complex exert a regulatory function but on a more limited subset of mRNAs and a population of longer poly(A) tails (Chen and Shyu,

2011). However, the CCR4-NOT complex seems to be responsible for most poly(A) tail controls in metazoan transcriptomes where it has been examined (Nousch et al., 2013; Schwede et al., 2008; Temme et al., 2004; Tucker et al., 2001; Yamashita et al., 2005). The CCR4-NOT complex integrates the effector functions in mechanisms initiated by a diversity of RNA-binding proteins and miRNAs (Figure 1-4). CCR4-NOT consists of two highly conserved modules: the CNOT1/2/3 proteins constitute a scaffolding module for all the subunits of the complex, while the catalytic module of the complex is formed by two deadenylases, EEP-type CCR4 and DEDD-type CAF1. Their functions partially overlap or compensate for each other *in vivo*, but CAF1 is believed to assume the bulk of the function in miRNA-directed deadenylation (Fabian et al., 2009). Beyond scaffolding the CCR4-NOT complex, the central CNOT1 subunit acts as a tether and directly interacts with GW182, TTP, Nanos, PUF, Smaug, and several other RNA-binding proteins in different cells and organisms (Wahle and Winkler, 2013).

Recruitment of the CCR4-NOT complex to mRNAs is associated with its deadenylation activities, but a different perspective on the function of this complex has recently emerged. The CCR4-NOT complex also recruits distinct activities such as decapping and exonucleases (Figure 1-4B) that are often coupled with deadenylation, but also with cap-binding and translation repression without mRNA deadenylation or decay (Figure 1-4C, 4D).

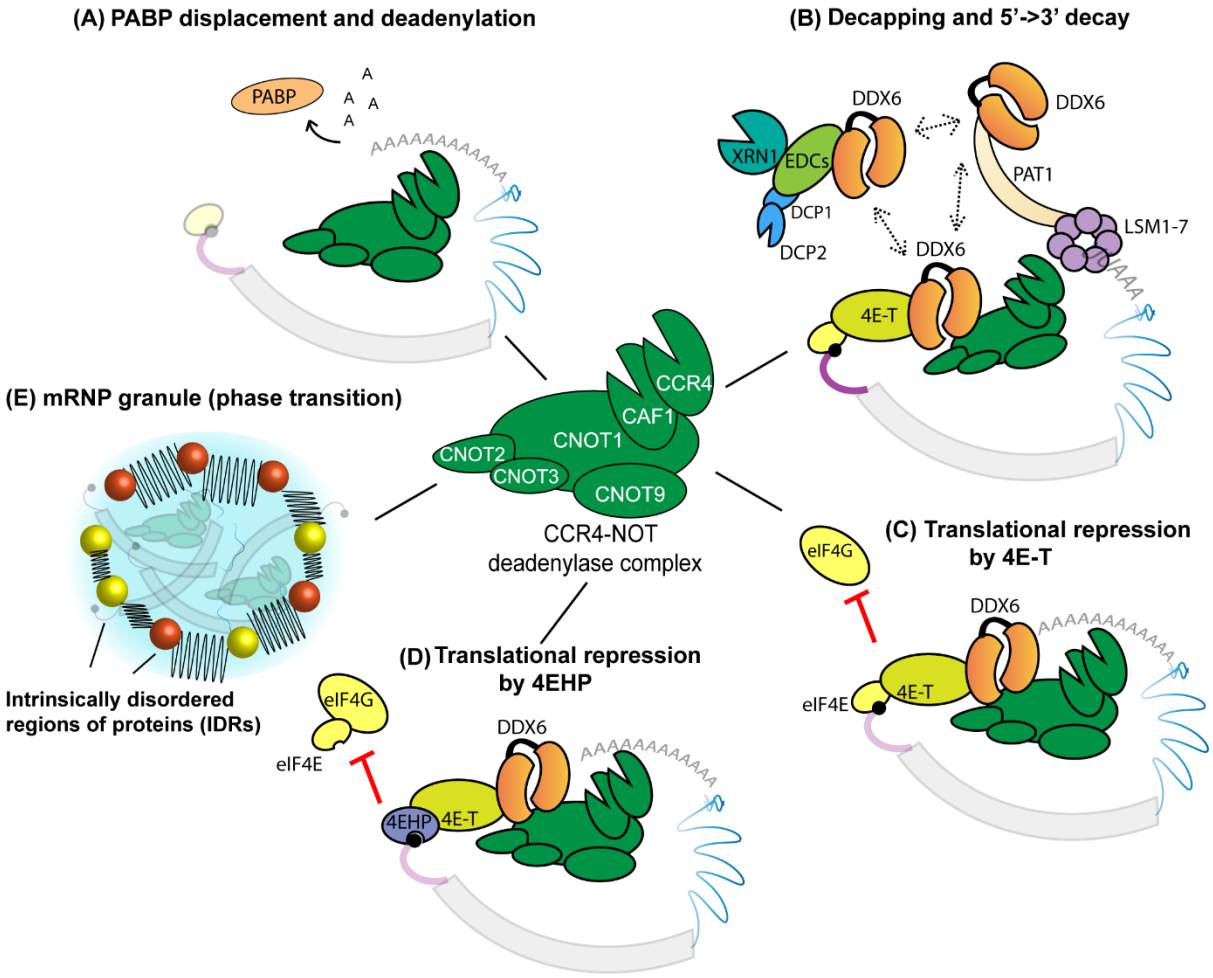

Figure 1-4. Roles of the CCR4-NOT complex and associated proteins in effecting 3`UTR-encoded gene regulation.

The CCR4-NOT complex contains at least eight subunits, of which only six are shown here. **(A)** Inhibition of mRNA circularization by PABP displacement and deadenylation. **(B)** CCR4-NOT-directed mRNA decay. The CCR4-NOT complex deadenylates the mRNA and recruits DDX6. DDX6 promotes decay through three mutually exclusive interactions, with 4E-T, EDC-3, and PAT1 (dashed lines). **(C-D)** Inhibition of translation through CCR4-NOT. Note that all mechanisms depicted target initiation. (C) DDX6 recruits 4E-T to prevent the binding of eIF4G to eIF4E. (D) 4EHP is recruited to the cap through 4E-T/DDX6/CCR4-NOT complex. **(E)** Assembly of an mRNP granule. CCR4-NOT and intrinsically disordered regions (IDRs)-encoding proteins are sequentially recruited to target mRNAs to promote mRNP formation, possibly enabling or promoting phase transition.

1.5 Mechanisms of miRNA-mediated gene silencing

Following target recognition by miRISC, effector proteins are recruited to the target mRNAs. This initiates a series of events that culminates in translation repression and/or mRNA deadenylation and decay. Below we review the two silencing mechanisms in detail.

1.5.1 mRNA deadenylation and decay

In addition to its role in translation initiation, PABP is a cofactor of deadenylases, including the CCR4-NOT complex (Fabian et al., 2009; Huntzinger et al., 2013). *In vitro*, PABP accelerates the deadenylation of long 3`UTRs for which the poly(A) tail is distant to the regulatory sequences (Flamand et al., 2016). The first step in deadenylation of an mRNA is thought to be the displacement of PABP proteins from the poly(A) tail by cofactors recruited through the GW182 protein and CCR4-NOT complex (Moretti et al., 2012; Zekri et al., 2013). Removal of the poly(A) tail is then catalyzed by the CAF-1 and CCR4 deadenylases subunits (Figure 1-4A).

In metazoans, deadenylation is often tightly coupled with mRNA decapping and decay (Figure 1-4B). Earlier studies showed that following the shortening of a poly(A) tail below a certain threshold, an mRNA is subjected to first-order decay (Chen et al., 2008). mRNA deadenylation and decay are clearly coupled in the early zebrafish embryo, where mRNA deadenylation instigated by the miR-430 family of miRNAs marks the initial step in the decay of an important fraction of maternal mRNAs in the Maternal-to-Zygotic Transition (MZT) (Giraldez et al., 2005; Giraldez et al., 2006). This is also obvious in *Drosophila* S2 cultured cells, where fully deadenylated mRNAs do not accumulate, and impairing the decapping enzymes Dcp1/2 is necessary to detect the deadenylated species (Eulalio et al., 2009a). The LSM1-7 proteins are thought to form a ring-like complex around the remnants of the shortened poly(A) tail and to promote mRNA decapping and decay (Tharun, 2009).

A key protein, which physically couples the CCR4-NOT complex with decapping and decay, is the DEAD-box protein DDX6. DDX6 directly interacts with CNOT1 subunit and multiple decapping/decay factors, either simultaneously or through mutually exclusive interactions (Chen et al., 2014; Mathys et al., 2014; Nishimura et al., 2015; Ozgur et al., 2015; Rouya et al., 2014; Sharif et al., 2013; Tritschler et al., 2009). Interestingly, DDX6 also interacts with eIF4E-transporter (4E-T). This interaction is thought to increase the local concentration of decapping factors such as DCP2 around the 5'-cap, thus enabling competition with eIF4E (Nishimura et al., 2015). The removal of the 5'-cap structure by DCP2 seals the mRNA's fate towards degradation via the 5'->3' decay pathway mediated by XRN1 (Arribas-Layton et al., 2013). The activity of DCP2 is greatly enhanced by DCP1 and additional factors such as enhancers of decapping (EDC-3, EDC-4), PAT1, and the LSM1-7 complex (Jonas and Izaurralde, 2013) (Figure 1-4B). Alternative routes of mRNA decay have also been proposed, which would proceed from the 3' end and through the cytoplasmic exosome complex (Chen and Shyu, 2011).

1.5.2 Translational repression

mRNA deadenylation abolishes the physical and functional synergy between the 5'-cap and poly(A) tail, resulting in translational repression (Mishima et al., 2006; Wakiyama et al., 2007). However, strong evidence indicates that the CCR4-NOT complex can also participate in direct translational repression, through mechanisms that do not involve its deadenylase activities (Figure 1-4C, 4D). Using luciferase reporters engineered to block deadenylation, an early study showed that tethering of *Xenopus* or human CAF1 is sufficient to repress mRNAs (Cooke et al., 2010). Several other reports, using different experimental designs and systems, have since then confirmed the role of CCR4-NOT as a direct translational repressor (Braun et al., 2011; Chapat et al., 2017; Chekulaeva et al., 2011; Flamand et al., 2016). Models proposed to explain this activity have

accumulated in recent years and were substantiated to different extents. Disruption of mRNA circularization by displacement of PABP through CCR4-NOT and its cofactors has been suggested as one mechanism (Zekri et al., 2013). Other mechanisms instead revolve around displacement of interactions with the 5'-cap of targeted mRNAs, and DDX6 is also central for these functions of CCR4-NOT.

DDX6 can recruit 4E-T whose interaction with eIF4E can displace eIF4G and thus mediate translational repression (Kamenska et al., 2016). Repression can also occur through the strong interaction between 4E-T and 4EHP (Cho et al., 2005; Joshi et al., 2004). 4EHP is an eIF4E-like cap-binding protein that does not interact with eIF4G and impairs ribosome recruitment (Rom et al., 1998). Recruitment of this dimer to CCR4-NOT through DDX6 was recently involved in translation repression by miRNAs (Chapat et al., 2017). A subset of mRNAs is translationally regulated through this 4EHP-4E-T mechanism in mammalian cells, among which DUSP6 plays an important role in fine-tuning the ERK signaling cascade (Jafarnejad et al., 2018). This last study is unique in identifying a physiological purpose to one of the many CCR4-NOT 'pure' translational repression mechanisms. Indeed, the physiological importance has yet to be determined for most of those mechanisms, which were identified in cell culture and/or *in vitro*. It remains possible that distinct mechanisms will be predominant in different cellular contexts or on particular mRNA targets. Discerning the biological importance of these mechanisms will likely require a combination of genomics, genetics and epistasis analyses with target mRNAs that exert important functions.

1.6 RNA-Binding Proteins (RBPs)

The human genome encodes more than 1,500 RBPs (reviewed in (Hentze et al., 2018)). Each one of these proteins is constituted of one or more RNA binding domains (RBD), which can be grouped

in RBP families, and auxiliary domains that enable other interactions or carry out enzymatic activities (Gerstberger et al., 2014). Canonical RBDs that are often involved in 3`UTR recognition include RNA recognition motifs (RRM), K-Homology (KH) domain, several types of zinc finger domains, double-stranded RNA binding domain (dsRBD), Piwi/Argonaute/Zwille (PAZ) domain, Pumilio/FBF (PUF) domain, and Trim-NHL domain proteins (Lunde et al., 2007). Using intra-molecular or extra-molecular combinations of RBDs, RBPs can improve RNA recognition specificity, affinity, and avidity. Distinct surfaces of RBDs, specific motifs and auxiliary domains mediate the protein-protein interactions required to recruit and activate effector activities to mRNAs.

1.6.1 PUF proteins

Eukaryotic Pumilio and FEM-3 binding factor (PUF) proteins are part of a family of RBPs that can instigate translational repression, deadenylation, and decay of targeted mRNAs. PUF proteins regulate a large number of mRNA targets involved in diverse biological functions. For example, *Drosophila* and *C. elegans* PUF proteins are important for the maintenance of stem cells (Wickens et al., 2002) and target mRNAs of central components of the Ras/MAPK, PI3K/Akt, NF-κB, and Notch signaling pathways (Kershner and Kimble, 2010). In mammalian cells, the precise dosage of PUF proteins is essential to fine-tune the expression of mRNAs encoding mitosis, DNA damage, and DNA replication factors. Recently, PUF proteins were shown to be involved in a network of interactions with the NORAD lncRNA at its center, which prevents chromosomal instability (CIN) (Lee et al., 2016).

The PUF family of proteins binds RNAs bearing the 5'-UGUR (where R = purine) sequence (Quenault et al., 2011). The determinants of those interactions are understood to such an extent that a PUF protein's specificity can be predicted (Hall, 2016). For example, the classical

Drosophila Pumilio protein uses its eight α-helical Pumilio repeats to bind the eight-nucleotide sequence 5′-UGUANAUA. Furthermore, Pumilio proteins can be co-expressed. In *Saccharomyces cerevisiae,* co-expression of PUF-proteins at different concentrations and with distinct binding affinities can result in competition for individual binding sites (Lapointe et al., 2017; Lapointe et al., 2015). Binding of PUF proteins to an mRNA typically leads to translational repression, deadenylation, and mRNA decapping. The yeast PUF-domain Mpt5p protein directly interacts with the ortholog of CAF1, one of the two catalytic subunits of the Carbon Catabolite Repressor-Negative on TATA (CCR4-NOT) deadenylase complex to the mRNA, through its RNA-binding domain (Goldstrohm et al., 2006). This interaction is conserved in metazoa, and *C. elegans* and human PUF homologs can also bind to the yeast CAF1 ortholog (Suh et al., 2009; Van Etten et al., 2012; Weidmann et al., 2014). PUF proteins can also repress mRNA expression by inducing their destabilization. Indeed, Mpt5p can recruit a eukaryotic translation initiation factor 4E (eIF4E)- binding protein to target mRNAs (Blewett and Goldstrohm, 2012). eIF4E-binding proteins block the interaction between eIF4E and eIF4G, and this typically prevents the recruitment of the 43S pre-initiation complex (PIC) to mRNAs (Haghighat et al., 1995). However, sometimes including this case, the interaction leads to the recruitment and activation of decapping and decay co-factors (Ferraiuolo et al., 2005; Nishimura et al., 2015).

1.6.2 Nanos and TRIM-NHL proteins

The outcome of PUF protein binding to mRNA targets can be altered through interactions with other RBPs. This is the case for the prototypical Pumilio protein in the regulation of *hunchback* mRNA in *Drosophila* (Sonoda and Wharton, 2001), wherein its functions are highly dependent on Nanos and Brain Tumour (Brat) proteins. The RNA-binding specificity of Nanos is defined by its interactions with Pumilio, and Nanos directly interacts with the CCR4-NOT deadenylase complex

to promote deadenylation of mRNAs (Curtis et al., 1997; Kadyrova et al., 2007; Kraemer et al., 1999; Sonoda and Wharton, 1999). Brat, a member of the broadly conserved TRIM-NHL family of proteins, forms a ternary complex with Pumilio and Nanos. This complex recruits the effector protein 4EHP to repress the translation of mRNAs (Cho et al., 2006). Unlike Nanos, Brat can stably bind RNA on its own through its NHL domain, and can also function independently of PUF proteins (Laver et al., 2015). Proteomic analysis of the CCR4-NOT complex also suggests an interaction with Brat (Temme et al., 2010). It remains unknown whether this is direct interaction and whether it contributes to and/or is necessary for mRNA repression. TRIM-NHL proteins exert a broader set of biological functions, beyond their interplay with Pumilio in the *Drosophila* embryo. They play critical roles in brain development, cell polarity, and sex determination (Tocchini and Ciosk, 2015). It is quite possible that this family drives different mechanisms in different cellular or physiological contexts, and that functional interactions with miRNAs or other RBP families may depend on the mRNA target and/or its genetic niche. In Chapter 4, we carefully investigate the role of the *C. elegans* NHL protein, NHL-2 in miRNA-mediated silencing.

1.6.3 HuR and TTP proteins

The presence of adenylate/uridylate (AU)-rich sequences in 3`UTRs have long been associated with the regulation of mRNA stability (Barreau et al., 2005). Early computational analysis of human mRNA datasets estimated that 8% of mRNAs harbor AU-rich elements (Bakheet et al., 2006). While AU-rich sequences may be expected to contribute to the destabilization of 3`UTR folding structures, they are also directly recognized by a diversity of RBPs. Tristetraprolin (TTP) and its paralogs butyrate response factors 1 and 2 (BRF-1/2) bind to AU-rich elements using their two zinc-finger domains and promote the decay of mRNAs (Lai et al., 2000). Here again, TTP or BRF direct mRNA destabilization by recruiting effectors of deadenylation, decapping, and 5’- and

3’-exonuclease activities (Lykke-Andersen and Wagner, 2005; Sandler et al., 2011). Interactions with effectors have been mapped to an auxiliary N-terminal domain, which is sufficient to trigger the decay of target mRNAs (Lykke-Andersen and Wagner, 2005). The XRN1 5’-> 3’ exonuclease is thought to be the enzyme effecting mRNA degradation instigated by TTP. It is recruited through the Enhancer of Decapping-4 (EDC4) scaffolding protein (Chang et al., 2014).

Not all AU-rich encoding mRNAs are subjected to degradation. In fact, closely similar sequences can instead lead to enhanced mRNA stability. Such a response often occurs when the HuR protein associates with AU-rich sequences (Brennan and Steitz, 2001). HuR is ubiquitously expressed and belongs to the Embryonic lethal abnormal vision (ELAV) family of proteins (Ma et al., 1996). The exact molecular mechanism used by HuR to confer mRNA stability is still being resolved (von Roretz et al., 2011). An early study showed that overexpression of HuR could slow down the decay of mRNAs without impacting their deadenylation rates (Peng et al., 1998). The prevailing model proposes that HuR can stabilize AU-rich encoding mRNAs through competition for binding with factors such as TTP or a subset of miRNAs. Some of the keys to predicting whether an AU-rich sequence dictates degradation, stabilization or no impact on an mRNA will likely lie in quantitative parameters such as stoichiometry of AU-rich elements and RBPs, and their binding affinities. Quantitative approaches such as those presented in Chapter 2 to study the stoichiometric aspects of miRNA-mediated silencing can be used here.

1.7 Cooperative and competitive interplay among RBPs and miRISC

RBPs and miRISC can interact among themselves and with each other to alter the fate of mRNAs through either cooperation or competition. Considering the importance of 3`UTR sequences and the diversity and density of potential binding sites for RBPs and miRNAs, it is hard to expect otherwise. The median length of human 3`UTRs is 1,200 nt (Jan et al., 2011). On average, each

mRNA 3`UTR is bound by 14 RBPs (Plass et al., 2017), and ~70% of vertebrate 3`UTRs encode multiple sites for different miRNA families (Friedman et al., 2009). Neither miRNA- nor RBP binding sites are distributed randomly in 3`UTR sequences. Early on, genomic studies have shown that miRNA-binding sites are more likely to be functional when located close to each other or located close to the ORF or the poly(A) tail (Grimson et al., 2007; Saetrom et al., 2007). Similarly, genomic analyses indicate that AU-rich sequences are associated with a greater functional output of nearby miRNA-binding sites, and computational analyses of the mammalian genomes indicate that recognition sites for PUF proteins and AU-rich sequences are enriched within 50 nt of binding sites for a subset of miRNAs (Jiang et al., 2013).

1.7.1 miRNA-miRNA cooperativity

Signs that miRNA-mediated silencing acts through a cooperative mechanism were already visible in the seminal discovery papers in *C. elegans*. The 3`UTR of *lin-14* encodes 7 potential base-pairing sites (Lee et al., 1993), while the *lin-41* 3`UTR harbors two *let-7* miRNA-binding sites, separated by intervening sequences of 27 nt in length (Reinhart et al., 2000). If each of these individual sites were independently functional, some degree of redundancy could be expected, with their individual impairment having limited to no consequence. Instead, both *let-7* sites in the *lin-41* 3`UTR are important *in vivo* (Vella et al., 2004). Likewise, binding sites for *lin-4* and *let-7*, and multiple sites for *lsy-6* functionally interact on the *lin-28* and *cog-1* mRNAs, respectively (Didiano and Hobert, 2008; Moss et al., 1997; Reinhart et al., 2000). *In vitro* and *in vivo* studies later demonstrated that miR-35 and miR-58 miRNAs cooperate in the deadenylation and the silencing of the *C. elegans egl-1/BIM* mRNA (Sherrard et al., 2017; Wu et al., 2010). In addition to the fore-mentioned early genomic studies, which support miRNA cooperativity, mammalian reporter assays clearly confirmed that a combination of sites exerts a much more potent silencing

output (Broderick et al., 2011). While some studies examined miRNA-binding site cooperativity on natural or fragments of 3`UTR sequences (Koscianska et al., 2015; Schouten et al., 2015), there are few detailed studies of miRNA-binding site interplay.

The mechanisms underlying miRNA cooperativity are still poorly resolved, but three models have been proposed, and two have been substantiated experimentally. First, miRISC binding to nearby miRNA-binding sites can enhance their affinity for the 3`UTR (Broderick et al., 2011; Flamand et al., 2017). This type of cooperativity in target binding is in fact required for some non-seed miRNA-binding sites to be stably bound by miRISC and to be functional (Flamand et al. 2017). A second model involves the cooperative recruitment of effector machineries. In an embryonic cell-free system, a reporter mRNA bearing a single miRNA-binding site was not deadenylated, and could not recruit the CCR4-NOT complex, whereas a reporter encoding three adjacent miRNA-binding sites did so efficiently (Flamand et al. 2017). Whether this mode of cooperativity is especially important in the embryo and/or in *C. elegans* is not known at present. A third, mutually not exclusive, possibility could involve the cooperative *activation* of effector activities. CCR4-NOT recruitment by miRISC on 3`UTRs may not be sufficient on its own to trigger mRNA deadenylation and decay. A stoichiometric threshold, a specific configuration of target sites, post-translational modifications and/or conformation changes of miRISC may be required to trigger effector activation. These variations would be consistent with other protein/nucleic acid interaction paradigms, such as transcription factors.

1.7.2 RBP-miRISC 3`UTR interactions

RBPs, miRNAs, and the associated machinery can regulate their activities through cooperative or competitive interactions. Likely, the mechanisms at work in cooperating miRNA-binding sites may also explain some of the RBP-miRNA cooperativity. Putative examples of direct interplay

may include the cooperation of TTP with miR-16 in regulating TNF-alpha mRNA (Jing et al., 2005), and AU-rich sequences near the miR-16 binding site in the 3`UTR of COX-2 mRNA (Young et al., 2012). Positive interplay can also be indirect through the modulation of global or local 3`UTR structures. Because they do not code, 3`UTRs can adopt complex folding structures, which can positively or negatively impact overlapping or nearby regulatory sequences. Structures can constitute determinants for the recognition of other RBPs, or limit binding to miRNA-binding sites. In turn, binding of miRISC or RBP to high-affinity sites can destabilize folding structures and facilitate access to nearby binding sites. This model explains the effect of Pumilio on the 3`UTR of the p27 tumor suppressor. Pumilio binding promotes a change in the local structure of the RNA that allows the binding of miR-221 and miR-222, leading to silencing of the p27 mRNA (Kedde et al., 2010). Similarly, a study showed that HuR could enhance the activity of *let-7* on c-Myc mRNA. This is also likely through a change in the local structure of the RNA resulting in the unmasking of the *let-7* binding site (Kim et al., 2009). In Chapter 4, we get to look at how interactions between NHL-2 protein and miRNAs affect gene silencing.

In the simplest form of antagonistic interaction, overlapping or nearby binding sites can lead to direct competition between RBPs and miRNAs/miRISC through steric hindrance. A survey by Keene and colleagues suggested that HuR prevents the function of abundant miRNAs on nearby and overlapping sites in a subset of mRNAs in HEK293 cells (Mukherjee et al., 2011). Similarly, Fillipowicz and colleagues showed that HuR could displace miRISC bound to a target mRNA thereby alleviating miRNA mediated repression. This displacement occurs when HuR binds to AU-rich sequences 20 to 50nt away from the miRNA-binding site (Kundu et al., 2012), again suggesting steric interference. The HuR example illustrates the fact that an RBP can have both positive or negative impacts on miRNA-binding site function, depending on 3`UTR structure and

binding site positioning. It also highlights that interactions between 3`UTR structures, regulatory sequences, and their trans-acting factors are precisely tuned through co-evolution.

1.7.3 Coordinated and sequential 3`UTR activities

Beyond simple positive or negative interplay, 3`UTR sequences can lead to the coordination of post-transcriptional mechanisms in both time and space. The mechanism underlying miRNA-mediated silencing is a coordinated series of events wherein mRNA translation repression precedes deadenylation, which in turn precedes decapping and decay. Translation repression can be resolved *in vitro* in a mammalian cell-free system (Mathonnet et al., 2007), *in vivo* in cell culture (Djuranovic et al., 2012), and even occur at distinct but subsequent developmental stages during early zebrafish embryo development (Bazzini et al., 2012). The biological purpose of this series of events, however, remains to be fully elucidated. Some of these steps in the silencing mechanism may be expected to be at least partially redundant with regard to the impact of gene expression. However, one possibility is that translation inhibition enables faster repression, e.g., when a binary decision is promptly required. Another possibility is that this allows for reversible repression in the early steps, whereas decapping and decay may offer a more permanent decision.

1.8 mRNPs: Going through phases in the lives of mRNAs

Mechanisms involving 3`UTR regulatory elements have long been associated with large mRNP granules. These granules can reach massive sizes by molecular standards (Brangwynne, 2013), often rivaling organelles. The list of large mRNP granules is rapidly expanding and includes P-bodies (originally named GW bodies), germ granules (also called polar granules and P granules, depending on species), stress granules, and the mRNA transport particles (Voronina et al., 2011), among others. Similarities and differences in the composition of large mRNPs have been documented (Eulalio et al., 2007a), mainly through comparison of associated markers by

immunofluorescence. For example, stress granules are often distinguished from co-expressed P-bodies through exclusive colocalization of G3BP and DCP2, respectively (Ingelfinger et al., 2002; Kedersha and Anderson, 2007; Tourriere et al., 2003). In the early embryo, germ granules are distinguished from P-bodies through their association with germline markers such as PIE-1 in *C. elegans* (Strome, 2005). The absence of membranes in these organelle-sized particles and their scale led to their non-specific description as 'large aggregates' of RNA and proteins. A function in local mRNA concentration or storage for germ granules was naturally inferred from their scale and their concentration of maternal mRNAs in the oocyte (Noble et al., 2008; Voronina et al., 2011). Their importance in storage and protection of subsets of mRNAs from degradation was substantiated by well-defined examples, including the above-described *nanos* mRNA in *Drosophila*. The mRNA storage/protection model for mRNPs is also often associated with seclusion from the translational machinery. For example, in the developing oocytes of *C. elegans,* P granules help store translationally silent transcripts to prevent premature differentiation (Boag et al., 2008). Later in the embryo, P granules selectively repress somatic mRNAs in the P-lineage blastomeres, but not germline mRNAs to maintain germline fate and totipotency (Gallo et al., 2010; Updike et al., 2014).

While a role in mRNA storage makes sense and appears to be well supported, the biochemical nature of large mRNPs has remained elusive since the identification of the electron-dense 'nuage' structures in the early days of germline and developmental biology (Wilsch-Bräuninger et al., 1997). A breakthrough was recently made in the mechanisms of assembly and disassembly of mRNP granules. Hyman and colleagues showed that P granules in fact form by phase separation. Granules have liquid-like properties that permit dynamic fusing and exchange of components, but segregate from their surroundings like oil from water (Brangwynne et al., 2009). Similar properties

were also described for P-bodies and stress granules *in vitro* (Lin et al., 2015; Molliex et al., 2015). Intrinsically disordered proteins (IDPs) or proteins with at least a portion of disordered regions (IDRs) are a critical component of phase transition and mRNPs (Brangwynne et al., 2015). It is suspected that most, if not all mRNP granules contain different IDPs/IDRs (Uversky, 2017), and the interactions and properties of these proteins can control mRNP contents. Another typical property is their propensity to scaffold multiple proteins through multivalent interaction networks (van der Lee et al., 2014). Alongside IDP/IDRs, mRNAs and their interactions contribute to mRNP dynamics, either in promoting (Lin et al., 2015), or modulating granule assembly (Hubstenberger et al., 2015; Seydoux, 2018). Thus, the nature of protein-protein and protein-RNA interactions which contribute to assembly and stability of mRNP granules are distinct from what is observed in stable complexes in aqueous phases. Phase separation instead is governed by weak multivalent interactions that segregate interacting macromolecules away from water at a critical concentration (Banani et al., 2017; Hyman et al., 2014; Li et al., 2012). Traditional protein-protein interaction studies based on co-immunoprecipitation and *in vitro* interaction assays may not be suitable to detect many, if not most of the interactions that occur in mRNPs. This, in turn, may be one of the reasons why proximity-based interaction mapping methods such as BioID were fruitful in mapping interactions in P-bodies and stress granules (Youn et al., 2018).

In light of the newly discovered properties of mRNPs, new and important questions have emerged. What are the folding and enzymatic differences that prevail in such phase-separated liquid droplets? How is the specific composition (if any) of an mRNP defined, and how are biochemical boundaries maintained or crossed between different types of mRNPs? Earlier work by the Seydoux group revealed that P granules and P-bodies closely interact, but do not merge in the *C. elegans* early embryo (Gallo et al., 2008). More recently, their work identified an important role for IDP

MEG-3 in modulating the structural stability of P granules. Different enrichments in PGL-1 and MEG-3 proteins significantly altered mRNP properties and could limit access to RNA (Smith et al., 2016). In the *Drosophila* oocyte, *nanos* mRNPs progress along the cytoskeleton from smaller localization particles to the larger germ granules at the posterior pole. The Gavis group used quantitative single-molecule imaging to analyze the localization dynamics and assembly of mRNP germ granules in the *Drosophila* oocyte. Interestingly, single mRNP complexes that contain individual *nanos* transcripts merge into multi-mRNA granules at the posterior pole. This localized 'growth' appears to be exponential, rather than additive, which could be interpreted as mRNPs merging through phase transition into the germ plasm. In contrast, the *oskar* mRNA localizes as multi-copy mRNPs which are segregated from other mRNP granules once it reaches the posterior pole, and this exclusivity contributes to proper germline specification (Little et al., 2015). This suggests that single- or multi-mRNPs, can be differentially transported and locally stored. It further strengthens and refines the links between mRNPs and the transport and localization of mRNA granules.

The possible implications of this mechanism reach far beyond *C. elegans* and *Drosophila* oocytes and embryo. For example, analogous mRNP granules are likely common in mammalian neurons. A study took advantage of the preferential precipitation of IDPs by the chemical biotinylated isoxazole (b-isox) to fractionate mRNPs from mouse brain tissue (Han et al., 2012; Kato et al., 2012). mRNAs that precipitated with b-isox had on average 5-fold longer 3`UTRs compared to mRNAs recovered in the soluble fraction. Moreover, precipitated mRNAs encoded roughly 10-fold more binding sites for Pumilio proteins. This further suggests that 3`UTRs and their ability to bind multiple RBPs play an important role in mRNP assembly.

Originally named GW bodies because they contained an important fraction of the miRISC component GW182, P-bodies (for processing bodies) were later renamed because they also co-localized with decapping and decay proteins (Eystathioy et al., 2002; Eystathioy et al., 2003). Because of this association, P-bodies have long been suspected to be sites of mRNA degradation (Sheth and Parker, 2003). They were also proposed as the site for RNAi, and several other mRNA decay activities (Jakymiw et al., 2005; Liu et al., 2005; Sheth and Parker, 2006; Unterholzner and Izaurralde, 2004). These functions however, had been inferred and not directly demonstrated, and several studies challenged this role for P-bodies over the years (Chu and Rana, 2006; Eulalio et al., 2007b). Early on, a study by Izaurralde's group revealed that while miRNA-mediated silencing promoted P-body formation, detectable P-bodies was not required for miRNA function (Eulalio et al., 2007b). More recently, the Weil group developed a FACS-based method to purify endogenous P-bodies and sequenced their RNA contents. With this method, they could not detect any mRNA decay intermediates (Hubstenberger et al., 2017). Interestingly, they also found that mRNAs in P-bodies were translationally repressed. They thus proposed that mRNP formation may increase the local concentration of translational repressors and thus maintain mRNA targets in a translationally repressed state. Similarly, another group monitored the dynamics of XRN1 (which mediates the 5'-> 3' activity in many mRNA decay pathways) using an elegant dual fluorescent reporter design. Surprisingly, they noted that mRNA decay occurred throughout the cytoplasm, but not in P-bodies. This led them to also suggest that P-bodies are sites for mRNA storage, and not decay (Horvathova et al., 2017). This model nonetheless remains at striking odds with the localized concentration of decapping and decay enzymes in P-bodies.

Part of the solution to this conundrum may come from examining the composition and properties of P-bodies in different cellular lineages. The Seydoux group showed that the biochemical

composition of P-bodies changes during early embryonic development, as it gains important decapping cofactors (Gallo et al., 2008). This stands to reason considering the dependence of mRNPs on the composition and concentration of proteins and mRNAs that are present in a particular context. P-bodies may have very different properties and functions in lineages as distinct as a neuron, an oocyte, an early blastomere, or an epithelial cell.

The properties of the proteins that are recruited to a 3`UTR target of miRISC or an RBP may also influence mRNP structure and activities. Our group's recent study in *C. elegans* embryos suggested that recruitment of the CCR4-NOT complex and the associated IDR proteins by miRISC could nucleate mRNP assembly on target mRNAs. Recruitment of cell-lineage specified IDR proteins (such as PGL-1 or MEG-1/2) or co-factors of decapping and decay may enable progression into larger mRNP and towards context-dependent functions (Wu et al., 2017). In keeping with the importance of cellular context, a recent study by the Simard lab showed that miRISC has a distinct composition in *C. elegans* germline. While germline miRNA target reporters were silenced, single-molecule FISH methods revealed that targeting led to juxtaposition to P granules (germ granules) and also stabilized the targeted mRNA (Dallaire et al., 2018).

Lastly, a recent intriguing study showed that interactions between GW182 and the Argonaute could result in the formation of miRISC droplets. This phase-separated condensate could, in turn, lead to sequestration of miRNA targets and acceleration of their deadenylation *in vitro* (Sheu-Gruttadauria and MacRae, 2018). Thus, it seems likely that resolving P-bodies' functions will be undissociable from the cellular expression and the sub-cellular concentration of mRNAs, IDRs, regulatory factors, and effector machinery. Advances in quantitative methods to locally trace translation, mRNA deadenylation, and decay in situ and in individual cell lineages may be important to resolve the apparent conflict in P-bodies' function.

1.9 GYF domain-containing proteins

Chapter 3 explains the function of *C. elegans* homolog of the GYF-family of proteins. Initially identified in the CD2BP2 protein, the Glycine-Tyrosine-Phenylalanine (GYF) domain recognizes proline-rich sequences (Freund et al., 1999). Through peptide substitution analysis, efficient interaction between the GYF domain of CD2BP2 and CD2 peptide was dependent on the core PPG motif (P=Proline, G=Glycine) (Kofler et al., 2004). Subsequent phage display studies revealed the PPG(W/F/Y/M/L) as a general recognition motif, with a bias towards tryptophan (PPGW) (Kofler et al., 2005a). As a result, the GYF domains are sub-divided into two families based on the amino acid following the core PPG: (i) CD2BP2-type GYF domains that have a strong preference for tryptophan ; (ii) SMY2-type GYF domains that preferentially bind peptides with a hydrophobic amino acid at the last position of the motif PPGΦ (Φ=any hydrophobic amino acid) (Kofler et al., 2005b). GYF domains form a compact fold with a single α-helix packed against a sheet. However, the SMY2-type GYF domain is characterized by a shorter β_1- β_2 sheet and an aspartate instead of tryptophan found in the β_1- β_2 loop of CD2BP2-type GYF domains (Kofler and Freund, 2006).

GYF domain-containing proteins' biological functions were deduced based on their identified interaction partners, deletion studies, or *in vitro* reporter assays. Across species, GYF domain-containing proteins are involved in several activities such as insulin-like growth factor signaling, neurodegeneration, splicing, translation control, and mRNA decay. Table 1.1 below summarizes the various GYF domain-containing proteins, their interaction partners, and their functions across species. Of interest to my work is the Grb10-interacting GYF protein-1/2 (GIGYF1/2), first described as regulators of the insulin signaling pathway (Giovannone et al., 2003). Subsequent studies in mice found that loss of Gigyf2 causes early post-natal fatality (Morita et al., 2012).

Mechanistically, the interaction between GIGYF2 and 4EHP, both in mammals and flies, promotes translation repression and mRNA decay (Peter et al., 2019; Peter et al., 2017; Ruscica et al., 2019). Furthermore, the interaction between GIGYF2 and AGO2 is thought to be important for the silencing of miRNA targets (Kryszke et al., 2016; Schopp et al., 2017). In Chapter 3, we study the physiological importance of 4EHP-GIGYF interaction for miRNAs' function and animal development.

Table 1.1. Functions of GYF domain-containing proteins.

Organism	GYF domain-containing protein	Interacting protein	Functions	References
Homo Sapiens	CD2BP2	CD2	T cell adhesion, signaling, splicing	(Hahn and Bierer, 1993; Heinze et al., 2007; Siliciano et al., 1985)
		PI31	Inhibition of proteasome	(McCutchen-Maloney et al., 2000; Zaiss et al., 2002)
	PERQ2	SF1	Splicing	(Krämer, 1992)
	GIGYF2	AGO2, TNRC6C	miRNA-mediated gene silencing	(Kryszke et al., 2016; Schopp et al., 2017)
		ZNF598	Ribosome quality control, Inflammatory signaling	(Garzia et al., 2017; Tollenaere et al., 2019)
		4EHP, DDX6	mRNA decay	(Weber et al., 2020)
Mus musculus	GIGYF2	4EHP Grb10	Translation repression Insulin-like growth factor signaling pathway, neurodegeneration	(Morita et al., 2012) (Giovannone et al., 2003; Giovannone et al., 2009)
Drosophila Melanogaster	GIGYF	4EHP, Me31B, HPat	mRNA decay	(Peter et al., 2019; Ruscica et al., 2019)
Arabidopsis thaliana	GYN4	At3g45630.1 (Orthologue of human CNOT4)	Ubiquitin ligase	(Kofler et al., 2005b)
Saccharomyces cerevisiae	SMY2	MSL5 EAP1	Splicing, mRNA export Translation inhibition	(Rutz and Séraphin, 2000) (Cosentino et al., 2000; Deloche et al., 2004; Matsuo et al., 2005)

1.10 Rationale and Thesis objectives

Significant progress has been made in understanding the mechanism of action of microRNAs. However, most often, miRNAs are studied as separate and autonomous regulatory units. A handful of recent studies now indicate that miRNA activity is largely affected by the cellular environment, miRNA/mRNA target stoichiometry, and other *trans*-acting factors simultaneously bound to 3`UTRs. These parameters that define the basis for functional outcomes of miRNA action in development are yet to be closely examined. This thesis encapsulates the work performed in two model systems (mammalian cell culture and *C. elegans*) and precisely aims at understanding the parameters regulating miRNA activity using a combination of genome editing techniques and biochemical tools.

Our first objective was to delineate the stoichiometric parameters that contribute to miRNA-mediated gene silencing. In Chapter 2, in HEK 293T cells, we quantified miRNA expression levels, their available fraction and investigated their effects on gene silencing. We then sought to understand the mechanistic and physiological contribution of miRISC cofactors in *C. elegans* development. In Chapter 3, we identify and characterize a novel effector of miRNA-mediated translation repression in the GYF-domain protein GYF-1. Finally, in Chapter 4, we focused on resolving the mechanism behind the cooperation between miRNAs and an RBP, NHL-2.

Chapter 2: On the availability of microRNA-induced silencing complexes, saturation of microRNA-binding sites and stoichiometry

Vinay K. Mayya & Thomas F. Duchaine (2015)

Nucleic Acids Res. 2015 Sep 3;43(15):7556-65. doi: 10.1093/nar/gkv720

2.1 Abstract

Several authors have suggested or inferred that modest changes in microRNA expression can potentiate or impinge on their capacity to mediate gene repression, and that doing so could play a significant role in diseases. Such interpretations are based on several assumptions, namely: i- changes in microRNA expression correlate with changes in availability of mature, functional miRISC, ii- changes in microRNA expression can significantly alter the stoichiometry of miRISC populations with their cognate targets, iii- this, in turn, can result in changes in miRISC silencing output. Here, we experimentally challenge those assumptions by quantifying and altering the availability of miRISC across several families of microRNAs. Doing so revealed a surprising fragmentation in the miRISC functional pool, striking differences in the availability of miRNA families, and saturability of miRNA-mediated silencing. Furthermore, we provide direct experimental evidence that only a limited subset of miRNAs, defined by a conjuncture of expression threshold, miRISC availability, and low target site abundance, is susceptible to competitive effects through microRNA-binding sites.

Keywords: microRNA, ceRNA, miRISC availability, miRNA/mRNA stoichiometry

2.2 Introduction

MicroRNAs (miRNAs) are ~22 nucleotide (nt)-long RNAs, which regulate a broad variety of biological processes by impinging on gene expression. Thus far, close to five hundred miRNA genes have been identified in the human genome (Landgraf et al., 2007), and they are suspected to regulate more than 60% of protein coding genes (Friedman et al., 2009). When embedded into Argonaute proteins (AGO1-4 in mammals) as part of the miRNA Induced Silencing Complex (miRISC), miRNAs direct target recognition through partial base-pairing with sites most often located in 3'-untranslated regions (3`UTRs). This initiates a series of events that culminate with the translational repression and the destabilisation of target mRNAs (Chekulaeva et al., 2011; Eulalio et al., 2008; Nishihara et al., 2013). The underlying mechanism involves deadenylation, de-capping and other activities that are scaffolded onto miRISC via the GW182 proteins (TNRC6 in mammals).

The extent of mRNA silencing mediated by miRNAs varies greatly, and the reasons for such a disparity are not fully understood. Silencing is sensitive to several constraints and parameters, including the sequence, structure, density and distribution of miRNA-binding sites in an mRNA (Grimson et al., 2007). Evidence is mounting that miRNA-mediated silencing can be further modulated through several context-dependent mechanisms. One such mechanism with far-reaching implications was postulated in the competing endogenous RNA (ceRNA) hypothesis (Salmena et al., 2011; Tay et al., 2014), whereby co-expressed RNA species, including mRNAs and long non-coding RNAs such as pseudogenes or circular RNAs (Cesana et al., 2011; Memczak et al., 2013), impinge on target mRNA silencing by competing for a common pool of miRNAs. A central prediction of this hypothesis is that changes in the availability of miRNAs, in contrast with their expression alone, could alter the potency of target mRNA silencing. Prior experimental

evidence indeed appeared to support this possibility: ectopic expression of RNAs encoding multiple binding sites for a particular miRNA (often called miRNA sponges) could de-repress endogenous and reporter miRNA targets (Ebert et al., 2007; Mukherji et al., 2011). Since then, several studies have interpreted both correlative and anti-correlative changes in expression of miRNAs and their target mRNAs in light of the ceRNA hypothesis. In some cases, coordinated changes in miRNA, ceRNA and mRNA expression were suspected to play a critical role in diseases including cancer (Fang et al., 2013; Kallen et al., 2013; Ling et al., 2013).

Several recent initiatives have turned to directly test the ceRNA hypothesis, both theoretically and experimentally, and identified some of its limitations. An emerging conclusion is that specific conditions of abundance and stoichiometry must be met for changes in competing RNA expression to affect miRNA-mediated silencing. For example, competition for miRNAs is predicted to be maximal when the concentration of targets and miRNA is nearly equal (Ala et al., 2013; Bosia et al., 2013; Figliuzzi et al., 2013). Conversely, target competition effects can fail due to high abundance of miRNA-binding sites (Denzler et al., 2014). Such interpretations are in line with a genome-wide assessment of the output of miRNAs, which revealed that only a fraction of the most abundant miRNAs, a select group characterized by low predicted target site-to-miRNA ratio, exert significant silencing (Mullokandov et al., 2012). Most recently, an elegant integration of gene expression, Argonaute iCLIP datasets and modelized target site affinities further indicated that only those miRNA families expressed at low target site-to-miRNA ratio are susceptible to target site competition effects (Bosson et al., 2014). Notwithstanding such insightful studies, decisive determination of effective stoichiometry of miRNAs and target sites remains a challenge as on one hand the cumulative concentration of target sites is modelized or inferred, and on the other hand effective miRISC concentration is affected by biochemical and sub-cellular compartmentalization.

We reasoned that direct empirical measurement of miRISC availability could better substantiate and refine the emerging views on critical stoichiometric aspects of miRNA-mediated silencing. Here, we sought to directly assess the relationships between miRISC availability, miRNA expression, and silencing outcome across a diverse set of cancer-linked miRNA families. Using quantitative target analogue-based miRISC capture, absolute quantification of miRNAs, and an array of reporter silencing assays, we demonstrate that miRISC availability is linked to, but distinct from miRNA expression, and greatly varies across miRNA families. Considering the availability of miRISC and its effects on silencing further refine the stoichiometric requirements for functional competition between co-expressed target RNAs, and unveil some of its key mechanistic bases.

2.3 Results

2.3.1 Quantitative capture of available miRISC using target site analogue oligonucleotides.

To profile the available population of miRISC, we used a strategy based on streptavidin-affinity capture of biotinylated 2'-O-methyl oligonucleotides (2'-O-Me), which mimic miRNA target sequences, and efficiently capture paralogous miRNAs (with the same seed sequence) (Hutvagner et al., 2004; Jannot et al., 2011; Wu et al., 2010) (Figure 2-1A). First, miRISC capture was conducted for the miR-20 family in HEK293T lysate over a 150-minute time-course. As a surrogate of miRISC, we detected Argonaute AGO2 (a core protein in miRISC) by western blot. For all capture experiments, similar results were observed when blotting for AGO1 or using a pan-AGO antibody that detects all the four human Argonautes (Nelson et al., 2007) (Figure A1-1A, B]. miRISC capture was progressive over the time course and reached a plateau between 45 and 60 minutes of incubation (Figure 2-1B). At this time, the miR-20 2'-O-Me target analogue captured 0.3% of total AGO2 in the lysate (Figure 2-1B, bottom left panel). We reasoned that this progressive binding might be reflective of a mixture of miRISC populations: a fraction already associated to cognate and/or non-cognate mRNA molecules, and a second available fraction, readily capturable. To test this hypothesis, we pre-treated the lysate with MNase, which preserves miRNAs but not mRNA targets (Chatterjee and Groszhans, 2009), and proceeded with the same capture time course. Quantification of four independent biological replicates indicates that both capture conditions yielded the same maxima at late time points, but capture is significantly accelerated by treatment with MNase (Figure 2-1B, bottom right panel). These results suggest that target analogue capture is sensitive to the availability of miRISC in cell lysates, with free miRISC being captured faster than target RNA-bound miRISC. As the 15-minute time point was the most reflective of the available pool of miRISC, later captures were carried out at this time point.

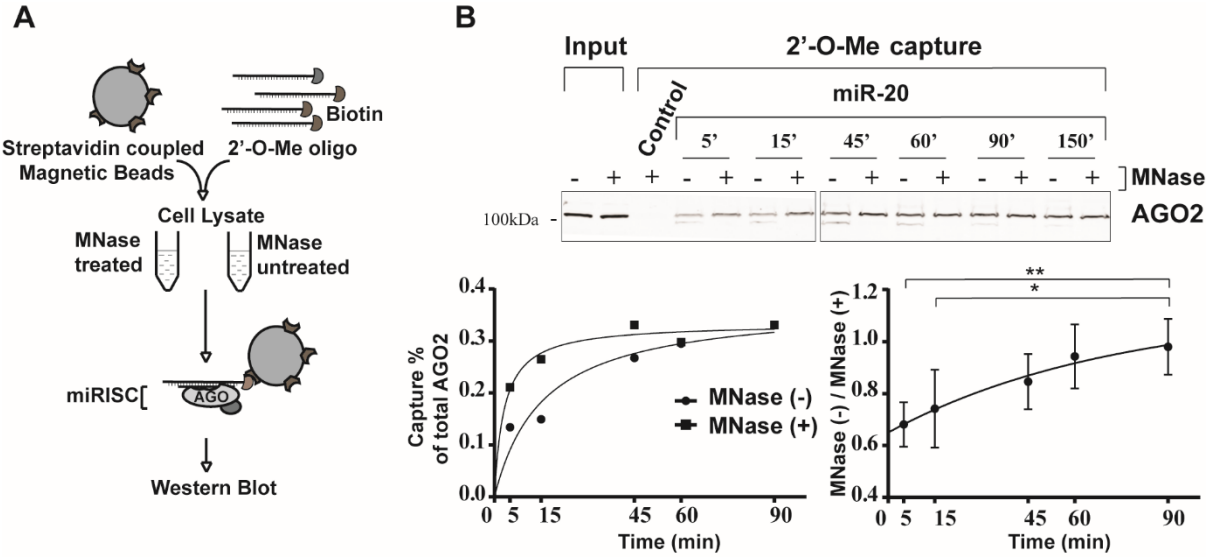

Figure 2-1: Quantitative capture of available miRISC using target site analogue oligonucleotides (2'-O-Me pull-down).

(A) Schematic representation of the capture strategy. Biotinylated 2'-O-methylated (2'-O-Me) oligonucleotides encoding a binding site for a particular miRNA family (here, *miR-20* and a C. *elegans* specific miRNA, *miR-35* as a control) are bound to streptavidin-coupled magnetic beads, and incubated for a defined time in HEK 293T protein lysates pre-treated or un-treated with MNase. Beads are pulled out, washed, and western blot is performed against AGO2, a core component of miRISC. **(B)** Bottom left panel: Quantification of the presented AGO2 western blot. Bottom right panel: Aggregate quantification from four independent biological replicate experiments. Data is presented as a ratio of untreated (MNase (-)) over MNase-treated (MNase (+)). Quantitative imaging was performed using the Odyssey imaging system (LiCor). A two-tailed Student's t test was used to calculate p-values (*: $p<0.05$, **: $p<0.005$).

2.3.2 Comparative quantitation of miRNA expression and miRISC capture for the miRNA families considered in this study.

miRNA expression profiles reflect a wide variety of intracellular and environmental cues, which are unique to cellular and organism contexts. We asked how the readily capturable miRISC pool

relates to miRNA expression levels. miRISC capture was compared for miR-19, miR-20, miR-92 families, members of which are encoded in the proto-oncogenic miR-17~92 polycistron, as well as let-7 and miR-26 miRNAs (Figure 2-2A). Major differences in capture were noticeable between miRNAs: a higher percentage of miRISC was captured using the miR-20 target analogue (median 0.43% of total AGO2 in lysates (n=4)) than miR-19 (0.19%) and miR-92 (0.12%) families (Figure 2-2A, box plot, bottom left panel). miR-26 did not capture miRISC significantly above background, whereas let-7 captured 0.02% of total AGO2 under the same conditions. While some spread of values is visible in box plots for individual captures of each miRNA family across independent lysates, the relative AGO2 capture of miRNA families remained strictly consistent in each individual lysate (lower right panel). Differences between miRNA families were unlikely due to selective small RNA sorting in distinct Argonautes, as evidence strongly argues against such a process in mammalian cells (Liu et al., 2004; Meister et al., 2004). 2'-O-Me baits were utilized in excess, and when capture was carried out for 2 hours, comparable depletion was achieved across- and within each miRNA families (Figure 2-2B and A1-2B,C). Capture of miR-19, miR-20, miR-92, miR-26 and let-7 paralogous miRNAs was largely independent of mismatches with central and 3' miRNA sequences, and was primarily dictated by seed complementary sequence.

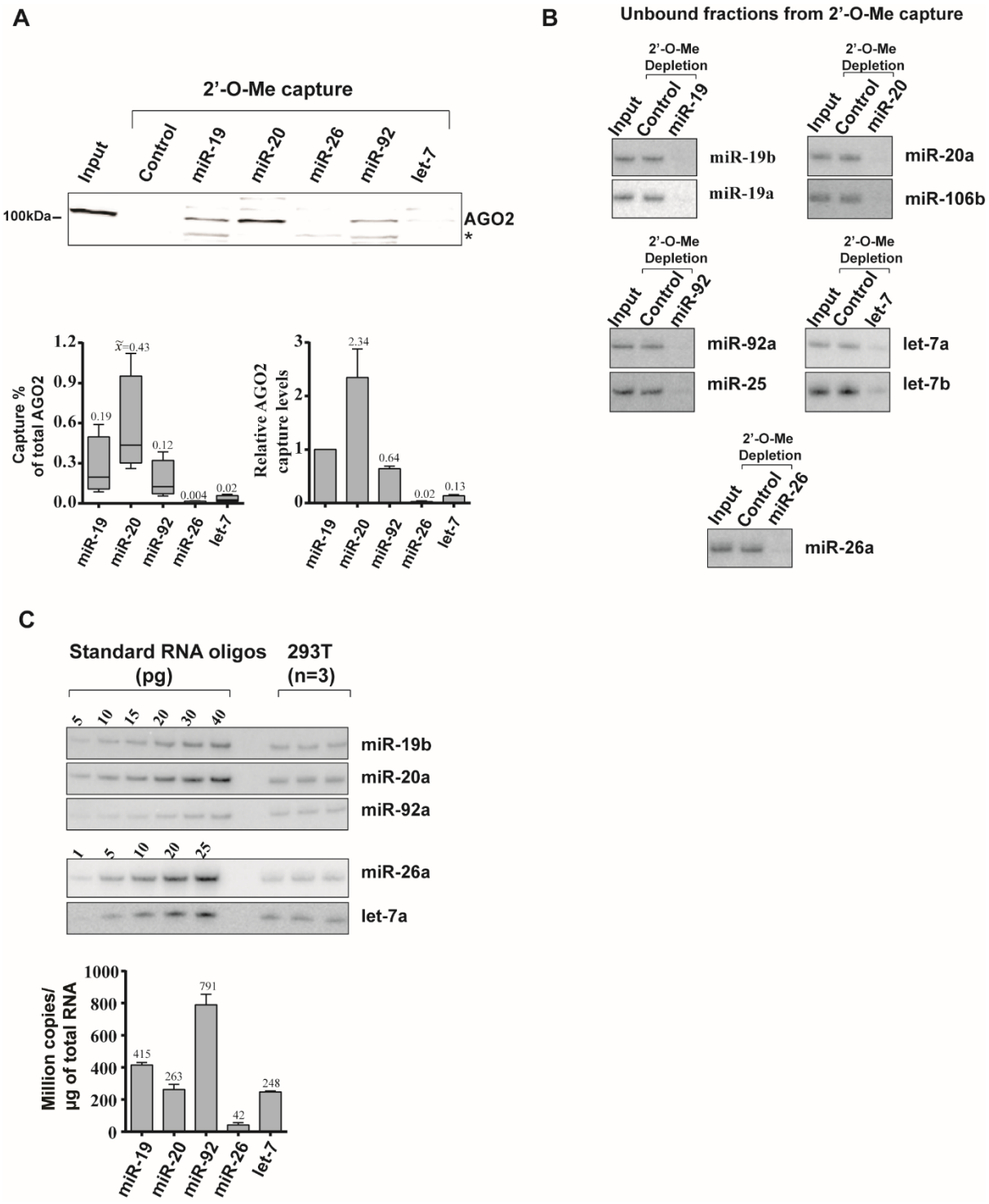

Figure 2-2: Comparative quantitation of miRNA expression and miRISC capture for the miRNA families considered in this study.

(A) miRISC capture was conducted as above, for the miR-19, -20, -92, -26 and let-7 families. Captured AGO2 was quantified from four independent biological replicates (bottom panels).

Results are presented as percentage of total AGO2 in HEK 293T lysate input (10µg) (box plot, bottom left, median values indicated above), and normalised against miR-19 capture for each individual lysate (bottom right, average values indicated above **(B)** Northern blot analyses of unbound miRNA fractions recovered after miRISC capture. **(C)** Quantitative northern blot analyses of each miRNA for three independent biological replicates. RNA oligonucleotides were used as standards, and copy numbers were calculated per microgram of isolated RNA (bottom, average values indicated above). All other paralogous miRNAs examined were less abundant (Supplemental materials). The asterisk (*) indicates a non-specific band.

We next set out to compare miRISC capture with miRNA abundance. Next-generation sequencing has proven invaluable for the identification and relative quantitation of miRNAs in different conditions, but its use in absolute quantitation without internal standards is limited by biases in library preparation (Hafner et al., 2011; Linsen et al., 2009; Zhuang et al., 2012). Instead we opted for standardized northern blots to quantify the expression of miRNAs. These analyses suggest that miR-92a is the most abundant of the examined miRNAs in HEK293T, at 791 x 10^6 copies/µg total RNA, ahead of miR-20a (263 x 10^6 copies/µg total RNA), miR-19b (415 x 10^6 copies/µg total RNA), and let-7a (248 x 10^6 copies/µg total RNA) (Figure 2-2C, Figure A1-3A). In comparison, their paralogs miR-17, miR-20b, miR-25, miR-93, miR-106b, let-7b, often abundantly detected in sequenced libraries (Hafner et al., 2010; Lee et al., 2010), were expressed at very low copy numbers or were undetectable (Figure A1-3B). Paralogue-specific detection using this method has been validated previously (Wu et al., 2010), and was further confirmed using total RNA isolated from mir-17-92 deletion MEFs (Figure A1-3C). Quantitative northern results were further verified using standardized, paralogue-specific, LNA-based qRT-PCR assays on miRNAs (Raymond et al., 2005) (Figure A1-3D,E). Strikingly, although miR-19, miR-20, and let-7 miRNAs are expressed at comparable levels, they exhibited marked differences in miRISC capture assays. miR-

20 is ~3-fold less abundant than miR-92, its expression being comparable to miR-19, whereas its capture yields 2.3-fold more miRISC than miR-19, and 3.7-fold more than miR-92. Furthermore, whereas let-7a and miR-20a are expressed at comparable levels in HEK293T cells, capture of miR-20 yields 117-fold more miRISC than let-7. Altogether, these results point to divergences between the expression levels of miRNAs and their functional availability as part of miRISC.

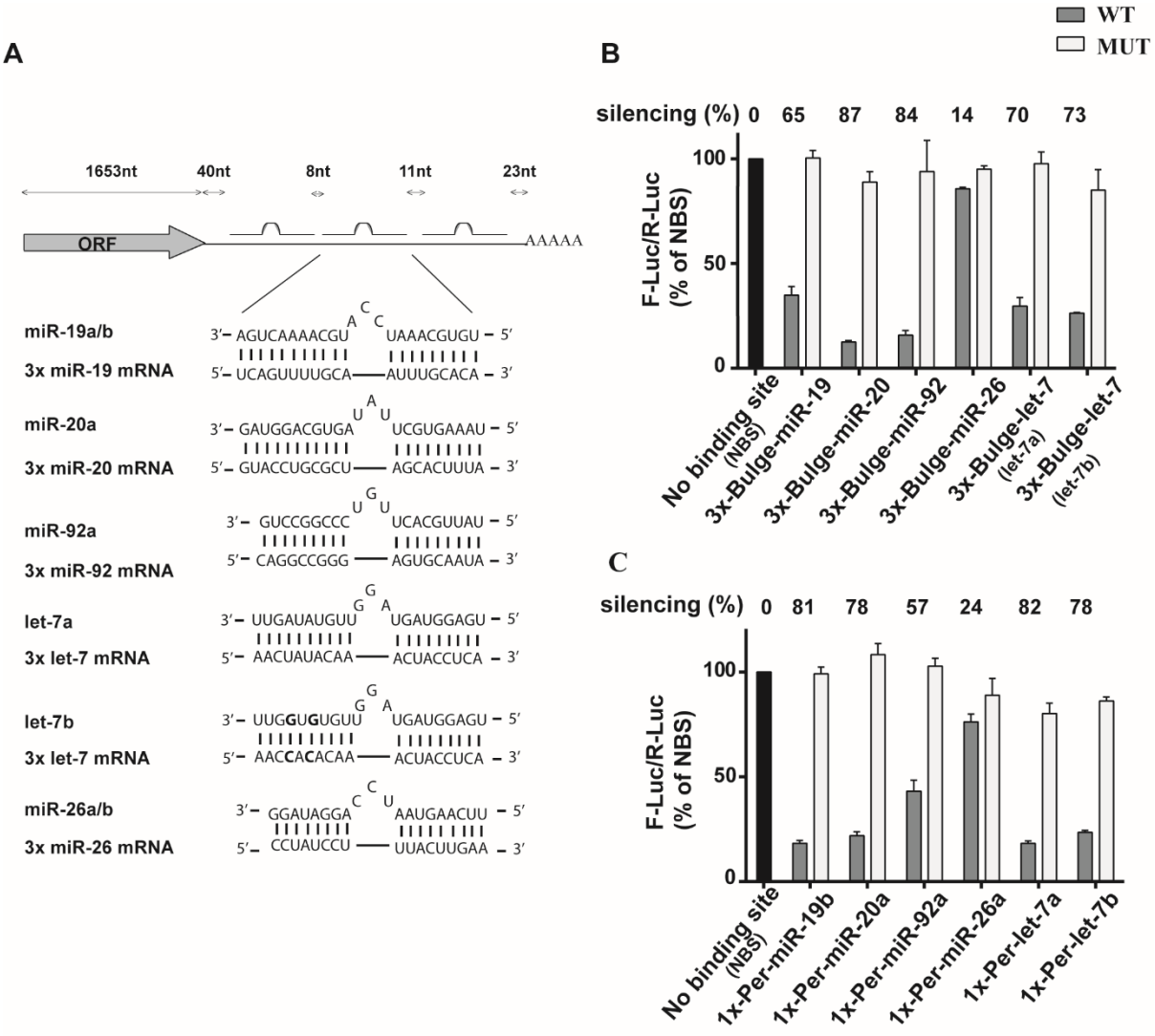

Figure 2-3: Comparative slicing and slicing-independent silencing by miRNA families.
(A) Schematic representation of 3x-Bulge Firefly luciferase (F-Luc) silencing reporters. The structures of mismatched (Bulge) sites are described. The spacing and positioning of sites are the same for all reporters [though miR-26 reporter has a minor disparity] (See supplementary table

S1). Mutated (MUT) reporters encode an additional 3-nt mutation in seed-complementary sequences (*See Materials and methods*). Differences between the let-7a and let-7b-based reporters are highlighted in bold. **(B)** HEK 293T cells were co-transfected with constructs expressing WT or MUT sites (as indicated) for miR-19, miR-92, miR-20, miR-26 or let-7, and *Renilla* luciferase (R-Luc) as an internal standard. Normalized counts are compared to the No binding site reporter (NBS), which is set as 100% for comparison. **(C)** Similar analyses were conducted with reporters expressing one perfectly matching site for each examined miRNA. All data are presented as mean ± standard deviation from technical triplicates of three independent biological experiments.

2.3.3 Comparative slicing and slicing-independent silencing by miRNA families.

Having profiled the expression and availability of the miR-19, 20, 92, 26, and let-7 miRNAs, we next compared their silencing output. As miRNA target sequences intricately interact with RNA structures and RNA binding proteins within endogenous 3`UTRs, we opted for a simple, well-controlled reporters to specifically contrast the impact of miRNAs. Firefly luciferase (FLuc) reporters were built to encode, in their 3' UTR, precisely positioned binding sites for each of the miRNAs. One version encoded three site copies with pairing mismatches at positions 9, 10 and 11, to prevent endo-nucleolytic (slicing) activity by AGO2, thus enabling the monitoring of miRNA-mediated repression (Filipowicz et al., 2008) (Figure 2-3A, B). A second version encoded a single, fully base-pairing site to monitor the slicing activity of miRISC (Figure 2-3C). Constructs were transfected in HEK293T and the potency of their silencing was determined and compared using *Renilla* luciferase (RLuc) activity as an internal reference. A let-7b-based reporter led to silencing virtually indistinguishable from a let-7a-based design, in spite of 3' end sequence differences between the paralogs. Furthermore, reporters bearing mismatches in the seed complementary region (bases 3-5) led to counts indistinguishable from the *No binding site* (NBS) reporter (Figure 2-3B, C; MUT and NBS lanes). These results indicate that our reporters account

for silencing by families of paralogous miRNAs, and reflect specificity as defined by the seed sequence. The extent of miRNA-mediated silencing significantly varied between miRNAs. While it is less abundantly expressed, the more available miR-20 miRNAs silenced cognate 3x Bulge reporter by 87%, significantly outperforming miR-19 (65%) and miR-92 (84%) (Figure 2-3B). let-7 silenced its cognate reporter to an extent comparable with miR-19 (70% vs. 65%), in spite of its limited availability.

Single, perfect site reporters (1xPer lanes, Figure 2-3C) also led to potent silencing, but with virtually the same silencing by miR-19, 20, and let-7 miRNAs (78-82%) despite the differences in their expression and availability. In contrast with the potent silencing exerted upon the 3x Bulge-miR-92 reporter, its 1xPer counterpart was silenced less (57%) than for the other detected miRNAs. However, for both 3x Bulge-miR-26 and 1xPer reporter, silencing was negligible compared to the other miRNAs. Altogether, these results indicate that neither the miRNA expression level nor their availability alone can predict the extent of reporter silencing through slicing or non-slicing mechanisms (see discussion).

2.3.4 Quantitative assessment of the effect of miRISC availability on miRNA reporter silencing.

To better discern the interplay of stoichiometric parameters in miRNA-mediated silencing, we elected to experimentally alter the availability of miRISC for each miRNA family along a continuum of controlled concentrations while following the impact on reporter silencing. For this, 3x-Bulge reporters were co-transfected with increasing concentrations of 2'-O-Me inhibitors to titrate miRISC availability (Figure 2-4, left panel, inhibitors), and dsRNAs that mimic endogenous miRNAs to increase it (Figure 2-4, right panel, miRNA mimics). Strikingly, miRNA families exerted qualitatively and quantitatively distinctive response profiles to miRNA inhibitors and

mimics. miR-20 and miR-92 reporters were progressively de-repressed with increasing concentrations of cognate miRNA inhibitors, but the addition of increasing concentrations of mimics did not lead to significantly more silencing, indicating saturation. miR-19 and let-7 reporters were responsive to both de-repression by miRNA inhibitors and enforced reporter repression by miRNA mimics. At the opposite end of the spectrum from miR-20, and consistent with its very low abundance, the miR-26 reporter was not significantly de-repressed by the addition of inhibitor, but its silencing was strongly improved (by more than 60%) with the miR-26 mimic, reaching saturation at 2-3nM. Importantly, neither inhibitors nor mimics affected MUT or NBS reporter expression within the range of concentrations examined (Figure A1-4). Interestingly, reporters reached saturation under high endogenous and/or mimic miRISC concentrations but reached different maxima. miR-20 and miR-92 reached maxima of silencing at 88 and 86%, respectively, more than let-7 (78%), miR-19 (79%), and miR-26 (80%). Finally, IC_{50} values for 2'-O-Me inhibitors were significantly different between the miRNA families and followed the relative order of miRISC availability reflected in capture experiments (Figure 2-2A): miR-17/20 (IC_{50} 11.22 nM) > miR-19 (IC_{50} 6.06 nM) > miR-92 (IC_{50} 2.76 nM) > let-7 (IC_{50} 1.31 nM) >>> miR-26. These results again confirm the distinction between miRNA expression and the availability of miRISC, and further suggest the functional fragmentation of miRNA/miRISC pools (see Discussion).

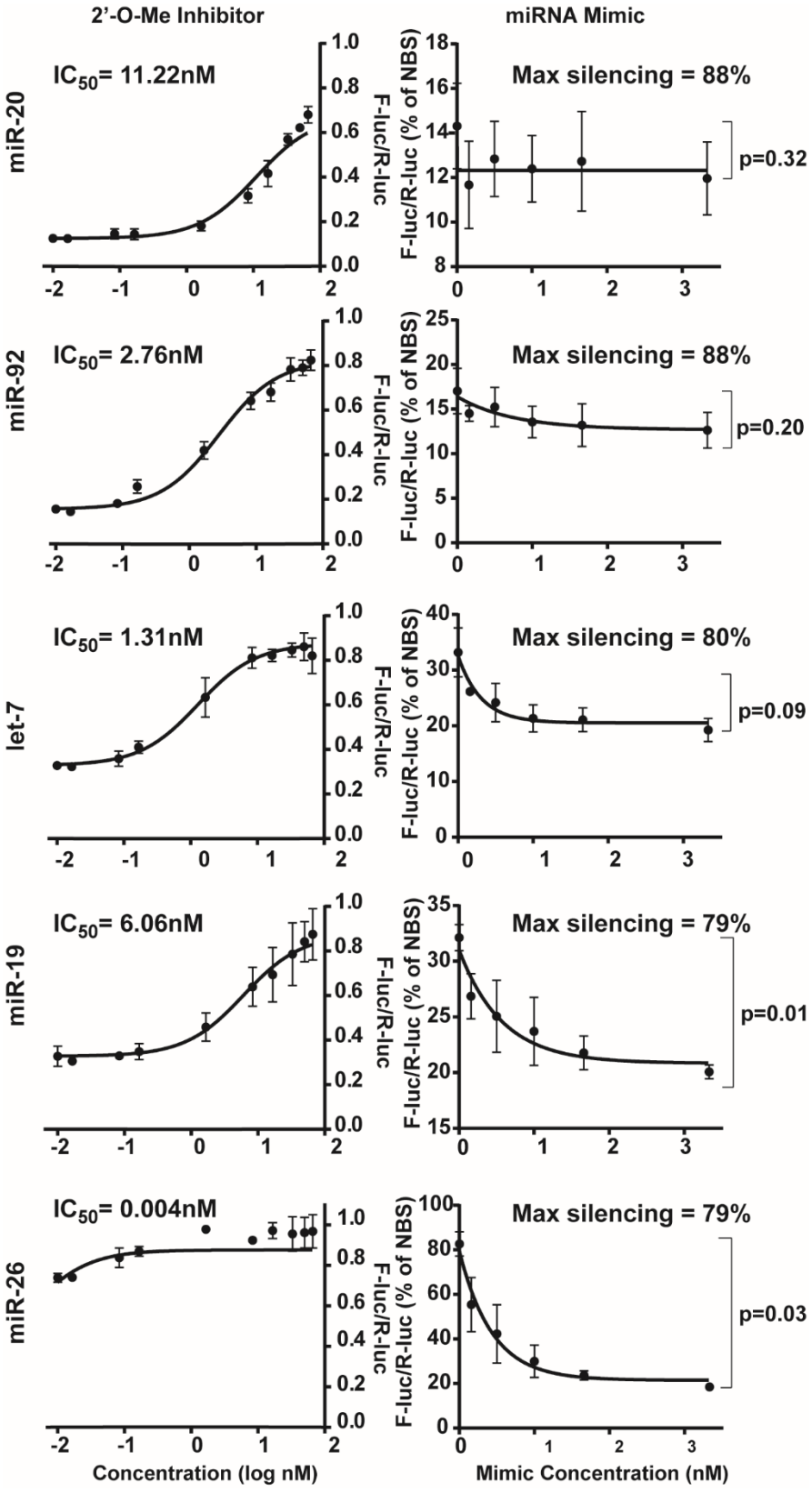
2'-O-Me Inhibitor
miRNA Mimic
miR-20
IC50= 11.22nM
Max silencing = 88%
p=0.32
miR-92
IC50= 2.76nM
Max silencing = 88%
p=0.20
let-7
IC50= 1.31nM
Max silencing = 80%
p=0.09
miR-19
IC50= 6.06nM
Max silencing = 79%
p=0.01
miR-26
IC50= 0.004nM
Max silencing = 79%
p=0.03
F-luc/R-luc
F-luc/R-luc (% of NBS)
Concentration (log nM)
Mimic Concentration (nM)

Figure 2-4: Quantitative assessment of the effect of miRISC availability on miRNA reporter silencing.

(Left panel) 3x-Bulge reporters were co-transfected with increasing concentrations (0-66nM) of 2'-O-Me inhibitors for the indicated miRNAs. The concentrations of inhibitors required to reach half-maximal inhibition (IC_{50}) for each reporter was calculated by normalizing FLuc-3xBulge (WT)/R-Luc ratios to FLuc-3xBulge (MUT)/R-Luc ratios and fitting the values into a sigmoidal curve, using four-parameter analyses. (Right panel) 3x-Bulge reporters were co-transfected with increasing concentrations (0-3.3nM) of dsRNA miRNA mimics for the indicated miRNAs. FLuc-3x-Bulge/RLuc ratios are compared to No binding site reporter (NBS)/RLuc, set as 100%. All data are presented as mean ± standard deviation from technical triplicates of at least three independent biological experiments. Two-tailed Student's t-test was used to calculate p-values.

2.3.5 Near-stoichiometric competing effects for miRNA targets.

Comparative dose-response data indicate that the stoichiometric ratio of endogenous miRISC pools to their reporters varies between miRNA families. While some are in excess and even saturate reporter silencing (miR-20 and miR-92), miR-26 miRISC populations are clearly sub-stoichiometric and cannot silence the reporter through slicing-independent mechanisms at endogenous concentrations. A subset represented by let-7 and miR-19 appears to program just enough miRISC to lie in a dynamic range of functional concentrations. Silencing mediated by such miRNA concentrations should be responsive to mild concentration variations of both available miRISC and competing mRNA target sites. To test this hypothesis, we co-expressed ectopic miR-19a/b (Figure 2-5A, miR-19++) or an mRNA encoding miR-19 binding sites previously validated to function as a competing target RNA, or sponge (Sponge-19) (Mu et al., 2009; Rao et al., 2012). We monitored and quantified the resulting miRISC availability (using 2'-O-Me capture) and reporter silencing (Figure 2-5A). Ectopic expression of miR-19a/b improved AGO2 miRISC capture by 3.3-fold, whereas co-expression of the cognate sponge at the highest concentration

transfected resulted in 0.6-fold capture of miR-19 miRISC of control levels (Figure 2-5A, bottom right panel). Ectopic expression of additional miR-19 indeed resulted in 20% more silencing (Figure 2-5A, bottom right panel).

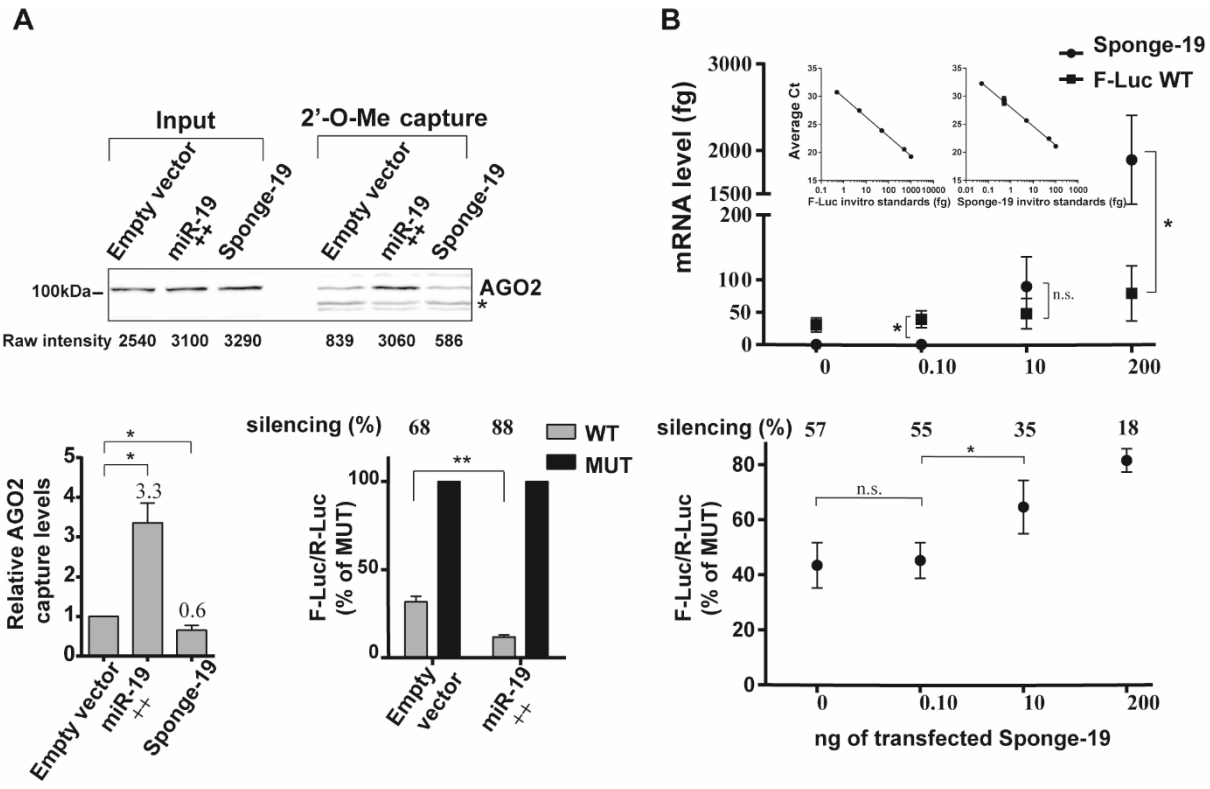

Figure 2-5: Near-stoichiometric competing effects for miRNA targets.
(A) miRISC captures and reporter silencing was quantified for lysates derived from cells co-expressing ectopic miR-19a/b (miR-19++) or a transcript encoding miR-19-binding sites (Sponge-19), with the 3xBulge-miR-19 reporter. Captured AGO2 signal was normalized to input and compared with capture from a lysate co-expressing FLuc without UTR ('Empty', bottom left). Silencing was determined from cells co-expressing ectopic miR-19a/b (miR-19++, bottom right), and are reported in comparison to the MUT construct (set at 100%). **(B)** Cells were co-transfected as in (A) with a fixed amount (10ng) of the 3x-Bulge-miR-19 reporter, and increasing amounts (0-200ng) of Sponge-19-encoding construct. Cells were harvested, and quantitative qRT-PCR analysis was performed on F-Luc reporter and Sponge-19 RNAs. Standard curves (indents) were

generated using samples with spiked-in *in vitro* transcribed F-Luc and Sponge-19 RNAs of known concentrations. 3x-Bulge-miR-19 silencing (bottom panel) for each Sponge-19 concentration was determined using luciferase assays as in (A). All data are presented as mean ± standard deviation from technical triplicates of three independent biological experiments. Two-tailed Student's t-test was used to calculate p-values (*: $p<0.05$, **: $p<0.005$).

To determine the effect of impinged miRISC availability near reporter stoichiometry, we co-transfected increasing amounts of Sponge-19 (0.1ng-200ng) with a fixed amount of 3x-Bulge-miR-19 reporter (10ng). We precisely quantified the reporter mRNA and Sponge-19 RNA species under each condition (Figure 2-5B, upper panel), and the resulting repression (or de-repression) was measured (Figure 2-5B, lower panel). At its lowest concentration, Sponge-19 did not have any significant effect on the miR-19 reporter repression by miR-19, whereas at the highest concentration tested, Sponge-19 de-repressed 3xBulge-miR-19 by 40% (Figure 2-5B). At 10ng of transfected Sponge-19 DNA, the resulting RNA reached near-stoichiometry with 3xBulge-miR-19 mRNA and drove a significant 20% de-repression of the reporter.

Altogether, these results experimentally demonstrate that under specific conditions of availability and stoichiometry with the co-expressed miRNA target sites, minor changes in miRISC availability can result in changes in silencing output.

2.4 Discussion

This work's main conclusions are in line with a few previous studies in challenging the up-front assumption of linkage between miRNA expression and silencing activity (Baccarini et al., 2011; Bosson et al., 2014; Hafner et al., 2010; Mullokandov et al., 2012). Using a unique design of miRISC capture and experimental alterations in miRISC availability, we add empirical evidence to a model wherein specific conditions of abundance, availability, and stoichiometry with target sites have to be met for changes in miRNA expression or target site competition to affect mRNA silencing. Our data also support the emerging view that such requirements are only fulfilled for a subset of miRNAs (Bosson et al., 2014; Mullokandov et al., 2012). The consequences of these strengthened conclusions are important, as functional validation of predicted miRNA targets is still largely conducted under ectopic and over-expression conditions. As such, several of the biological functions that had been allotted to changes in miRNA expression or competitive effects between miRNA-binding sites will have to be revisited.

Previous work, and the results of this manuscript identify four reasons for the disconnect between miRNA expression and their silencing activity; fragmentation in biochemically distinct complexes, sub-cellular localization of miRISC, target site competitive effects, and direct stoichiometric titration of miRNAs by mRNAs. First, fragmentation of the miRISC pool is suggested by the disagreement between miRISC capture and the expression of miRNA families (Figure 2-2). It is further hinted to by the results of miRISC titration on the silencing output (Figure 2-4): IC_{50} values follow the overall trend of silencing but do not always reflect it. Part of this fragmentation is likely the result of the non-homogenous distribution of mature miRNAs among complexes, rendering a significant fraction unavailable for direct involvement in silencing and capture using pull-down methods. One possible mechanism for this is the existence of one or

several miRISC-like complexes with distinct biochemical behavior. This possibility was recently supported in *Drosophila* cells and primary mammalian tissue (La Rocca et al., 2015; Wu et al., 2013), and may also occur in the course of an alternative mechanism of miRISC assembly (Janas et al., 2012). We note that since our experiments were limited to HEK293T cells, it is possible that the composition of miRNA-associated complexes, and thus miRNA functional availability, may differ substantially in other systems. A second mechanism is the fragmentation of the miRISC pool by sub-cellular localization. At least a subset of miRNAs, which includes miR-16, localizes in the nucleus, and the importance of this fraction varies largely across miRNA families (Mullokandov et al., 2012). P-bodies, wherein at least part of miRISC components localize (Liu et al., 2005; Sen and Blau, 2005), are another candidate structure for the sequestration of miRNAs. However, to this day, it is still unclear if- or to what extent P-bodies partition the target recognition and silencing functions of the miRISC.

Results from our miRISC capture and dose-response assays highlight the potential importance of target site competition in modulating the output of miRNAs, but also point to limiting conditions of miRISC availability and target site stoichiometry. Notwithstanding those important parameters, a recent study examined the contribution of target site affinity in potentiating target site competitive effects (Bosson et al., 2014). Even though imperfect base-pairing miRNA-binding sites allow a single miRNA to regulate multiple target mRNAs (Baccarini et al., 2011), the kinetics of miRISC-target site association suggest that exchange rate is slow in comparison to perfectly base-pairing sites, which dictate a slicing-dependent mechanism (Hutvagner and Zamore, 2002). Sequence and positioning of the base-pairing nucleotides of miRNAs with natural miRNA-binding sites can modulate the affinity of miRISC and hence modulate exchange rates (Wee et al., 2012). As miRNAs co-evolved with cognate target site sequences, the kinetics of exchange between

competing target sites may be atoned to regulate the silencing potential on the critical mRNAs involved. Hastened exchange of miRISC between target sites could limit the functional competition between target sites, whereas high-affinity association to a specific target site sequence/structure could potentiate target site competition effects. It is tempting to imagine that miRNA-binding sites encoded in naturally occurring competing RNA species, such as circular RNAs and pseudogenes, co-evolved with miRNAs (whether an entire family or a specific miRNA) to trap and retain bound miRISC more efficiently. As our experimental designs were largely based on 2'-O-Me oligonucleotides, which may not strictly reflect affinities of native miRNA-binding sites, we did not systematically examine the importance of target site affinity here. As such, it will be informative to extend quantitation of non-slicing exchange rates for each miRNA families in a complex, competitive context, in a defined cellular transcriptome.

The titration curves presented in Figure 2-4 are strikingly reminiscent of the threshold model of miRNA molecular titration proposed by Mukherji and colleagues (Mukherji et al., 2011). It also provides another explanation for the discordance between miRNA expression and their output. Modest changes to a defined miRISC pool, while prevailing at a lower concentration than its cognate target mRNA, would be expected to have a limited effect on target silencing. Conversely, an mRNA bearing target sites saturated with excess miRISC should be buffered from changes in expression and/or availability. In this line of thought, the very fact that miRNA-mediated silencing is saturable by miRISC bears important mechanistic and biological implications. Saturation clearly raises the aspect of redundancy for distinct miRISC pools, programmed by distinct miRNA families, when they co-occupy the same target mRNA. Even if a particular miRISC pool's availability is in the dynamic concentration range with an mRNA target, a saturation of second or even more target sites should pre-empt sensitive changes in silencing outcome.

We postulate that the different scenarios of expression, availability, and stoichiometry experimentally revealed here can be selected to serve distinct physiological purposes and may unlock different properties of the miRISC machinery. The extreme abundance of a simple miRISC pool, programmed by a single miRNA family, such as miR-430 in the zebrafish embryo (Giraldez et al., 2006), is a logical fit for the rapid clearance of maternal transcripts at MZT. A different scenario should prevail in fully differentiated somatic cells reaching a homeostatic state. In this case, modest to moderate changes in miRNA expression, several of which may act redundantly, will rarely result in a drastic phenotype. Nonetheless, a subset of miRNAs should lie in the dynamic or responsive range of concentrations, with the available pool of miRISC being near-stoichiometric with biologically critical mRNA targets to allow a sensitive modulation of silencing in response to environmental and signaling cues. Re-visiting the properties of the miRISC in each of these states will potentially resolve the complexity in miRNA-mediated silencing mechanisms.

2.5 Acknowledgements

We want to thank Dr. Nahum Sonenberg, Dr. Martin Simard, Dr. Francois Major, and Ahilya N. Sawh for their comments on the manuscript. We also thank Dr. Carine Lussier, Caroline Thivierge, Mathieu Flamand for useful suggestions throughout the project, and Dr. Russell Jones for reagents.

2.6 Funding

This work was supported by the Canadian Institute of Health Research (CIHR) MOP 123352 (T.F.D.), and the Fonds de la Rercherche en Santé du Québec (FRQS), Chercheur-Boursier Salary Award J2 to (T.F.D.). V.M. was supported by the Graduate Excellence Fellowship Award from the Faculty of Medicine and the CIHR/FRQS of the McGill Integrated Cancer Research Training Program [grant number FRN53888]

2.7 Material and Methods

2.7.1 Plasmids

For the silencing assays, oligonucleotides encoding binding sites (1x-Perfect/ 3x-Bulge) (Table A1-1) for each of the miRNAs (IDT) were annealed and inserted downstream of Firefly luciferase gene between XBaI/NotI sites of the pmiRGLO vector (Promega). The construct used for ectopic expression of miR-19a/b was described and validated in (Mu et al., 2009). The Sponge-19 plasmid was a generous gift from Dr. Kai Fu (University of Nebraska) (Rao et al., 2012).

2.7.2 2'-O-Me Capture and western blot

HEK 293T cells cultured in DMEM supplemented with 10% Foetal bovine serum (Wisent) and gentamycin were plated on 10-cm plates (BD Falcon). After 3 days, cells were collected and resuspended in ice-cold lysis buffer (25 mM HEPES-KOH pH 7.4, 120 mM NaCl, 1 mM EDTA, 2.5% glycerol, 0.5% Triton-X, 2 mM DTT), supplemented with protease and phosphatase inhibitor cocktail (Sigma). MyOne T1 streptavidin beads (25 µL; Invitrogen) were washed three times with 1X binding and washing buffer (10 mM Tris-HCl pH 7.5, 1 mM EDTA, 2 M NaCl). The slurry was then resuspended in the same buffer to obtain a final concentration of 5 mg/mL, and 10 µL of specific 2'-O-Me oligonucleotide (10 µM) was added. After incubation at RT for 30 min., the beads were washed, 1.75 mg of protein lysate was added, and the mixture was incubated in a rotating wheel for 15 min. The beads were again washed and resuspended in 2X SDS buffer. To monitor the efficiency of RISC capture following incubation of specific 2'-O-Me oligonucleotides with the beads the protein lysate was added, and the mixture was incubated in a rotating wheel for 120 min. The unbound fraction was then recovered, and RNA was extracted using QIAzol (Qiagen) for northern analyses. For experiments involving expression of sponge and ectopic expression of miR-19a/b, the plasmids were transfected at 70-80% confluency for HEK 293T cells

plated in 10-cm dishes. The expression of the sponge was induced the following day by addition of doxycycline (1 µg/mL) and cells were harvested on the next day (24 h).

For the detection of Argonautes, AGO1 (1:1,000) from Cell signalling; AGO2 (1:1,000) from Abcam#135025; AGO1-4 (1:500) from Millipore #2A8 each diluted in blocking buffer were used (Odyssey, LiCor). Bound primary antibodies were detected using Goat anti-Rabbit IR dye (1:10,000) or Goat anti-Mouse IR dye (1:10,000) using an Odyssey imaging system from LiCor.

2.7.3 Luciferase assay

At 70-80% confluency, HEK 293T cells plated on 24 wells were co-transfected with 10 ng of each of the pmiRGLO reporters and varying concentrations of miRNA inhibitors/mimics (Qiagen). After 48 h of transfection, cells were lysed and Firefly and *Renilla* luciferase activities were determined using dual luciferase kit (Promega, BioTek).

2.7.4 Data and Statistical analyses

IC_{50} values were obtained by normalising F-Luc/R-Luc values of the WT reporter over the non-responsive (MUT) version. The curve was fit using four-parameter analysis with a Hill's constant = 1. All data are presented as mean ± standard deviation. Student's t-test was employed for comparisons between samples with * $p<0.05$, ** $p<0.005$.

2.7.5 Quantitative northern Blot analysis

Standard RNA oligos of miR-19b, miR-20a, miR-26a, miR-92a, let-7a, let-7b, miR-17, miR-20b, miR-25, miR-93 and miR-106b obtained from IDT were each diluted to concentrations of 1, 5, 10, 15, 20, 25, 30 and 40 pg/µl. Total RNA (2.75/5.5 µg) from HEK293T cells and the standards were resolved on 15% TBE-Urea gel (Bio-Rad), transferred onto to Hybond-XL membrane (Amersham) and UV-crosslinked. Hybridisation was carried out using ^{32}P-labelled Starfire probes

(miRfire IDT) at 25 °C overnight in ULTRAHyb Oligo Hybridisation buffer (Ambion). Following hybridisation, membranes were washed, exposed onto an imaging plate (Fujifilm) and developed using a phosphoimager (Typhoon). Intensity of the signal was quantified using ImageJ software.

2.7.6 qRT-PCR analysis

Synthetic RNA oligonucleotides were used as quantitative standards and the absolute levels of miRNAs were quantified as described in (Raymond et al., 2005). Templates for *in vitro* transcription of F-Luc and Sponge-19 RNAs were prepared by PCR using primers encoding T7 RNA polymerase promoter sequence (Table A1-1). Following *in vitro* transcription (Ambion), the samples were treated with DNase I and purified using RNA spin column (Roche). Reverse transcription of known amounts of *in vitro* transcripts RNA spiked in HEK 293T RNA was performed (Bio-Rad) alongside RNA extracted from cells expressing 3x-Bulge-miR-19 and the MUT version of the reporter. qPCR was performed using a SYBR green-based method (Qiagen) (see Table A1-1). Quantitation of F-Luc and Sponge-19 mRNAs was then determined using the standard curve obtained using *in vitro* transcribed templates.

Chapter 3: microRNA-mediated translation repression through GYF-1 and IFE-4 in *C. elegans* development

Mayya VK, Flamand MN, Lambert AM, Jafarnejad SM, Wohlschlegel JA, Sonenberg N, Duchaine TF.

Nucleic Acids Research Breakthrough article, 2021 *doi: 10.1093/nar/gkab162*

3.1 Abstract

microRNA (miRNA)-mediated gene silencing is enacted through the recruitment of effector proteins that direct translational repression or degradation of mRNA targets, but the relative importance of their activities for animal development remains unknown. Our concerted proteomic surveys identified the uncharacterized GYF-domain encoding protein GYF-1 and its direct interaction with IFE-4, the ortholog of the mammalian translation repressor 4EHP, as key miRNA effector proteins in *C. elegans*. Recruitment of GYF-1 protein to mRNA reporters *in vitro* or *in vivo* leads to potent translation repression without affecting the poly(A) tail or impinging on mRNA stability. Loss of *gyf-1* is synthetic lethal with hypomorphic alleles of embryonic *miR-35-42* and larval (L4) *let-7* miRNAs, which is phenocopied through engineered mutations in *gyf-1* that abolish interaction with IFE-4. GYF-1/4EHP function is cascade-specific, as loss of *gyf-1* had no noticeable impact on the functions of other miRNAs, including *lin-4* and *lsy-6*. Overall, our findings reveal the first direct effector of miRNA-mediated translational repression in *C. elegans* and its physiological importance for the function of several, but likely not all miRNAs.

Keywords: *C. elegans*, development, microRNA, translation repression, 4EHP, GYF domain, *let-7, miR-35, lsy-6*

3.2 Introduction

microRNAs (miRNAs) are ~22nt long RNA molecules that direct the regulation of a wide variety of biological processes by impinging on gene expression (Ameres and Zamore, 2013). While embedded into Argonaute proteins (ALG-1/2 in *C. elegans*) as part of the miRNA-induced silencing complex (miRISC), miRNAs guide the recognition of complementary regions located in the 3′untranslated regions (UTR) of messenger RNAs (mRNAs). Following target recognition, the GW182 protein (AIN-1/2 in *C. elegans*), a core component of miRISC, recruits effector proteins such as the CCR4-NOT deadenylase complex to silence genes through translational repression and/or mRNA decay (Duchaine and Fabian, 2019; Jonas and Izaurralde, 2015).

The relative contribution of mRNA translational repression and decay in the overall silencing of miRNA targets under physiological conditions remains largely unclear. Noticeable mechanistic differences have emerged in distinct systems and cell types. Different concentrations of miRNAs and effectors, and the density and distribution of miRNA-binding sites in mRNA 3′UTRs are possible explanations for such differences (Iwakawa and Tomari, 2015). Several studies have suggested that translation repression is the initial effect of silencing and precedes mRNA decay (Bazzini et al., 2012; Djuranovic et al., 2012; Fabian et al., 2009; Mathonnet et al., 2007), whereas other reports have argued that mRNA decay could account for the bulk of miRNA-mediated silencing (Guo et al., 2010).

A well-characterized translation inhibition mechanism involves a 5′-cap-binding protein, 4EHP (eIF4E2), which interferes with the recognition of the 5′-cap by the translation initiation complex eIF4F (Rom et al., 1998). In *Drosophila,* RNA-binding proteins Bicoid and Brain Tumor (Brat) recruit 4EHP to repress the translation of *caudal* and *hunchback* mRNAs, respectively, ensuring

proper embryonic development (Cho et al., 2006; Cho et al., 2005). 4EHP-mediated translational regulation of *HoxB4* mRNA is also essential for murine germ cell development (Villaescusa et al., 2009). More recent studies in mammalian cells have shown that 4EHP represses the translation of a select group of mRNAs, directed through recruitment of the miRISC/CCR4-NOT/DDX6/4E-T complex by miRNAs (Chapat et al., 2017; Jafarnejad et al., 2018). 4EHP can also form a translation repressor complex with the GIGYF2 protein, which is involved in the silencing of miRNA reporters (Schopp et al., 2017). Furthermore, knockout of *4ehp* or *Gigyf2* in mice causes prenatal and early postnatal lethality, respectively (Giovannone et al., 2009; Morita et al., 2012). However, the physiological importance of the 4EHP-GIGYF2 interaction for the function of miRNAs or for animal development is unknown.

When combined with mass spectrometry, affinity purification from various tissues and cells has been successful in identifying functional miRISC cofactors (Chu and Rana, 2006; Kakumani et al., 2020; Wu et al., 2017). Here, we performed comparative proteomics in *C. elegans* embryo on known components of the miRNA pathway and identified a novel miRISC cofactor, GYF-1, and its direct binding partner IFE-4, an ortholog of 4EHP. *gyf-1* mutations exacerbated the defects of certain miRNAs but did not impact others. Through genome editing and the derived cell-free miRNA-mediated silencing systems, we show that interactions between GYF-1 and IFE-4 generated potent translational repression of target mRNAs without eliciting their deadenylation or reducing their stability. Our results identify the first direct translational repressor in miRNA-mediated silencing in *C. elegans* and reveal its physiological significance in a subset of the developmental cascades governed by miRNAs.

3.3 Results

3.3.1 Concerted proteomics identifies GYF-1 association with miRISC and 4EHP

To identify new components of the miRNA-Induced Silencing Complex (miRISC), we compared the interactomes of a miRISC core component AIN-1 (GW182 ortholog), the miRISC cofactor NHL-2 (Hammell et al., 2009b), and the scaffolding subunit of the CCR4-NOT deadenylase complex, NTL-1 (CNOT1 ortholog; (Wu et al., 2017)) using immunoprecipitation (IP) coupled with Multi-Dimensional Protein Identification Technology (MuDPIT) (Washburn et al., 2001; Wolters et al., 2001). Each Co-IP dataset included at least three independent biological replicates (three for NHL-2 [unpublished], three for NTL-1, and six for AIN-1), and proteins detected in control samples were removed. Among the common interactors shared between all three baits were known components of the miRNA-induced silencing mechanism, mRNP granules (P-body, germ granule components; (Wu et al., 2017)), and several novel interactors of unknown function. Among the latter was the uncharacterized protein C18H9.3, detected in 11 out of a total of 12 independent datasets (Figure 3-1A and Table A2-1). Comparative alignment of the C18H9.3 protein sequence across other eukaryote proteomes revealed homology for a domain found in the yeast SMY2 protein, named Glycine-Tyrosine-Phenylalanine (GYF) domain (Figure 3-1B and Table A2-2). The SMY2-type GYF domain which recognizes the proline-rich motif PPGΦ (where P = proline, G = glycine, Φ = any hydrophobic amino acid) (Kofler and Freund, 2006) was implicated in translational control through the function of *hs*GIGYF2 proteins (Morita et al., 2012). Because C18H9.3 is the first *C. elegans* protein identified to encode this domain, we chose to name it GYF-1. To further confirm the physical interactions between GYF-1 and the miRISC, we performed reciprocal IP and MuDPIT using GYF-1 as bait. GYF-1 protein was immunoprecipitated from *C. elegans* embryos expressing an endogenous 3xFLAG-tagged protein

engineered via CRISPR/Cas9 (Figure 3-1C, upper panel). A total of 32 proteins were detected in all 3 independent biological replicates that were absent in all untagged (N2) samples, among which miRISC components AIN-1 paralog AIN-2 and the miRNA-dedicated argonaute, ALG-1 (ranked 5 and 12, respectively) (Figure 3-1C, bottom panel and Table A2-3). The 4EHP ortholog IFE-4 was recovered with 45.56% peptide coverage on average, above all other detected interactions, suggesting a stable and likely direct interaction.

Mammalian GIGYF2 and *dm*GIGYF proteins interact with 4EHP through the canonical motif $YXYX_4L\Phi$ (where Y = tyrosine, X = any amino acid, L = leucine, and Φ = any hydrophobic amino acid) (Morita et al., 2012; Ruscica et al., 2019). A similar motif, $FXYX_4L\Phi$, is present in the N-terminal region of GYF-1 (Figure 3-1D, upper panel). To test whether GYF-1 directly interacts with IFE-4, we generated GST-tagged constructs encoding fragments of GYF-1 and a construct wherein the conserved IFE-4 binding motif was mutated to alanines ($FXYX_4L\Phi$ to $AXAX_4AA$). A stable interaction of IFE-4 with the N-terminal region of GYF-1 was detected, and the mutation of the IFE-4 binding motif strongly impaired this interaction (Figure 3-1D, bottom panel). Residual binding, above the background level, with the IFE-4 binding mutant suggests the possible presence of a distinct, weaker IFE-4 binding site. In agreement with this, a lesser interaction between the C-terminal fragment of GYF-1 and IFE-4 could be detected in a pull-down assay. Interestingly, while cloning full-length *gyf-1* cDNA*,* we detected a splice variant (*gyf-1* Δ*ife-4 binding motif*) of *gyf-1,* which did not encode the canonical IFE-4 binding motif (Figure 3-1E). A GST pull-down with this isoform confirmed the loss of robust interaction of IFE-4 with GYF-1 (ΔIFE-4 binding motif). Together, these results confirm that the conserved IFE-4 binding motif in the N-terminal region of GYF-1 is a direct binding site for IFE-4 and that this interaction may be subject to biological regulation by alternative splicing.

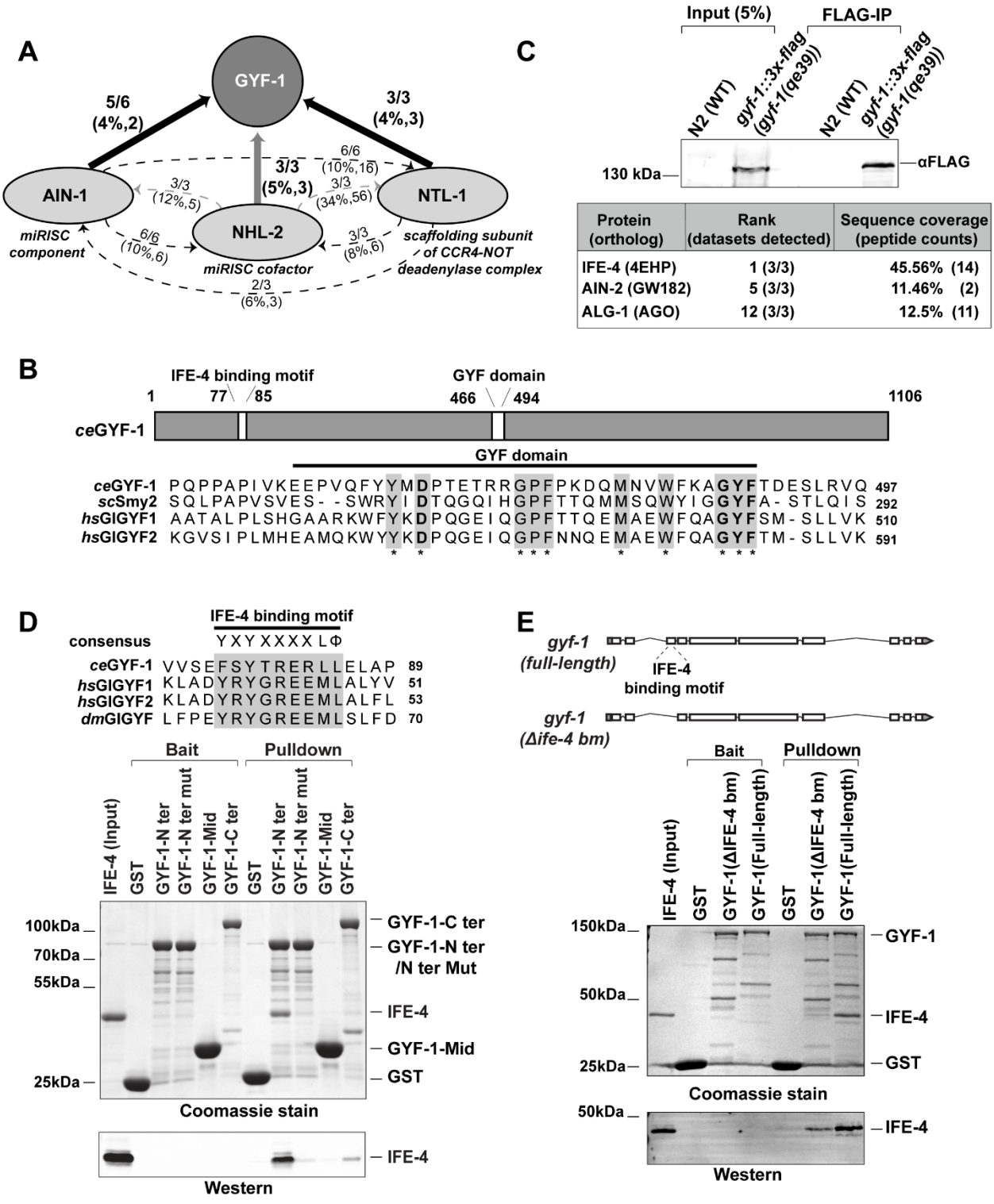

Figure 3-1. Concerted proteomics identifies GYF-1 association with miRISC and 4EHP.
(A) A network of proteins converging on GYF-1, as detected by MuDPIT analyses in *C. elegans* embryonic extracts. FLAG immunoprecipitations were carried out on endogenously-tagged

(genome-edited) AIN-1, NHL-2, and NTL-1. Arrowheads indicate detected interactions. The number of independent IPs in which GYF-1 was detected is indicated along with peptide coverage percentage and counts in brackets. Grey arrowheads indicate RNase A untreated interactions. **(B)** Schematic representation of the *ce*GYF-1 protein. The protein contains an N-terminal IFE-4 binding motif and a central GYF domain (top). The protein sequence of the C18H9.3 (*ce*GYF-1) GYF domain was aligned with other Smy2-type GYF domains (*Sc*Smy2, *hs*GIGYF1, and *hs*GIGYF2) (bottom). The conserved amino acids encompassing the GYF domain are highlighted in grey, while the amino acid Aspartate 466 that determines a Smy2-type GYF domain is in bold. **(C)** Western blot of embryo lysates and FLAG immunoprecipitations (FLAG-IP) from wild-type (N2) and animals expressing FLAG-tagged GYF-1 (top). The table indicates the proteins that were detected in GYF-1 MuDPIT analyses. The proteins were ranked based on NSAF values. **(D)** Sequence alignment of the IFE-4 binding motif present in *ce*GYF-1, *hs*GIGYF1/2, and *dm*GIGYF proteins. The consensus sequence $YXYX_4L\Phi$ is highlighted in grey (top). *In vitro* pull-down assay on GST-tagged WT or mutant fragments of GYF-1 and His-tagged IFE-4 purified recombinants (bottom). **(E)** Schematic representation of the two *gyf-1* isoforms: *gyf*-1 (full-length) and *gyf-1(*Δ*ife-4 binding motif)* (top). A GST pull-down assay showing the interaction between GST-tagged GYF-1 (full-length or ΔIFE-4 binding motif) with purified His-tagged IFE-4 (bottom). The input, baits, and pull-downs were analyzed by SDS-PAGE and Coomassie staining. Western blotting was performed using an anti-His antibody.

The GYF domain proteins can interact with several partners through the PPGΦ motif. A search for PPGΦ motif-containing proteins in factors with known function in post-transcriptional gene silencing (PTGS) identified the PPGL sequence in the mRNA decapping cofactor PATR-1 (ortholog of mammalian PatL1). To test whether GYF-1 can directly interact with PATR-1, we performed *in vitro* pull-down using full-length GST-tagged GYF-1 as bait and His-tagged PATR-1 as prey. GST-GYF-1 interacted with recombinant PATR-1, and mutation of the PATR-1 PPGL motif (to AAGA) abolished this interaction (Figure A2-1A and Figure A2-1B). Conversely, mutation of the GYF domain of GYF-1 abrogated the interaction with recombinant wild-type

PATR-1 (Figure A2-1C). This result shows that the GYF motif of GYF-1 interacts with the PPGL motif of PATR-1 *in vitro*, and possibly other proteins bearing this motif (see Discussion).

3.3.2 *gyf-1* is synthetic lethal with *let-7* and *miR-35* hypomorphs

To investigate a possible role for GYF-1 in the miRNA-regulated developmental pathways, we engineered a loss-of-function (*lof*) allele by inserting a stop codon cassette in the fourth exon of *gyf-1* through CRISPR/Cas9 genome editing (*gyf-1(qe27)*) (Figure 3-2A). The lesion triggered mRNA destabilization, presumably through nonsense-mediated decay (NMD). Quantitative PCR analysis of *gyf-1* mRNA in embryos indicated a ~5-fold reduction in mRNA (Figure A2-2A). Western blot using a newly developed polyclonal antiserum confirmed that the bulk (>90%) of the GYF-1 protein signal was lost in this allele. A single band of unknown significance could still be seen, potentially reflecting another isoform (Figure A2-2E). *gyf-1(qe27)* appeared WT at 16°C but was afflicted by a two-third reduction in brood size at 25°C (Figure A2-2B). Notably, a pleiotropy of phenotypes could be observed at 25°C, including embryonic lethality, larval arrest, dumpy, high incidence of males, and low penetrance of the bursting vulva at the L4-to-adult transition (<5%) (Figure A2-2C). Some of these phenotypes are compatible with defects in miRNA-induced silencing (Alvarez-Saavedra and Horvitz, 2010; Ecsedi et al., 2015), but their complexity could indicate several other mechanisms of action and functions for GYF-1. To examine the role of *gyf-1* in miRNA-induced silencing, we employed a sensitized genetic assay based on the temperature-sensitive allele of *let-7(n2853)*. This allele encodes a point mutation in the seed sequence of *let-7* miRNA, which impairs the repression of the *lin-41* mRNA target and results in a temperature-sensitive vulval bursting at the L4-to-adult transition (Ecsedi et al., 2015). The mild ~20% penetrance of this phenotype at 16ºC can be suppressed or exacerbated upon disruption of components of the miRISC or its cofactors (Flamand et al., 2016). F1s from a cross between *gyf-*

1(qe27) and *let-7(n2853)* animals were individually picked, and their progeny (F2) was monitored at the permissive temperature (16ºC). In comparison with *let-7(n2853)* animals (26%), *let-7(n2853)*; *gyf-1(qe27/wt)* animals exhibited a striking increase in L4-to-adult bursting (61%) and 100% of the *gyf-1(qe27); let-7(n2853)* homozygous animals (20/20) died due to bursting, with no viable progeny recoverable (Figure 3-2B). Interestingly, the surviving *let-7(n2853)*; *gyf-1(qe27/wt)* heterozygous animals often died as young adults because of an egg-laying defect. This genetic interaction was further confirmed with point mutations in *gyf-1* (see below) and *gyf-1*(RNAi) by injection in *let-7(n2853)* animals (Figure A2-2D). Together, these results show that *gyf-1 lof* is synthetic lethal with *let-7* and that this function is dosage-sensitive.

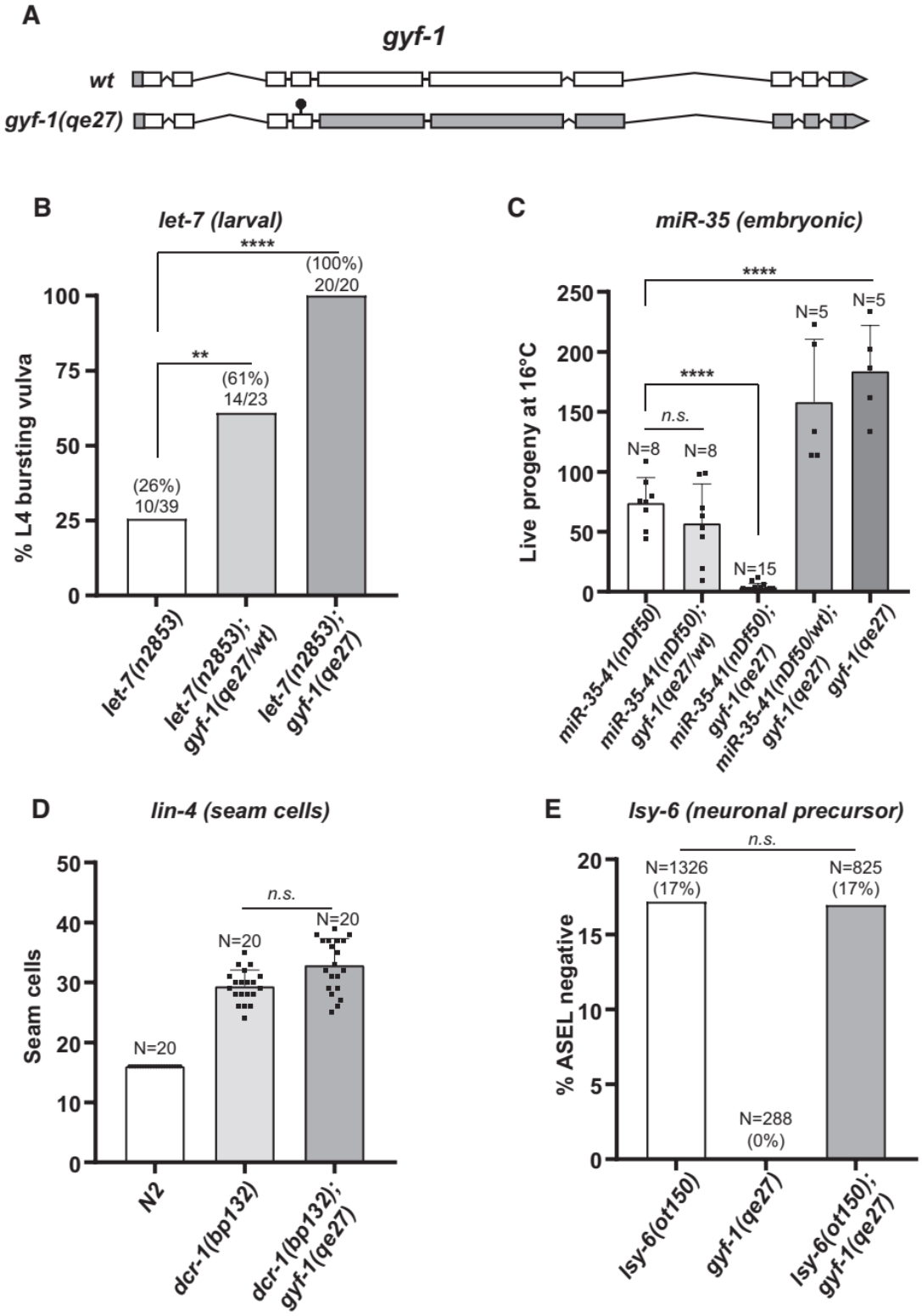
A
gyf-1
wt
gyf-1(qe27)
B
let-7 (larval)
% L4 bursting vulva
(26%)
10/39
(61%)
14/23
(100%)
20/20
**
****
let-7(n2853)
let-7(n2853); gyf-1(qe27/wt)
let-7(n2853); gyf-1(qe27)
C
miR-35 (embryonic)
Live progeny at 16°C
n.s.
****
N=8
N=8
N=15
N=5
N=5
miR-35-41(nDf50)
miR-35-41(nDf50); gyf-1(qe27/wt)
miR-35-41(nDf50); gyf-1(qe27)
miR-35-41(nDf50/wt); gyf-1(qe27)
gyf-1(qe27)
D
lin-4 (seam cells)
Seam cells
n.s.
N=20
N=20
N=20
N2
dcr-1(bp132)
dcr-1(bp132); gyf-1(qe27)
E
lsy-6 (neuronal precursor)
% ASEL negative
n.s.
N=1326
(17%)
N=288
(0%)
N=825
(17%)
lsy-6(ot150)
gyf-1(qe27)
lsy-6(ot150); gyf-1(qe27)

Figure 3-2. *gyf-1* is synthetic lethal with *let-7* and *miR-35* hypomorphs.
(A) Schematic representation of the *gyf-1* locus, with the white and grey boxes indicating the coding and non-coding regions, respectively. A null allele of *gyf-1* was generated by inserting a stop codon (black circle) using the CRISPR/Cas9 gene-editing technique. **(B)** Percent bursting vulva phenotype was quantified at 16°C for animals with wild-type *gyf-1*, *gyf-1(qe27/wt)*$^{-}$, *gyf-1(qe27)* alleles in *let-7(n2853)* background. The number of bursting animals is indicated over the bars. Statistical significance was assessed using two-tailed chi-square analysis (**** $P < 0.00005$, ** $P < 0.005$). **(C)** Progeny produced by hermaphrodites of each genotype was counted at 16°C. Each black square within the bars indicates independent replicates. **(D)** Number of seam cells, quantified by the expression of seam cell-specific reporter *scm::gfp* in WT, *dcr-1(bp132)*, and *dcr-1(bp132);gyf-1(qe27)* animals. **(E)** Loss of ASEL-specific expression of *plim-6::gfp* reporter was quantified in *lsy-6* and *gyf-1* single mutants, and *lsy-6; gyf-1* double mutants. N = animals scored for each genotype. The error bars represent standard deviation and the *P*-value (**** $P < 0.00005$) was determined using the two-tailed Student's *t*-test.

We next assayed for *gyf-1* genetic interactions with miRNAs implicated in other developmental events in *C. elegans*. The *miR-35-42* family of miRNAs is essential for early embryonic development (Alvarez-Saavedra and Horvitz, 2010; Wu et al., 2010). Its eight members are abundantly expressed in oocytes and early embryos (Alvarez-Saavedra and Horvitz, 2010; Lau et al., 2001; McJunkin and Ambros, 2014), and animals expressing only *miR-42* (*nDf50*) are viable at lower temperatures (16^{o}C) (Alvarez-Saavedra and Horvitz, 2010; Liu et al., 2011). To explore a possible role of GYF-1 in the functions of this family of miRNAs, *nDf50; gyf-1(qe27/wt)* were isolated and maintained at 16°C, and live progeny from individual picks was quantified (Figure 3-2C). Although *miR-35-41* deletion (*nDf50*) alone led to a reduced brood size (70 ± 21), the compound mutation strain *gyf-1(qe27)*; *nDf50* led to a near-complete eradication of any viable progeny (3 ± 3). However, this hypomorph was not as sensitive to *gyf-1* dosage as the *let-7(n2853)* mutant, as the brood size of the *nDf50; gyf-1(qe27/wt)* was virtually indistinguishable from *nDf50*

animals. Together, these data demonstrate that loss of *gyf-1* greatly exacerbates *let-7* and *miR-35-41* deletion defects in embryogenesis and suggest that different miRNA cascades may exhibit different sensitivities to *gyf-1* dosage.

We further studied genetic interactions of *gyf-1* with other miRNA-involving developmental cascades. The *dcr-1(bp132)* mutant animals exhibit an increased number of seam cells and defects in alae formation that are visible in adult animals. This phenotype is thought to be attributed to the reduced levels of *lin-4* miRNA and misregulation of *lin-28* mRNA, but might also involve other miRNAs such as *miR-48*, *miR-84*, and *miR-241* in early larval decisions (Ren and Zhang, 2010; Ren et al., 2016). Notwithstanding this, the *gyf-1(qe27)* allele did not modify the phenotype of *dcr-1(bp132)* on seam cell numbers (Figure 3-2D). While wild-type and *dcr-1(bp132)* animals presented an average of 16 and 30 pairs of seam cells, respectively, when quantified with an *scm-1::gfp* reporter in young adults, loss of *gyf-1* did not impact this phenotype. Lastly, *gyf-1* had no detectable impact on *lsy-6* function in left/right neuronal asymmetry (Figure 3-2E) in an ASEL/ASER reporter assay performed in the *lsy-6(ot150)* hypomorphic allele (Johnston and Hobert, 2003). Thus, our results show that while *gyf-1* is essential for the function of the miRNAs *let-7* and *miR-35-42* upon genetic perturbation, it does not appear to be required for the function of all miRNAs.

3.3.3 Loss of the IFE-4 binding motif or the GYF domain of GYF-1 exacerbate *let-7* defects

Next, we sought to corroborate the importance of the interaction between GYF-1 and IFE-4 for *let-7* activity by mutational analysis. For this, we mutated the sequence encoding the IFE-4 binding site in the *gyf-1* locus through CRISPR/Cas9 genome editing ((FXYX$_4$LΦ to AXAX$_4$AA), *qe71*, referred henceforth as *gyf-1*$^{ife\text{-}4\ bm}$). This engineered genomic lesion effectively disrupted the interaction between GYF-1 and IFE-4 in the co-immunoprecipitation assay (Figure A2-2E). Using

a similar approach, we generated the *gyf-1(qe72)* mutant wherein conserved key residues involved in the GYF domain's interaction with PPGΦ-motif were mutated to alanines ((GYF to AAA), *gyf-1*$^{gyf\ dm}$) (Figure 3-33A). The two *gyf-1* mutant strains were then crossed with *let-7(n2853),* and L4-to-adult bursting was quantified in the double mutants [*let-7(n2853); gyf-1*$^{ife\text{-}4\ bm}$ and *let-7(n2853); gyf-1*$^{gyf\ dm}$] (Figure 3-3B). Compared to the *let-7(n2853)* single mutant (24%), composite mutant strains with either *gyf-1*$^{ife\text{-}4\ bm}$ or *gyf-1*$^{gyf\ dm}$ exacerbated bursting to 56% and 39%, respectively. This result demonstrates that the IFE-4 binding motif, and to a lesser degree the GYF domain, of GYF-1, partake in the *let-7* activity.

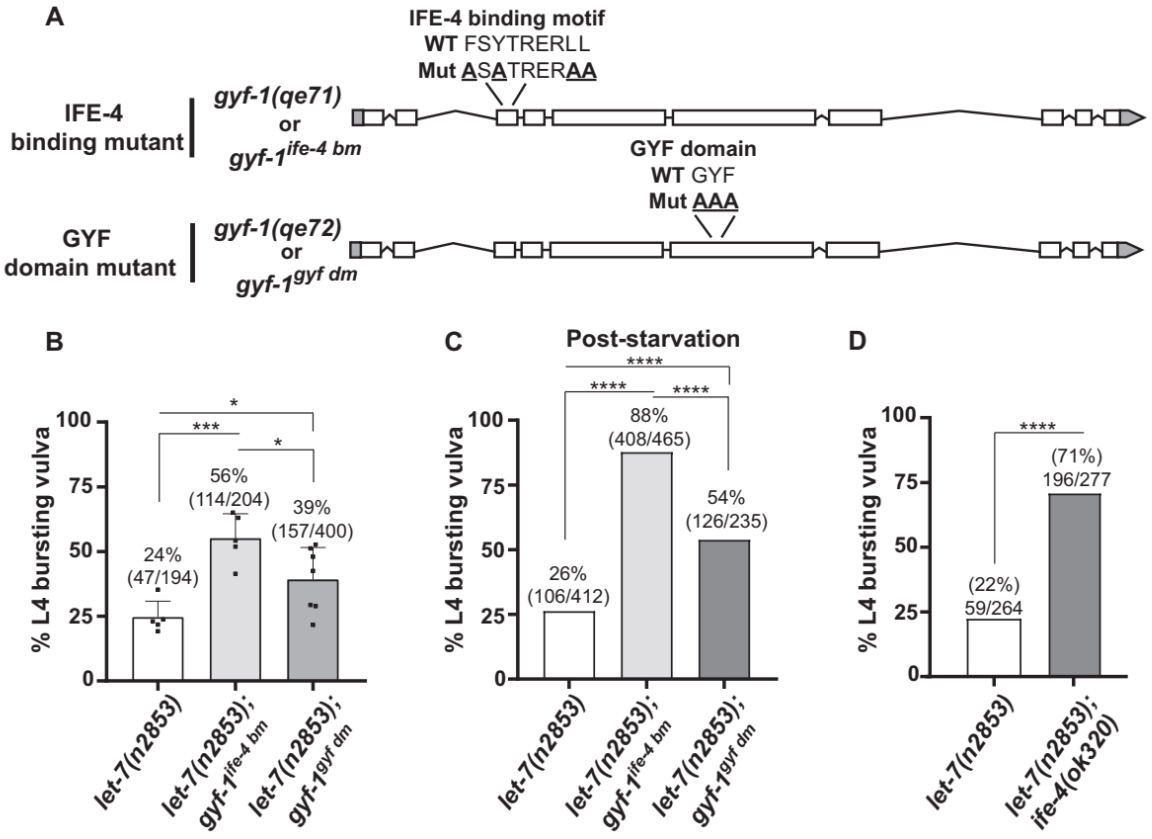

Figure 3-3. Loss of the IFE-4 binding motif or the GYF domain of GYF-1 exacerbate *let-7* defects.

(A) A schematic representation of the two *gyf-1* mutants (*gyf-1*$^{ife\text{-}4\ bm}$ and *gyf-1*$^{gyf\ dm}$) generated by the CRISPR/Cas9 gene-editing technique. The residues mutated are shown above the schematics.

(B) Homozygous double mutants for both *let-7(n2853); gyf-1*$^{ife\text{-}4\ bm}$/*gyf-1*$^{gyf\ dm}$ were monitored for L4-to-adult bursting when maintained at 16°C. The number of bursting animals is indicated over the bars. The error bars represent standard deviation and the *P*-value (*** $P < 0.0005$, * $P < 0.05$) was determined using the two-tailed Student's *t*-test. **(C)** Animals grown in a food-deprived condition to induce stress were returned to favorable conditions, and percent L4 bursting vulva was monitored. **(D)** The percent bursting vulva phenotype was quantified at 16°C for animals with wild-type *ife-4* and *ife-4(ok320)* alleles in *let-7(n2853)* background. Statistical significance in (C) and (D) was assessed using two-tailed chi-square analysis (**** $P < 0.0005$).

Genetic programs ensure developmental robustness to avert environmental stresses (Hammell et al., 2009a; Karp et al., 2011; Li et al., 2009; Posadas and Carthew, 2014). For example, signaling cues from diapause signals correct cell lineage defects caused by shortages in *let-7* functions (Ilbay and Ambros, 2019). We thus examined the impact of *gyf-1*$^{ife\text{-}4\ bm}$ and *gyf-1*$^{gyf\ dm}$ mutations on *let-7* functions in populations recovering from unfavorable (starvation) conditions. To this end, we induced L1 arrest by food deprivation (Baugh, 2013) in *gyf-1*$^{ife\text{-}4\ bm}$*; let-7(n2853)* and *gyf-1*$^{gyf\ dm}$*; let-7(n2853)* animals and quantified L4-to-adult transition failure (bursting) in the recovering populations. Both mutations exacerbated the bursting phenotype observed in *let-7(n2853)* animals (26%), with 88% for *gyf-1*$^{ife\text{-}4\ bm}$*; let-7(n2853)* and 54% for the *gyf-1*$^{gyf\ dm}$*; let-7(n2853)* genotype (Figure 3-3C). Curiously, this exacerbation of the *let-7* phenotype by the *gyf-1*$^{ife\text{-}4\ bm}$ and *gyf-1*$^{gyf\ dm}$ mutations persisted in the next generation, indicating trans-generational inheritance (Figure A2-3A). Lastly, to better delineate the contribution of the GYF-1 cofactor IFE-4 in *let-7* function, a null allele of *ife-4(ok320)* (Dinkova et al., 2005) was crossed with *let-7(n2853)* and *ife-4(ok320); let-7(n2853)*, and L4-to-adult bursting was quantified. 71% of the animals burst in comparison with 22% in the *let-7(n2853)* genotype (Figure 3-3D).

Overall, these results validate the functional importance of the GYF-1 and 4EHP proteins, and their direct interaction, in *let-7* functions and indicate that the GYF domain of GYF-1 also partakes in the *let-7* functions, although to a lesser extent. Furthermore, these results indicate that contribution of the IFE-4 binding motif and GYF domain can gain importance in developmental pathways upon environmental perturbations of nutrients or temperature.

3.3.4 GYF-1/4EHP is a potent translational repressor

To investigate the molecular function of GYF-1, we employed the λN:BoxB protein/mRNA tethering system (Baron-Benhamou et al., 2004; Pillai et al., 2004) by engineering a strain wherein a sequence encoding the λN-tag was embedded in the *gyf-1* locus using CRISPR/Cas9 genome editing. Cell-free embryonic extracts, proficient for miRNA-mediated silencing and deadenylation (Wu and Duchaine, 2011; Wu et al., 2010), were then prepared from animals expressing either untagged (wt) or the GYF-1- λN fusion protein. *In vitro* transcribed *Renilla* luciferase (RL) reporters bearing 5BoxB sites or 3x-*miR-35* miRNA-binding sites (as a control) in their 3′ UTR region (Figure 3-4A) were incubated in the two extracts, along with a firefly luciferase (FL) internal control. mRNA and their expression were monitored using normalized luciferase assays (Figure 3-4B). Importantly, the control reporters were expressed in the two extracts with comparable efficiencies (Figure A2-4A). In comparison to the control (wt) extract, RL reporters bearing 5BoxB sites were strongly repressed in the *gyf-1-λn* extract (Figure 3-4B). Tethering GYF-1 to the reporter mRNA led to more potent silencing (>95% repression) than the 3x-miR-35 reporter (~70%) at the 3h time-point, which is known to be potently silenced through deadenylation (Wu et al., 2010). To determine if GYF-1 promotes mRNA deadenylation and/or destabilization *in vitro*, RL-5BoxB and RL-3xmiR-35 reporters were metabolically labeled with ^{32}P, and their stability was monitored after incubation in the different extracts through denaturing

PAGE and autoradiography. The 3x-miR-35 reporter was rapidly deadenylated in both extracts, with a virtually indistinguishable deadenylation half-time ($t_{d1/2}$) (*wt*: 56 min vs. *gyf-1-λn*: 52 min) (Figure 3-4C, Figure A2-4B). Consistent with previous observations in *C. elegans* embryonic extracts (Wu et al., 2010; Wu et al., 2017), fully deadenylated mRNAs remained stable, and no acceleration of decay could be detected. No deadenylation or destabilization was detectable for the RL-5BoxB reporter in any of the tested extracts (Figure 3-4C).

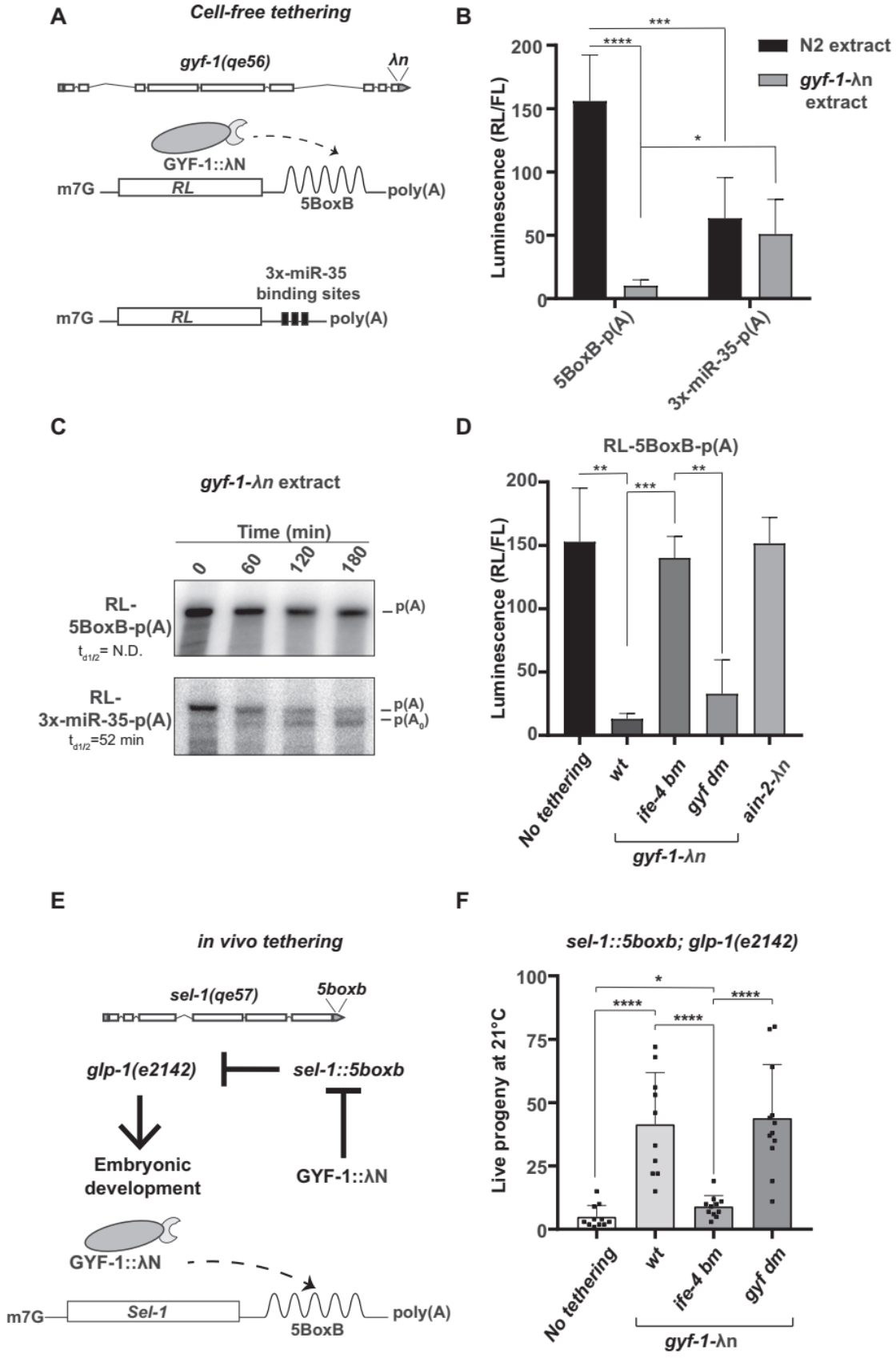
A
Cell-free tethering
gyf-1(qe56)
λn
GYF-1::λN
m7G
RL
5BoxB
poly(A)
3x-miR-35
binding sites
B
N2 extract
gyf-1-λn
extract
Luminescence (RL/FL)
5BoxB-p(A)
3x-miR-35-p(A)
C
gyf-1-λn extract
Time (min)
0
60
120
180
RL-
5BoxB-p(A)
t1/2= N.D.
p(A)
RL-
3x-miR-35-p(A)
t1/2=52 min
p(A0)
D
RL-5BoxB-p(A)
Luminescence (RL/FL)
No tethering
wt
ife-4 bm
gyf dm
ain-2-λn
gyf-1-λn
E
in vivo tethering
sel-1(qe57)
5boxb
glp-1(e2142)
sel-1::5boxb
Embryonic
development
GYF-1::λN
Sel-1
F
sel-1::5boxb; glp-1(e2142)
Live progeny at 21°C

Figure 3-4. GYF-1/4EHP is a potent translational repressor.
(A) A schematic representation of the *gyf-1* locus encoding a λN-tag at the C-terminus engineered through CRISPR/Cas9 (top). *In vitro* transcribed reporters were used to monitoring translation and deadenylation activity in extracts derived from engineered strains (bottom). **(B-C)** Reporters bearing either 5boxB sites or 3x miR-35 binding sites were incubated in embryonic extracts expressing either wild-type (N2) or λN-tag GYF-1. RL and FL activities were measured after 3 hours using the Dual-Luciferase Reporter assay system (Promega). RL activity was normalized to that of the FL control, $n = 6$ (B). The RNA was extracted at indicated time points and analyzed by UREA-PAGE (C). p(A) denotes the position of the adenylated reporter mRNA, while p(A_0) indicates the position of the deadenylated reporter mRNA. Half-deadenylation rates ($t_{d1/2}$) were quantified using ImageJ. Images are representative of three independent experiments conducted using two different batches of extract preparations. $t_{d1/2}$ = N.D. indicates *not detected*. **(D)** Extracts expressing untagged-GYF-1 (No tethering), GYF-1-λN (WT), GYF-1-λN (IFE-4 BM/GYF DM), and AIN-2-λN were incubated with RL-5BoxB-p(A) reporters. RL and FL activities were measured as described in (B). RL activity was normalized to that of the FL control, $n = 3$. **(E)** The *sel-1* locus was engineered by the CRISPR/Cas9 gene-editing technique to encode 5BoxB sites in its 3`UTR (*sel-1(qe57)* (top). *Sel-1* loss-of-function can suppress the temperature-sensitive embryonic lethality phenotype in the loss-of-function mutation of *glp-1(e2142)* (middle). Animals expressing untagged-GYF-1 (No tethering) or λN-tagged GYF-1 (WT/IFE-4 BM/ GYF DM) were crossed with *sel-1(qe57); glp-1(e2142)* alleles. (bottom). **(F)** Live progeny of each genotype was counted at 21°C. Each black square within the bars indicates independent replicates, $n = 10$. The error bars represent standard deviation, and the *P*-value (**** $P < 0.00005$, *** $P < 0.0005$, ** $P < 0.005$, * $P < 0.05$) was determined using the two-tailed Student's *t*-test.

Taken together, these results show that GYF-1 recruitment to an mRNA directs potent translational repression without eliciting its deadenylation or destabilization.

We next tested the contribution of the IFE-4 binding motif and GYF domain of GYF-1 in translational repression by performing similar experiments in extracts derived from *gyf-1*$^{ife\text{-}4\ bm}$ and *gyf-1*$^{gyf\ dm}$ engineered strains (Figure 3-3A) wherein the *gyf-1* locus also carried the λn-tag coding

sequence. *N2 (wt)* extract where no λn fusion is tethered and *ain-2-λn* extracts where AIN-2 is tethered but does not lead to any silencing were used as negative controls. Tethering in the *gyf-1*$^{ife\text{-}4\ bm}$*-λn* extract entirely prevented the translational repression observed in the *wt gyf-1-λn* extract (Figure 3-4D). In contrast, silencing in the *gyf-1*$^{gyf\ dm}$*λn* extract did not significantly differ from the *wt gyf-1- λN*. Again, this was not due to batch-to-batch differences in the potency of extracts (Figure A2-4A). Thus, these results show that GYF-1 requires IFE-4 protein to effect translational repression when recruited to an mRNA.

To confirm the molecular function of the GYF-1/IFE-4 effector complex-induced repression *in vivo*, we designed a genetic assay based on the activity of engineered GYF-1 mutants (wt, *gyf-1*$^{gyf\ dm}$, *gyf-1*$^{ife\text{-}4\ bm}$) on a CRISPR-edited endogenous mRNA reporter locus. The temperature-sensitive allele of *glp-1*(*e2142*) is embryonic lethal at non-permissive temperatures (21ºC and above), and loss of *sel-1* expression suppresses this phenotype (Flamand et al., 2017; Kodoyianni et al., 1992; Priess et al., 1987). Using CRISPR/Cas9 editing, 5BoxB sites were introduced in the 3′ UTR sequence of the *sel-1* locus (Figure 3-4E), and the engineered strain was crossed with strains expressing wt or mutant versions of GYF-1-λN fusion protein. Live progeny was then monitored at *glp-1*(*e2142*) non-permissive (21°C) temperature. As expected, animals expressing the *sel-1* mRNAs containing 5BoxB sites as part of their 3′ UTRs, but no GYF-1-λN fusion protein, did not produce viable progeny (Figure 3-4F, *no tethering*). Partial but effective rescue of embryonic lethality was observed in animals wherein wild-type GYF-1 was tethered to *sel-1* mRNA *in vivo*, indicating potent gene silencing (Figure 3-4F). qPCR analysis indicated no change in *sel-1* mRNA levels upon GYF-1 tethering (Figure A2-4C), suggesting, as with *in vitro* experiments, translational repression without mRNA destabilization. Strikingly mirroring *in vitro* tethering

results, *gyf-1*$^{ife\text{-}4\ bm}$ animals poorly suppressed *glp-1* phenotype, while *gyf-1*$^{gyf\ dm}$ suppressed embryonic lethality as well as *wt gyf-1-λn*.

Our results collectively indicate that GYF-1 is a potent translation repressor that primarily requires IFE-4 interaction to silence mRNAs both *in vitro* and *in vivo*, and that this silencing occurs without mRNA deadenylation or decay.

3.4 Discussion

In this study, concerted interaction proteomics identified the GYF domain protein GYF-1 as a novel miRISC-associated protein in *C. elegans*. Precision genome engineering highlighted the physiological importance of GYF-1 interaction with the cap-binding IFE-4 protein in key developmental events orchestrated by the *miR-35* and *let-7* families of miRNAs. We further showed that GYF-1 directly interacts with IFE-4 to potently repress the translation of mRNAs without eliciting mRNA deadenylation and decay. Overall, our results support a model where GYF-1 acts as a cofactor of miRISC to repress the translation of a select subset of miRNA targets during the development of *C. elegans* (Figure 3-5).

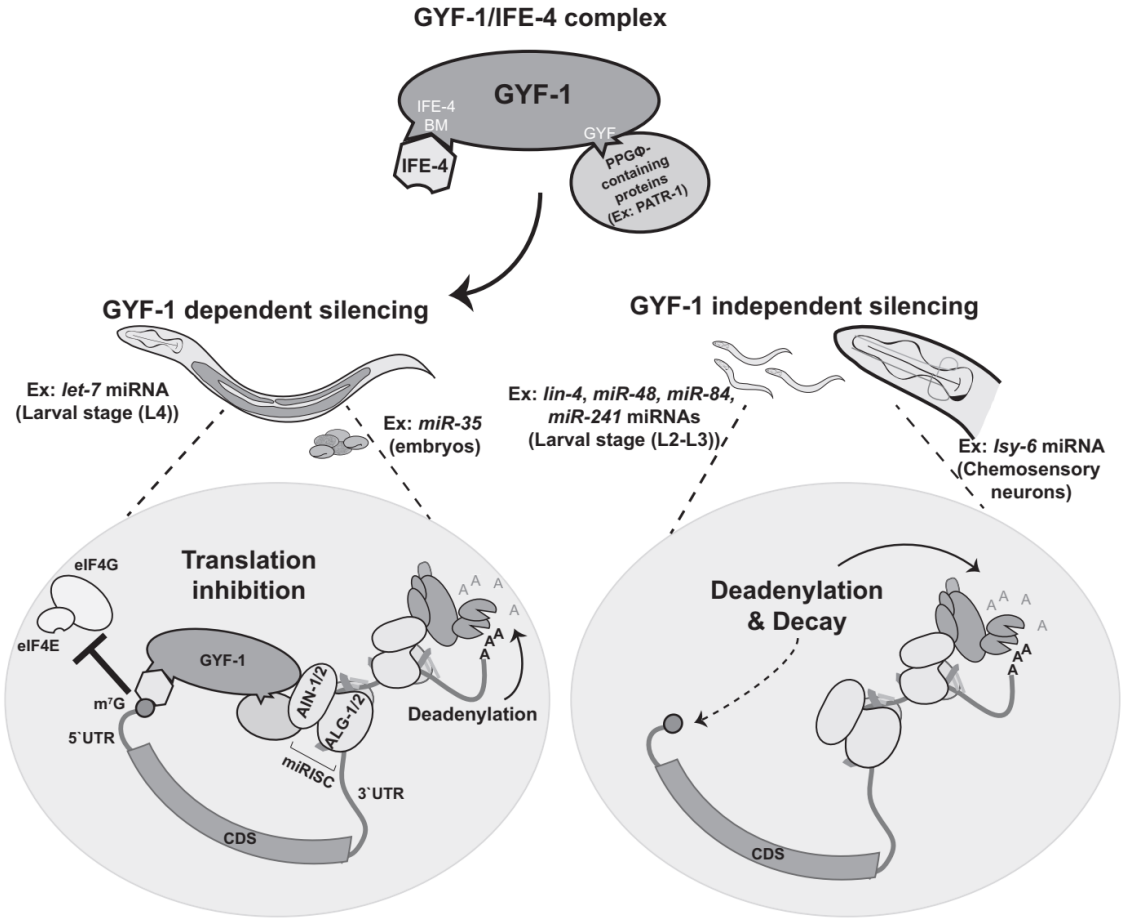

Figure 3-5. Model: GYF-1-dependency in miRNA-mediated silencing depends on the developmental context.
Through interactions with miRISC (larval *let-7* or embryonic *miR-35)*, the GYF-1/IFE-4 effector complex inhibits translation by interfering with the recognition of the 5′- cap by the translation initiation complex. For other miRNA/targets such as *lin-4, miR-48, miR-84, miR-241* (larval) and *lsy-6* (neuronal) miRNAs, GYF-1 is completely dispensable, and other silencing mechanisms such as deadenylation and decay fully compensate for the loss of GYF-1-mediated translation repression.

Recent studies implicated the human and *Drosophila* homologs of GYF-1 in post-transcriptional gene silencing (Kryszke et al., 2016; Peter et al., 2017; Ruscica et al., 2019; Schopp et al., 2017). In contrast to GYF-1, the homologs appear to function through translational repression and mRNA deadenylation and decay. *hs*GIGYF2, one of the two human GYF-1 homologs, silences miRNA reporters through interactions with 4EHP but also engages the CCR4-NOT deadenylase complex (Amaya Ramirez et al., 2018). *dm*GIGYF, the only known *Drosophila* homolog, interacts with 4EHP, Me31B (CGH-1/DDX6 ortholog), and HPat, the ortholog of PATR-1 (Peter et al., 2019; Ruscica et al., 2019), and silences luciferase reporters upon tethering in cell culture assays. Curiously, *dm*GIGYF has not been linked to miRNA-mediated silencing. The conservation of the mechanism by the GYF domain proteins will likely extend to a combination of translation repression, deadenylation and decay. Beyond IFE-4/4EHP, the diversity of the effectors recruited by this family of protein will be reflected through the interactions of the GYF domain with binding partners bearing the PPGΦ motif. Here, we mapped a PATR-1 interaction with GYF-1 to the PPGΦ motif *in vitro* (Figure A2-1). However, PATR-1 was not detected in our proteomic survey, and no evidence of decapping or decay, which could have been expected from such an interaction, was detected. While the orthologs of PATR-1 were characterized as de-capping cofactors, some studies indicate that they can also function as translation repressors (Christou-Kent et al., 2018; Marnef et al., 2010). GYF-1 tethering to reporters elicited neither deadenylation nor decay, and

mutation of the GYF domain had no impact on reporter silencing *in vitro*, in stark contrast with a mutation in the IFE-4/4EHP binding motif which fully impaired silencing. These results thus suggest that *C. elegans* GYF-1 primarily relies on its interaction with IFE-4 and translational repression to effect mRNA silencing. This view is in agreement with *in vivo* data as well, with results from the genetic interactions of the two modules of GYF-1 with the *let-7* hypomorph (Figure 3-3) and from *in vivo* tethering assays (Figure 3-4F). Notwithstanding this, the GYF domain did have a minor but significant contribution in target silencing in both assays, suggesting that PATR-1 and/or other PPGΦ motif-containing proteins participate in GYF-1/IFE-4-mediated translation repression. Additionally, the alternative splicing isoform GYF-1(ΔIFE-4 binding motif), which lacks the 4EHP-binding motif (Figure 3-1E), could reflect a physiological switch between silencing mechanisms. Fine mapping of the expression of this isoform may reveal the existence of other functions for the *gyf-1* gene, beyond its functions as a translational repressor. Alternatively, under particular conditions of stoichiometry and interaction kinetics within the holo-miRISC, this isoform could act as a dominant-negative by competing with other effector proteins or complexes.

The subtle and mild phenotype of the *gyf-1* alleles on their own at 16ºC drastically contrasts with their dosage-sensitive synthetic lethality with the *let-7* miRNA hypomorph. A possible interpretation for this observation is that translational repression through GYF-1 is one of several effectors mobilized by miRISC, and that deadenylation and decay may partially but incompletely compensate for the loss of translational repression in the *gyf-1* mutant. Further attrition of silencing potency of one or several miRNA targets in hypomorphic alleles may thrust the gene regulation system beyond a phenocritical threshold. In addition, the distinct quality or kinetics of the different silencing effectors of miRISC could be expected to become critical during infection, disease, or

environmental stress. The flexibility of the miRNA-mediated silencing mechanism and the importance of translation repression were also highlighted in embryonic stem cells wherein loss of DDX6, a cofactor of miRISC, leads to the translational upregulation of miRNA targets without eliciting mRNA decay (Freimer et al., 2018). Our an interpretation provides a refined perspective on a long-standing debate in the field of miRNA-mediated silencing: whether translational repression or mRNA decay accounts for the bulk of miRNA's silencing activities (Bagga et al., 2005; Bazzini et al., 2012; Djuranovic et al., 2012; Eichhorn et al., 2014; Fabian et al., 2009; Guo et al., 2010; Jonas and Izaurralde, 2015; Mathonnet et al., 2007).

A similar interpretation may also explain the striking differences in the importance of GYF-1 for the function of *let-7* and *miR-35* miRNAs on the one hand, and the absence of detectable functional implication in the *lsy-6* and *lin-4* cascades on the other (Figure 3-2 and Figure 3-5). Our data aligns with a growing number of publications based on model organisms, which indicate that miRISC effector activities change according to cellular and mRNA contexts (Wu et al., 2017). For example, as a result of extracellular cues, cells assemble functionally different miRISCs in *Drosophila* (Wu et al., 2013). Another recent study showed how differences in the composition of miRISC between germline and somatic tissues led to different mechanistic outcomes (Dallaire et al., 2018). Lastly, distinct 3′UTR sequences may mobilize different effectors as part of competitive or cooperative interactions, a theme that is prevalent in miRNA-mediated deadenylation in *C. elegans* embryo (Wu et al., 2010). Biochemical differences in miRISC composition or properties, their domain of expression, between the larval *let-7* and embryonic *lsy-6* cascades, for example, could thus explain the striking differences in GYF-1 impact in different developmental contexts.

Whether the involvement of GYF-1 is determined by cell fate or can differ between mRNAs and 3′UTR isoforms within the same expression domain remains to be investigated. The bursting

phenotype at the L4-to-adult transition observed in *let-7*(*n2853*) alleles is accounted for by the misregulation of *lin-41* mRNA alone (Ecsedi et al., 2015). In wild-type animals, *let-7* binds to the two complementary sequences in the 3′ UTR of *lin-41* and targets the mRNA for degradation (Bagga et al., 2005), but homozygous *gyf-1 lof* leads to <5% bursting at the permissive temperature. This suggests that *lin-41* mRNA decay is the prevalent mechanism in this cascade. Another interpretation is that this only reflects the contribution that cannot be compensated for, upon loss of miRNA-mediated translation repression through the GYF-1/IFE-4 complex. Revisiting the functional elements of the *lin-41* 3′ UTR in its native developmental context, and those of other phenocritical miRNA targets in different developmental cascades, is now more accessible than ever through precision genome editing. Careful re-examination of the mechanistic impact of those elements could provide a clearer view of the intersect, compensation or unique contribution of the effectors of miRNA-mediated silencing.

In conclusion, the discovery of the novel GYF-domain protein GYF-1 and precision genome-editing in *C. elegans* allowed a direct assessment of the physiological importance of miRNA-mediated translational repression in an animal's development and unveiled the surprising systems' flexibility among miRNA's silencing mechanisms.

3.6 Data Availability

Mass spectrometry proteomics data were deposited to the ProteomeXchange Consortium via the PRIDE partner repository, with the dataset identifier PXD023610.

3.5 Acknowledgements

We want to apologize to authors whose directly related work may not have been cited in this manuscript. We thank Dr. Victor Ambros for providing the *miR-35-41(nDf50)* strain and the Caenorhabditis Genetics Center (CGC) for the *glp-1(e2142),* and *ife-4(ok320)* strains used in this study.

3.6 Funding

This work was supported by the Canadian Institutes of Health Research (CIHR) MOP-123352 (to T.F.D.); The Charlotte and Leo Karassik Foundation Ph.D. fellowship award to V.K.M.

3.7 Material And Methods

3.7.1 Worm strains

N2 Bristol (WT), *let-7 (n2853)*, *wIs51(scm-1:: gfp),* VT2700 *(wIs51(scm-1:: gfp); dcr-1(bp132)),* FD237*(wIs51(scm-1::gfp); dcr-1(bp132); gyf-1 null),* (*glp-1 (e2142)*, *nDf50 (miR-35-41),* MH2636 *(otIs114(Plim-6::GFP,rol-6(d)),lsy-6(ot150))*, FD81 (*gyf-1 null*; *otIs114(Plim-6::GFP,rol-6(d)),lsy-6(ot150))*, FD76 (*gyf-1(qe27)*), FD119 (*gyf-1(qe39),* FD152 (*gyf-1(56*), FD198 (*gyf-1(qe71))*, FD199 (*gyf-1(qe72))*, FD165 (*sel-1*::*5boxb; glp-1(e2142)*), FD193 (*sel-1*::*5boxb; glp-1(e2142); gyf-1::λN*), FD261 (*sel-1::5boxb; glp-1 (e2142); gyf-1(qe71)*), FD262 (*sel-1::5boxb; glp-1 (e2142); gyf-1(qe72)*). All strains were maintained at 16°C.

3.7.2 CRISPR

The different alleles of *gyf-1* and *sel-1* were generated using a modified protocol (Paix et al., 2015). mRNP complex was assembled with rCas9 and *in vitro*-transcribed modified sgRNA(F+E) (Ward, 2015). Injection mixes contained 1.2µg/µL Cas9, 300mM KCl, 12.5mM HEPES pH7.4, 50ng/µL dpy-10 sgRNA, 200ng/µL gene-specific sgRNA, 13.75ng/µL dpy-10 repair ssODN and 110ng/µL ssODN gene-specific repair template (see Table A2-4). Approximately 15 germlines of N2 gravid adults grown on *cku-80* RNAi plates were injected. Roller (heterozygotes for *dpy-10*) or dumpy animals were screened for edits by PCR.

3.7.3 Immunoprecipitation (IP) and Multidimensional Protein Identification (MuDPIT)

Embryonic pellets expressing either wild-type (N2) or FLAG-tagged GYF-1 (FD119) were homogenized in lysis buffer (50 mM Tris-HCl pH 8, 150 mM NaCl, 1 mM EDTA, 1% Triton X-100 with Complete EDTA-free protease inhibitors [Roche]) and cleared by 17,500 × *g* centrifugation. The lysates were treated with RNaseA, and FLAG-tagged GYF-1 was purified using anti-FLAG M2 Affinity Gel (Sigma-Aldrich A2220). For each IP, 5 mg of proteins

were used at a concentration of 2 mg/mL in lysis buffer. IP was carried out at 4°C for 2 hours with 50 µl of bead slurry per IP. Beads were washed four times in lysis buffer, and proteins were eluted with ammonium hydroxide solution. One tenth of the eluate was resolved by SDS-PAGE, and western blot analysis was performed using an anti-FLAG-M2 antibody. Non-transgenic N2 embryos were used as controls for the purifications. MuDPIT was performed as described in (Duchaine et al., 2006).

3.7.4 RNAi

RNAi was performed as described in (Fire et al., 1998). The genomic sequence of *gyf-1* was amplified using the primers listed in Table S4. Using the PCR products as a template, RNA was *in vitro* transcribed using the T7 MegaScript kit (Ambion). The RNA was then purified using mini Quick Spin RNA columns (Roche). Larval stage-4 (L4) animals were injected with 100ng/µL dsRNA, and bursting phenotype was monitored in the injected mother's progeny.

3.7.5 Antibody generation

The GYF-1 polyclonal antiserum was raised against the GYF domain region of GYF-1 by injecting rabbits with purified recombinants of the GYF domain. Likewise, IFE-4 polyclonal antiserum was raised against the full region of IFE-4. The primers used to clone the constructs for producing the recombinants are listed in Table A2-4. Serum was used at a 1:1000 dilution in Odyssey blocking buffer (Li-Cor).

3.7.6 qRT-PCR

RNA was reverse transcribed using the Bio-Rad iScript Supermix for 5 minutes at 25°C, 30 minutes at 42°C, and 1 minute at 95°C. The cDNA was diluted four-fold in water before using it for PCR (Bio-Rad iQ Supermix), with the following cycling parameters: initial denaturation at 95° for 2 minutes, denaturation for 15 seconds at 95°C, 59°C for 30 seconds and 72°C for 30 seconds,

for 40 cycles. Reactions were followed by a melting curve analysis with the Eppendorf Realplex instrument and software. The RNA levels were normalized using the delta-delta Ct method with *act-1* mRNA as an internal control.

3.7.7 Translation and deadenylation assays

Preparation of embryonic extracts were performed as described in (Wu et al., 2010). In brief, embryonic extracts were incubated with mRNA (1 nM) at 16°C for 0 to 4.5 hours, as indicated. Luciferase activities were measured using the Dual-Luciferase Reporter assay system (Promega). For deadenylation assays, 1 ng of ^{32}P-labeled RNA was incubated in embryonic extracts for 0 to 3 hours. Half-deadenylation times were calculated by determining the intersect of the non-deadenylated and deadenylated RNA species over time using polynomial regression (order 2), using quantification of autoradiography with ImageJ.

3.7.8 Protein expression and purification

All recombinant proteins were expressed in either BL21-CodonPlus (DE3)-RIPL or ArcticExpress (DE3) competent cells (Agilent Technologies) grown in LB medium overnight at 13-16°C. For GST-recombinants, the cells were lysed using a sonicator (FisherScientific) in GST-lysis buffer (10 mM Tris-HCl, pH 8.0, 150 mM NaCl, 1 mM EDTA) supplemented with lysozyme (500 µg/mL), 1% Triton-X100 and protease inhibitor cocktail (Sigma).

For His-tagged recombinants (IFE-4, PATR-1), the cells were lysed in His-lysis buffer (20 mM sodium phosphate, 0.5 M NaCl, 20 mM Imidazole, 10% glycerol) supplemented with lysozyme, Triton-X100, and protease inhibitor cocktail. The protein was purified from cleared cell lysate using Ni-Sepharose 6 Fast Flow resin (GE Healthcare) in a Poly-Prep column (Bio-Rad). Following multiple washing steps with His-lysis buffer containing 60 mM imidazole, recombinants were eluted in His-lysis buffer containing 250 mM imidazole. Each fraction was

analyzed by SDS-PAGE and Coomassie staining. Pure fractions were then concentrated using 50K centrifugal filter units (Amicon).

3.7.9 GST pull-down

Approximately 5 µg of GST or GST-fusion proteins were incubated in Glutathione-Sepharose beads (GE Healthcare) in the GST-lysis buffer at 4°C overnight. The bead-bound proteins were then incubated in GST-lysis buffer containing 5% BSA at 4°C for 2 hours. Meanwhile, His-tagged recombinants (~50 µg) were pre-cleared in Glutathione-Sepharose beads. The pre-cleared protein was then incubated with bead-bound proteins in phosphate-buffered saline containing 0.1% Tween20 (PBST). After 2 hours of incubation, the beads were washed three times with PBST containing 500 mM KCl and eluted with a 2x-SDS loading buffer. The pull-downs were then analyzed by SDS-PAGE and subsequent Coomassie staining. For specific detection of His-tagged recombinants, anti-His (1:1,000) (Abcam) was used. Bound primary antibodies were detected using Goat anti-Mouse IRDye (1:10,000) using an Odyssey imaging system (Li-Cor).

Chapter 4: Enhancement of microRNA-mediated deadenylation by the TRIM-NHL protein NHL-2 and DEAD-box protein CGH-1

Vinay K. Mayya, Mathieu N. Flamand, Elva Vidya, Nahum Sonenberg, James A. Wohlschlegel, Christopher M. Hammell, Thomas F. Duchaine*

Manuscript in preparation

*Correspondence: Thomas.duchaine@mcgill.ca

4.1 Abstract

The *C. elegans* NHL-2, a member of the broadly conserved TRIM-NHL family of RNA-binding proteins, enhances post-transcriptional repression of a subset of miRNA targets. Here, a co-immunoprecipitation and proteomic survey on NHL-2 detected interactions with components of miRISC, processing bodies (P-bodies), the CCR4-NOT deadenylase complex, and other RNA-binding proteins. Recruitment of NHL-2 to the 3`UTR of mRNAs triggered weak mRNA deadenylation, but this activity was greatly potentiated by juxtaposition to miRNA-binding sites. CRISPR-Cas9 engineering of 3`UTR sequences *in vivo* further supported the function of enhancement of miRNA-mediated silencing *in vivo.* Finally, we demonstrate that NHL-2 directly associates with the DEAD-box RNA helicase CGH-1 (*C. elegans* ortholog of DDX6) in a temperature-dependent manner to support a model where the NHL-2/CGH-1 interaction potentiates miRNA-mediated deadenylation by remodeling the RNP. Altogether our findings shed light on the mechanistic basis of cooperativity between miRNAs, and the RNA-binding protein NHL-2.

Keywords: microRNA, NHL-2, CGH-1, cooperativity, deadenylation, P-bodies.

4.2 Introduction

Post-transcriptional regulation of gene expression is often mediated through the recognition of *cis*-regulatory sequences and structures in the 3`UTRs of mRNAs by *trans*-acting factors, some of which involve microRNA Induced Silencing Complex (miRISC), their associated machinery, and RNA-binding proteins (RBPs) (Mayya and Duchaine, 2019). *Trans*-acting factors, in turn, recruit effector proteins such as CCR4-NOT deadenylase, the decapping complex, and thus mediate gene repression (Duchaine and Fabian, 2019; Jonas and Izaurralde, 2015).

Considering the vast number of binding sites for miRNAs in 3`UTRs, multiple miRNAs can bind within a 3`UTR and alter mRNAs' fate through cooperative or competitive interplay (Friedman et al., 2009). For instance, proper neuronal patterning in *C. elegans* requires the repression of *cog-1* mRNA through the cooperative action of two *lsy-6* miRNA-binding sites in its 3` UTR (Didiano and Hobert, 2008; Johnston and Hobert, 2003). Recent *in vitro* and *in vivo* studies have provided more clarity on the mechanism underlying cooperativity. The presence of two or more miRNA-binding sites on target mRNAs can enable the recruitment of deadenylase complex to provide robust gene silencing (Flamand et al., 2017; Wu et al., 2010). Likewise, RBPs and miRNAs interactions within a 3`UTR are also thought to function cooperatively (Jiang and Coller, 2012). Examples of a positive interplay between RBP and miRNAs include the cooperation of TTP with miR-16 in regulating TNF-alpha mRNA, and the modulation of local 3`UTR structures in c-Myc mRNA by HuR that increases *let-7* miRNA activity (Jing et al., 2005; Kim et al., 2009). The mechanisms behind miRNA-RBP interactions occurring on 3`UTR of mRNAs remain poorly understood.

The broadly conserved Tripartite motif (TRIM)- NCL-1/H2TA/LIN-41 (NHL) family of RBPs are important regulators of development, cell polarity, and sex determination (Tocchini and Ciosk,

2015). The N-terminal TRIM contains three main domains: a RING finger, two B-Box-type zinc fingers, and a coiled-coil domain that can participate in protein-protein interactions and in some cases may act as an E3 ubiquitin ligase. The C-terminus consists of the NHL domain, which comprises five to six repeats of ~40 amino acids that fold into a β-propeller structure to bind directly to RNA (Davis et al., 2018; Loedige et al., 2015; Loedige et al., 2014). A subset of TRIM-NHL RBPs are implicated in post-transcriptional gene regulation. For instance, the *Drosophila* Brat recruits the effector protein 4EHP to repress the translation of *hunchback* mRNA (Cho et al., 2006). In *C. elegans*, *nhl-2* is required to efficiently repress *cog-1* and *hbl-1* mRNAs by *lsy-6* and *let-7* miRNAs, respectively (Hammell et al., 2009b). More recently, *in vitro* binding assays using the NHL domain of NHL-2 revealed a strong binding preference for poly(U)-enriched RNAs (Davis et al., 2018). The endogenous targets and the exact mechanistic roles of NHL-2 in post-transcriptional gene repression are unclear.

Translationally repressed mRNAs and components of the miRISC and its associated machinery localize to P-bodies (Ding et al., 2005; Eystathioy et al., 2003; Liu et al., 2005). P-bodies are cytoplasmic membrane-less ribonucleoprotein (RNP) granules suspected to be sites for mRNA degradation and/or mRNA storage. An essential protein required for the assembly of RNPs is the conserved RNA dependent DEAD-box ATPase DDX6/RCK/Me31B/Dhh1/CGH-1 (Cougot et al., 2004; Eulalio et al., 2007b; Minshall et al., 2009; Serman et al., 2007; Sheth and Parker, 2003). Results from several groups show that DDX6 and its orthologs also enhance translation repression (Chu and Rana, 2006; Coller and Parker, 2005; Minshall et al., 2009). For instance, DDX6 interacts directly with CNOT1 subunit of the CCR4-NOT deadenylase complex to repress miRNA targets (Chen et al., 2014; Mathys et al., 2014; Rouya et al., 2014). In *C. elegans*, CGH-1 binds and

stabilizes specific maternal transcripts during oogenesis (Boag et al., 2008). CGH-1 also colocalizes with NHL-2 in somatic cells *in vivo* (Hammell et al., 2009b).

Here, we uncovered the interactome of NHL-2 and identified extensive interactions with core components of miRISC, the CCR4-NOT deadenylase complex, P-bodies, and other RBPs. We show that tethering NHL-2 protein, *in vitro* and *in vivo*, greatly enhances the potency of miRNA-mediated deadenylation of target mRNAs. We further show a direct interaction between NHL-2 and the RNA helicase, CGH-1, and abolishing this interaction exacerbated miRNA defects. We propose a model wherein reorganization of RNP through CGH-1 and NHL-2 interaction promotes miRNA-mediated deadenylation.

4.3 Results

4.3.1 NHL-2 interacts with miRISC, CCR4-NOT complex, and the P-Body associated protein, CGH-1.

Comparative proteomic analyses on a core component of miRISC AIN-1 (GW182 ortholog) and the scaffolding subunit of CCR4-NOT deadenylase complex, NTL-1 (CNOT1 ortholog) using immunoprecipitation (IP) coupled with Multi-Dimensional Protein Identification Technology (MuDPIT) (Washburn et al., 2001; Wolters et al., 2001) revealed extensive overlapping interactions with P-body proteins, germ granule components, and several other cytoplasmic ribonucleoproteins including the TRIM-NHL protein, NHL-2 (Wu et al., 2017). We performed reciprocal IP and MuDPIT using NHL-2 as bait with or without RNase A treatment. NHL-2 was immunoprecipitated from *C. elegans* embryos expressing an endogenous 3xFLAG-tagged NHL-2 protein engineered using the CRISPR/Cas9 gene-editing (Figure 4-1A, top panel). A total of 103 proteins were detected in at least 2 of 3 independent biological replicates (51 proteins in RNase untreated, 52 proteins in RNase treated purifications) absent in all untagged (N2) samples, among which are miRISC components AIN-1, AIN-2, and the miRNA-dedicated Argonaute, ALG-1 (Figure 4-1B). Several components of the CCR4-NOT deadenylase complex and P-body were also recovered with high percent peptide coverage on average (see Table A3-1 and A3-2 for a complete list). Gene ontology (GO) cellular component analysis using g: Profiler web server (Raudvere et al., 2019) revealed a strong enrichment for P-body proteins with a total of 11 out of 51 NHL-2 RNase untreated interactions ($p_{adj} = 1.068 \times 10^{-17}$) (Table A3-3). Furthermore, 8 out of the nine components of the CCR4-NOT complex were detected ($p_{adj} = 1.622 \times 10^{-17}$). We confirmed the interaction between NHL-2 and the scaffolding subunit of the CCR4-NOT deadenylase complex, NTL-1, by co-immunoprecipitation (Co-IP) assay (Figure 4-1D). GST-pulldown assays did not

reveal a direct interaction between NTL-1 and NHL-2 (data not shown), although NHL-2 may recruit the CCR4-NOT complex through other subunits.

CGH-1 and its ortholog DDX6 are very abundant proteins (~10 fold more abundant than CNOT1) (Lee et al., 2020; Schwanhausser et al., 2011) and were disqualified through MuDPIT analysis by the detection of peptides in our negative control. Since our IP samples were prepared at 4°C, and the CGH-1 / NHL-2 interaction is stabilized at higher temperatures (see below), temperature may have disfavored this interaction in our MuDPIT datasets. In light of the importance of CGH-1 for P-body integrity and the function of some miRNAs, we directly tested its interaction with NHL-2 *in vitro.* To test whether NHL-2 physically interacts with CGH-1, we performed co-immunoprecipitation using CRISPR-tagged CGH-1 expressing 3x-FLAG tag as bait (Figure 4-1D). NHL-2 co-immunoprecipitated with CGH-1, and this interaction was resistant to RNase treatment, suggesting that it occurs independently of RNA. To test whether NHL-2 directly interacts with CGH-1, we performed *in vitro* pull-down using full-length GST-tagged NHL-2 as bait and His-tagged CGH-1 as prey. GST-NHL-2 interacts weakly with CGH-1 at lower temperatures (4°C and 16°C), and strongly at 30°C (Figure 4- 1E). In a reciprocal pull-down using TAP-tagged CGH-1 as a bait, we demonstrated that the two B-Box domains of NHL-2 were sufficient to interact with CGH-1(Figure A4-1, lane 6). As with the full-length protein, the B-Box of NHL-2 interaction with CGH-1 was dependent on the temperature. The addition of a non-hydrolysable analog of ATP, AMP-PNP, stabilized the interaction between CGH-1 and B-Box1/2 proteins, regardless of the temperature. These results show that the B-Box1/2 domain of NHL-2 directly interacts with CGH-1 and suggests that conformational changes stabilized by ATP and temperature promote NHL-2/CGH-1 interaction.

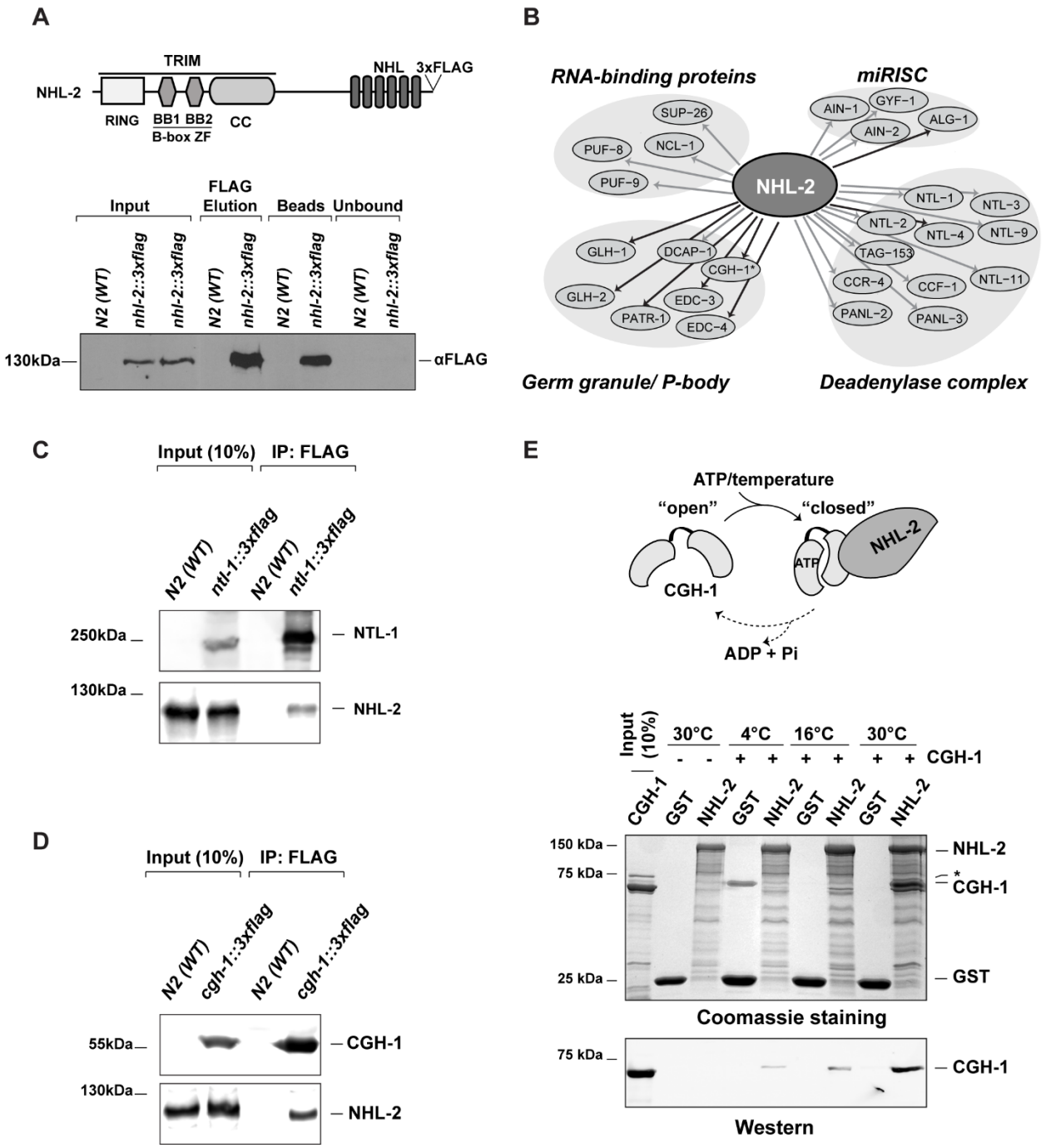

Figure 4-1. NHL-2 interacts with miRISC, CCR4-NOT complex, and CGH-1.
(A) Protein domain structure of *C.elegans* NHL-2. The N-terminal region of NHL-2 contains a RING motif, two B-box domains, and a coiled-coil region. The C-terminal region of NHL-2 contains six NHL repeats. A 3X-FLAG tag was inserted at the C-terminus through CRISPR/Cas9 gene-editing technique (top panel). Western blot of embryonic lysates and FLAG immunoprecipitations from wild-type (N2) and *nhl-2::3xflag* expressing animals (Bottom panel).

(B) A network of proteins detected by MuDPIT analyses in *C. elegans* embryonic lysates. FLAG immunoprecipitations were carried out on endogenously-tagged NHL-2. Arrowheads indicate detected interactions. Grey arrowheads indicate RNase untreated, black arrowheads indicate RNase treated interactions. * indicates interaction detected through co-ip and GST-pulldown assays. **(C-D)** Western blots of embryo lysates and FLAG immunoprecipitations from wild-type (N2) and animals expressing FLAG-tagged NTL-1 (D) or FLAG-tagged CGH-1 (E) are shown. NTL-1 and CGH-1 were detected using anti-FLAG M2 antibodies, while NHL-2 was detected using a polyclonal NHL-2 antiserum. **(E)** A schematic model for interaction between CGH-1 and NHL-2: Increase in temperature or ATP binding stabilizes CGH-1 to its active conformation and promotes interaction with NHL-2 (top). A GST pull-down assay showing the interaction between GST-tagged NHL-2 with purified His-tagged CGH-1 (bottom). The input, baits, and pull-downs were analyzed by SDS-PAGE and Coomassie staining. Western blotting was performed using an anti-His antibody.

4.3.2 NHL-2 cooperates with miRNAs to potentiate deadenylation of target mRNAs

To investigate the molecular function of NHL-2, we employed the λN:BoxB protein/mRNA tethering system (Baron-Benhamou et al., 2004; Pillai et al., 2004) by engineering a strain wherein a sequence encoding the λN-peptide was embedded in the C-terminus of *nhl-2* locus using CRISPR/Cas9 genome editing. Cell-free embryonic extracts, proficient for miRNA-mediated silencing and deadenylation (Wu and Duchaine, 2011; Wu et al., 2010), were then prepared from animals expressing either untagged (wt) or the NHL-2- λN fusion protein. *In vitro* transcribed *Renilla* luciferase (RL) reporters bearing 5x-BoxB stemloops, 3x-*miR-35* miRNA-binding sites (as a control), or both in the 3' UTR (Figure 4-2A) were assayed. The translation of each reporter was first monitored using luciferase activity (Figure 4-2B). In comparison to the control (wt) untagged extract, RL reporters bearing both 3x-miR-35 and 5x-BoxB sites were strongly repressed

in the *nhl-2-λn* extract. Repression was more potent than for either 3x-miR-35 reporter or 5x-BoxB reporter alone.

To determine if NHL-2 participates in mRNA deadenylation and/or destabilization, the same reporters were labeled with ^{32}P, and their stability was monitored after incubation in the different extracts through denaturing PAGE and autoradiography. Consistent with prior experiments (Wu et al., 2010), the 3x-miR-35 reporter was rapidly deadenylated, with a similar deadenylation half-time ($t_{d1/2}$) in both extracts (*wt*: 143 min vs. *nhl-2-λn*: 118 min) (Figure 4-2C, lower panel). Surprisingly, reporters bearing both 5x-BoxB and 3x-miR-35 sites were rapidly deadenylated in *nhl-2- λn* extract ($t_{d1/2}$ = 60 min), compared to the same reporter in control (*wt)* extract ($t_{d1/2}$ > 270 min) (Figure 4-2C, middle panel). A modest deadenylation rate ($t_{d1/2}$ > 270 min) was detectable for the 5x-BoxB reporter upon tethering of NHL-2 alone (Figure 4-2C, upper panel). Taken together, these results show that while NHL-2 can elicit some deadenylation of target mRNAs, its cooperation with miRNAs greatly enhances the rate of deadenylation, leading to potent gene silencing.

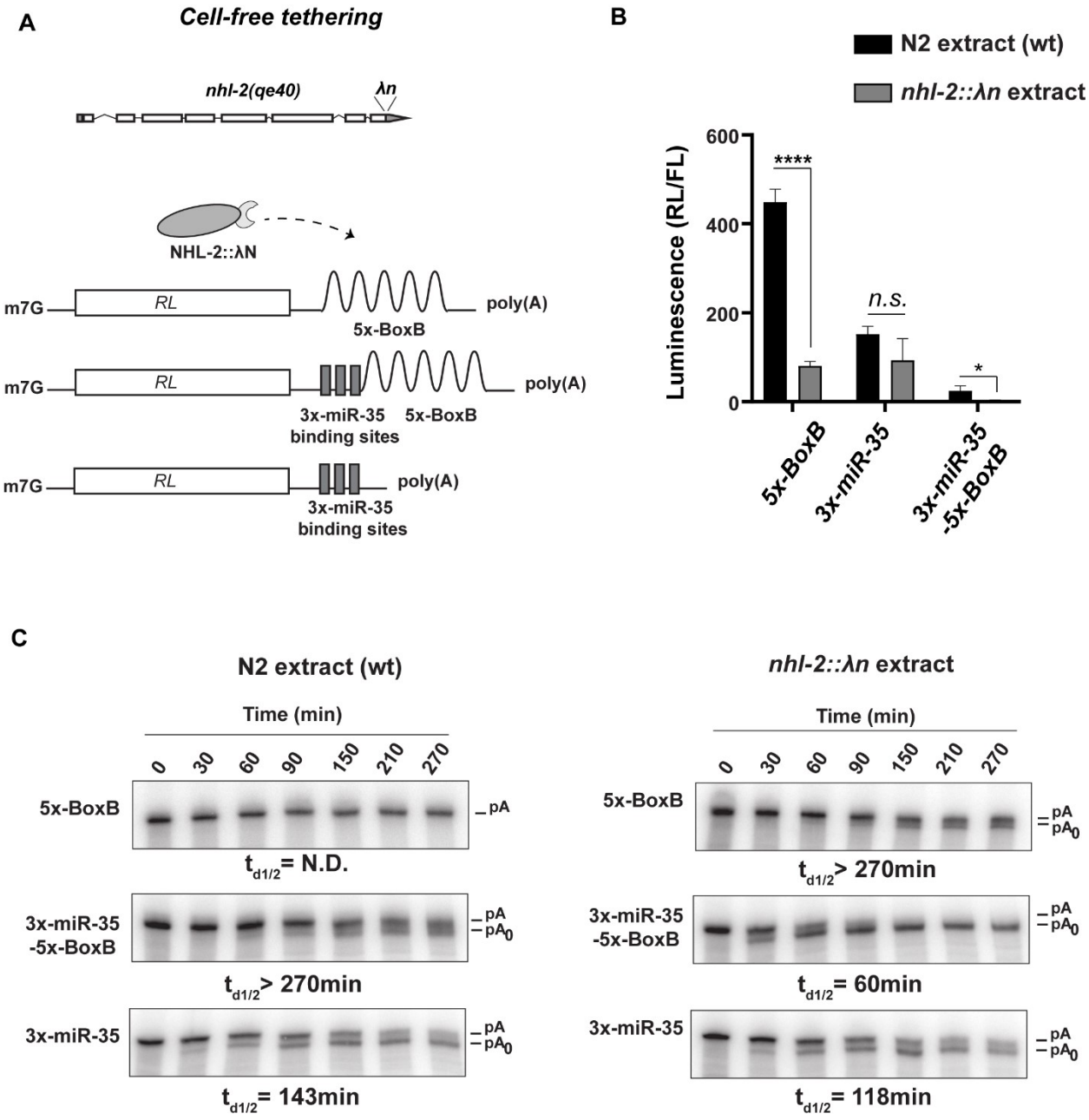

Figure 4-2: NHL-2 cooperates with miRISC to promote miRNA-mediated deadenylation. **(A)** *in vitro* transcribed reporters used to monitor translation and deadenylation activity (bottom). **(B-C)** Reporters bearing either 5x-BoxB sites, 3x-miR-35 binding sites or, both 5x-Boxb and 3x-miR-35 sites were incubated in embryonic extracts expressing either wild-type (N2) or λN-tagged NHL-2. RL and FL activities were measured after 4 ½ hours using the dual-luciferase reporter assay system (Promega)(B). RL activity was normalized to that of the FL control, $n = 3$. The RNA was extracted at indicated time points and analyzed by Urea-PAGE (C) p(A) denotes the position

of the poly-adenylated reporter mRNA, while p(A_0) indicates the position of the deadenylated reporter mRNA. Half-deadenylation rates ($t_{d1/2}$) were quantified using ImageJ. Images are representative of three independent experiments conducted using two different batches of extract preparations. The error bars represent standard deviation, and the *P*-value (**** $P < 0.00005$, * $P < 0.05$) was determined using the two-tailed Student's *t*-test.

4.3.3 Cooperative interactions between NHL-2 and miRNAs enhance miRNA-mediated silencing *in vivo.*

To validate the cooperative function of NHL-2 and miRNAs *in vivo*, we designed a genetic assay based on the activity of *miR-35* miRNA and NHL-2- λN on CRISPR-edited endogenous mRNA reporter loci (Flamand et al., 2017; Mayya et al., 2021). The temperature-sensitive allele of *glp-1*(*e2142*) is embryonic lethal at non-permissive temperatures (21^{o}C and above), and loss of *sel-1* expression suppresses this phenotype (Flamand et al., 2017; Kodoyianni et al., 1992; Priess et al., 1987). Using CRISPR/Cas9 gene-editing, 5x-BoxB alone or 5x-BoxB alongside 3 copies of *miR-35* binding sites were introduced in the 3'UTR sequence of the *sel-1* locus (Figure 4-3A), and the engineered strains were crossed with strains expressing wt or λN-tagged NHL-2 fusion protein. Live progeny was then scored at *glp-1*(*e2142*) non-permissive (21°C) temperature. As expected, animals expressing the *sel-1* mRNAs encoding 5x-BoxB sites as part of their 3' UTRs without NHL-2-λN fusion protein, produced very few viable progeny (3 ± 1 animals) (Figure 4-3B). Partial rescue of embryonic lethality (9 ± 2 animals) was observed in animals expressing *sel-1* mRNAs encoding both 5x-BoxB and 3x-miR-35 sites as part of their 3`UTRs, indicating some activity by *miR-35* miRNA. When NHL-2 was tethered in animals expressing *sel-1* mRNAs encoding both 5x-BoxB and 3x-miR-35, an efficient rescue of embryonic lethality (59 ± 4 animals) was observed. This repression was more potent than in animals expressing *sel-1*-5x-BoxB sites (24 ± 3 animals).

This indicates that NHL-2 can functionally cooperate with miRNAs to silence genes *in vivo.* qPCR analysis indicated no change in *sel-1* mRNA levels upon NHL-2 tethering to either 5x-BoxB or 5x-BoxB and 3x-miR-35 site containing *sel-1* (Figure 4-3C), suggesting an absence of mRNA destabilization.

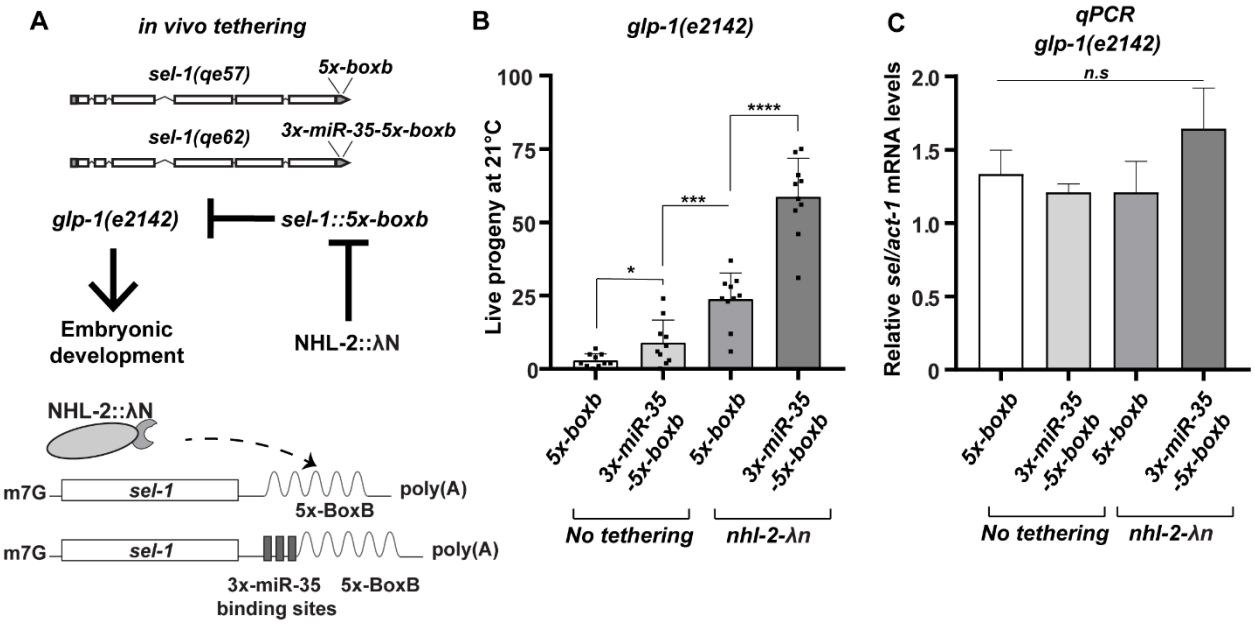

Figure 4-3. NHL-2 cooperates with miRNAs *in vivo*.
(A) The *sel-1* locus was engineered by the CRISPR/Cas9 gene-editing technique to encode *sel-1* mRNA bearing either 5boxb or both 5boxb and 3x-miR-35 sites in its 3`UTR (top). *sel-1* loss-of-function can suppress the temperature-sensitive embryonic lethality phenotype in the loss-of-function mutation of *glp-1(e2142)* (middle). Animals expressing a λN-tagged version of NHL-1 were crossed with animals expressing the two variants of *sel-1* mRNA to allow *in vivo* tethering of NHL-2 proteins to *sel-1* mRNA (bottom). **(B)** The number of live progeny was then measured in *sel-1((qe57)/(qe62))* and *glp-1(e2142)* double mutants with or without tethering of NHL-2. Each black dot within the bars indicates independent replicates. The error bars represent standard deviation, and the P-value (*** $P < 0.0005$, ** $P < 0.005$) was determined using the two-tailed Student's t-test. Progeny of 10 animals for each genotype was scored.

Our results collectively show that NHL-2 cooperates with miRNAs to silence mRNAs both *in vitro* and *in vivo*, and that this silencing occurs through rapid deadenylation and does not seem to involve mRNA decay.

4.3.4 Loss of interaction between NHL-2 and CGH-1 exacerbates *lsy-6* miRNA-associated defects.

Previous *in vitro* studies had shown a pair of cysteine residues in the B-box-1 domain of NHL-2 were responsible for the interaction with CGH-1 (Christopher Hammell, unpublished). To investigate if the interaction between CGH-1 and NHL-2 is important for miRNA function *in vivo*, we mutated the cysteine residues of B-box-1 encoding sequences in the *nhl-2* locus through CRISPR/Cas9 genome editing ((SDLCENCTTA to SDLAENATTA), *qe70*, referred henceforth as *nhl-2*$^{cgh\text{-}1\ bm}$). The mutant strain, *nhl-2*$^{cgh\text{-}1\ bm}$ was then crossed with the hypomorphic *lsy-6(ot150)* allele, which encodes point-mutations in the *lsy-6* promoter that leads to a reduction in *lsy-6* miRNA levels. *lsy-6(ot150)* animals display ~10% defects in neuronal left/right asymmetry (ASEL and ASER) (Johnston and Hobert, 2003). Mutations in the B-Box-1 domain of NHL-2 (*nhl-2*$^{cgh\text{-}1\ bm}$) in *lsy-6(ot150)* significantly exacerbated the ASEL phenotype (Figure 4-4A).

Overall, this result indicates the functional importance of NHL-2 and CGH-1, and their direct interaction in *lsy-6* miRNA function.

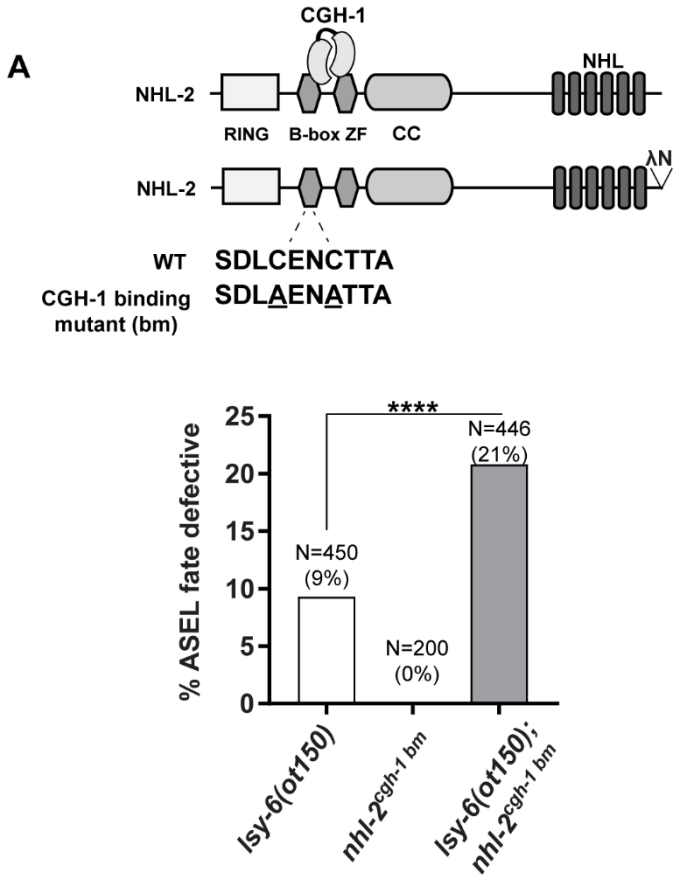

Figure 4-4. Loss of interaction between NHL-2 and CGH-1 exacerbates *lsy-6* miRNA-associated defects.

(A) A schematic representation of the mutations performed in the B-Box-1 domain of NHL-2 by the CRISPR/Cas9 gene-editing technique (top). Loss of ASEL-specific expression of plim-6::GFP reporter was quantified in *lys-6(ot150)* and *nhl-2*$^{cgh\text{-}1\ bm}$ single mutants, and *lys-6(ot150); nhl-2*$^{cgh\text{-}1\ bm}$ double mutants (bottom). N = animals scored for each genotype. Statistical significance was assessed using two-tailed chi-square analysis (****$P < 0.00005$).

4.4 Discussion

Cooperativity between RBPs and miRNAs has thus far been loosely characterized without much mechanistic resolution. By performing proteomics on a previously identified co-factor of miRISC, the TRIM-NHL protein NHL-2 (Hammell et al., 2009b), we identified interactions with components of miRISC, P-Bodies, the CCR4-NOT complex, and other RBPs. Upon juxtaposition of miRISC and NHL-2 on 3`UTRs of mRNAs, we observed an increase in deadenylation rate, leading to potent repression. Functional cooperativity between NHL-2 and miRNAs was also observed *in vivo.* Moreover, NHL-2 directly interacts with the P-body-associated protein, CGH-1, and loss of this interaction functionally impairs silencing mediated by *lsy-6* miRNA.

Members of the DEAD-box helicases play essential roles in the formation of membrane-less organelles such as P-bodies and P granules. For instance, depletion of DDX6 in HeLa cells results in the disappearance of P-bodies (Minshall et al., 2009; Serman et al., 2007), while depletion of GLH proteins, the *C. elegans* ortholog of Vasa DEAD-box helicases, causes defects in the assembly of P granules (Spike et al., 2008). Current models suggest that extensive interactions between DEAD-box helicase proteins and RNA lead to remodeling of RNPs and drive phase separation of these RNPs into liquid droplets (Banani et al., 2016; Fromm et al., 2014; Rao and Parker, 2017). Interestingly, loss of NHL-2 also reduces P granules suggesting a role for NHL-2 in P granule formation (Hyenne et al., 2008). In light of these studies, along with our findings here highlighting the importance of NHL-2/CGH-1 interaction in *lsy-6* miRNA function, we postulate a model wherein cooperative interactions between NHL-2 and miRNAs enable recruitment of the ATPase CGH-1 to target mRNAs, which, in turn, promotes remodeling of the RNPs to form P-bodies (Figure 4-5). Next steps will include immunofluorescence experiments on *nhl-2* and *cgh-1* mutants to test if there are defects in P-bodies.

Our data shows that cooperative interactions between miRISC and NHL-2 increase the rate of deadenylation. While miRISCs can cooperatively recruit the CCR4-NOT complex, we looked into an alternate, non-exclusive hypothesis, that NHL-2 enables the recruitment of multiple copies of the deadenylase complex, leading to the increase in deadenylation rate. We directly tested this hypothesis by performing deadenylated RNA immunoprecipitation assays (Flamand et al., 2017) on reporter mRNAs encoding both 5x-BoxB and miRNA-binding sites. We did not detect an increase in the number of copies of the CCR4-NOT complex recruited through the combination of NHL-2 and miRISC. This result suggests that the increase in the rate of deadenylation of miRNA targets by NHL-2 is perhaps also due to RNP reorganization and the formation of P-bodies. We propose that the P-bodies provide an environment for mRNA seclusion and enhanced deadenylation. Recent *in vitro* reconstitution of phase-separated miRISC droplets showed sequestration of miRNA targets and accelerated deadenylation occurring within these droplets, suggesting that this may be a common theme in P-bodies as well (Sheu-Gruttadauria and MacRae, 2018). Alternatively, liquid-liquid phase separation may enable a switch to a more active conformation of the CCR4-NOT complex. Similar reconstitution experiments performed using wild-type and mutant forms of NHL-2 and CGH-1 and monitoring the deadenylation rates of miRNA targets will test this model.

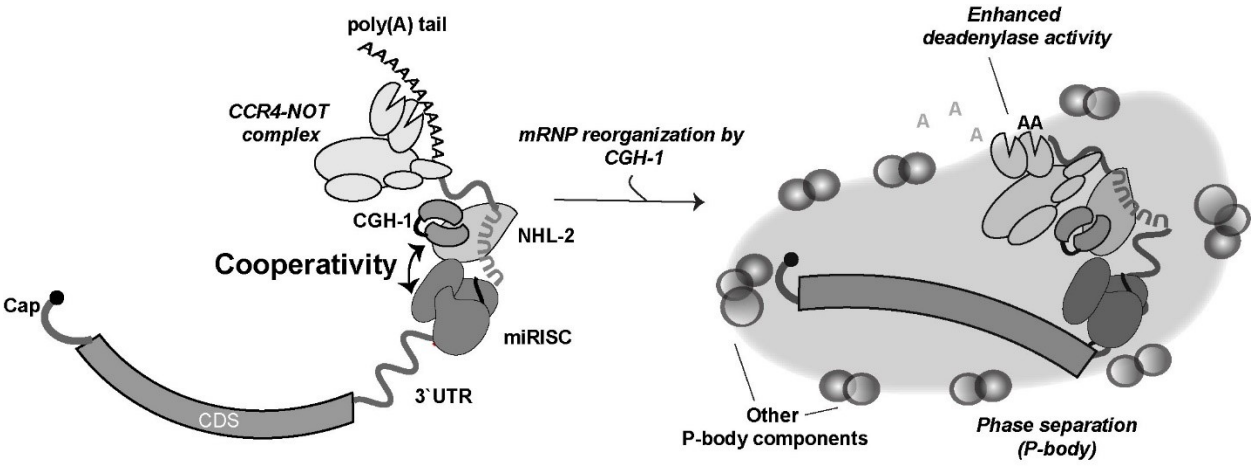

Figure 4-5. Model. Cooperativity between miRISC and NHL-2 enhances the rate of deadenylation.
NHL-2 cooperates with miRNAs to silence target mRNAs. We propose that the interaction of NHL-2 with DEAD-Box helicase, CGH-1, causes a reorganization in RNP and the formation of P-bodies, which altogether contributes to the increase in deadenylation rate of target mRNAs.

Protein-protein interactions occurring within P-bodies are poorly understood since many of these interactions are very transient and difficult to detect. *In vitro* reconstitution and *in vivo* experiments have demonstrated the DEAD-box helicases in their ATP-bound form to promote phase separation, while hydrolysis of ATP disassembles the RNPs (Hondele et al., 2019; Ma et al., 2013; Minshall et al., 2009; Mugler et al., 2016). Accordingly, a recent study utilized mutations within the DEAD motif of GLH-1 to lock the protein in its bound state with P granules and examine what happens to GLH-1 interactions (Marnik et al., 2019). The same mutations could be engineered in CGH-1 and used to identify interactions unique to P-bodies.

The contribution of the RING domain of NHL-2 to miRNA-mediated silencing and P-body formation is currently unknown. As some members of the TRIM-NHL family of proteins use their RING domains to ubiquitinate target proteins (Kudryashova et al., 2005; Raheja et al., 2014), the

RING domain of NHL-2 could also act as an E3 ubiquitin ligase and regulate nascent polypeptides encoded by miRNA targets. More recently, a study showed that loss of ubiquitination of the decapping activator (DCP1) was associated with defects in P-body formation (Tenekeci et al., 2016). In line with this finding, NHL-2 could also contribute to the reorganization of RNPs and P-body formation through its E3-ubiquitin ligase activity. The next step would be to use CRISPR/Cas9 gene-editing technique to engineer specific domain-deletions and examine their effects on miRNA-mediated silencing and P-body formation.

NHL-2 is a poly(U) binding protein (Davis et al., 2018); however, our experiments enforced the recruitment of NHL-2 to mRNAs through the use of λN:BoxB protein/mRNA tethering system (Figure 4-2 and Figure 4-3). While this approach allowed us to specifically test the effect of bound NHL-2 on mRNAs without clouding from other poly(U)-binding RBPs, we currently do not know if poly(U) sequences alone are sufficient to recruit NHL-2 to target mRNAs. As poly(U) binding sites in 3'UTR are common, especially in *C. elegans*, one would expect wide-spread regulation of the transcript, yet, *nhl-2* null animals are viable and only display weak penetrance of heterochronic phenotypes (Hammell et al., 2009b; Hyenne et al., 2008). Thus, we suspect that the specificity of NHL-2 depends on miRISC. Future experiments involving the genome-wide mapping of NHL-2-binding sites using RNA-IP sequencing should identify endogenous targets bound by NHL-2. These generated datasets will then have to be compared with validated miRNA-binding sites (Broughton et al., 2016; Zisoulis et al., 2010). The genome of *C. elegans* is AU-rich, and computational analysis of 3`UTRs shows enrichment for AU-elements near miRNA-binding sites (Consortium, 1998; Jiang et al., 2013). The functional output of natural 3`UTRs bearing binding sites for NHL-2 and miRNAs can then be detailed by engineering precise mutations in poly(U) sequences of 3`UTRs and monitoring the translation and fate of RNA.

4.5 Acknowledgements

We would like to apologize to authors whose directly related work may have not been cited in this manuscript. We thank all the lab members for their valuable feedback on the manuscript.

4.6. Funding

This work was supported by the Canadian Institutes of Health Research (CIHR) MOP-123352 (to T.F.D.); The Charlotte and Leo Karassik Foundation PhD fellowship award to V.K.M.

4.7 Material and Methods

4.7.1 Worm strains

N2 Bristol (WT), *let-7* (n2853), FD03(*nhl-2*::3xFLAG), FD120 (*nhl-2*::λN), FD165(*sel-1*::5boxb), FD166(*sel-1*::3x-mir-35-5boxb), FD167(*sel-1*::5boxb; *nhl-2*:: λN), FD177(*sel-1*::3x-mir-35-5boxb; *nhl-2*:: λN). All strains were maintained at 16°C except for phenotypic assays, which were performed at 20 or 25ºC.

4.7.2 Genome Editing

Genome editing for the *nhl-2::3xFLAG* insertion was carried out as in (Ward, 2015) using the CTCATCAGCAAGTTTCAGTG guide sequence, and a PCR repair template. The repair template was amplified using the forward primer 5′-GGACTTCCTGTTCCAACTCC-3′ and reverse primer 5′-GAAGACGGCTAGAAATGAGAAA-3′ using a synthetic template. For *nhl-2*:: λN, the genome editing protocol was modified from (Paix et al., 2015). mRNP complex was assembled with rCAS9 and *in vitro* transcribed modified sgRNA(F+E)(Ward, 2015). Injection mixes contained 1.2µg/µL Cas9, 300mM KCl, 12.5mM Hepes pH7.4. 50ng/µL dpy-10 sgRNA, 200ng/µL gene specific sgRNA, 13.75ng/µL dpy-10 repair ssODN and 110ng/µL of ssODN repair template

(TACAAGAAAAAAAGCTTATATAGGAATTGGGGTAACCTCCTCAATTAGCAGCTTTC
CATTGAGCTTGTTTTTCAGCTCTTCTTTCTCTTCTTCTAGTTTGAGCATCTCCACCCCC
GCCTCCCCCCTGAAACTTGCTGATGAGCGAAGTTGCATGAGGAACTGGA). The following guide RNA was used: (ATCAGCAAGTTTCAGTGAGG). Approximately 15 germlines of N2 gravid adults grown on *cku-80* RNAi plates were injected. Roller (heterozygotes for *dpy-10*) or dumpy animals were screened for λN insertion by PCR.

4.7.3 Translation and Deadenylation assays

Embryonic extracts were performed as described in (Wu et al., 2010). Half-deadenylation times were calculated by determining the intersection of the non-deadenylated and deadenylated RNA species over time using polynomial regression (order 2), using quantification of autoradiography with ImageJ.

4.7.4 Immunoprecipitation (IP) and Multidimensional Protein Identification (MuDPIT)

Embryo pellets were homogenized in lysis buffer (50 mM Tris-HCl pH 8, 150 mM NaCl, 1 mM EDTA, 1% Triton X-100 with Complete EDTA-free protease inhibitors (Roche)) and cleared by 17500 × *g* centrifugation. FLAG-tagged proteins were purified using anti-FLAG M2 Affinity Gel (Sigma-Aldrich A2220). 4 mg of proteins were used for each IP at a concentration of 2mg/mL in lysis buffer. 50 µl of bead slurry was used by IP, which were carried out at 4°C for 2 hours. Beads were washed four times in lysis buffer, and proteins were eluted using the 3xFLAG peptide (Sigma-Aldrich F4799) or ammonium hydroxide solution. 10% the eluate was resolved by SDS-PAGE and western blot analysis was performed using anti-FLAG-M2 antibody. Non-transgenic N2 embryos were used as controls for the purifications. MuDPIT was performed as described in (Duchaine et al., 2006).

4.7.5. Gene Ontology (GO) term analysis

Proteins (51) identified by MuDPIT in at least two independent NHL-2 purifications were analysed for GO cellular component annotations using g:prolifer (https://biit.cs.ut.ee/gprofiler/gost) (Raudvere et al., 2019). Proteins found in the negative control at more than 1 peptide in the N2 (WT) strain were excluded.

Chapter 5: General Discussion

While investigating development in *C. elegans*, the groups of Ambros and Ruvkun identified the *lin-4* gene to regulate *lin-14* gene (Arasu et al., 1991; Wightman et al., 1991). The subsequent cloning and characterization of the *lin-4* gene identified a 22-nt transcript that would bind to complementary sequences in the 3`UTR of *lin-14* to post-transcriptionally regulate *lin-14* gene expression (Lee et al., 1993; Wightman et al., 1993). This discovery of *lin-4* miRNA paved the way to identifying other miRNAs, not only in *C. elegans* but in several other species (Lagos-Quintana et al., 2001; Pasquinelli et al., 2000; Reinhart et al., 2000). To this date, miRbase (v22), a database that catalogs names and sequences of miRNAs, contains miRNAs from over 250 organisms (Kozomara et al., 2018). The identification of miRNAs has also enabled many groups to study individual miRNAs function and their target mRNA counterparts. However, we are still far away from completely understanding the breadth of miRNA action. *What determines the silencing output that is driven by miRNAs? How do miRISC cofactors affect miRNA-mediated silencing? What are the biological implications of miRNAs?* The thesis presented here addresses these questions using a combination of biochemical, proteomic, and genetic assays.

5.1 *C. elegans* and cell line models to study microRNA function

miRNAs form intricate connections with their cofactors, and these connections determine the overall impact of gene silencing on animal development. For this reason, animal models such as *C. elegans, Drosophila melanogaster, Danio rerio, and Mus musculus* have been used to elucidate the exact functions of miRNAs by exploiting the *in vivo* genetics and cell biology that these model systems have to offer. Indeed, studies using animal models have largely contributed to our understanding of miRNA function in different cellular processes, including proliferation, differentiation, apoptosis, all of which are affected in human diseases (Pal and Kasinski, 2017). *C. elegans,* in particular, is an appropriate choice of a model for miRNA research as defects in some

miRNAs cause overtly visible phenotypes (Ambros and Ruvkun, 2018). Moreover, *C. elegans* express fewer conserved miRNA family members (Ibáñez-Ventoso et al., 2008) and thus studying the function of miRNAs becomes easier due to less redundancy. Advances in CRISPR approaches have enabled researchers to edit specific regions in the *C. elegans* genome in a matter of weeks. As *C. elegans* are hermaphrodites that self-fertilize, bi-allelic mutations can be easily obtained from heterozygous mothers. The advantages of such a model system were instrumental in identifying the physiological roles of GYF-1 and NHL-2 in Chapters 3 and 4. The questions asked in these chapters could not have been answered using *in vitro* cell line models. On the contrary, quantitative analyses of miRNA-mediated silencing require biochemical approaches that typically can be employed in cell lines only. Cell lines offer a pure population of cells that remain consistent and allow the generation of reproducible results (Kaur and Dufour, 2012). In Chapter 2, using HEK 293T cells as a model, we used quantitative biochemical approaches to assess the relationship between miRISC availability, miRNA expression, and silencing outcomes. This thesis utilizes both *C. elegans* and cell line models to understand the biological and molecular functions of various miRNAs.

5.2 Genetic and proteomic approaches in identifying miRISC cofactors and their function

A readout for any given miRNA silencing effect is the direct measurement of the impact on protein synthesis. Through quantitative-based mass-spectrometry approaches using SILAC (stable isotope labeling with amino acids in cell culture), we now know that while a single miRNA can repress several hundreds of proteins, overexpression of miRNAs in mammalian cell lines cause mostly mild repression and rarely exceeds fourfold (Baek et al., 2008; Lim et al., 2005; Selbach et al., 2008). In stark contrast, some miRNAs (*lsy-6, let-7, lin-4, etc.)* elicit near-complete repression of target mRNAs to ensure proper development (Johnston and Hobert, 2003; Moss et al., 1997; Slack

et al., 2000).Thus, some miRNAs function as molecular switches while other miRNAs only act as fine-tuners of gene expression. For several years now, research groups have focused on understanding how individual miRNAs can differ in their overall silencing output. As the core component of miRISC, the Argonaute protein is necessary for any silencing to occur (reviewed in (Peters and Meister, 2007)). An interpretation in the field is that Argonaute proteins act as a molecular scaffold. Depending on the cell type, developmental stage, or alternative environmental conditions, the core miRISC may interact with different cofactors. Each of these cofactors can have its own activity or interact with other proteins that increase miRNA-mediated silencing activity. For instance, in Chapter 4, we showed that miRISC cofactor, NHL-2 increases the rate of miRNA-mediated deadenylation of target mRNAs. Our data suggest that the interaction of NHL-2 with CGH-1 leads to the reorganization of RNPs that accelerate deadenylase activity. With such an interpretation in mind, the absence, substitution, or post-translational modifications of a cofactor might affect miRNA activity. Could any one of these reasons explain why in Chapter 3, GYF-1 does not impact the function of *lsy-6* and *lin-4* miRNAs? While we know that GYF-1 is expressed in all the stages of *C. elegans* development, we do not know if GYF-1 is expressed in all cells or if GYF-1 undergoes post-translational modifications or substitution by another abundant cofactor in specific cell types. We now have the tools to address these questions. Affinity purification of *lsy-6* or *lin-4* miRNAs combined with proteomics can be used to investigate the composition of miRISC.

Early on, the identification of cofactors of miRISC relied primarily on classical forward genetic screens. But redundancy within proteins and miRNA family members can often mask the effect of loss of a single gene. Thus, reverse genetic screens using RNAi in sensitized miRNA backgrounds contributed to identifying proteins that regulate miRNA activity (Hurschler et al., 2011; Nolde et

al., 2007; Parry et al., 2007; Rausch et al., 2015). While RNAi is an easy and rapid approach, knockdown efficiencies can vary between experiments and sometimes fail to produce any phenotype even in sensitized miRNA backgrounds. This could be why previous genetic screens using RNAi (Parry et al., 2007; Rausch et al., 2015) failed to identify GYF-1 as a regulator of miRNA activity. An alternative approach has been to look at proteins associated with the Argonaute, and then through either genetics or knockdown experiments, uncover the function of miRNA-associated proteins (Chu and Rana, 2006; Hammell et al., 2009b; Kakumani et al., 2020). This was seen in chapter 3, by comparing proteomic datasets of key components involved in the miRNA pathway, we identified several uncharacterized proteins beyond GYF-1. We have now begun to expand the characterization of other attractive candidates, including STAM-1 (See Appendix A5.1 for a complete list) obtained through this proteomics-based discovery approach. The *C. elegans* STAM-1 (ortholog of human STAM and STAM2) is an accessory protein of the endosomal sorting complex required for transport (ESCRT) (Rusten et al., 2012), and might perhaps play a role in vesicular-based transport of miRNAs between subcellular compartments. Preliminary studies indicate that STAM-1 is important for *lsy-6* miRNA activity (See Appendix A5.2). Biochemical and genetic assays employed in chapters 3 and 4, along with immunofluorescence procedures, could thus be used to study the underlying mechanisms regulating the subcellular localization of miRNAs and their biological significance. Similar experiments can be performed in other model systems and ask if our findings in *C. elegans* are conserved and relevant to organism development and disease.

The past decade has seen the emergence of CRISPR/Cas9 tools augment our ability to precisely edit genomes and examine the function of a gene in its endogenous context. Indeed, this allowed us to engineer null alleles of *gyf-1* and express various tagged versions of GYF-1 and NHL-2.

Also, targeted point mutations engineered in *gyf-1* and *nhl-2* loci uncovered the contribution of individual molecular determinants to miRNA function. Moving forward, an exciting application of CRISPR/Cas9 technology would be to identify biologically relevant targets of miRNAs and other RBPs. Methods such as ribosome profiling or CLIP have been widely used to this end. However, these approaches generate a long list of candidate genes with false positives and eventually require *in vivo* validation. Instead, a recent work used a CRISPR screen in *C. elegans* and identified a single target gene (*egl-1*) alone sufficient to induce embryonic lethality observed in *miR-35-42* family mutants (Yang et al., 2020). It would be of great interest to extend this method to identify biologically relevant targets of other miRNAs, GYF-1, NHL-2, and other RBPs. Additionally, previously validated miRNA targets through reporter assays or overexpression experiments should be revisited, and this time validated with the use of CRISPR. This would help us to confirm previous candidates and possibly to identify functionally relevant miRNA targets.

5.3 Quantitative approaches to unveil properties of miRNA-mediated silencing

In addition to the discovery and characterization of miRISC cofactors in specific cell type/developmental stage, studying the kinetic properties of miRISC can reveal the mechanisms miRNAs use to efficiently mediate gene silencing. In Chapter 2, we observed a disconnect between miRNA expression levels, the available miRISC pool, and their silencing activity. Reasons for this observation likely include differences in target site accessibility and binding affinity of miRNAs and subcellular localization of miRISC. Approaches such as single-molecule imaging techniques that allow direct and continuous observation of the events leading up to gene silencing will be key in revealing the importance of the dynamic nature of miRISC. Using the cell-free *C. elegans* embryonic extract system used in Chapters 3 and 4 that offer a near-physiological environment to monitor the events mentioned earlier, we developed a single-molecule imaging technique to

unravel the steps starting from miRISC target recognition to CCR4-NOT recruitment (see appendix A4).

Until recently, the rates at which miRISC associate and disassociate its target mRNA were quantified using batch-averaging techniques (Wee et al., 2012). Recent improvements in fluorescent protein photostability, the sensitivity of camera detectors, robust software algorithms that track fluorescently labeled proteins, and analytical tools to improve the signal-to-noise ratios have enabled researchers to observe and precisely examine the individual domains of miRISC that contribute to target recognition (Chandradoss et al., 2015; Li and Zhang, 2012; Salomon et al., 2015; Shashkova and Leake, 2017). An extension of this approach will be to study the assembly of cofactors and effector machinery such as the CCR4-NOT complex on the target mRNA. We designed a fluorescently labeled bait bearing the 3`UTR of *elg-1* mRNA, which is known to harbor two functionally cooperating miRNA-binding sites (Sherrard et al., 2017; Wu et al., 2010). With the application of the CRISPR/Cas9 gene-editing technique, functional tags that can be fluorescently labeled were introduced to ALG-1, AIN-2, and NTL-1. Such an approach has never been attempted before as introducing fluorescent tags to endogenous loci has been difficult before the advent of CRISPR/Cas9. Future experiments using total internal reflection fluorescence microscopy will help determine the kinetics of miRNAs and the deadenylase complex.

The single-molecule imaging system that we have developed can also be broadly applicable to studying the role of miRISC cofactors and RBPs. Chapter 4 proposed a model where NHL-2/CGH-1 interaction reorganizes the mRNP leading to an increase in the rate of mRNA deadenylation. This model can be tested in the single-molecule imaging setup, using fluorescence resonance energy transfer (FRET). Protein conformational changes or reorganization of mRNP can be studied

by measuring fluorescence intensity changes due to FRET efficiencies, and therefore would be an invaluable tool in investigating the role of conformational dynamics in miRNA function.

5.4 Insights into miRNA-mediated silencing mechanisms

For several years, the relative contributions and biological significances of translational repression and mRNA destabilization, the two silencing mechanisms initiated by miRNAs, have remained elusive. Steady-state measurements of proteins and miRNA targets indicate that mRNA destabilization could apparently account for most of the miRNA-mediated silencing in certain cell types (Eichhorn et al., 2014; Guo et al., 2010). In contrast, kinetic analyses conducted in mammalian and *Drosophila* cells, and zebrafish embryos revealed that translation repression precedes mRNA deadenylation and decay (Bazzini et al., 2012; Béthune et al., 2012; Djuranovic et al., 2012; Giraldez et al., 2006). As mRNA destabilization can be a consequence of translation repression (Chan et al., 2018; Huch and Nissan, 2014; Roy and Jacobson, 2013), only by uncoupling translation repression from mRNA decay can we truly study the two silencing mechanisms and identify their biological significance. This is not a simple issue to tackle since both translation repression and mRNA decay mechanisms share similar effector proteins and are intimately connected to each other. Chapter 3 identified the physiological purpose for a "pure" miRNA-mediated translational repression. Importantly, we observed instances where loss of translation repression could not be compensated through mRNA destabilization mechanisms. Apart from the composition of miRISC and differences in developmental stages, the silencing mechanisms likely depend on the sequence of target mRNAs (density and distribution of *cis*-regulatory elements in the 3`UTR). Careful examination of the individual contribution of *cis*-regulatory elements enabled by CRISPR-based technologies to the silencing mechanisms could help us understand the interplay between translation repression and mRNA decay.

5.5 Current frontiers in 3`UTR research

[*The discussion points presented in this section are taken from my review article, (Mayya and Duchaine, 2019)*]

Great strides have been made in understanding the mechanisms underlying 3`UTR regulatory sequences and the factors that recognize and affect them. However, several problems remain unsolved and important new ones recently emerged. The resolution in the functions of phase transition mRNPs provides an example of an old problem that was recently visited with a new perspective. Other important problems came into focus with the emergence of next-generation sequencing, including alternative cleavage and polyadenylation (APA) (Edwalds-Gilbert et al., 1997), which generates significant diversity in 3`UTR isoforms. High-throughput sequencing identified multiple APA sites in at least 70% of known mammalian genes (Derti et al., 2012; Hoque et al., 2012). Most tissue-specific genes express single UTRs, but more than half of ubiquitously expressed genes are produced as multiple 3`UTR isoforms (Lianoglou et al., 2013). A different choice of polyadenylation sites in a 3`UTR has the potential to profoundly re-shape its structure and response elements, thus impacting mRNA stability, translation and localization. An interesting recent study even showed that an mRNA APA can alter the localization and expression of the membrane protein it encodes (Berkovits and Mayr, 2015). Not only is there an important diversity of 3`UTR isoforms, they are also dynamic in different cellular states. On average, proliferating cells (including several tumour-derived cell lines) express shorter 3'UTRs in mRNAs that are more stable and translated into more protein compared to the longer 3'UTR mRNAs expressed in differentiated cells (Ji et al., 2009; Mayr and Bartel, 2009; Sandberg et al., 2008). This led to the idea that shorter 3`UTR isoforms allowed mRNAs to avoid regulation by miRNAs and RBPs. This is likely an over-simplification and is not always the case, however, as shorter 3`UTRs can also

mean more potent deadenylation (Flamand et al., 2016), and longer 3`UTRs can also mean regulatory sequences being buried in a more complex structure (Thivierge et al., 2018). Furthermore, some tissues like the brain (Hilgers et al., 2011; Ji et al., 2009; Miura et al., 2013; Ulitsky et al., 2012) have on average much longer 3`UTRs, potentially multiplying the folding structures and/or regulatory input, and thus the complexity of functional interplay.

The folding structures of 3`UTRs remain largely under-appreciated. This in itself is an important frontier, as structures can profoundly impact gene regulation (for reviews, see (Jacobs et al., 2012; Kwok et al., 2015). Significant advances in chemical probes and next-generation sequencing now enable us to obtain genome-wide *in vivo* structures at single nucleotide resolution (Bevilacqua et al., 2016). Structures can be derived from *in vivo* transcripts, thus providing a perspective on the impact of developmental and cellular contexts, and the prevailing 3`UTR interactions (Spitale et al., 2015). Along those lines, a recent study analyzed changes in structures in zebrafish transcripts during maternal-to-zygotic transition (MZT) (Beaudoin et al., 2018), and revealed the interplay between ribosomes and the unwinding of mRNA secondary structures.

Improvements in throughput, library generation methods, and cost-effectiveness of next generation sequencing now enable an integrated genomic perspective on multiple regulatory mechanisms. Massively parallel reporter assays (MPRA) have been used in the past to identify functional *cis*-regulatory elements in transcription and splicing (Melnikov et al., 2012; Rosenberg et al., 2015). Thousands of random sequences with unique tags are fused to reporters and introduced into cells, and their regulatory output is then quantified using high-throughput sequencing. A recent study used a similar technique to identify *cis*-regulatory elements in the 3`UTRs of maternal mRNAs in zebrafish that regulate mRNA decay (Rabani et al., 2017). The authors identified 2 stabilizing

elements (polyU and UUAG sequences) and four destabilizing elements (GC- rich, AU-rich, Pumilio-binding sites and miR-430-binding sequences).

Because so many mechanisms mobilize the deadenylase complex and its activities, sequencing libraries that allow the capture of poly(A) tail size, the end of the 3`UTR isoform, and the abundance of transcripts will provide insight on the impact of these key features on gene expression.

5.6 Conclusion

The work presented in this thesis reveals how regulatory elements in 3`UTRs are recognized by miRNAs and their cofactors, and the mechanisms leading to the decisions on the fate of mRNAs. While genomic approaches would successfully unveil the complexity and breadth of some of these mechanisms, each 3`UTR is also unique and has co-evolved closely in its genetic and cellular niche with its regulatory factors. Deciphering the 3`UTR code will thus also require detailing this uniqueness for each 3`UTR. Embracing genetics once more, this time through genome edition in model organisms, my thesis offers powerful new possibilities in linking the sequences of 3`UTRs, miRNAs, and their cofactors with mRNA fates in their physiological context.

REFERENCES

Abbott, A.L., Alvarez-Saavedra, E., Miska, E.A., Lau, N.C., Bartel, D.P., Horvitz, H.R., and Ambros, V. (2005). The let-7 MicroRNA family members mir-48, mir-84, and mir-241 function together to regulate developmental timing in Caenorhabditis elegans. Dev Cell *9*, 403-414.

Ala, U., Karreth, F.A., Bosia, C., Pagnani, A., Taulli, R., Leopold, V., Tay, Y., Provero, P., Zecchina, R., and Pandolfi, P.P. (2013). Integrated transcriptional and competitive endogenous RNA networks are cross-regulated in permissive molecular environments. Proc Natl Acad Sci U S A *110*, 7154-7159.

Altuvia, Y., Landgraf, P., Lithwick, G., Elefant, N., Pfeffer, S., Aravin, A., Brownstein, M.J., Tuschl, T., and Margalit, H. (2005). Clustering and conservation patterns of human microRNAs. Nucleic Acids Res *33*, 2697-2706.

Alvarez-Saavedra, E., and Horvitz, H.R. (2010). Many families of C. elegans microRNAs are not essential for development or viability. Curr Biol *20*, 367-373.

Amaya Ramirez, C.C., Hubbe, P., Mandel, N., and Bethune, J. (2018). 4EHP-independent repression of endogenous mRNAs by the RNA-binding protein GIGYF2. Nucleic Acids Res *46*, 5792-5808.

Ambros, V., and Ruvkun, G. (2018). Recent Molecular Genetic Explorations of *Caenorhabditis elegans* MicroRNAs. Genetics *209*, 651-673.

Ameres, S.L., and Zamore, P.D. (2013). Diversifying microRNA sequence and function. Nature Reviews Molecular Cell Biology *14*, 475-488.

Arasu, P., Wightman, B., and Ruvkun, G. (1991). Temporal regulation of lin-14 by the antagonistic action of two other heterochronic genes, lin-4 and lin-28. Genes & development *5*, 1825-1833.

Arribas-Layton, M., Wu, D., Lykke-Andersen, J., and Song, H. (2013). Structural and functional control of the eukaryotic mRNA decapping machinery. Biochimica et Biophysica Acta (BBA) - Gene Regulatory Mechanisms *1829*, 580-589.

Babiarz, J.E., Ruby, J.G., Wang, Y., Bartel, D.P., and Blelloch, R. (2008). Mouse ES cells express endogenous shRNAs, siRNAs, and other Microprocessor-independent, Dicer-dependent small RNAs. Genes & development *22*, 2773-2785.

Baccarini, A., Chauhan, H., Gardner, T.J., Jayaprakash, A.D., Sachidanandam, R., and Brown, B.D. (2011). Kinetic analysis reveals the fate of a microRNA following target regulation in mammalian cells. Curr Biol *21*, 369-376.

Baek, D., Villén, J., Shin, C., Camargo, F.D., Gygi, S.P., and Bartel, D.P. (2008). The impact of microRNAs on protein output. Nature *455*, 64-71.

Bagga, S., Bracht, J., Hunter, S., Massirer, K., Holtz, J., Eachus, R., and Pasquinelli, A.E. (2005). Regulation by let-7 and lin-4 miRNAs Results in Target mRNA Degradation. Cell *122*, 553-563.

Bakheet, T., Williams, B.R., and Khabar, K.S. (2006). ARED 3.0: the large and diverse AU-rich transcriptome. Nucleic Acids Res *34*, D111-114.

Banani, S.F., Lee, H.O., Hyman, A.A., and Rosen, M.K. (2017). Biomolecular condensates: organizers of cellular biochemistry. Nature Reviews Molecular Cell Biology *18*, 285.

Banani, S.F., Rice, A.M., Peeples, W.B., Lin, Y., Jain, S., Parker, R., and Rosen, M.K. (2016). Compositional Control of Phase-Separated Cellular Bodies. Cell *166*, 651-663.

Baron-Benhamou, J., Gehring, N.H., Kulozik, A.E., and Hentze, M.W. (2004). Using the lambdaN peptide to tether proteins to RNAs. Methods Mol Biol *257*, 135-154.

Barreau, C., Paillard, L., and Osborne, H.B. (2005). AU-rich elements and associated factors: are there unifying principles? Nucleic Acids Res *33*, 7138-7150.

Baugh, L.R. (2013). To Grow or Not to Grow: Nutritional Control of Development During *Caenorhabditis elegans* L1 Arrest. Genetics *194*, 539-555.

Bazzini, A.A., Lee, M.T., and Giraldez, A.J. (2012). Ribosome Profiling Shows That miR-430 Reduces Translation Before Causing mRNA Decay in Zebrafish. Science *336*, 233-237.

Beaudoin, J.-D., Novoa, E.M., Vejnar, C.E., Yartseva, V., Takacs, C.M., Kellis, M., and Giraldez, A.J. (2018). Analyses of mRNA structure dynamics identify embryonic gene regulatory programs. Nat Struct Mol Biol *25*, 677-686.

Bentwich, I., Avniel, A., Karov, Y., Aharonov, R., Gilad, S., Barad, O., Barzilai, A., Einat, P., Einav, U., Meiri, E*., et al.* (2005). Identification of hundreds of conserved and nonconserved human microRNAs. Nature Genetics *37*, 766-770.

Berkovits, B.D., and Mayr, C. (2015). Alternative 3′ UTRs act as scaffolds to regulate membrane protein localization. Nature *522*, 363.

Bernstein, E., Caudy, A.A., Hammond, S.M., and Hannon, G.J. (2001). Role for a bidentate ribonuclease in the initiation step of RNA interference. Nature *409*, 363-366.

Béthune, J., Artus-Revel, C.G., and Filipowicz, W. (2012). Kinetic analysis reveals successive steps leading to miRNA-mediated silencing in mammalian cells. EMBO Rep *13*, 716-723.
Bevilacqua, P.C., Ritchey, L.E., Su, Z., and Assmann, S.M. (2016). Genome-Wide Analysis of RNA Secondary Structure. Annual Review of Genetics *50*, 235-266.

Blewett, N.H., and Goldstrohm, A.C. (2012). A Eukaryotic Translation Initiation Factor 4E-Binding Protein Promotes mRNA Decapping and Is Required for PUF Repression. Molecular and cellular biology *32*, 4181-4194.

Boag, P.R., Atalay, A., Robida, S., Reinke, V., and Blackwell, T.K. (2008). Protection of specific maternal messenger RNAs by the P body protein CGH-1 (Dhh1/RCK) during Caenorhabditis elegans oogenesis. J Cell Biol *182*, 543-557.

Bohmert, K., Camus, I., Bellini, C., Bouchez, D., Caboche, M., and Benning, C. (1998). AGO1 defines a novel locus of Arabidopsis controlling leaf development. EMBO J *17*, 170-180.

Bohnsack, M.T., Czaplinski, K., and Gorlich, D. (2004). Exportin 5 is a RanGTP-dependent dsRNA-binding protein that mediates nuclear export of pre-miRNAs. RNA *10*, 185-191.

Borchert, G.M., Lanier, W., and Davidson, B.L. (2006). RNA polymerase III transcribes human microRNAs. Nat Struct Mol Biol *13*, 1097-1101.

Bosia, C., Pagnani, A., and Zecchina, R. (2013). Modelling Competing Endogenous RNA Networks. PloS one *8*, e66609.

Bosson, A.D., Zamudio, J.R., and Sharp, P.A. (2014). Endogenous miRNA and target concentrations determine susceptibility to potential ceRNA competition. Molecular cell *56*, 347-359.

Brancati, G., and Großhans, H. (2018). An interplay of miRNA abundance and target site architecture determines miRNA activity and specificity. Nucleic Acids Res *46*, 3259-3269.

Brangwynne, C.P. (2013). Phase transitions and size scaling of membrane-less organelles. J Cell Biol *203*, 875-881.

Brangwynne, C.P., Eckmann, C.R., Courson, D.S., Rybarska, A., Hoege, C., Gharakhani, J., Jülicher, F., and Hyman, A.A. (2009). Germline P Granules Are Liquid Droplets That Localize by Controlled Dissolution/Condensation. Science *324*, 1729.

Brangwynne, Clifford P., Tompa, P., and Pappu, Rohit V. (2015). Polymer physics of intracellular phase transitions. Nature Physics *11*, 899.

Braun, J.E., Huntzinger, E., Fauser, M., and Izaurralde, E. (2011). GW182 proteins directly recruit cytoplasmic deadenylase complexes to miRNA targets. Molecular cell *44*, 120-133.
Braun, J.E., Huntzinger, E., and Izaurralde, E. (2013). The Role of GW182 Proteins in miRNA-Mediated Gene Silencing. In Ten Years of Progress in GW/P Body Research, E.K.L. Chan, and M.J. Fritzler, eds. (New York, NY: Springer New York), pp. 147-163.

Brennan, C.M., and Steitz, J.A. (2001). HuR and mRNA stability. Cellular and molecular life sciences : CMLS *58*, 266-277.

Brennecke, J., Stark, A., Russell, R.B., and Cohen, S.M. (2005). Principles of microRNA-target recognition. PLoS Biol *3*, e85.

Broderick, J.A., Salomon, W.E., Ryder, S.P., Aronin, N., and Zamore, P.D. (2011). Argonaute protein identity and pairing geometry determine cooperativity in mammalian RNA silencing. RNA *17*, 1858-1869.

Broughton, James P., Lovci, Michael T., Huang, Jessica L., Yeo, Gene W., and Pasquinelli, Amy E. (2016). Pairing beyond the Seed Supports MicroRNA Targeting Specificity. Molecular cell *64*, 320-333.

Brown, K.C., Svendsen, J.M., Tucci, R.M., Montgomery, B.E., and Montgomery, T.A. (2017). ALG-5 is a miRNA-associated Argonaute required for proper developmental timing in the Caenorhabditis elegans germline. Nucleic Acids Res *45*, 9093-9107.

Cesana, M., Cacchiarelli, D., Legnini, I., Santini, T., Sthandier, O., Chinappi, M., Tramontano, A., and Bozzoni, I. (2011). A long noncoding RNA controls muscle differentiation by functioning as a competing endogenous RNA. Cell *147*, 358-369.

Chan, L.Y., Mugler, C.F., Heinrich, S., Vallotton, P., and Weis, K. (2018). Non-invasive measurement of mRNA decay reveals translation initiation as the major determinant of mRNA stability. Elife *7*, e32536.

Chandradoss, S.D., Schirle, N.T., Szczepaniak, M., MacRae, I.J., and Joo, C. (2015). A Dynamic Search Process Underlies MicroRNA Targeting. Cell *162*, 96-107.

Chang, C.T., Bercovich, N., Loh, B., Jonas, S., and Izaurralde, E. (2014). The activation of the decapping enzyme DCP2 by DCP1 occurs on the EDC4 scaffold and involves a conserved loop in DCP1. Nucleic Acids Res *42*, 5217-5233.

Chapat, C., Jafarnejad, S.M., Matta-Camacho, E., Hesketh, G.G., Gelbart, I.A., Attig, J., Gkogkas, C.G., Alain, T., Stern-Ginossar, N., Fabian, M.R.*, et al.* (2017). Cap-binding protein 4EHP effects translation silencing by microRNAs. Proc Natl Acad Sci U S A *114*, 5425-5430.

Chatterjee, S., and Groszhans, H. (2009). Active turnover modulates mature microRNA activity in Caenorhabditis elegans. Nature *461*, 546-549.
Chekulaeva, M., Mathys, H., Zipprich, J.T., Attig, J., Colic, M., Parker, R., and Filipowicz, W. (2011). miRNA repression involves GW182-mediated recruitment of CCR4-NOT through conserved W-containing motifs. Nat Struct Mol Biol *18*, 1218-1226.

Cheloufi, S., Dos Santos, C.O., Chong, M.M.W., and Hannon, G.J. (2010). A dicer-independent miRNA biogenesis pathway that requires Ago catalysis. Nature *465*, 584-589.

Chen, C.-Y.A., Ezzeddine, N., and Shyu, A.-B. (2008). Messenger RNA Half-Life Measurements in Mammalian Cells. Methods in enzymology *448*, 335-357.

Chen, C.-Y.A., and Shyu, A.-B. (2011). Mechanisms of deadenylation-dependent decay. Wiley interdisciplinary reviews RNA *2*, 167-183.

Chen, Y., Boland, A., Kuzuoğlu-Öztürk, D., Bawankar, P., Loh, B., Chang, C.-T., Weichenrieder, O., and Izaurralde, E. (2014). A DDX6-CNOT1 Complex and W-Binding Pockets in CNOT9 Reveal Direct Links between miRNA Target Recognition and Silencing. Molecular cell *54*, 737-750.

Chendrimada, T.P., Finn, K.J., Ji, X., Baillat, D., Gregory, R.I., Liebhaber, S.A., Pasquinelli, A.E., and Shiekhattar, R. (2007). MicroRNA silencing through RISC recruitment of eIF6. Nature *447*, 823-828.

Chi, S.W., Zang, J.B., Mele, A., and Darnell, R.B. (2009). Argonaute HITS-CLIP decodes microRNA–mRNA interaction maps. Nature *460*, 479-486.

Cho, P.F., Gamberi, C., Cho-Park, Y.A., Cho-Park, I.B., Lasko, P., and Sonenberg, N. (2006). Cap-dependent translational inhibition establishes two opposing morphogen gradients in Drosophila embryos. Curr Biol *16*, 2035-2041.

Cho, P.F., Poulin, F., Cho-Park, Y.A., Cho-Park, I.B., Chicoine, J.D., Lasko, P., and Sonenberg, N. (2005). A New Paradigm for Translational Control: Inhibition via 5′-3′ mRNA Tethering by Bicoid and the eIF4E Cognate 4EHP. Cell *121*, 411-423.

Christou-Kent, M., Kherraf, Z.-E., Amiri-Yekta, A., Le Blévec, E., Karaouzène, T., Conne, B., Escoffier, J., Assou, S., Guttin, A., Lambert, E*., et al.* (2018). PATL2 is a key actor of oocyte maturation whose invalidation causes infertility in women and mice. EMBO Molecular Medicine *10*, e8515.

Chu, C.Y., and Rana, T.M. (2006). Translation repression in human cells by microRNA-induced gene silencing requires RCK/p54. PLoS Biol *4*, e210.

Cogoni, C., and Macino, G. (1999). Gene silencing in Neurospora crassa requires a protein homologous to RNA-dependent RNA polymerase. Nature *399*, 166-169.

Coller, J., and Parker, R. (2005). General translational repression by activators of mRNA decapping. Cell *122*, 875-886.

Consortium, C.e.S. (1998). Genome sequence of the nematode C. elegans: a platform for investigating biology. Science *282*, 2012-2018.

Cooke, A., Prigge, A., and Wickens, M. (2010). Translational repression by deadenylases. J Biol Chem *285*, 28506-28513.

Cosentino, G.P., Schmelzle, T., Haghighat, A., Helliwell, S.B., Hall, M.N., and Sonenberg, N. (2000). Eap1p, a novel eukaryotic translation initiation factor 4E-associated protein in Saccharomyces cerevisiae. Molecular and cellular biology *20*, 4604-4613.

Cougot, N., Babajko, S., and Séraphin, B. (2004). Cytoplasmic foci are sites of mRNA decay in human cells. J Cell Biol *165*, 31-40.

Curtis, D., Treiber, D.K., Tao, F., Zamore, P.D., Williamson, J.R., and Lehmann, R. (1997). A CCHC metal-binding domain in Nanos is essential for translational regulation. EMBO J *16*, 834-843.

Dallaire, A., Frédérick, P.M., and Simard, M.J. (2018). Somatic and Germline MicroRNAs Form Distinct Silencing Complexes to Regulate Their Target mRNAs Differently. Dev Cell *47*, 239-247.e234.

Davis, G.M., Tu, S., Anderson, J.W.T., Colson, R.N., Gunzburg, M.J., Francisco, M.A., Ray, D., Shrubsole, S.P., Sobotka, J.A., Seroussi, U.*, et al.* (2018). The TRIM-NHL protein NHL-2 is a co-factor in the nuclear and somatic RNAi pathways in C. elegans. Elife *7*, e35478.

Deloche, O., de la Cruz, J., Kressler, D., Doère, M., and Linder, P. (2004). A membrane transport defect leads to a rapid attenuation of translation initiation in Saccharomyces cerevisiae. Molecular cell *13*, 357-366.

Denzler, R., Agarwal, V., Stefano, J., Bartel, D.P., and Stoffel, M. (2014). Assessing the ceRNA hypothesis with quantitative measurements of miRNA and target abundance. Molecular cell *54*, 766-776.

Derti, A., Garrett-Engele, P., Macisaac, K.D., Stevens, R.C., Sriram, S., Chen, R., Rohl, C.A., Johnson, J.M., and Babak, T. (2012). A quantitative atlas of polyadenylation in five mammals. Genome Res *22*, 1173-1183.

Didiano, D., and Hobert, O. (2008). Molecular architecture of a miRNA-regulated 3′ UTR. RNA *14*, 1297-1317.

Ding, L., Spencer, A., Morita, K., and Han, M. (2005). The Developmental Timing Regulator AIN-1 Interacts with miRISCs and May Target the Argonaute Protein ALG-1 to Cytoplasmic P Bodies in C. elegans. Molecular cell *19*, 437-447.

Dinkova, T.D., Keiper, B.D., Korneeva, N.L., Aamodt, E.J., and Rhoads, R.E. (2005). Translation of a small subset of Caenorhabditis elegans mRNAs is dependent on a specific eukaryotic translation initiation factor 4E isoform. Molecular and cellular biology *25*, 100-113.

Djuranovic, S., Nahvi, A., and Green, R. (2012). miRNA-Mediated Gene Silencing by Translational Repression Followed by mRNA Deadenylation and Decay. Science *336*, 237-240.

Doench, J.G., and Sharp, P.A. (2004). Specificity of microRNA target selection in translational repression. Genes & development *18*, 504-511.

Duchaine, T.F., and Fabian, M.R. (2019). Mechanistic Insights into MicroRNA-Mediated Gene Silencing. Cold Spring Harb Perspect Biol *11*.

Duchaine, T.F., Wohlschlegel, J.A., Kennedy, S., Bei, Y., Conte, D., Jr., Pang, K., Brownell, D.R., Harding, S., Mitani, S., Ruvkun, G.*, et al.* (2006). Functional proteomics reveals the biochemical niche of C. elegans DCR-1 in multiple small-RNA-mediated pathways. Cell *124*, 343-354.

Ebert, M.S., Neilson, J.R., and Sharp, P.A. (2007). MicroRNA sponges: competitive inhibitors of small RNAs in mammalian cells. Nature methods *4*, 721-726.

Ecsedi, M., Rausch, M., and Großhans, H. (2015). The let-7 microRNA directs vulval development through a single target. Dev Cell *32*, 335-344.

Edwalds-Gilbert, G., Veraldi, K.L., and Milcarek, C. (1997). Alternative poly(A) site selection in complex transcription units: means to an end? Nucleic Acids Res *25*, 2547-2561.

Eichhorn, S.W., Guo, H., McGeary, S.E., Rodriguez-Mias, R.A., Shin, C., Baek, D., Hsu, S.-H., Ghoshal, K., Villén, J., and Bartel, D.P. (2014). mRNA destabilization is the dominant effect of mammalian microRNAs by the time substantial repression ensues. Molecular cell *56*, 104-115.

Elkayam, E., Faehnle, C.R., Morales, M., Sun, J., Li, H., and Joshua-Tor, L. (2017). Multivalent Recruitment of Human Argonaute by GW182. Molecular cell *67*, 646-658.e643.

Eulalio, A., Behm-Ansmant, I., and Izaurralde, E. (2007a). P bodies: at the crossroads of post-transcriptional pathways. Nat Rev Mol Cell Biol *8*, 9.

Eulalio, A., Behm-Ansmant, I., Schweizer, D., and Izaurralde, E. (2007b). P-body formation is a consequence, not the cause, of RNA-mediated gene silencing. Molecular and cellular biology *27*, 3970-3981.

Eulalio, A., Huntzinger, E., and Izaurralde, E. (2008). Getting to the root of miRNA-mediated gene silencing. Cell *132*, 9-14.

Eulalio, A., Huntzinger, E., Nishihara, T., Rehwinkel, J., Fauser, M., and Izaurralde, E. (2009a). Deadenylation is a widespread effect of miRNA regulation. RNA *15*, 21-32.

Eulalio, A., Tritschler, F., and Izaurralde, E. (2009b). The GW182 protein family in animal cells: new insights into domains required for miRNA-mediated gene silencing. RNA *15*, 1433-1442.

Eystathioy, T., Chan, E.K., Tenenbaum, S.A., Keene, J.D., Griffith, K., and Fritzler, M.J. (2002). A phosphorylated cytoplasmic autoantigen, GW182, associates with a unique population of human mRNAs within novel cytoplasmic speckles. Mol Biol Cell *13*, 1338-1351.

Eystathioy, T., Jakymiw, A., Chan, E.K., Séraphin, B., Cougot, N., and Fritzler, M.J. (2003). The GW182 protein colocalizes with mRNA degradation associated proteins hDcp1 and hLSm4 in cytoplasmic GW bodies. RNA *9*, 1171-1173.

Fabian, M.R., Cieplak, M.K., Frank, F., Morita, M., Green, J., Srikumar, T., Nagar, B., Yamamoto, T., Raught, B., Duchaine, T.F., *et al.* (2011). miRNA-mediated deadenylation is orchestrated by GW182 through two conserved motifs that interact with CCR4-NOT. Nat Struct Mol Biol *18*, 1211-1217.

Fabian, M.R., Mathonnet, G., Sundermeier, T., Mathys, H., Zipprich, J.T., Svitkin, Y.V., Rivas, F., Jinek, M., Wohlschlegel, J., Doudna, J.A., *et al.* (2009). Mammalian miRNA RISC recruits CAF1 and PABP to affect PABP-dependent deadenylation. Molecular cell *35*, 868-880.

Fang, L., Du, W.W., Yang, X., Chen, K., Ghanekar, A., Levy, G., Yang, W., Yee, A.J., Lu, W.Y., Xuan, J.W., *et al.* (2013). Versican 3'-untranslated region (3'-UTR) functions as a ceRNA in inducing the development of hepatocellular carcinoma by regulating miRNA activity. FASEB J *27*, 907-919.

Ferraiuolo, M.A., Basak, S., Dostie, J., Murray, E.L., Schoenberg, D.R., and Sonenberg, N. (2005). A role for the eIF4E-binding protein 4E-T in P-body formation and mRNA decay. J Cell Biol *170*, 913-924.

Figliuzzi, M., Marinari, E., and De Martino, A. (2013). MicroRNAs as a selective channel of communication between competing RNAs: a steady-state theory. Biophysical journal *104*, 1203-1213.

Filipowicz, W., Bhattacharyya, S.N., and Sonenberg, N. (2008). Mechanisms of post-transcriptional regulation by microRNAs: are the answers in sight? Nature reviews Genetics *9*, 102-114.

Fire, A., Xu, S., Montgomery, M.K., Kostas, S.A., Driver, S.E., and Mello, C.C. (1998). Potent and specific genetic interference by double-stranded RNA in Caenorhabditis elegans. Nature *391*, 806-811.

Flamand, M.N., Gan, H.H., Mayya, V.K., Gunsalus, K.C., and Duchaine, T.F. (2017). A non-canonical site reveals the cooperative mechanisms of microRNA-mediated silencing. Nucleic Acids Res *45*, 7212-7225.

Flamand, M.N., Wu, E., Vashisht, A., Jannot, G., Keiper, B.D., Simard, M.J., Wohlschlegel, J., and Duchaine, T.F. (2016). Poly(A)-binding proteins are required for microRNA-mediated silencing and to promote target deadenylation in C. elegans. Nucleic Acids Res *44*, 5924-5935.

Förstemann, K., Horwich, M.D., Wee, L., Tomari, Y., and Zamore, P.D. (2007). Drosophila microRNAs are sorted into functionally distinct argonaute complexes after production by dicer-1. Cell *130*, 287-297.

Freimer, J.W., Hu, T.J., and Blelloch, R. (2018). Decoupling the impact of microRNAs on translational repression versus RNA degradation in embryonic stem cells. Elife *7*, e38014.

Freund, C., Dötsch, V., Nishizawa, K., Reinherz, E.L., and Wagner, G. (1999). The GYF domain is a novel structural fold that is involved in lymphoid signaling through proline-rich sequences. Nat Struct Mol Biol *6*, 656-660.

Friedman, R.C., Farh, K.K.-H., Burge, C.B., and Bartel, D.P. (2009). Most mammalian mRNAs are conserved targets of microRNAs. Genome Research *19*, 92-105.

Fromm, S.A., Kamenz, J., Nöldeke, E.R., Neu, A., Zocher, G., and Sprangers, R. (2014). In vitro reconstitution of a cellular phase-transition process that involves the mRNA decapping machinery. Angew Chem Int Ed Engl *53*, 7354-7359.

Gallie, D.R. (1991). The cap and poly(A) tail function synergistically to regulate mRNA translational efficiency. Genes & development *5*, 2108-2116.

Gallo, C.M., Munro, E., Rasoloson, D., Merritt, C., and Seydoux, G. (2008). Processing bodies and germ granules are distinct RNA granules that interact in C. elegans embryos. Dev Biol *323*, 76-87.

Gallo, C.M., Wang, J.T., Motegi, F., and Seydoux, G. (2010). Cytoplasmic partitioning of P granule components is not required to specify the germline in C. elegans. Science *330*, 1685-1689.

Garzia, A., Jafarnejad, S.M., Meyer, C., Chapat, C., Gogakos, T., Morozov, P., Amiri, M., Shapiro, M., Molina, H., Tuschl, T.*, et al.* (2017). The E3 ubiquitin ligase and RNA-binding protein ZNF598 orchestrates ribosome quality control of premature polyadenylated mRNAs. Nat Commun *8*, 16056-16056.
Gerstberger, S., Hafner, M., and Tuschl, T. (2014). A census of human RNA-binding proteins. Nature reviews Genetics *15*, 829-845.

Giovannone, B., Lee, E., Laviola, L., Giorgino, F., Cleveland, K.A., and Smith, R.J. (2003). Two novel proteins that are linked to insulin-like growth factor (IGF-I) receptors by the Grb10 adapter and modulate IGF-I signaling. J Biol Chem *278*, 31564-31573.

Giovannone, B., Tsiaras, W.G., de la Monte, S., Klysik, J., Lautier, C., Karashchuk, G., Goldwurm, S., and Smith, R.J. (2009). GIGYF2 gene disruption in mice results in neurodegeneration and altered insulin-like growth factor signaling. Hum Mol Genet *18*, 4629-4639.

Giraldez, A.J., Cinalli, R.M., Glasner, M.E., Enright, A.J., Thomson, J.M., Baskerville, S., Hammond, S.M., Bartel, D.P., and Schier, A.F. (2005). MicroRNAs Regulate Brain Morphogenesis in Zebrafish. Science *308*, 833.

Giraldez, A.J., Mishima, Y., Rihel, J., Grocock, R.J., Van Dongen, S., Inoue, K., Enright, A.J., and Schier, A.F. (2006). Zebrafish MiR-430 Promotes Deadenylation and Clearance of Maternal mRNAs. Science *312*, 75.

Goldstrohm, A.C., Hook, B.A., Seay, D.J., and Wickens, M. (2006). PUF proteins bind Pop2p to regulate messenger RNAs. Nat Struct Mol Biol *13*, 533-539.

Grimson, A., Farh, K.K.-H., Johnston, W.K., Garrett-Engele, P., Lim, L.P., and Bartel, D.P. (2007). MicroRNA Targeting Specificity in Mammals: Determinants Beyond Seed Pairing. Molecular cell *27*, 91-105.

Grishok, A., Pasquinelli, A.E., Conte, D., Li, N., Parrish, S., Ha, I., Baillie, D.L., Fire, A., Ruvkun, G., and Mello, C.C. (2001). Genes and mechanisms related to RNA interference regulate expression of the small temporal RNAs that control C. elegans developmental timing. Cell *106*, 23-34.

Grosswendt, S., Filipchyk, A., Manzano, M., Klironomos, F., Schilling, M., Herzog, M., Gottwein, E., and Rajewsky, N. (2014). Unambiguous identification of miRNA:target site interactions by different types of ligation reactions. Molecular cell *54*, 1042-1054.

Gu, S., Jin, L., Zhang, F., Sarnow, P., and Kay, M.A. (2009). Biological basis for restriction of microRNA targets to the 3' untranslated region in mammalian mRNAs. Nat Struct Mol Biol *16*, 144-150.

Guang, S., Bochner, A.F., Burkhart, K.B., Burton, N., Pavelec, D.M., and Kennedy, S. (2010). Small regulatory RNAs inhibit RNA polymerase II during the elongation phase of transcription. Nature *465*, 1097-1101.

Guil, S., and Cáceres, J.F. (2007). The multifunctional RNA-binding protein hnRNP A1 is required for processing of miR-18a. Nat Struct Mol Biol *14*, 591-596.
Guo, H., Ingolia, N.T., Weissman, J.S., and Bartel, D.P. (2010). Mammalian microRNAs predominantly act to decrease target mRNA levels. Nature *466*, 835-840.

Hafner, M., Landthaler, M., Burger, L., Khorshid, M., Hausser, J., Berninger, P., Rothballer, A., Ascano, M., Jr., Jungkamp, A.C., Munschauer, M.*, et al.* (2010). Transcriptome-wide identification of RNA-binding protein and microRNA target sites by PAR-CLIP. Cell *141*, 129-141.

Hafner, M., Renwick, N., Brown, M., Mihailovic, A., Holoch, D., Lin, C., Pena, J.T., Nusbaum, J.D., Morozov, P., Ludwig, J.*, et al.* (2011). RNA-ligase-dependent biases in miRNA representation in deep-sequenced small RNA cDNA libraries. RNA *17*, 1697-1712.

Hagan, J.P., Piskounova, E., and Gregory, R.I. (2009). Lin28 recruits the TUTase Zcchc11 to inhibit let-7 maturation in mouse embryonic stem cells. Nat Struct Mol Biol *16*, 1021-1025.

Haghighat, A., Mader, S., Pause, A., and Sonenberg, N. (1995). Repression of cap-dependent translation by 4E-binding protein 1: competition with p220 for binding to eukaryotic initiation factor-4E. EMBO J *14*, 5701-5709.

Hahn, W.C., and Bierer, B.E. (1993). Separable portions of the CD2 cytoplasmic domain involved in signaling and ligand avidity regulation. J Exp Med *178*, 1831-1836.

Hall, T.M.T. (2016). De-coding and re-coding RNA recognition by PUF and PPR repeat proteins. Current Opinion in Structural Biology *36*, 116-121.

Hammell, C.M., Karp, X., and Ambros, V. (2009a). A feedback circuit involving let-7-family miRNAs and DAF-12 integrates environmental signals and developmental timing in Caenorhabditis elegans. Proc Natl Acad Sci U S A *106*, 18668-18673.

Hammell, C.M., Lubin, I., Boag, P.R., Blackwell, T.K., and Ambros, V. (2009b). nhl-2 Modulates microRNA activity in Caenorhabditis elegans. Cell *136*, 926-938.

Han, Tina W., Kato, M., Xie, S., Wu, Leeju C., Mirzaei, H., Pei, J., Chen, M., Xie, Y., Allen, J., Xiao, G.*, et al.* (2012). Cell-free Formation of RNA Granules: Bound RNAs Identify Features and Components of Cellular Assemblies. Cell *149*, 768-779.

Heinze, M., Kofler, M., and Freund, C. (2007). Investigating the functional role of CD2BP2 in T cells. International Immunology *19*, 1313-1318.

Hentze, M.W., Castello, A., Schwarzl, T., and Preiss, T. (2018). A brave new world of RNA-binding proteins. Nature Reviews Molecular Cell Biology *19*, 327.

Heo, I., Joo, C., Kim, Y.-K., Ha, M., Yoon, M.-J., Cho, J., Yeom, K.-H., Han, J., and Kim, V.N. (2009). TUT4 in Concert with Lin28 Suppresses MicroRNA Biogenesis through Pre-MicroRNA Uridylation. Cell *138*, 696-708.
Hesse, M., and Arenz, C. (2014). MicroRNA maturation and human disease. Methods Mol Biol *1095*, 11-25.

Hilgers, V., Perry, M.W., Hendrix, D., Stark, A., Levine, M., and Haley, B. (2011). Neural-specific elongation of 3′ UTRs during *Drosophila* development. Proc Natl Acad Sci U S A *108*, 15864-15869.

Hondele, M., Sachdev, R., Heinrich, S., Wang, J., Vallotton, P., Fontoura, B.M.A., and Weis, K. (2019). DEAD-box ATPases are global regulators of phase-separated organelles. Nature *573*, 144-148.

Hoque, M., Ji, Z., Zheng, D., Luo, W., Li, W., You, B., Park, J.Y., Yehia, G., and Tian, B. (2012). Analysis of alternative cleavage and polyadenylation by 3′ region extraction and deep sequencing. Nature Methods *10*, 133.

Horvathova, I., Voigt, F., Kotrys, A.V., Zhan, Y., Artus-Revel, C.G., Eglinger, J., Stadler, M.B., Giorgetti, L., and Chao, J.A. (2017). The Dynamics of mRNA Turnover Revealed by Single-Molecule Imaging in Single Cells. Molecular cell *68*, 615-625.e619.

Hubstenberger, A., Cameron, C., Noble, S.L., Keenan, S., and Evans, T.C. (2015). Modifiers of solid RNP granules control normal RNP dynamics and mRNA activity in early development. J Cell Biol *211*, 703-716.

Hubstenberger, A., Courel, M., Bénard, M., Souquere, S., Ernoult-Lange, M., Chouaib, R., Yi, Z., Morlot, J.-B., Munier, A., Fradet, M.*, et al.* (2017). P-Body Purification Reveals the Condensation of Repressed mRNA Regulons. Molecular cell *68*, 144-157.e145.

Huch, S., and Nissan, T. (2014). Interrelations between translation and general mRNA degradation in yeast. WIREs RNA *5*, 747-763.

Humphreys, D.T., Westman, B.J., Martin, D.I., and Preiss, T. (2005). MicroRNAs control translation initiation by inhibiting eukaryotic initiation factor 4E/cap and poly(A) tail function. Proc Natl Acad Sci U S A *102*, 16961-16966.

Huntzinger, E., Kuzuoğlu-Öztürk, D., Braun, J.E., Eulalio, A., Wohlbold, L., and Izaurralde, E. (2013). The interactions of GW182 proteins with PABP and deadenylases are required for both translational repression and degradation of miRNA targets. Nucleic Acids Res *41*, 978-994.

Hurschler, B.A., Harris, D.T., and Grosshans, H. (2011). The type II poly(A)-binding protein PABP-2 genetically interacts with the let-7 miRNA and elicits heterochronic phenotypes in Caenorhabditis elegans. Nucleic Acids Res *39*, 5647-5657.

Hutvagner, G., McLachlan, J., Pasquinelli, A.E., Balint, E., Tuschl, T., and Zamore, P.D. (2001). A cellular function for the RNA-interference enzyme Dicer in the maturation of the let-7 small temporal RNA. Science *293*, 834-838.

Hutvagner, G., and Simard, M.J. (2008). Argonaute proteins: key players in RNA silencing. Nat Rev Mol Cell Biol *9*, 22-32.

Hutvagner, G., Simard, M.J., Mello, C.C., and Zamore, P.D. (2004). Sequence-specific inhibition of small RNA function. PLoS Biol *2*, E98.

Hutvagner, G., and Zamore, P.D. (2002). A microRNA in a multiple-turnover RNAi enzyme complex. Science *297*, 2056-2060.

Hyenne, V., Desrosiers, M., and Labbe, J.C. (2008). C. elegans Brat homologs regulate PAR protein-dependent polarity and asymmetric cell division. Dev Biol *321*, 368-378.

Hyman, A.A., Weber, C.A., and Jülicher, F. (2014). Liquid-Liquid Phase Separation in Biology. Annual Review of Cell and Developmental Biology *30*, 39-58.

Ibáñez-Ventoso, C., Vora, M., and Driscoll, M. (2008). Sequence relationships among C. elegans, D. melanogaster and human microRNAs highlight the extensive conservation of microRNAs in biology. PloS one *3*, e2818.

Ilbay, O., and Ambros, V. (2019). Pheromones and Nutritional Signals Regulate the Developmental Reliance on let-7 Family MicroRNAs in C. elegans. Curr Biol *29*, 1735-1745.e1734.

Ingelfinger, D., Arndt-Jovin, D.J., Lührmann, R., and Achsel, T. (2002). The human LSm1-7 proteins colocalize with the mRNA-degrading enzymes Dcp1/2 and Xrnl in distinct cytoplasmic foci. RNA *8*, 1489-1501.

Iwakawa, H.-o., and Tomari, Y. (2015). The Functions of MicroRNAs: mRNA Decay and Translational Repression. Trends in Cell Biology *25*, 651-665.

Jacobs, E., Mills, J.D., and Janitz, M. (2012). The Role of RNA Structure in Posttranscriptional Regulation of Gene Expression. Journal of Genetics and Genomics *39*, 535-543.

Jafarnejad, S.M., Chapat, C., Matta-Camacho, E., Gelbart, I.A., Hesketh, G.G., Arguello, M., Garzia, A., Kim, S.-H., Attig, J., Shapiro, M.*, et al.* (2018). Translational control of ERK signaling through miRNA/4EHP-directed silencing. Elife *7*, e35034.

Jakymiw, A., Lian, S., Eystathioy, T., Li, S., Satoh, M., Hamel, J.C., Fritzler, M.J., and Chan, E.K. (2005). Disruption of GW bodies impairs mammalian RNA interference. Nature cell biology *7*, 1267-1274.

Jan, C.H., Friedman, R.C., Ruby, J.G., and Bartel, D.P. (2011). Formation, Regulation and Evolution of Caenorhabditis elegans 3′UTRs. Nature *469*, 97-101.

Janas, M.M., Wang, B., Harris, A.S., Aguiar, M., Shaffer, J.M., Subrahmanyam, Y.V., Behlke, M.A., Wucherpfennig, K.W., Gygi, S.P., Gagnon, E.*, et al.* (2012). Alternative RISC assembly: binding and repression of microRNA-mRNA duplexes by human Ago proteins. RNA *18*, 2041-2055.

Jannot, G., Vasquez-Rifo, A., and Simard, M.J. (2011). Argonaute pull-down and RISC analysis using 2'-O-methylated oligonucleotides affinity matrices. Methods Mol Biol *725*, 233-249.

Ji, Z., Lee, J.Y., Pan, Z., Jiang, B., and Tian, B. (2009). Progressive lengthening of 3' untranslated regions of mRNAs by alternative polyadenylation during mouse embryonic development. Proc Natl Acad Sci U S A *106*, 7028-7033.

Jiang, P., and Coller, H. (2012). Functional interactions between microRNAs and RNA binding proteins. Microrna *1*, 70-79.

Jiang, P., Singh, M., and Coller, H.A. (2013). Computational assessment of the cooperativity between RNA binding proteins and MicroRNAs in Transcript Decay. PLoS Comput Biol *9*, e1003075.

Jing, Q., Huang, S., Guth, S., Zarubin, T., Motoyama, A., Chen, J., Di Padova, F., Lin, S.-C., Gram, H., and Han, J. (2005). Involvement of MicroRNA in AU-Rich Element-Mediated mRNA Instability. Cell *120*, 623-634.

Johnston, R.J., and Hobert, O. (2003). A microRNA controlling left/right neuronal asymmetry in Caenorhabditis elegans. Nature *426*, 845-849.

Jonas, S., and Izaurralde, E. (2013). The role of disordered protein regions in the assembly of decapping complexes and RNP granules. Genes & development *27*, 2628-2641.

Jonas, S., and Izaurralde, E. (2015). Towards a molecular understanding of microRNA-mediated gene silencing. Nature Reviews Genetics *16*, 421-433.

Joshi, B., Cameron, A., and Jagus, R. (2004). Characterization of mammalian eIF4E-family members. European journal of biochemistry *271*, 2189-2203.

Kadyrova, L.Y., Habara, Y., Lee, T.H., and Wharton, R.P. (2007). Translational control of maternal *Cyclin B* mRNA by Nanos in the *Drosophila* germline. Development *134*, 1519-1527.

Kakumani, P.K., Harvey, L.M., Houle, F., Guitart, T., Gebauer, F., and Simard, M.J. (2020). CSDE1 controls gene expression through the miRNA-mediated decay machinery. Life Sci Alliance *3*.

Kallen, A.N., Zhou, X.B., Xu, J., Qiao, C., Ma, J., Yan, L., Lu, L., Liu, C., Yi, J.S., Zhang, H.*, et al.* (2013). The imprinted H19 lncRNA antagonizes let-7 microRNAs. Molecular cell *52*, 101-112.

Kamenska, A., Simpson, C., Vindry, C., Broomhead, H., Benard, M., Ernoult-Lange, M., Lee, B.P., Harries, L.W., Weil, D., and Standart, N. (2016). The DDX6-4E-T interaction mediates translational repression and P-body assembly. Nucleic Acids Res *44*, 6318-6334.

Karp, X., Hammell, M., Ow, M.C., and Ambros, V. (2011). Effect of life history on microRNA expression during C. elegans development. RNA *17*, 639-651.

Kato, M., Han, Tina W., Xie, S., Shi, K., Du, X., Wu, Leeju C., Mirzaei, H., Goldsmith, Elizabeth J., Longgood, J., Pei, J.*, et al.* (2012). Cell-free Formation of RNA Granules: Low Complexity Sequence Domains Form Dynamic Fibers within Hydrogels. Cell *149*, 753-767.

Kaur, G., and Dufour, J.M. (2012). Cell lines: Valuable tools or useless artifacts. Spermatogenesis *2*, 1-5.

Kedde, M., van Kouwenhove, M., Zwart, W., Oude Vrielink, J.A., Elkon, R., and Agami, R. (2010). A Pumilio-induced RNA structure switch in p27-3' UTR controls miR-221 and miR-222 accessibility. Nature cell biology *12*, 1014-1020.

Kedersha, N., and Anderson, P. (2007). Mammalian Stress Granules and Processing Bodies. In Methods in Enzymology (Academic Press), pp. 61-81.

Keppler, A., Kindermann, M., Gendreizig, S., Pick, H., Vogel, H., and Johnsson, K. (2004). Labeling of fusion proteins of O6-alkylguanine-DNA alkyltransferase with small molecules in vivo and in vitro. Methods *32*, 437-444.

Kershner, A.M., and Kimble, J. (2010). Genome-wide analysis of mRNA targets for *Caenorhabditis elegans* FBF, a conserved stem cell regulator. Proc Natl Acad Sci U S A *107*, 3936-3941.

Ketting, R.F., Fischer, S.E., Bernstein, E., Sijen, T., Hannon, G.J., and Plasterk, R.H. (2001). Dicer functions in RNA interference and in synthesis of small RNA involved in developmental timing in C. elegans. Genes & development *15*, 2654-2659.

Khvorova, A., Reynolds, A., and Jayasena, S.D. (2003). Functional siRNAs and miRNAs exhibit strand bias. Cell *115*, 209-216.

Kim, H.H., Kuwano, Y., Srikantan, S., Lee, E.K., Martindale, J.L., and Gorospe, M. (2009). HuR recruits let-7/RISC to repress c-Myc expression. Genes & development *23*, 1743-1748.

Klum, S.M., Chandradoss, S.D., Schirle, N.T., Joo, C., and MacRae, I.J. (2018). Helix-7 in Argonaute2 shapes the microRNA seed region for rapid target recognition. EMBO J *37*, 75-88.
Knight, S.W., and Bass, B.L. (2001). A role for the RNase III enzyme DCR-1 in RNA interference and germ line development in *Caenorhabditis elegans*. Science *293*, 2269-2271.

Kodoyianni, V., Maine, E.M., and Kimble, J. (1992). Molecular basis of loss-of-function mutations in the glp-1 gene of Caenorhabditis elegans. Mol Biol Cell *3*, 1199-1213.

Kofler, M., Heuer, K., Zech, T., and Freund, C. (2004). Recognition sequences for the GYF domain reveal a possible spliceosomal function of CD2BP2. J Biol Chem *279*, 28292-28297.

Kofler, M., Motzny, K., Beyermann, M., and Freund, C. (2005a). Novel interaction partners of the CD2BP2-GYF domain. J Biol Chem *280*, 33397-33402.

Kofler, M., Motzny, K., and Freund, C. (2005b). GYF Domain Proteomics Reveals Interaction Sites in Known and Novel Target Proteins. Molecular & Cellular Proteomics *4*, 1797-1811.

Kofler, M.M., and Freund, C. (2006). The GYF domain. The FEBS Journal *273*, 245-256.

Koscianska, E., Witkos, T.M., Kozlowska, E., Wojciechowska, M., and Krzyzosiak, W.J. (2015). Cooperation meets competition in microRNA-mediated DMPK transcript regulation. Nucleic Acids Res *43*, 9500-9518.

Kozomara, A., Birgaoanu, M., and Griffiths-Jones, S. (2018). miRBase: from microRNA sequences to function. Nucleic Acids Res *47*, D155-D162.

Kraemer, B., Crittenden, S., Gallegos, M., Moulder, G., Barstead, R., Kimble, J., and Wickens, M. (1999). NANOS-3 and FBF proteins physically interact to control the sperm–oocyte switch in Caenorhabditis elegans. Current Biology *9*, 1009-1018.

Krämer, A. (1992). Purification of splicing factor SF1, a heat-stable protein that functions in the assembly of a presplicing complex. Molecular and cellular biology *12*, 4545-4552.

Kryszke, M.H., Adjeriou, B., Liang, F., Chen, H., and Dautry, F. (2016). Post-transcriptional gene silencing activity of human GIGYF2. Biochem Biophys Res Commun *475*, 289-294.

Kudryashova, E., Kudryashov, D., Kramerova, I., and Spencer, M.J. (2005). Trim32 is a ubiquitin ligase mutated in limb girdle muscular dystrophy type 2H that binds to skeletal muscle myosin and ubiquitinates actin. Journal of Molecular Biology *354*, 413-424.

Kundu, P., Fabian, M.R., Sonenberg, N., Bhattacharyya, S.N., and Filipowicz, W. (2012). HuR protein attenuates miRNA-mediated repression by promoting miRISC dissociation from the target RNA. Nucleic Acids Res *40*, 5088-5100.

Kwok, C.K., Tang, Y., Assmann, S.M., and Bevilacqua, P.C. (2015). The RNA structurome: transcriptome-wide structure probing with next-generation sequencing. Trends in Biochemical Sciences *40*, 221-232.

La Rocca, G., Olejniczak, S.H., Gonzalez, A.J., Briskin, D., Vidigal, J.A., Spraggon, L., DeMatteo, R.G., Radler, M.R., Lindsten, T., Ventura, A.*, et al.* (2015). In vivo, Argonaute-bound microRNAs exist predominantly in a reservoir of low molecular weight complexes not associated with mRNA. Proc Natl Acad Sci U S A.

Lagos-Quintana, M., Rauhut, R., Lendeckel, W., and Tuschl, T. (2001). Identification of novel genes coding for small expressed RNAs. Science *294*, 853-858.

Lai, E.C., Tam, B., and Rubin, G.M. (2005). Pervasive regulation of Drosophila Notch target genes by GY-box-, Brd-box-, and K-box-class microRNAs. Genes & development *19*, 1067-1080.

Lai, W.S., Carballo, E., Thorn, J.M., Kennington, E.A., and Blackshear, P.J. (2000). Interactions of CCCH Zinc Finger Proteins with mRNA: binding of Tristetraprolin-related Zinc FInger proteins to AU-rich elements and destabilization of mRNA. Journal of Biological Chemistry *275*, 17827-17837.

Landgraf, P., Rusu, M., Sheridan, R., Sewer, A., Iovino, N., Aravin, A., Pfeffer, S., Rice, A., Kamphorst, A.O., Landthaler, M.*, et al.* (2007). A mammalian microRNA expression atlas based on small RNA library sequencing. Cell *129*, 1401-1414.

Lapointe, C.P., Preston, M.A., Wilinski, D., Saunders, H.A.J., Campbell, Z.T., and Wickens, M. (2017). Architecture and dynamics of overlapped RNA regulatory networks. RNA *23*, 1636-1647.

Lapointe, C.P., Wilinski, D., Saunders, H.A., and Wickens, M. (2015). Protein-RNA networks revealed through covalent RNA marks. Nat Methods *12*, 1163-1170.

Lau, N.C., Lim, L.P., Weinstein, E.G., and Bartel, D.P. (2001). An abundant class of tiny RNAs with probable regulatory roles in Caenorhabditis elegans. Science *294*, 858-862.

Laver, J.D., Li, X., Ray, D., Cook, K.B., Hahn, N.A., Nabeel-Shah, S., Kekis, M., Luo, H., Marsolais, A.J., Fung, K.Y.*, et al.* (2015). Brain tumor is a sequence-specific RNA-binding protein that directs maternal mRNA clearance during the Drosophila maternal-to-zygotic transition. Genome Biology *16*, 94.

Lazzaretti, D., Tournier, I., and Izaurralde, E. (2009). The C-terminal domains of human TNRC6A, TNRC6B, and TNRC6C silence bound transcripts independently of Argonaute proteins. RNA *15*, 1059-1066.

Lee, C.-Y.S., Putnam, A., Lu, T., He, S., Ouyang, J.P.T., and Seydoux, G. (2020). Recruitment of mRNAs to P granules by condensation with intrinsically-disordered proteins. Elife *9*, e52896.
Lee, L.W., Zhang, S., Etheridge, A., Ma, L., Martin, D., Galas, D., and Wang, K. (2010). Complexity of the microRNA repertoire revealed by next-generation sequencing. Rna *16*, 2170-2180.

Lee, R.C., and Ambros, V. (2001). An extensive class of small RNAs in Caenorhabditis elegans. Science *294*, 862-864.

Lee, R.C., Feinbaum, R.L., and Ambros, V. (1993). The C. elegans heterochronic gene lin-4 encodes small RNAs with antisense complementarity to lin-14. Cell *75*, 843-854.

Lee, S., Kopp, F., Chang, T.C., Sataluri, A., Chen, B., Sivakumar, S., Yu, H., Xie, Y., and Mendell, J.T. (2016). Noncoding RNA NORAD Regulates Genomic Stability by Sequestering PUMILIO Proteins. Cell *164*, 69-80.

Lee, Y., Ahn, C., Han, J., Choi, H., Kim, J., Yim, J., Lee, J., Provost, P., Rådmark, O., Kim, S.*, et al.* (2003). The nuclear RNase III Drosha initiates microRNA processing. Nature *425*, 415-419.

Lee, Y., Jeon, K., Lee, J.-T., Kim, S., and Kim, V.N. (2002). MicroRNA maturation: stepwise processing and subcellular localization. EMBO J *21*, 4663-4670.

Lee, Y., Kim, M., Han, J., Yeom, K.H., Lee, S., Baek, S.H., and Kim, V.N. (2004). MicroRNA genes are transcribed by RNA polymerase II. EMBO J *23*, 4051-4060.

Leung, A.K., Young, A.G., Bhutkar, A., Zheng, G.X., Bosson, A.D., Nielsen, C.B., and Sharp, P.A. (2011). Genome-wide identification of Ago2 binding sites from mouse embryonic stem cells with and without mature microRNAs. Nat Struct Mol Biol *18*, 237-244.

Lewis, B.P., Burge, C.B., and Bartel, D.P. (2005). Conserved seed pairing, often flanked by adenosines, indicates that thousands of human genes are microRNA targets. Cell *120*, 15-20.

Lewis, B.P., Shih, I.H., Jones-Rhoades, M.W., Bartel, D.P., and Burge, C.B. (2003). Prediction of mammalian microRNA targets. Cell *115*, 787-798.

Li, P., Banjade, S., Cheng, H.C., Kim, S., Chen, B., Guo, L., Llaguno, M., Hollingsworth, J.V., King, D.S., Banani, S.F.*, et al.* (2012). Phase transitions in the assembly of multivalent signalling proteins. Nature *483*, 336-340.

Li, X., Cassidy, J.J., Reinke, C.A., Fischboeck, S., and Carthew, R.W. (2009). A microRNA imparts robustness against environmental fluctuation during development. Cell *137*, 273-282.

Li, Y., and Zhang, C.-y. (2012). Analysis of MicroRNA-Induced Silencing Complex-Involved MicroRNA-Target Recognition by Single-Molecule Fluorescence Resonance Energy Transfer. Analytical Chemistry *84*, 5097-5102.
Lianoglou, S., Garg, V., Yang, J.L., Leslie, C.S., and Mayr, C. (2013). Ubiquitously transcribed genes use alternative polyadenylation to achieve tissue-specific expression. Genes & development *27*, 2380-2396.

Lim, L.P., Lau, N.C., Garrett-Engele, P., Grimson, A., Schelter, J.M., Castle, J., Bartel, D.P., Linsley, P.S., and Johnson, J.M. (2005). Microarray analysis shows that some microRNAs downregulate large numbers of target mRNAs. Nature *433*, 769-773.

Lim, L.P., Lau, N.C., Weinstein, E.G., Abdelhakim, A., Yekta, S., Rhoades, M.W., Burge, C.B., and Bartel, D.P. (2003). The microRNAs of Caenorhabditis elegans. Genes & development *17*, 991-1008.

Lin, Y., Protter, David S.W., Rosen, Michael K., and Parker, R. (2015). Formation and Maturation of Phase-Separated Liquid Droplets by RNA-Binding Proteins. Molecular cell *60*, 208-219.

Ling, S., Birnbaum, Y., Nanhwan, M.K., Thomas, B., Bajaj, M., and Ye, Y. (2013). MicroRNA-dependent cross-talk between VEGF and HIF1alpha in the diabetic retina. Cellular signalling *25*, 2840-2847.

Linsen, S.E.V., de Wit, E., Janssens, G., Heater, S., Chapman, L., Parkin, R.K., Fritz, B., Wyman, S.K., de Bruijn, E., Voest, E.E.*, et al.* (2009). Limitations and possibilities of small RNA digital gene expression profiling. Nat Meth *6*, 474-476.

Little, S.C., Sinsimer, K.S., Lee, J.J., Wieschaus, E.F., and Gavis, E.R. (2015). Independent and coordinate trafficking of single Drosophila germ plasm mRNAs. Nature cell biology *17*, 558.

Liu, J., Carmell, M.A., Rivas, F.V., Marsden, C.G., Thomson, J.M., Song, J.J., Hammond, S.M., Joshua-Tor, L., and Hannon, G.J. (2004). Argonaute2 is the catalytic engine of mammalian RNAi. Science *305*, 1437-1441.

Liu, J., Rivas, F.V., Wohlschlegel, J., Yates, J.R., 3rd, Parker, R., and Hannon, G.J. (2005). A role for the P-body component GW182 in microRNA function. Nature cell biology *7*, 1261-1266.

Liu, M., Liu, P., Zhang, L., Cai, Q., Gao, G., Zhang, W., Zhu, Z., Liu, D., and Fan, Q. (2011). mir-35 is involved in intestine cell G1/S transition and germ cell proliferation in C. elegans. Cell Res *21*, 1605-1618.

Loeb, G.B., Khan, A.A., Canner, D., Hiatt, J.B., Shendure, J., Darnell, R.B., Leslie, C.S., and Rudensky, A.Y. (2012). Transcriptome-wide miR-155 binding map reveals widespread noncanonical microRNA targeting. Molecular cell *48*, 760-770.

Loedige, I., Jakob, L., Treiber, T., Ray, D., Stotz, M., Treiber, N., Hennig, J., Cook, K.B., Morris, Q., Hughes, T.R.*, et al.* (2015). The Crystal Structure of the NHL Domain in Complex with RNA Reveals the Molecular Basis of Drosophila Brain-Tumor-Mediated Gene Regulation. Cell Reports *13*, 1206-1220.

Loedige, I., Stotz, M., Qamar, S., Kramer, K., Hennig, J., Schubert, T., Löffler, P., Längst, G., Merkl, R., Urlaub, H.*, et al.* (2014). The NHL domain of BRAT is an RNA-binding domain that directly contacts the hunchback mRNA for regulation. Genes & development *28*, 749-764.

Lund, E., Guttinger, S., Calado, A., Dahlberg, J.E., and Kutay, U. (2004). Nuclear export of microRNA precursors. Science *303*, 95-98.

Lunde, B.M., Moore, C., and Varani, G. (2007). RNA-binding proteins: modular design for efficient function. Nature Reviews Molecular Cell Biology *8*, 479-490.

Lykke-Andersen, J., and Wagner, E. (2005). Recruitment and activation of mRNA decay enzymes by two ARE-mediated decay activation domains in the proteins TTP and BRF-1. Genes & development *19*, 351-361.

Ma, W.-J., Cheng, S., Campbell, C., Wright, A., and Furneaux, H. (1996). Cloning and Characterization of HuR, a Ubiquitously Expressed Elav-like Protein. Journal of Biological Chemistry *271*, 8144-8151.

Ma, W.K., Cloutier, S.C., and Tran, E.J. (2013). The DEAD-box protein Dbp2 functions with the RNA-binding protein Yra1 to promote mRNP assembly. Journal of molecular biology *425*, 3824-3838.

Marnef, A., Maldonado, M., Bugaut, A., Balasubramanian, S., Kress, M., Weil, D., and Standart, N. (2010). Distinct functions of maternal and somatic Pat1 protein paralogs. RNA *16*, 2094-2107.

Marnik, E.A., Fuqua, J.H., Sharp, C.S., Rochester, J.D., Xu, E.L., Holbrook, S.E., and Updike, D.L. (2019). Germline Maintenance Through the Multifaceted Activities of GLH/Vasa in *Caenorhabditis elegans* P Granules. Genetics *213*, 923-939.

Mathonnet, G., Fabian, M.R., Svitkin, Y.V., Parsyan, A., Huck, L., Murata, T., Biffo, S., Merrick, W.C., Darzynkiewicz, E., Pillai, R.S.*, et al.* (2007). MicroRNA Inhibition of Translation Initiation in Vitro by Targeting the Cap-Binding Complex eIF4F. Science *317*, 1764-1767.

Mathys, H., Basquin, J., Ozgur, S., Czarnocki-Cieciura, M., Bonneau, F., Aartse, A., Dziembowski, A., Nowotny, M., Conti, E., and Filipowicz, W. (2014). Structural and Biochemical Insights to the Role of the CCR4-NOT Complex and DDX6 ATPase in MicroRNA Repression. Molecular cell *54*, 751-765.

Matsuo, R., Kubota, H., Obata, T., Kito, K., Ota, K., Kitazono, T., Ibayashi, S., Sasaki, T., Iida, M., and Ito, T. (2005). The yeast eIF4E-associated protein Eap1p attenuates GCN4 translation upon TOR-inactivation. FEBS Lett *579*, 2433-2438.

Mayr, C., and Bartel, D.P. (2009). Widespread shortening of 3'UTRs by alternative cleavage and polyadenylation activates oncogenes in cancer cells. Cell *138*, 673-684.

Mayya, V.K., and Duchaine, T.F. (2019). Ciphers and Executioners: How 3'-Untranslated Regions Determine the Fate of Messenger RNAs. Front Genet *10*, 6-6.

Mayya, V.K., Flamand, M.N., Lambert, A.M., Jafarnejad, S.M., Wohlschlegel, J.A., Sonenberg, N., and Duchaine, T.F. (2021). microRNA-mediated translation repression through GYF-1 and IFE-4 in C. elegans development. Nucleic Acids Res.

McCutchen-Maloney, S.L., Matsuda, K., Shimbara, N., Binns, D.D., Tanaka, K., Slaughter, C.A., and DeMartino, G.N. (2000). cDNA cloning, expression, and functional characterization of PI31, a proline-rich inhibitor of the proteasome. J Biol Chem *275*, 18557-18565.

McJunkin, K., and Ambros, V. (2014). The embryonic mir-35 family of microRNAs promotes multiple aspects of fecundity in Caenorhabditis elegans. G3 (Bethesda) *4*, 1747-1754.

Meister, G., Landthaler, M., Patkaniowska, A., Dorsett, Y., Teng, G., and Tuschl, T. (2004). Human Argonaute2 mediates RNA cleavage targeted by miRNAs and siRNAs. Mol Cell *15*, 185-197.

Melnikov, A., Murugan, A., Zhang, X., Tesileanu, T., Wang, L., Rogov, P., Feizi, S., Gnirke, A., Callan Jr, C.G., Kinney, J.B.*, et al.* (2012). Systematic dissection and optimization of inducible enhancers in human cells using a massively parallel reporter assay. Nature Biotechnology *30*, 271.

Memczak, S., Jens, M., Elefsinioti, A., Torti, F., Krueger, J., Rybak, A., Maier, L., Mackowiak, S.D., Gregersen, L.H., Munschauer, M.*, et al.* (2013). Circular RNAs are a large class of animal RNAs with regulatory potency. Nature *495*, 333-338.

Minshall, N., Kress, M., Weil, D., and Standart, N. (2009). Role of p54 RNA helicase activity and its C-terminal domain in translational repression, P-body localization and assembly. Mol Biol Cell *20*, 2464-2472.

Mishima, Y., Giraldez, A.J., Takeda, Y., Fujiwara, T., Sakamoto, H., Schier, A.F., and Inoue, K. (2006). Differential regulation of germline mRNAs in soma and germ cells by zebrafish miR-430. Curr Biol *16*, 2135-2142.

Miura, P., Shenker, S., Andreu-Agullo, C., Westholm, J.O., and Lai, E.C. (2013). Widespread and extensive lengthening of 3′ UTRs in the mammalian brain. Genome Research *23*, 812-825.

Molliex, A., Temirov, J., Lee, J., Coughlin, M., Kanagaraj, A.P., Kim, H.J., Mittag, T., and Taylor, J.P. (2015). Phase separation by low complexity domains promotes stress granule assembly and drives pathological fibrillization. Cell *163*, 123-133.

Moretti, F., Kaiser, C., Zdanowicz-Specht, A., and Hentze, M.W. (2012). PABP and the poly(A) tail augment microRNA repression by facilitated miRISC binding. Nat Struct Mol Biol *19*, 603.

Morita, M., Ler, L.W., Fabian, M.R., Siddiqui, N., Mullin, M., Henderson, V.C., Alain, T., Fonseca, B.D., Karashchuk, G., Bennett, C.F.*, et al.* (2012). A novel 4EHP-GIGYF2 translational repressor complex is essential for mammalian development. Molecular and cellular biology *32*, 3585-3593.

Moss, E.G., Lee, R.C., and Ambros, V. (1997). The Cold Shock Domain protein LIN-28 controls developmental timing in *C. elegans* and is regulated by the *lin-4* RNA. Cell *88*, 637-646.

Mourelatos, Z., Dostie, J., Paushkin, S., Sharma, A., Charroux, B., Abel, L., Rappsilber, J., Mann, M., and Dreyfuss, G. (2002). miRNPs: a novel class of ribonucleoproteins containing numerous microRNAs. Genes & development *16*, 720-728.

Mu, P., Han, Y.C., Betel, D., Yao, E., Squatrito, M., Ogrodowski, P., de Stanchina, E., D'Andrea, A., Sander, C., and Ventura, A. (2009). Genetic dissection of the miR-17~92 cluster of microRNAs in Myc-induced B-cell lymphomas. Genes & development *23*, 2806-2811.

Mugler, C.F., Hondele, M., Heinrich, S., Sachdev, R., Vallotton, P., Koek, A.Y., Chan, L.Y., and Weis, K. (2016). ATPase activity of the DEAD-box protein Dhh1 controls processing body formation. Elife *5*, e18746.

Mukherjee, N., Corcoran, D.L., Nusbaum, J.D., Reid, D.W., Georgiev, S., Hafner, M., Ascano, M., Tuschl, T., Ohler, U., and Keene, J.D. (2011). Integrative regulatory mapping indicates that the RNA-binding protein HuR (ELAVL1) couples pre-mRNA processing and mRNA stability. Molecular cell *43*, 327-339.

Mukherji, S., Ebert, M.S., Zheng, G.X.Y., Tsang, J.S., Sharp, P.A., and van Oudenaarden, A. (2011). MicroRNAs can generate thresholds in target gene expression. Nat Genet *43*, 854-859.

Mullokandov, G., Baccarini, A., Ruzo, A., Jayaprakash, A.D., Tung, N., Israelow, B., Evans, M.J., Sachidanandam, R., and Brown, B.D. (2012). High-throughput assessment of microRNA activity and function using microRNA sensor and decoy libraries. Nat Methods *9*, 840-846.

Nelson, M.R., Leidal, A.M., and Smibert, C.A. (2004). Drosophila Cup is an eIF4E-binding protein that functions in Smaug-mediated translational repression. EMBO J *23*, 150-159.

Nelson, P.T., De Planell-Saguer, M., Lamprinaki, S., Kiriakidou, M., Zhang, P., O'Doherty, U., and Mourelatos, Z. (2007). A novel monoclonal antibody against human Argonaute proteins reveals unexpected characteristics of miRNAs in human blood cells. RNA *13*, 1787-1792.

Newman, M.A., Thomson, J.M., and Hammond, S.M. (2008). Lin-28 interaction with the Let-7 precursor loop mediates regulated microRNA processing. RNA *14*, 1539-1549.
Nishihara, T., Zekri, L., Braun, J.E., and Izaurralde, E. (2013). miRISC recruits decapping factors to miRNA targets to enhance their degradation. Nucleic Acids Res *41*, 8692-8705.

Nishimura, T., Padamsi, Z., Fakim, H., Milette, S., Dunham, Wade H., Gingras, A.-C., and Fabian, Marc R. (2015). The eIF4E-Binding Protein 4E-T Is a Component of the mRNA Decay Machinery that Bridges the 5′ and 3′ Termini of Target mRNAs. Cell Reports *11*, 1425-1436.

Noble, S.L., Allen, B.L., Goh, L.K., Nordick, K., and Evans, T.C. (2008). Maternal mRNAs are regulated by diverse P body-related mRNP granules during early Caenorhabditis elegans development. J Cell Biol *182*, 559-572.

Nolde, M.J., Saka, N., Reinert, K.L., and Slack, F.J. (2007). The Caenorhabditis elegans pumilio homolog, puf-9, is required for the 3'UTR-mediated repression of the let-7 microRNA target gene, hbl-1. Dev Biol *305*, 551-563.

Nousch, M., Techritz, N., Hampel, D., Millonigg, S., and Eckmann, C.R. (2013). The Ccr4-Not deadenylase complex constitutes the main poly(A) removal activity in C. elegans. Journal of cell science *126*, 4274-4285.

Ozgur, S., Basquin, J., Kamenska, A., Filipowicz, W., Standart, N., and Conti, E. (2015). Structure of a Human 4E-T/DDX6/CNOT1 Complex Reveals the Different Interplay of DDX6-Binding Proteins with the CCR4-NOT Complex. Cell Rep *13*, 703-711.

Ozsolak, F., Poling, L.L., Wang, Z., Liu, H., Liu, X.S., Roeder, R.G., Zhang, X., Song, J.S., and Fisher, D.E. (2008). Chromatin structure analyses identify miRNA promoters. Genes & development *22*, 3172-3183.

Paix, A., Folkmann, A., Rasoloson, D., and Seydoux, G. (2015). High Efficiency, Homology-Directed Genome Editing in Caenorhabditis elegans Using CRISPR-Cas9 Ribonucleoprotein Complexes. Genetics *201*, 47-54.

Pal, A.S., and Kasinski, A.L. (2017). Animal Models to Study MicroRNA Function. Adv Cancer Res *135*, 53-118.

Parry, D.H., Xu, J., and Ruvkun, G. (2007). A whole-genome RNAi Screen for C. elegans miRNA pathway genes. Curr Biol *17*, 2013-2022.

Pasquinelli, A.E., Reinhart, B.J., Slack, F., Martindale, M.Q., Kuroda, M.I., Maller, B., Hayward, D.C., Ball, E.E., Degnan, B., Muller, P.*, et al.* (2000). Conservation of the sequence and temporal expression of let-7 heterochronic regulatory RNA. Nature *408*, 86-89.

Peng, S.S., Chen, C.Y., Xu, N., and Shyu, A.B. (1998). RNA stabilization by the AU-rich element binding protein, HuR, an ELAV protein. EMBO J *17*, 3461-3470.
Peter, D., Ruscica, V., Bawankar, P., Weber, R., Helms, S., Valkov, E., Igreja, C., and Izaurralde, E. (2019). Molecular basis for GIGYF-Me31B complex assembly in 4EHP-mediated translational repression. Genes & development *33*, 1355-1360.

Peter, D., Weber, R., Sandmeir, F., Wohlbold, L., Helms, S., Bawankar, P., Valkov, E., Igreja, C., and Izaurralde, E. (2017). GIGYF1/2 proteins use auxiliary sequences to selectively bind to 4EHP and repress target mRNA expression. Genes & development *31*, 1147-1161.

Peters, L., and Meister, G. (2007). Argonaute Proteins: Mediators of RNA Silencing. Molecular cell *26*, 611-623.

Petersen, C.P., Bordeleau, M.-E., Pelletier, J., and Sharp, P.A. (2006). Short RNAs Repress Translation after Initiation in Mammalian Cells. Molecular cell *21*, 533-542.

Pillai, R.S., Artus, C.G., and Filipowicz, W. (2004). Tethering of human Ago proteins to mRNA mimics the miRNA-mediated repression of protein synthesis. RNA *10*, 1518-1525.

Piskounova, E., Polytarchou, C., Thornton, James E., LaPierre, Robert J., Pothoulakis, C., Hagan, John P., Iliopoulos, D., and Gregory, Richard I. (2011). Lin28A and Lin28B Inhibit let-7 MicroRNA Biogenesis by Distinct Mechanisms. Cell *147*, 1066-1079.

Plass, M., Rasmussen, S.H., and Krogh, A. (2017). Highly accessible AU-rich regions in 3' untranslated regions are hotspots for binding of regulatory factors. PLOS Computational Biology *13*, e1005460.

Posadas, D.M., and Carthew, R.W. (2014). MicroRNAs and their roles in developmental canalization. Curr Opin Genet Dev *27*, 1-6.

Priess, J.R., Schnabel, H., and Schnabel, R. (1987). The glp-1 locus and cellular interactions in early C. elegans embryos. Cell *51*, 601-611.

Quenault, T., Lithgow, T., and Traven, A. (2011). PUF proteins: repression, activation and mRNA localization. Trends in cell biology *21*, 104-112.

Rabani, M., Pieper, L., Chew, G.-L., and Schier, A.F. (2017). A massively parallel reporter assay of 3`UTR sequences identifies *in vivo* rules for mRNA degradation. Molecular cell *68*, 1083-1094.e1085.

Raheja, R., Liu, Y., Hukkelhoven, E., Yeh, N., and Koff, A. (2014). The ability of TRIM3 to induce growth arrest depends on RING-dependent E3 ligase activity. Biochem J *458*, 537-545.

Rao, B.S., and Parker, R. (2017). Numerous interactions act redundantly to assemble a tunable size of P bodies in *Saccharomyces cerevisiae*. Proc Natl Acad Sci U S A *114*, E9569-E9578.

Rao, E., Jiang, C., Ji, M., Huang, X., Iqbal, J., Lenz, G., Wright, G., Staudt, L.M., Zhao, Y., McKeithan, T.W., *et al.* (2012). The miRNA-17 approximately 92 cluster mediates chemoresistance and enhances tumor growth in mantle cell lymphoma via PI3K/AKT pathway activation. Leukemia *26*, 1064-1072.

Raudvere, U., Kolberg, L., Kuzmin, I., Arak, T., Adler, P., Peterson, H., and Vilo, J. (2019). g:Profiler: a web server for functional enrichment analysis and conversions of gene lists (2019 update). Nucleic Acids Res *47*, W191-W198.

Rausch, M., Ecsedi, M., Bartake, H., Müllner, A., and Grosshans, H. (2015). A genetic interactome of the let-7 microRNA in C. elegans. Dev Biol *401*, 276-286.

Raymond, C.K., Roberts, B.S., Garrett-Engele, P., Lim, L.P., and Johnson, J.M. (2005). Simple, quantitative primer-extension PCR assay for direct monitoring of microRNAs and short-interfering RNAs. RNA *11*, 1737-1744.

Reinhart, B.J., Slack, F.J., Basson, M., Pasquinelli, A.E., Bettinger, J.C., Rougvie, A.E., Horvitz, H.R., and Ruvkun, G. (2000). The 21-nucleotide let-7 RNA regulates developmental timing in Caenorhabditis elegans. Nature *403*, 901-906.

Reinhart, B.J., Weinstein, E.G., Rhoades, M.W., Bartel, B., and Bartel, D.P. (2002). MicroRNAs in plants. Genes & development *16*, 1616-1626.

Ren, H., and Zhang, H. (2010). Wnt signaling controls temporal identities of seam cells in Caenorhabditis elegans. Developmental Biology *345*, 144-155.

Ren, Z., Veksler-Lublinsky, I., Morrissey, D., and Ambros, V. (2016). Staufen Negatively Modulates MicroRNA Activity in Caenorhabditis elegans. G3 (Bethesda) *6*, 1227-1237.

Rhoades, M.W., Reinhart, B.J., Lim, L.P., Burge, C.B., Bartel, B., and Bartel, D.P. (2002). Prediction of plant microRNA targets. Cell *110*, 513-520.

Rodriguez, A., Griffiths-Jones, S., Ashurst, J.L., and Bradley, A. (2004). Identification of Mammalian microRNA Host Genes and Transcription Units. Genome Research *14*, 1902-1910.

Rom, E., Kim, H.C., Gingras, A.C., Marcotrigiano, J., Favre, D., Olsen, H., Burley, S.K., and Sonenberg, N. (1998). Cloning and characterization of 4EHP, a novel mammalian eIF4E-related cap-binding protein. J Biol Chem *273*, 13104-13109.

Rosenberg, Alexander B., Patwardhan, Rupali P., Shendure, J., and Seelig, G. (2015). Learning the Sequence Determinants of Alternative Splicing from Millions of Random Sequences. Cell *163*, 698-711.

Rouya, C., Siddiqui, N., Morita, M., Duchaine, T.F., Fabian, M.R., and Sonenberg, N. (2014). Human DDX6 effects miRNA-mediated gene silencing via direct binding to CNOT1. RNA *20*, 1398-1409.

Roy, B., and Jacobson, A. (2013). The intimate relationships of mRNA decay and translation. Trends Genet *29*, 691-699.

Ruby, J.G., Jan, C.H., and Bartel, D.P. (2007). Intronic microRNA precursors that bypass Drosha processing. Nature *448*, 83-86.

Ruscica, V., Bawankar, P., Peter, D., Helms, S., Igreja, C., and Izaurralde, E. (2019). Direct role for the Drosophila GIGYF protein in 4EHP-mediated mRNA repression. Nucleic Acids Res *47*, 7035-7048.

Rusten, T.E., Vaccari, T., and Stenmark, H. (2012). Shaping development with ESCRTs. Nature cell biology *14*, 38-45.

Rutz, B., and Séraphin, B. (2000). A dual role for BBP/ScSF1 in nuclear pre-mRNA retention and splicing. EMBO J *19*, 1873-1886.

Sachs, A.B., Sarnow, P., and Hentze, M.W. (1997). Starting at the beginning, middle, and end: translation initiation in eukaryotes. Cell *89*, 831-838.

Saetrom, P., Heale, B.S., Snove, O., Jr., Aagaard, L., Alluin, J., and Rossi, J.J. (2007). Distance constraints between microRNA target sites dictate efficacy and cooperativity. Nucleic Acids Res *35*, 2333-2342.

Saini, H.K., Griffiths-Jones, S., and Enright, A.J. (2007). Genomic analysis of human microRNA transcripts. Proc Natl Acad Sci U S A *104*, 17719.

Salmena, L., Poliseno, L., Tay, Y., Kats, L., and Pandolfi, P.P. (2011). A ceRNA hypothesis: the Rosetta Stone of a hidden RNA language? Cell *146*, 353-358.

Salomon, W.E., Jolly, S.M., Moore, M.J., Zamore, P.D., and Serebrov, V. (2015). Single-Molecule Imaging Reveals that Argonaute Reshapes the Binding Properties of Its Nucleic Acid Guides. Cell *162*, 84-95.

Sandberg, R., Neilson, J.R., Sarma, A., Sharp, P.A., and Burge, C.B. (2008). Proliferating cells express mRNAs with shortened 3′ UTRs and fewer microRNA target sites. Science *320*, 1643-1647.

Sandler, H., Kreth, J., Timmers, H.T., and Stoecklin, G. (2011). Not1 mediates recruitment of the deadenylase Caf1 to mRNAs targeted for degradation by tristetraprolin. Nucleic Acids Res *39*, 4373-4386.

Schirle, N.T., and MacRae, I.J. (2012). The crystal structure of human Argonaute2. Science *336*, 1037-1040.

Schirle, N.T., Sheu-Gruttadauria, J., and MacRae, I.J. (2014). Structural basis for microRNA targeting. Science *346*, 608-613.

Schopp, I.M., Amaya Ramirez, C.C., Debeljak, J., Kreibich, E., Skribbe, M., Wild, K., and Béthune, J. (2017). Split-BioID a conditional proteomics approach to monitor the composition of spatiotemporally defined protein complexes. Nat Commun *8*, 15690-15690.

Schouten, M., Fratantoni, S.A., Hubens, C.J., Piersma, S.R., Pham, T.V., Bielefeld, P., Voskuyl, R.A., Lucassen, P.J., Jimenez, C.R., and Fitzsimons, C.P. (2015). MicroRNA-124 and -137 cooperativity controls caspase-3 activity through BCL2L13 in hippocampal neural stem cells. Scientific Reports *5*, 12448.

Schwanhausser, B., Busse, D., Li, N., Dittmar, G., Schuchhardt, J., Wolf, J., Chen, W., and Selbach, M. (2011). Global quantification of mammalian gene expression control. Nature *473*, 337-342.

Schwartz, D.C., and Parker, R. (1999). Mutations in Translation Initiation Factors Lead to Increased Rates of Deadenylation and Decapping of mRNAs in Saccharomyces cerevisiae. Molecular and cellular biology *19*, 5247-5256.

Schwede, A., Ellis, L., Luther, J., Carrington, M., Stoecklin, G., and Clayton, C. (2008). A role for Caf1 in mRNA deadenylation and decay in trypanosomes and human cells. Nucleic Acids Res *36*, 3374-3388.

Selbach, M., Schwanhäusser, B., Thierfelder, N., Fang, Z., Khanin, R., and Rajewsky, N. (2008). Widespread changes in protein synthesis induced by microRNAs. Nature *455*, 58-63.

Sen, G.L., and Blau, H.M. (2005). Argonaute 2/RISC resides in sites of mammalian mRNA decay known as cytoplasmic bodies. Nature cell biology *7*, 633-636.

Serman, A., Le Roy, F., Aigueperse, C., Kress, M., Dautry, F., and Weil, D. (2007). GW body disassembly triggered by siRNAs independently of their silencing activity. Nucleic Acids Res *35*, 4715-4727.

Seydoux, G. (2018). The P Granules of C. elegans: A Genetic Model for the Study of RNA–Protein Condensates. Journal of Molecular Biology.

Sharif, H., Ozgur, S., Sharma, K., Basquin, C., Urlaub, H., and Conti, E. (2013). Structural analysis of the yeast Dhh1-Pat1 complex reveals how Dhh1 engages Pat1, Edc3 and RNA in mutually exclusive interactions. Nucleic Acids Res *41*, 8377-8390.

Shashkova, S., and Leake, M.C. (2017). Single-molecule fluorescence microscopy review: shedding new light on old problems. Biosci Rep *37*, BSR20170031.

Sherrard, R., Luehr, S., Holzkamp, H., McJunkin, K., Memar, N., and Conradt, B. (2017). miRNAs cooperate in apoptosis regulation during C. elegans development. Genes & Development *31*, 209-222.

Sheth, U., and Parker, R. (2003). Decapping and decay of messenger RNA occur in cytoplasmic processing bodies. Science *300*, 805-808.

Sheth, U., and Parker, R. (2006). Targeting of aberrant mRNAs to cytoplasmic processing bodies. Cell *125*, 1095-1109.

Sheu-Gruttadauria, J., and MacRae, I.J. (2018). Phase Transitions in the Assembly and Function of Human miRISC. Cell *173*, 946-957.e916.

Siliciano, R.F., Pratt, J.C., Schmidt, R.E., Ritz, J., and Reinherz, E.L. (1985). Activation of cytolytic T lymphocyte and natural killer cell function through the T11 sheep erythrocyte binding protein. Nature *317*, 428-430.

Siomi, M.C., Sato, K., Pezic, D., and Aravin, A.A. (2011). PIWI-interacting small RNAs: the vanguard of genome defence. Nature Reviews Molecular Cell Biology *12*, 246-258.

Slack, F.J., Basson, M., Liu, Z., Ambros, V., Horvitz, H.R., and Ruvkun, G. (2000). The lin-41 RBCC gene acts in the C. elegans heterochronic pathway between the let-7 regulatory RNA and the LIN-29 transcription factor. Molecular cell *5*, 659-669.

Smith, J., Calidas, D., Schmidt, H., Lu, T., Rasoloson, D., and Seydoux, G. (2016). Spatial patterning of P granules by RNA-induced phase separation of the intrinsically-disordered protein MEG-3. Elife *5*, e21337.

Sonoda, J., and Wharton, R.P. (1999). Recruitment of Nanos to hunchback mRNA by Pumilio. Genes & development *13*, 2704-2712.

Sonoda, J., and Wharton, R.P. (2001). Drosophila Brain Tumor is a translational repressor. Genes & development *15*, 762-773.

Spike, C., Meyer, N., Racen, E., Orsborn, A., Kirchner, J., Kuznicki, K., Yee, C., Bennett, K., and Strome, S. (2008). Genetic analysis of the Caenorhabditis elegans GLH family of P-granule proteins. Genetics *178*, 1973-1987.

Spitale, R.C., Flynn, R.A., Zhang, Q.C., Crisalli, P., Lee, B., Jung, J.-W., Kuchelmeister, H.Y., Batista, P.J., Torre, E.A., Kool, E.T.*, et al.* (2015). Structural imprints in vivo decode RNA regulatory mechanisms. Nature *519*, 486.

Strome, S. (2005). Specification of the germ line. Wormbook, 1-10.

Suh, N., Crittenden, S.L., Goldstrohm, A., Hook, B., Thompson, B., Wickens, M., and Kimble, J. (2009). FBF and Its Dual Control of gld-1 Expression in the Caenorhabditis elegans Germline. Genetics *181*, 1249-1260.

Tabara, H., Sarkissian, M., Kelly, W.G., Fleenor, J., Grishok, A., Timmons, L., Fire, A., and Mello, C.C. (1999). The rde-1 gene, RNA interference, and transposon silencing in C. elegans. Cell *99*, 123-132.

Takimoto, K., Wakiyama, M., and Yokoyama, S. (2009). Mammalian GW182 contains multiple Argonaute-binding sites and functions in microRNA-mediated translational repression. RNA *15*, 1078-1089.

Tay, Y., Rinn, J., and Pandolfi, P.P. (2014). The multilayered complexity of ceRNA crosstalk and competition. Nature *505*, 344-352.

Temme, C., Zaessinger, S., Meyer, S., Simonelig, M., and Wahle, E. (2004). A complex containing the CCR4 and CAF1 proteins is involved in mRNA deadenylation in Drosophila. EMBO J *23*, 2862-2871.

Temme, C., Zhang, L., Kremmer, E., Ihling, C., Chartier, A., Sinz, A., Simonelig, M., and Wahle, E. (2010). Subunits of the Drosophila CCR4-NOT complex and their roles in mRNA deadenylation. RNA *16*, 1356-1370.

Tenekeci, U., Poppe, M., Beuerlein, K., Buro, C., Müller, H., Weiser, H., Kettner-Buhrow, D., Porada, K., Newel, D., Xu, M.*, et al.* (2016). K63-Ubiquitylation and TRAF6 Pathways Regulate Mammalian P-Body Formation and mRNA Decapping. Molecular cell *62*, 943-957.

Tharun, S. (2009). Lsm1-7-Pat1 complex: A link between 3' and 5'-ends in mRNA decay? RNA Biology *6*, 228-232.

Thivierge, C., Tseng, H.W., Mayya, V.K., Lussier, C., Gravel, S.P., and Duchaine, T.F. (2018). Alternative polyadenylation confers Pten mRNAs stability and resistance to microRNAs. Nucleic Acids Res.

Tocchini, C., and Ciosk, R. (2015). TRIM-NHL proteins in development and disease. Seminars in cell & developmental biology *47-48*, 52-59.

Tollenaere, M.A.X., Tiedje, C., Rasmussen, S., Nielsen, J.C., Vind, A.C., Blasius, M., Batth, T.S., Mailand, N., Olsen, J.V., Gaestel, M.*, et al.* (2019). GIGYF1/2-Driven Cooperation between ZNF598 and TTP in Posttranscriptional Regulation of Inflammatory Signaling. Cell Rep *26*, 3511-3521.e3514.

Tomari, Y., Du, T., and Zamore, P.D. (2007). Sorting of Drosophila small silencing RNAs. Cell *130*, 299-308.

Tourriere, H., Chebli, K., Zekri, L., Courselaud, B., Blanchard, J.M., Bertrand, E., and Tazi, J. (2003). The RasGAP-associated endoribonuclease G3BP assembles stress granules. J Cell Biol *160*, 823-831.

Tritschler, F., Braun, J.E., Eulalio, A., Truffault, V., Izaurralde, E., and Weichenrieder, O. (2009). Structural Basis for the Mutually Exclusive Anchoring of P Body Components EDC3 and Tral to the DEAD Box Protein DDX6/Me31B. Molecular cell *33*, 661-668.

Tucker, M., Valencia-Sanchez, M.A., Staples, R.R., Chen, J., Denis, C.L., and Parker, R. (2001). The Transcription Factor Associated Ccr4 and Caf1 Proteins Are Components of the Major Cytoplasmic mRNA Deadenylase in Saccharomyces cerevisiae. Cell *104*, 377-386.

Ulitsky, I., Shkumatava, A., Jan, C.H., Subtelny, A.O., Koppstein, D., Bell, G.W., Sive, H., and Bartel, D.P. (2012). Extensive alternative polyadenylation during zebrafish development. Genome Research *22*, 2054-2066.

Unterholzner, L., and Izaurralde, E. (2004). SMG7 acts as a molecular link between mRNA surveillance and mRNA decay. Mol Cell *16*, 587-596.

Updike, Dustin L., Knutson, Andrew K.a., Egelhofer, Thea A., Campbell, Anne C., and Strome, S. (2014). Germ-Granule Components Prevent Somatic Development in the C. elegans Germline. Current Biology *24*, 970-975.

Uversky, V.N. (2017). Intrinsically disordered proteins in overcrowded milieu: Membrane-less organelles, phase separation, and intrinsic disorder. Current Opinion in Structural Biology *44*, 18-30.

van der Lee, R., Buljan, M., Lang, B., Weatheritt, R.J., Daughdrill, G.W., Dunker, A.K., Fuxreiter, M., Gough, J., Gsponer, J., Jones, D.T.*, et al.* (2014). Classification of intrinsically disordered regions and proteins. Chemical reviews *114*, 6589-6631.

Van Etten, J., Schagat, T.L., Hrit, J., Weidmann, C.A., Brumbaugh, J., Coon, J.J., and Goldstrohm, A.C. (2012). Human Pumilio Proteins Recruit Multiple Deadenylases to Efficiently Repress Messenger RNAs. J Biol Chem *287*, 36370-36383.

Vasquez-Rifo, A., Jannot, G., Armisen, J., Labouesse, M., Bukhari, S.I.A., Rondeau, E.L., Miska, E.A., and Simard, M.J. (2012). Developmental Characterization of the MicroRNA-Specific C. elegans Argonautes alg-1 and alg-2. PloS one *7*, e33750.

Vella, M.C., Choi, E.-Y., Lin, S.-Y., Reinert, K., and Slack, F.J. (2004). The C. elegans microRNA let-7 binds to imperfect let-7 complementary sites from the lin-41 3′UTR. Genes & development *18*, 132-137.

Villaescusa, J.C., Buratti, C., Penkov, D., Mathiasen, L., Planagumà, J., Ferretti, E., and Blasi, F. (2009). Cytoplasmic Prep1 Interacts with 4EHP Inhibiting Hoxb4 Translation. PloS one *4*, e5213.

Viswanathan, S.R., Daley, G.Q., and Gregory, R.I. (2008). Selective Blockade of MicroRNA Processing by Lin28. Science *320*, 97-100.

von Roretz, C., Di Marco, S., Mazroui, R., and Gallouzi, I.E. (2011). Turnover of AU-rich-containing mRNAs during stress: a matter of survival. Wiley interdisciplinary reviews RNA *2*, 336-347.

Voronina, E., Seydoux, G., Sassone-Corsi, P., and Nagamori, I. (2011). RNA Granules in Germ Cells. Cold Spring Harbor Perspectives in Biology *3*, a002774.

Wahle, E., and Winkler, G.S. (2013). RNA decay machines: Deadenylation by the Ccr4–Not and Pan2–Pan3 complexes. Biochimica et Biophysica Acta (BBA) - Gene Regulatory Mechanisms *1829*, 561-570.

Wakiyama, M., Takimoto, K., Ohara, O., and Yokoyama, S. (2007). Let-7 microRNA-mediated mRNA deadenylation and translational repression in a mammalian cell-free system. Genes & development *21*, 1857-1862.

Wang, D., Zhang, Z., O'Loughlin, E., Lee, T., Houel, S., O'Carroll, D., Tarakhovsky, A., Ahn, N.G., and Yi, R. (2012). Quantitative functions of Argonaute proteins in mammalian development. Genes & development *26*, 693-704.

Wang, Y., Juranek, S., Li, H., Sheng, G., Tuschl, T., and Patel, D.J. (2008). Structure of an argonaute silencing complex with a seed-containing guide DNA and target RNA duplex. Nature *456*, 921-926.

Ward, J.D. (2015). Rapid and precise engineering of the Caenorhabditis elegans genome with lethal mutation co-conversion and inactivation of NHEJ repair. Genetics *199*, 363-377.

Washburn, M.P., Wolters, D., and Yates, J.R., 3rd (2001). Large-scale analysis of the yeast proteome by multidimensional protein identification technology. Nat Biotechnol *19*, 242-247.

Weber, R., Chung, M.-Y., Keskeny, C., Zinnall, U., Landthaler, M., Valkov, E., Izaurralde, E., and Igreja, C. (2020). 4EHP and GIGYF1/2 Mediate Translation-Coupled Messenger RNA Decay. Cell Reports *33*, 108262.

Wee, L.M., Flores-Jasso, C.F., Salomon, W.E., and Zamore, P.D. (2012). Argonaute divides its RNA guide into domains with distinct functions and RNA-binding properties. Cell *151*, 1055-1067.

Weidmann, C.A., Raynard, N.A., Blewett, N.H., Van Etten, J., and Goldstrohm, A.C. (2014). The RNA binding domain of Pumilio antagonizes poly-adenosine binding protein and accelerates deadenylation. RNA *20*, 1298-1319.

Wells, S.E., Hillner, P.E., Vale, R.D., and Sachs, A.B. (1998). Circularization of mRNA by Eukaryotic Translation Initiation Factors. Molecular cell *2*, 135-140.

Wickens, M., Bernstein, D.S., Kimble, J., and Parker, R. (2002). A PUF family portrait: 3'UTR regulation as a way of life. Trends in genetics : TIG *18*, 150-157.

Wightman, B., Bürglin, T.R., Gatto, J., Arasu, P., and Ruvkun, G. (1991). Negative regulatory sequences in the lin-14 3'-untranslated region are necessary to generate a temporal switch during Caenorhabditis elegans development. Genes & development *5*, 1813-1824.

Wightman, B., Ha, I., and Ruvkun, G. (1993). Posttranscriptional regulation of the heterochronic gene lin-14 by lin-4 mediates temporal pattern formation in C. elegans. Cell *75*, 855-862.

Wilsch-Bräuninger, M., Schwarz, H., and Nüsslein-Volhard, C. (1997). A Sponge-like Structure Involved in the Association and Transport of Maternal Products during Drosophila Oogenesis. J Cell Biol *139*, 817-829.

Wolters, D.A., Washburn, M.P., and Yates, J.R., 3rd (2001). An automated multidimensional protein identification technology for shotgun proteomics. Anal Chem *73*, 5683-5690.

Wu, E., and Duchaine, T.F. (2011). Cell-free microRNA-mediated translation repression in Caenorhabditis elegans. Methods Mol Biol *725*, 219-232.

Wu, E., Thivierge, C., Flamand, M., Mathonnet, G., Vashisht, A.A., Wohlschlegel, J., Fabian, M.R., Sonenberg, N., and Duchaine, T.F. (2010). Pervasive and cooperative deadenylation of 3'UTRs by embryonic microRNA families. Molecular cell *40*, 558-570.

Wu, E., Vashisht, A.A., Chapat, C., Flamand, M.N., Cohen, E., Sarov, M., Tabach, Y., Sonenberg, N., Wohlschlegel, J., and Duchaine, T.F. (2017). A continuum of mRNP complexes in embryonic microRNA-mediated silencing. Nucleic Acids Res *45*, 2081-2098.

Wu, P.H., Isaji, M., and Carthew, R.W. (2013). Functionally diverse microRNA effector complexes are regulated by extracellular signaling. Molecular cell *52*, 113-123.

Xie, M., Li, M., Vilborg, A., Lee, N., Shu, M.D., Yartseva, V., Šestan, N., and Steitz, J.A. (2013). Mammalian 5'-capped microRNA precursors that generate a single microRNA. Cell *155*, 1568-1580.

Yamashita, A., Chang, T.-C., Yamashita, Y., Zhu, W., Zhong, Z., Chen, C.-Y.A., and Shyu, A.-B. (2005). Concerted action of poly(A) nucleases and decapping enzyme in mammalian mRNA turnover. Nat Struct Mol Biol *12*, 1054.

Yang, B., Schwartz, M., and McJunkin, K. (2020). In vivo CRISPR screening for phenotypic targets of the *mir-35-42* family in C. elegans. Genes & development *34*, 1227-1238.

Yang, J.-S., Maurin, T., Robine, N., Rasmussen, K.D., Jeffrey, K.L., Chandwani, R., Papapetrou, E.P., Sadelain, M., O'Carroll, D., and Lai, E.C. (2010). Conserved vertebrate *mir-451* provides a platform for Dicer-independent, Ago2-mediated microRNA biogenesis. Proc Natl Acad Sci U S A *107*, 15163-15168.

Yi, R., Qin, Y., Macara, I.G., and Cullen, B.R. (2003). Exportin-5 mediates the nuclear export of pre-microRNAs and short hairpin RNAs. Genes & development *17*, 3011-3016.

Yigit, E., Batista, P.J., Bei, Y., Pang, K.M., Chen, C.C., Tolia, N.H., Joshua-Tor, L., Mitani, S., Simard, M.J., and Mello, C.C. (2006). Analysis of the C. elegans Argonaute family reveals that distinct Argonautes act sequentially during RNAi. Cell *127*, 747-757.

Youn, J.Y., Dunham, W.H., Hong, S.J., Knight, J.D.R., Bashkurov, M., Chen, G.I., Bagci, H., Rathod, B., MacLeod, G., Eng, S.W.M.*, et al.* (2018). High-Density Proximity Mapping Reveals the Subcellular Organization of mRNA-Associated Granules and Bodies. Molecular cell *69*, 517-532.e511.

Young, L.E., Moore, A.E., Sokol, L., Meisner-Kober, N., and Dixon, D.A. (2012). The mRNA Stability Factor HuR Inhibits MicroRNA-16 Targeting of Cyclooxygenase-2. Molecular Cancer Research *10*, 167-180.

Zaiss, D.M., Standera, S., Kloetzel, P.M., and Sijts, A.J. (2002). PI31 is a modulator of proteasome formation and antigen processing. Proc Natl Acad Sci U S A *99*, 14344-14349.

Zdanowicz, A., Thermann, R., Kowalska, J., Jemielity, J., Duncan, K., Preiss, T., Darzynkiewicz, E., and Hentze, M.W. (2009). Drosophila miR2 primarily targets the m7GpppN cap structure for translational repression. Molecular cell *35*, 881-888.

Zekri, L., Kuzuoğlu-Öztürk, D., and Izaurralde, E. (2013). GW182 proteins cause PABP dissociation from silenced miRNA targets in the absence of deadenylation. EMBO J *32*, 1052-1065.

Zeng, Y., Yi, R., and Cullen, B.R. (2005). Recognition and cleavage of primary microRNA precursors by the nuclear processing enzyme Drosha. EMBO J *24*, 138-148.

Zhang, H., Kolb, F.A., Jaskiewicz, L., Westhof, E., and Filipowicz, W. (2004). Single processing center models for human Dicer and bacterial RNase III. Cell *118*, 57-68.
Zhuang, F., Fuchs, R.T., Sun, Z., Zheng, Y., and Robb, G.B. (2012). Structural bias in T4 RNA ligase-mediated 3'-adapter ligation. Nucleic Acids Res *40*, e54.

Zielezinski, A., and Karlowski, W.M. (2015). Early origin and adaptive evolution of the GW182 protein family, the key component of RNA silencing in animals. RNA biology *12*, 761-770.

Zisoulis, D.G., Lovci, M.T., Wilbert, M.L., Hutt, K.R., Liang, T.Y., Pasquinelli, A.E., and Yeo, G.W. (2010). Comprehensive discovery of endogenous Argonaute binding sites in Caenorhabditis elegans. Nat Struct Mol Biol *17*, 173-179.

APPENDIX 1: Supplemental information to chapter 2

On the availability of microRNA-induced silencing complexes, saturation of microRNA-binding sites and stoichiometry

Vinay K. Mayya & Thomas F. Duchaine (2015)

Nucleic Acids Res. 2015 Sep 3;43(15):7556-65. doi: 10.1093/nar/gkv720

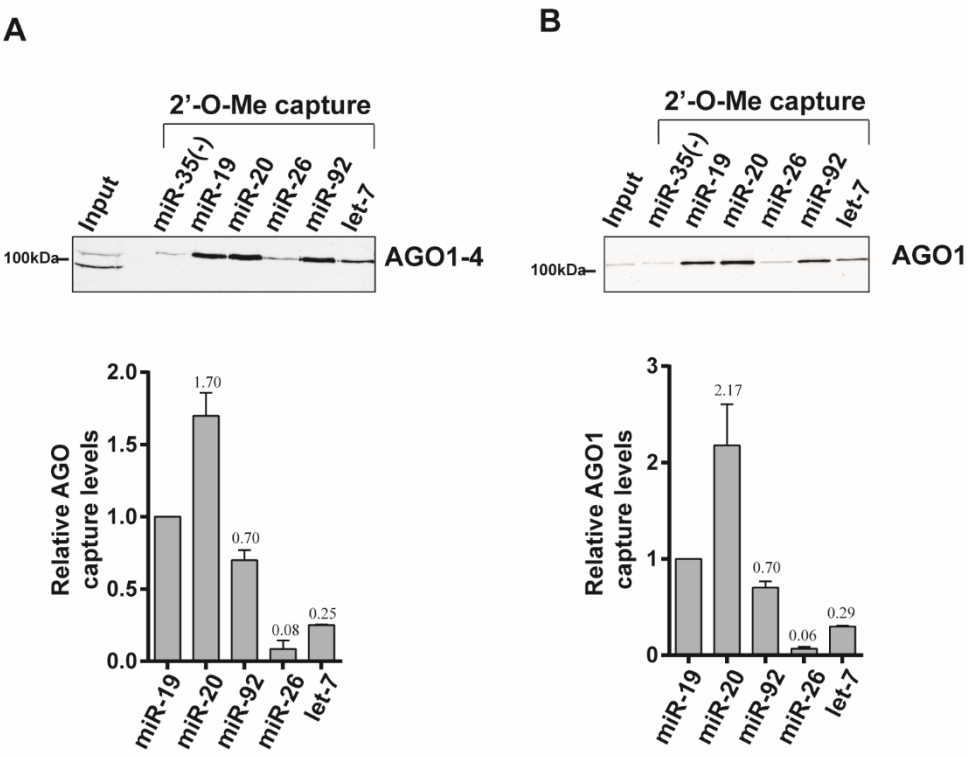

Figure A1-1. Refers to Figure 2-2. 2'-*O*-Me miRISC capture in HEK 293T cells.
miRISC capture was conducted as explained in Figure 2-1A for the miR-19, -20, -92, -26 and let-7 families. Captured AGO1-4 **(A)** or AGO1 **(B)** were quantified and normalized relatively to miR-19 capture for each individual lysate (Bottom) from two independent biological replicates.

A

```
hsa-miR-19b   UGUGCAAAUCCAUGCAAAACUGA
hsa-miR-19a   UGUGCAAAUCuAUGCAAAACUGA

hsa-miR-20a   UAAAGUGCUUAUAGUGCAGGUAG
hsa-miR-20b   cAAAGUGCUcAUAGUGCAGGUAG
hsa-miR-17    cAAAGUGCUUAcAGUGCAGGUAG
hsa-miR-106a  aAAAGUGCUUAcAGUGCAGGUAG
hsa-miR-106b  UAAAGUGCUgAcAGUGCAGaU
hsa-miR-93    cAAAGUGCUguUcGUGCAGGUAG

hsa-miR-92a   UAUUGCACUUGUCCCGGCCUGU
hsa-miR-92b   UAUUGCACUcGUCCCGGCCUcc
hsa-miR-25    cAUUGCACUUGUCuCGGuCUGa
hsa-miR-32    UAUUGCACaUuaCuaaGuugca
hsa-miR-363   UAUUGCACUUGUCCCGGCCUGU
hsa-miR-367   UAUUGCACUUGUCCCGGCCUGU

hsa-let-7a    UGAGGUAGUAGGUUGUAUAGUU
hsa-let-7b    UGAGGUAGUAGGUUGUgUgGUU
hsa-let-7c    UGAGGUAGUAGGUUGUAUgGUU
hsa-let-7d    aGAGGUAGUAGGUUGcAUaGUU
hsa-let-7e    UGAGGUAGgAGGUUGUAUAGUU
hsa-let-7f    UGAGGUAGUAGaUUGUAUAGUU
hsa-let-7g    UGAGGUAGUAGuUUGUAcAGUU
hsa-let-7i    UGAGGUAGUAGuUUGUgcuGUU
```

B

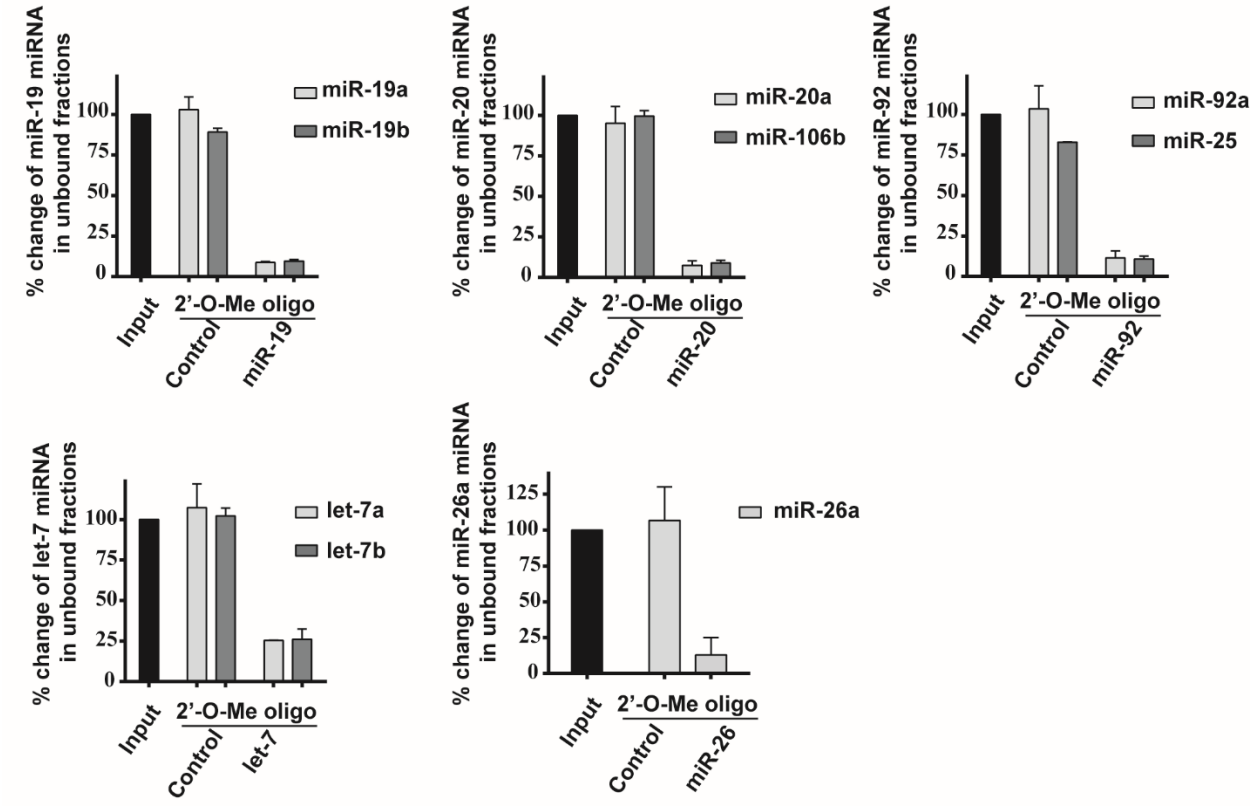

Figure A1-2. Refers to Figure 2-2.
(A) Alignment of all known family members of miRNAs considered in this study. The seed region is highlighted in grey. Bases that differ from consensus are depicted in lowercase. **(B)** Quantification of northern analyses shown in Figure 2-2B. Results are presented as percentages of miRNA present in unbound fractions following RISC capture. These are compared to Input which is set to 100% for comparison. All data are presented as mean ± standard deviation of two biological independent experiments.

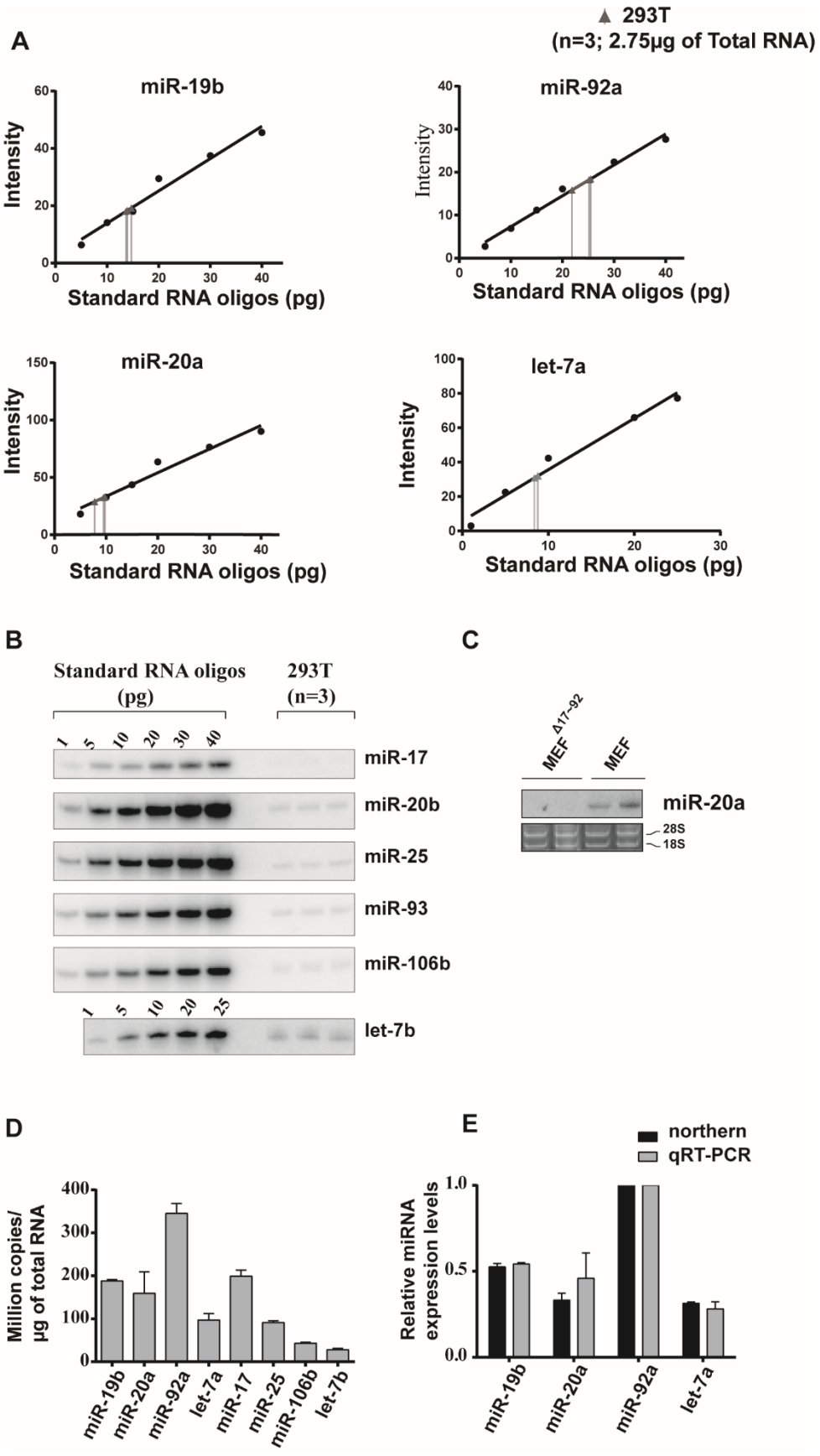
A
293T
(n=3; 2.75µg of Total RNA)
miR-19b
miR-92a
miR-20a
let-7a
Intensity
Standard RNA oligos (pg)
B
Standard RNA oligos
(pg)
293T
(n=3)
1
5
10
20
30
40
25
miR-17
miR-20b
miR-25
miR-93
miR-106b
let-7b
C
MEF Δ17-92
MEF
miR-20a
28S
18S
D
Million copies/
µg of total RNA
400
300
200
100
0
miR-19b
miR-20a
miR-92a
let-7a
miR-17
miR-25
miR-106b
let-7b
E
northern
qRT-PCR
Relative miRNA
expression levels
1.0
0.5
0.0
miR-19b
miR-20a
miR-92a
let-7a

Figure A1-3. Refers to Figure 2-2. Quantitative analyses on the HEK 293T miRNAs examined in this study.

(A) Standard curves were generated using RNA oligonucleotides, and used to quantify miR-19b, miR-20a, miR-92a and let-7a. **(B)** Northern blot quantification of miR-17, miR-20b, miR-25, miR-93, miR-106b and let-7b for three independent biological replicates. **(C)** Hybridisation probe specificity is assessed by northern blot analysis of miR-20a in MEFs deficient of miR-17~92 cluster. 28S and 18S rRNA were used as loading controls. **(D)** qRT-PCR analyses of each miRNA for three independent biological replicates. RNA oligonucleotides were used as standards and copy numbers were calculated per microgram of isolated RNA. **(E)** Relative miRNA expression levels between northern blot analyses and qRT-PCR analyses. Values are normalised against miR-92a copy numbers.

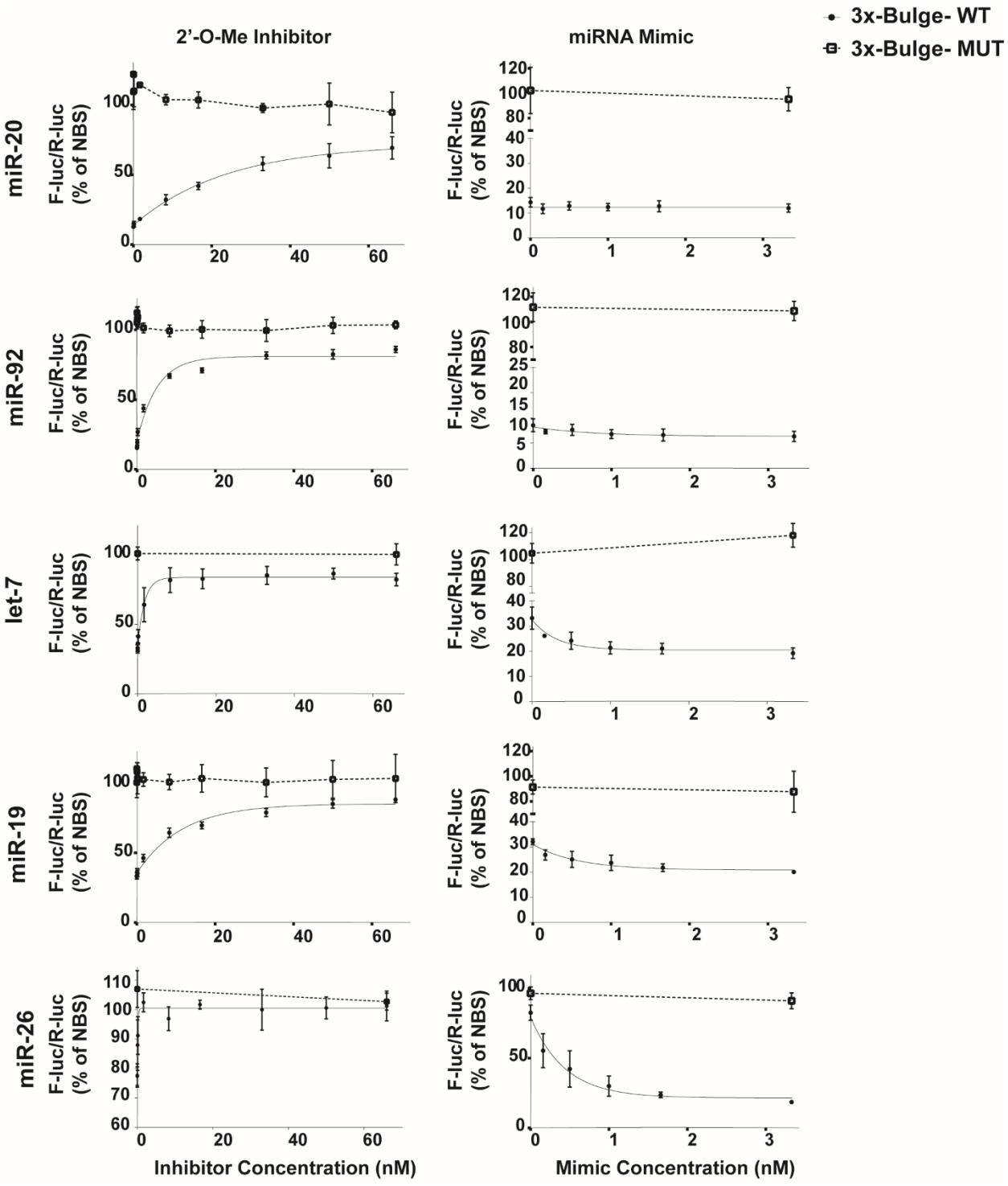

Figure A1-4. Refers to Figure 2-4. Luciferase reporter silencing and de-repression assays on 3x-Bulge reporters.

(Left panel) HEK 293T cells were co-transfected with 3x-Bulge reporters and increasing concentrations (0-66nM) of 2'-*O*-Me inhibitors for the indicated miRNAs. FLuc-3x-Bulge/R-Luc

ratios are compared to F-Luc only (no binding site)/R-Luc, set as 100%. (Right panel) 3x-Bulge reporters were co-transfected with increasing concentrations (0-3.3nM) of dsRNA miRNA mimics for the indicated miRNAs. All data are presented as average ± standard deviation from technical triplicates of at-least three independent biological experiments.

F-Luc-T7-Fwd	GAAATTAATACGACTCACTATAGGGAATCCGGTACTGTTGGT
pmiRGLO-Rev	TGCCGGTCAGTCCTTTAGGC
GFP-T7-Fwd	GAAATTAATACGACTCACTATAGGGTTTAGTGAACCGTCA
pTRIPZ-Rev	GATGTGGAATGTGTGCGAGG
F-Luc-qPCR-Fwd	CGAGCACTTCTTCATCGTGG
F-Luc-qPCR-Rev	GAAGATGTTGGGGTGTTGCA
GFP-qPCR-Fwd	GTGACCACCCTGACCTACG
GFP-qPCR-Rev	TTGAAGAAGATGGTGCGCTC
Gene Specific_17/20a	CATGATCAGCTGGGCCAAGACTACCTGCAC
Gene Specific_19b	CATGATCAGCTGGGCCAAGATCAGTTTTGC
Gene Specific_92a	CATGATCAGCTGGGCCAAGAACAGGCCGGG
Gene Specific_106b	CATGATCAGCTGGGCCAAGAATCTGCACTG
Gene Specific_25	CATGATCAGCTGGGCCAAGATCAGACCGAG
Gene Specific_let7a	CATGATCAGCTGGGCCAAGAAACTATACAA
Gene Specific_let7b	CATGATCAGCTGGGCCAAGAAACCACACAA
Universal qPCR	CATGATCAGCTGGGCCAAGA
LNA_miR-17	C+AA+AGTGCTTACAGT
LNA_miR-20a	T+AA+AGTGCTTATAGT
LNA_miR-19b	T+GT+GCAAATCCATGC
LNA_miR-92a	T+AT+TGCACTTGTCCC
LNA_miR-106b	T+AA+AG+TGCTGACAG
LNA_miR-25	C+AT+TGCACTTGTCTC
LNA_miR-let7a/b	T+GA+GGTAGTAGGTTG
1xPer-miR19b Fwd	CTAGATCAGTTTTGCATGGATTTGCACAGC
1xPer-miR19b Rev	GGCCGCTGTGCAAATCCATGCAAAACTGAT
1xPer-mut miR19b Fwd	CTAGATCAGTTTTGCAACCATTTCGTCAGC
1xPer-mut miR19b Rev	GGCCGCTGACGAAATGGTTGCAAAACTGAT
3x-Bulge-miR19 Fwd	CTAGATCAGTTTTGCAATTTGCACACCGCGGTATCAGTTTTGCAATTTGCACAGAATTCATATGTCAGTTTTGCAATTTGCACAGC
3x-Bulge-miR19 Rev	GGCCGCTGTGCAAATTGCAAAACTGACATATGAATTCTGTGCAAATTGCAAAACTGATACCGCGGTGTGCAAATTGCAAAACTGAT
3x-Bulge-mutmiR19 Fwd	CTAGATCAGTTTTGCAATTTCGTCACCGCGGTATCAGTTTTGCAATTTCGTCAGAATTCATATGTCAGTTTTGCAATTTCGTCAGC
3x-Bulge-mut miR19 Rev	GGCCGCTGACGAAATTGCAAAACTGACATATGAATTCTGACGAAATTGCAAAACTGATACCGCGGTGACGAAATTGCAAAACTGAT
1xPer-miR-20a Fwd	CTAGACTACCTGCACTATAAGCACTTTAGC

1xPer-miR-20a Rev	GGCCGCTAAAGTGCTTATAGTGCAGGTAGT
1xPer-mut miR-20a Fwd	CTAGACTACCTGCACTTATAGCAGAATAGC
1xPer-mut miR-20a Rev	GGCCGCTATTCTGCTATAAGTGCAGGTAGT
3x-Bulge-miR20 Fwd	CTAGACTACCTGCACTAGCACTTTACCGCGGTACTACCTGCACTAGCACTTTAGAATTCATATGCTACCTGCACTAGCACTTTAGC
3x-Bulge-miR20 Rev	GGCCGCTAAAGTGCTAGTGCAGGTAGCATATGAATTCTAAAGTGCTAGTGCAGGTAGTACCGCGGTAAAGTGCTAGTGCAGGTAGT
3x-Bulge-mutmiR20 Fwd	CTAGACTACCTGCACTAGCAGAATACCGCGGTACTACCTGCACTAGCAGAATAGAATTCATATGCTACCTGCACTAGCAGAATAGC
3x-Bulge-mut miR20 Rev	GGCCGCTATTCTGCTAGTGCAGGTAGCATATGAATTCTATTCTGCTAGTGCAGGTAGTACCGCGGTATTCTGCTAGTGCAGGTAGT
1xPer-let-7a Fwd	CTAGAAACTATACAACCTACTACCTCAGC
1xPer-let-7a Rev	GGCCGCTGAGGTAGTAGGTTGTATAGTTT
1xPer-mut let-7a Fwd	CTAGAAACTATACAAGGAACTAGGACAGC
1xPer-mut let-7a Rev	GGCCGCTGTCCTAGTTCCTTGTATAGTTT
3x-Bulge-let-7a Fwd	CTAGAAACTATACAAACTACCTCACCGCGGTAAACTATACAAACTACCTCAGAATTCATATGAACTATACAAACTACCTCAGC
3x-Bulge-let-7a Rev	GGCCGCTGAGGTAGTTTGTATAGTTCATATGAATTCTGAGGTAGTTTGTATAGTTTACCGCGGTGAGGTAGTTTGTATAGTTT
3x-Bulge-mut let-7a Fwd	CTAGAAACTATACAAACTAGGACACCGCGGTAAACTATACAAACTAGGACAGAATTCATATGAACTATACAAACTAGGACAGC
3x-Bulge-mut-let-7a Rev	GGCCGCTGTCCTAGTTTGTATAGTTCATATGAATTCTGTCCTAGTTTGTATAGTTTACCGCGGTGTCCTAGTTTGTATAGTTT
1xPer-let-7b Fwd	CTAGAAACCACACAACCTACTACCTCAGC
1xPer-let-7b Rev	GGCCGCTGAGGTAGTAGGTTGTGTGGTTT
1xPer-mut let-7b Fwd	CTAGAAACCACACAAGGAACTAGGACAGC
1xPer-mut let-7b Rev	GGCCGCTGTCCTAGTTCCTTGTGTGGTTT
3x-Bulge-let-7b Fwd	CTAGAAACCACACAAACTACCTCACCGCGGTAAACCACACAAACTACCTCAGAATTCATATGAACCACACAAACTACCTCAGC
3x-Bulge-let-7b Rev	GGCCGCTGAGGTAGTTTGTGTGGTTCATATGAATTCTGAGGTAGTTTGTGTGGTTTACCGCGGTGAGGTAGTTTGTGTGGTTT
3x-Bulge-mut let-7b Fwd	CTAGAAACCACACAAACTAGGACACCGCGGTAAACCACACAAACTAGGACAGAATTCATATGAACCACACAAACTAGGACAGC

3x-Bulge-mut let-7b Rev	GGCCGCTGTCCTAGTTTGTGTGGTTCATATGAATT CTGTCCTAGTTTGTGTGGTTTACCGCGGTGTCCTA GTTTGTGTGGTTT
1xPer-miR-26a Fwd	CTAGAAGCCTATCCTGGATTACTTGAAGC
1xPer-miR-26a Rev	GGCCGCTTCAAGTAATCCAGGATAGGCTT
1xPer mut miR-26a Fwd	CTAGAAGCCTATCCTCCTTTACAACAAGC
1xPer-mut miR-26a Rev	GGCCGCTTGTTGTAAAGGAGGATAGGCTT
3x-Bulge-miR-26Fwd	TCGAGCCTATCCTTTACTTGAAGAATTCCCTATCC TTTACTTGAAGAATTCCCTATCCTTTACTTGAAGC
3x-Bulge-miR-26 Rev	GGCCGCTTCAAGTAAAGGATAGGGAATTCTTCAA GTAAAGGATAGGGAATTCTTCAAGTAAAGGATAG GC
3x-Bulge-mut miR-26 Fwd	TCGAGCCTATCCTTTACAACAAGAATTCCCTATCC TTTACAACAAGAATTCCCTATCCTTTACAACAAGC
3x-Bulge-mut miR-26 Rev	GGCCGCTTGTTGTAAAGGATAGGGAATTCTTGTT GTAAAGGATAGGGAATTCTTGTTGTAAAGGATAG GC

Table A1-1. Refers to Material and Methods (Chapter 2). List of oligonucleotides used in this study

APPENDIX 2: Supplemental information to Chapter 3

microRNA-mediated translation repression through GYF-1 and IFE-4 in *C. elegans* development

Mayya VK[1,2], Flamand MN[1,2,3], Lambert AM[1,2], Jafarnejad SM[4], Wohlschlegel JA[5], Sonenberg N[1,2], Duchaine TF[1,2]

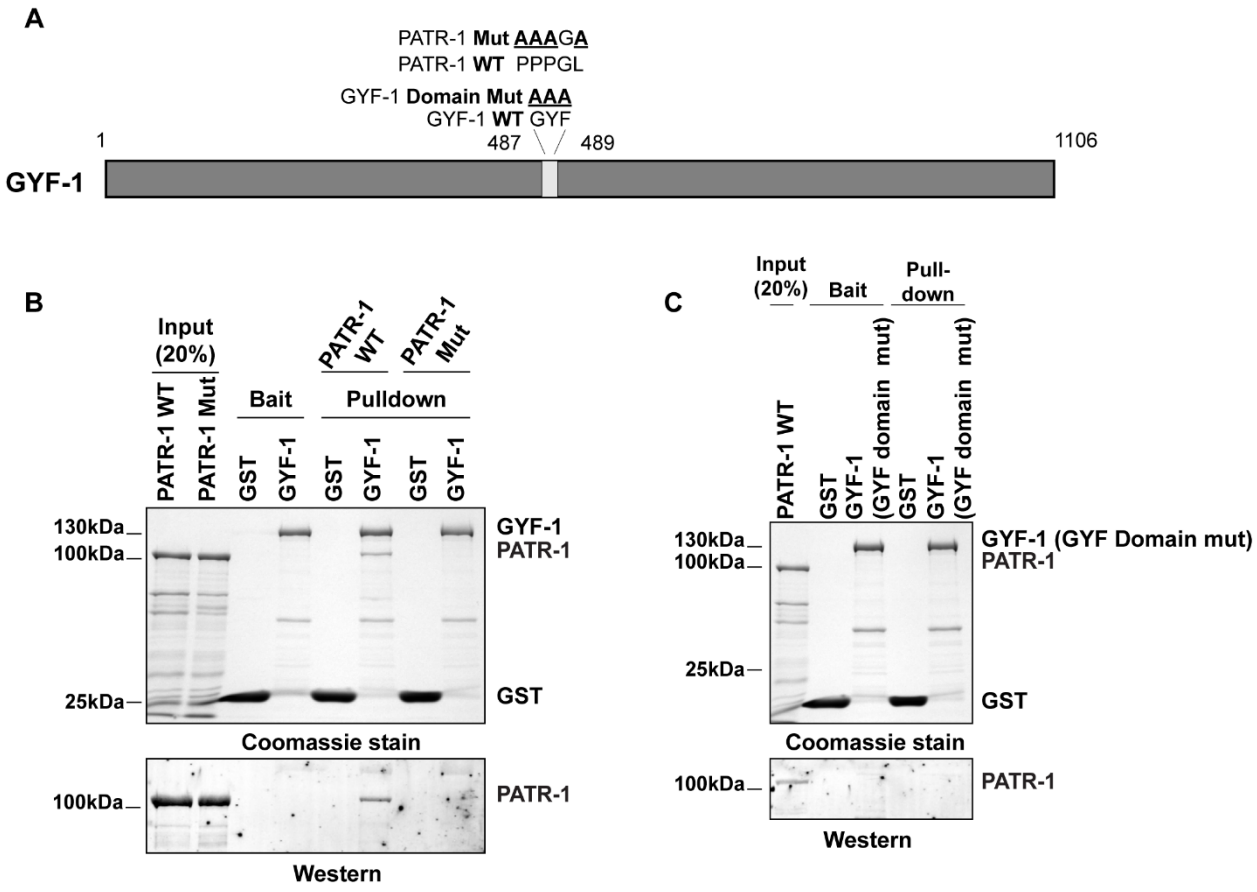

Figure A2-1. Refers to Figure 3-1. GYF-1 interacts with the decapping cofactor PATR-1. **(A)** A schematic representation of wild-type GYF-1 protein. The residues mutated in the GYF domain (GYF DM) of GYF-1 and PPGΦ-motif of PATR-1 are indicated. **(B)** A GST pull-down assay showing the interaction of GST-tagged GYF-1 (WT) with purified His-tagged PATR-1 **(C)** A GST pull-down assay showing an absence of interaction between GST-tagged GYF-1 (GYF domain mut) and purified His-tagged PATR-1. The input, baits, and pull-downs were analyzed by SDS-PAGE and Coomassie staining. Western blotting was performed using an anti-His antibody.

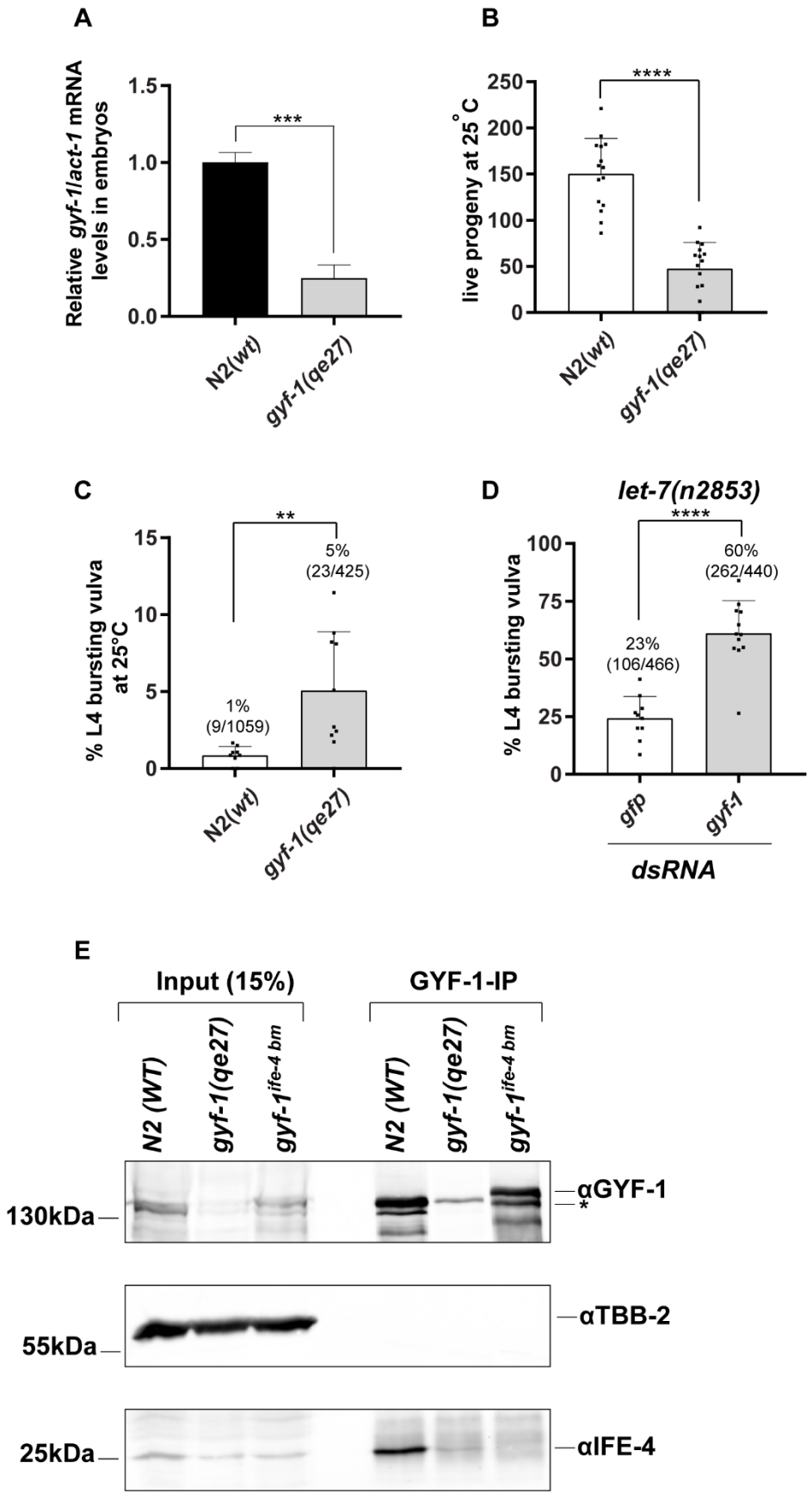
A
Relative gyf-1/act-1 mRNA levels in embryos
1.5
1.0
0.5
0.0
***
N2(wt)
gyf-1(qe27)
B
live progeny at 25 °C
250
200
150
100
50
0
****
N2(wt)
gyf-1(qe27)
C
% L4 bursting vulva at 25°C
15
10
5
0
**
1%
(9/1059)
5%
(23/425)
N2(wt)
gyf-1(qe27)
D
let-7(n2853)
% L4 bursting vulva
100
75
50
25
0
****
23%
(106/466)
60%
(262/440)
gfp
gyf-1
dsRNA
E
Input (15%)
GYF-1-IP
N2 (WT)
gyf-1(qe27)
gyf-1ife-4 bm
N2 (WT)
gyf-1(qe27)
gyf-1ife-4 bm
130kDa
αGYF-1
*
55kDa
αTBB-2
25kDa
αIFE-4

Figure A2-2. Refers to Figure 3-2. Loss of gyf-1 exacerbates the bursting phenotype in let-7(n2853) animals.

(A) Relative expression of *gyf-1* mRNA in embryos was quantified by qRT-PCR and normalized to the level of *act-1* mRNA. **(B)** Brood sizes were quantified for N2(wt) and *gyf-1(qe27)* allele. Experiments were carried out at 25ºC. n=10. **(C)** The percent bursting vulva was quantified at 25 °C in N2(wt) and *gyf-1(qe27)* animals. The number of bursting animals is indicated over the bars. **(D)** *let-7(n2853)* L4 animals were injected with *dsRNA* against *gyf*-1, and F1 animals were scored for the bursting phenotype. Each black square within the bars indicates independent replicates. The error bars represent standard deviation, and the *P*-value (*** $P < 0.0005$, ** $P < 0.005$) was determined using the two-tailed Student's *t*-test. **(E)** Western blots of embryo lysates and GYF-1 immunoprecipitations from wild-type (N2), *gyf-1(qe27),* and *gyf-1*$^{ife\text{-}4\ bm}$. GYF-1 and IFE-4 proteins were detected using polyclonal GYF-1 and IFE-4 antiserum, respectively. Tubulin served as a loading control. * denotes an isoform of GYF-1.

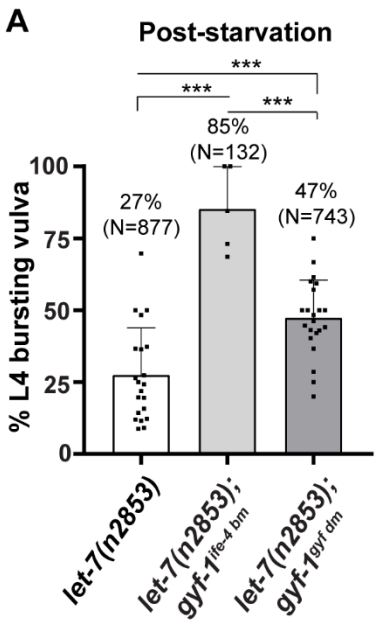

Figure A2-3. Refers to Figure 3-3. The exacerbation of the *let-7* bursting phenotype in *gyf-1*$^{ife\text{-}4\ bm}$ and *gyf-1*$^{gyf\ dm}$ animals post-starvation persists in the subsequent generation.
(A) F1 animals homozygous for both *let-7(n2853); gyf-1*$^{ife\text{-}4\ bm}$/*gyf-1*$^{gyf\ dm}$, whose mothers (P0) were starved (at L4-stage) were monitored for percent bursting phenotype when maintained at 16°C. The number of bursting animals is indicated over the bars. Each black square within the bars indicates independent replicates. The error bars represent standard deviation, and the *P*-value (*** $P < 0.0005$) was determined using the two-tailed Student's *t*-test.

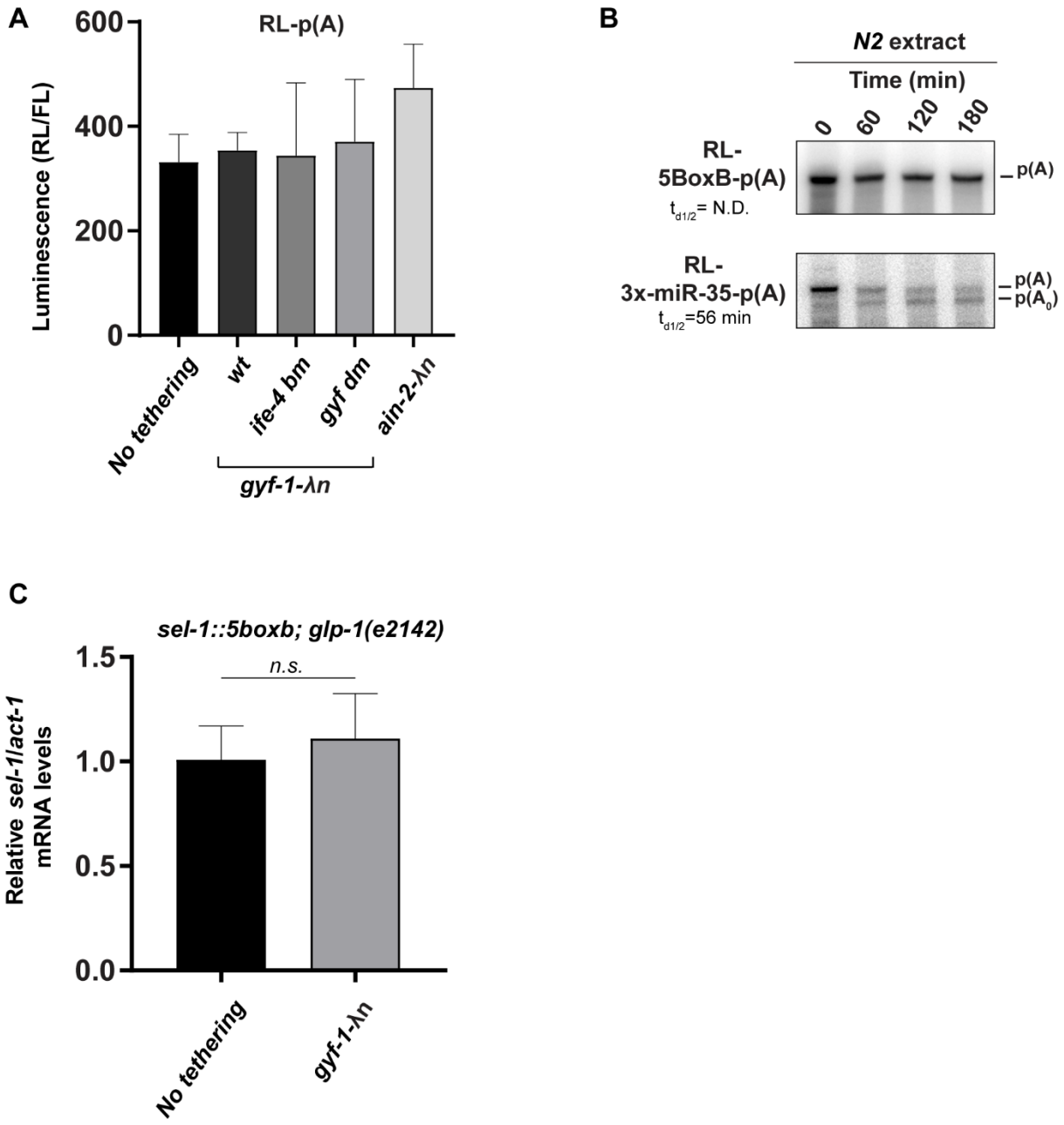

Figure A2-4. Refers to Figure 3-4. In vitro and in vivo tethering of GYF-1 wt and mutants.
(A) Cell-free extracts from wild-type (N2/no tethering), *gyf-1-λn, gyf-1-λn (ife-4 bm), gyf-1-λn (gyf dm),* and *ain-2-λn* have similar translation efficiencies. Control reporters (RL-p(A)) were incubated in the above-mentioned embryonic extracts. RL and FL activities were measured after 3 hours using the Dual-Luciferase Reporter assay system (Promega). RL activity was normalized to that of the FL control, $n = 3$. **(B)** Reporters bearing 5boxb or 3x-miR-35 sites were incubated in wild-type(N2) extracts. The RNA was extracted at indicated time points and analyzed by UREA-

PAGE. p(A) denotes the position of the adenylated reporter mRNA, while p(A_0) indicates the position of the deadenylated reporter mRNA. Half-deadenylation rates ($t_{d1/2}$) were quantified using ImageJ. **(C)** Relative expression of *sel-1* mRNA in embryos of *sel-1::5boxb;glp-1(e2142); gyf-1(wt/no tethering)/gyf-1-λn* animals was quantified by qRT-PCR and normalized to the level of *act-1* mRNA. Error bars represent the standard deviation of three independent biological replicates.

Protein	Sequence ID	Homology
GYF-1	C18H9.3	GIGYF1/2
STAM-1	C34G6.7	STAM1/2 (signal transducing adaptor molecule
UNC-116	R05D3.7	KIF5A/C (kinesin family member)
SUP-26	R10E4.2	RBMS1/2/3 (RNA binding motif single stranded interacting)
VPS-4	Y34D9A.10	VPS4A/B (vacuolar protein sorting)
NOL-58	W01B11.3	NOP-58
RFC-4	F31E3.3	RFC4 (replication factor C subunit 4)
LIN-66	B0513.1	Unknown
ACDH-7	T25G12.5	ACADM (acyl-CoA dehydrogenase medium chain)
UAF-2	Y116A8C.35	U2AF1L5
TRCS-2	T01B7.6	Unknown
KFB-6	F31D4.3	FKBP prolyl isomerase 4

Table A2-1: Refers to Figure 3-1. List of overlapping proteins detected in FLAG immunoprecipitations of AIN-1, NTL-1, and NHL-2 are presented.
From (Wu et al., 2017) and Chapter 4 proteomic datasets. Homology data for each protein was obtained from Wormbase WS277.

Protein	Species	Protein similarity (%)	Protein identity (%)	Gaps (%)
GIGYF1	*Homo sapiens*	35	20	31
GIGYF2	*Homo sapiens*	35	21	35
GIGYF	*Drosophila melanogaster*	33	19	37
SMY2	*Saccharomyces cerevisiae*	36	21	29
gigyf2	*Danio rerio*	36	22	33

Table A2-2: Refers to Figure 3-1. Sequence alignments of GYF-domain encoding proteins

in *C. elegans*, *H. sapiens*, *D. melanogaster*, *S. cerevisiae*, and *D. rerio* were performed using NCBI protein BLAST. Percent similarity, identity, and gaps are listed.

Sequence ID	Protein	GYF-1 (1) NSAFE5	GYF-1 (2) NSAFE5	GYF-1 (3) NSAFE5	Average NSAFE5	Homology
C05D9.5	IFE-4	1341.145	350.9329	2193.899	1295.326	4EHP
F08B6.4b	UNC-87	63.70569	113.6712	16.50797	64.62828	Unknown
F52H3.7b	LEC-2	51.42287	100.3567	14.80571	55.52843	LGALS9
T09B4.5a	T09B4.5	68.00469	77.19297	12.58712	52.59493	Unknown
B0041.2d	AIN-2	133.782	10.65667	5.502657	49.98043	GW182
F29D10.4	HUM-1	40.43188	90.58171	3.741806	44.91847	MYO1E
F54D8.2	COX-6A	62.04669	20.75831	32.15615	38.32038	COX6A1/2
Y116A8C.42	SNR-1	35.03813	19.53723	45.39692	33.32409	SNRPD3
Y53G8AR.9	Y53G8AR.9	45.38272	37.95805	13.06663	32.1358	ZC3H10
C49H3.5c	NTL-4	30.00747	15.05892	38.87897	27.98179	CNOT4
ZK105.1	ZK105.1	34.15904	21.42793	22.12896	25.90531	Unknown
F48F7.1a	ALG-1	42.80107	18.56232	8.215543	23.19298	AGO
F55F8.5	WDR-12	14.47285	39.34149	14.06374	22.62602	WDR12
H10E21.4	H10E21.4	20.19146	22.51749	17.44062	20.04986	Unknown
F26F12.7	LET-418	28.65885	23.24386	2.250403	18.05104	CHD3/4
F53B7.3	ISY-1	17.84714	19.9031	15.41568	17.72197	ISY1-RAB43
T28H10.3	T28H10.3	24.0666	14.37805	13.36359	17.26941	LGMN
C36B1.8a	GLS-1	16.65619	11.39827	19.61862	15.89103	Unknown
F42C5.7	GRL-4	15.12757	12.65268	19.59994	15.7934	Unknown
B0432.4	MISC-1	15.5725	13.02482	13.45094	14.01609	SLC25A11
C26E6.4	RPB-2	17.30858	17.81769	3.450115	12.8588	POLR2B
JC8.2	JC8.2	20.40765	8.534466	8.813677	12.58526	PWP1
T01B7.6	TRCS-2	12.23411	5.116297	15.85104	11.06715	Unknown
F36F2.6	FCP-1	14.46187	12.09589	6.245807	10.93452	CTDP1
Y37D8A.9a	MRG-1	9.482956	7.931533	12.28653	9.900339	MORF4L1/2
D1081.7	D1081.7	14.86218	6.215353	7.22103	9.432854	Unknown
C05E4.9b	ICL-1	9.202753	6.157737	9.538788	8.299759	Unknown
Y54H5A.1	Y54H5A.1	7.012783	8.798223	9.086064	8.299023	GRWD1
B0464.5b	SPK-1	6.826913	7.613363	8.845244	7.76184	SRPK2
C52E12.1	ZNF-598	12.02029	4.308752	6.674574	7.667872	ZNF598
C55B7.1	GLH-2	9.784776	2.727991	6.338789	6.283852	DDX4
T21G5.3	GLH-1	6.245328	3.48239	8.091718	5.939812	DDX4

Table A2-3: List of GYF-1 interactors. Refers to Figure 3-1.

Proteins (32) identified by MuDPIT in three independent GYF-1 purifications are ordered based on normalized spectral counts (NSAF-E5). Homology data for each protein was obtained from Wormbase WS277.

Template generation for dsRNA	
*gyf-1*_Fwd	TAATACGACTCACTATAGGGCGGACAATCACC AACCAGTC
*gyf-1*_Rev	TAATACGACTCACTATAGGGCAGGACGTTCAG ATGATTGAGG
*gfp*_Fwd	TAATACGACTCACTATAGGG CATGGCCAACACTTGTCACT
*gfp*_Rev	TAATACGACTCACTATAGGG TCCCAGCAGCTGTTACAAACT
CRISPR	
*gyf-1(qe27)*_Repair template	CACCGGATCGTGGCACCGGTACAACTCCTCGT GGTGGgaattcttaattaaTGGATCTGTTGGTCGAGCA AGTGGAGCATTCTTTGC
*gyf-1(qe27)*_sgRNA	GCAGCTAATACGACTCACTATAG GGTACAACTCCTCGTGGTGGGTTTAAGAGCTA TGCTG
*gyf-1(qe27)*_genotyping_Fwd	GCTGGAGCTGCTTATGGAAG
*gyf-1(qe27)*_genotyping_Rev	GGGTTGTACAAAGCGTCAGC
*gyf-1(qe39)*_Repair template	GGCTGAATAGAATGTTAAAGCTGGAAAAAGA AATGACTCATCTACTTGTCGTCATCGTCTTTGT AGTCGATGTCATGATCTTTATAATCACCGTCAT GGTCTTTGTAGTCACGGCGCGAAGGATTCACC GGAGCCGATGGGACTGCGTCG
*gyf-1(qe39)*_sgRNA	GCAGCTAATACGACTCACTATAG AAAAGAAATGACTCATCTAA GTTTAAGAGCTATGCTG
*gyf-1(qe39)*_genotyping_Fwd	TTGTTCGCGAATTCATCAAG
*gyf-1(qe39)*_genotyping_Rev	GGGTTGGAGGAATTTAATTTGG
*gyf-1(qe56)*_Repair template	CGACGCAGTCCCATCGGCTCCGGTGAATCCTT CGCGCCGTGGGGGAGGCGGGGGTGGAGATGC TCAAACTAGAAGAAGAGAAAGAAGAGCTGAA AAACAAGCTCAATGGAAAGCTGCTAATTAGAT GAGTCATTTCTTTTTCCAGCTTTAACATTCTAT TC
*gyf-1(qe71)*_Repair template	CGCATCAGGCATAATCGATCCGGTTGGAGCCA GCTCGGCAGCACGTTCGCGCGTGGCCGAGgcTT CgGAtACgACTGGCGAAGAGAGGACCGCGGCG GCTGCAGCAGCG
*gyf-1(qe71)*_sgRNA	GCAGCTAATACGACTCACTATAGG TACGAGAATTCCGAAACCAC GTTTAAGAGCTATGCT
*gyf-1(qe71)*_genotyping_Fwd	GGGTCATGGTCCCCGTGGTAC

*gyf-1(qe71)*_genotyping_Rev	CTAGAATACAATGTGCACACG
*gyf-1(qe72)*_Repair template	CGTTTTCGCCTCTCTGAACTCGAAGTGATTCAT CCGTAGCAGCAGCTGCTTTGAACCATACATTC ATTTGATCTTTAGGGAAAGGAC
*gyf-1(qe72)*_sgRNA	GCAGCTAATACGACTCACTATAGGATGAATGT ATGGTTCAAAGCGTTTAAGAGCTGT
*gyf-1(qe72)*_genotyping_Fwd	CCTTCTGATCCATCAGCGTG
*gyf-1(qe72)*_genotyping_Rev	CACTCCACCAAATGCAGCTG
*dpy-10*_MutationFix_Repair template	CACTTGAACTTCAATACGGCAAGATGAGAATG ACTGGAAACCGTACCGCTCGTGGTGCCTATGG TAGCGGAGCTTCACATGGCTTCAGACCAACAG CCTAT
*dpy-10*_MutationFix_sgRNA	GCAGCTAATACGACTCACTATAGGGCTACCAT AGGCACCGCATGGTTTAAGAGCTATGCT
*dpy-10*_repair template	CACTTGAACTTCAATACGGCAAGATGAGAATG ACTGGAAACCGTACCGCATGCGGTGCCTATGG TAGCGGAGCTTCACATGGCTTCAGACCAACAG CCTAT
*dpy-10*_sgRNA	GCAGCTAATACGACTCACTATAG GCTACCATAGGCACCACGAG GTTTAAGAGCTATGCTGG
*sel-1(qe57)*_sgRNA	GCAGCTAATACGACTCACTATAG GGGACAGCGTAGACCCGAGT GTTTAAGAGCTATGCTG
5BoxB-Sel-1_repair template_Fwd	CTTTTAATAGTTGTAATATTCACATCAGCCTAC TCGTAAGTCCAACTACTAAACTG
5BoxB-Sel-1_repair template_Rev	GGCAAATGTTTGATGATTAGAAGGGACAGCGT AGACCTCGAGATAATATCCTCGATAG
*sel-1(qe57)*_genotyping_Fwd	TCTTTACCTGGCTAAACGTTTCT
*sel-1(qe57)*_genotyping_Rev	CGGCAAGTAAATCACACGAAAT
qPCR	
*gyf-1(qe27)*_Fwd	GCTGCTATCGCTGGAGACAA
*gyf-1(qe27)*_Rev	GTAGCAGGAGACGATACGGC
*act-1*_Fwd	CGTGTTCCCATCCATTGTCG
*act-1*_Rev	AGTTGGTGACGATACCGTGCTC
Constructs for recombinants	
GYF-1_N-Ter_Fwd	GTCGACTTATGTCGTCAGTTTCGTCC
GYF-1_N-Ter_Rev	GCGGCCGCTCATTCTTTTACAATCGGAGC
GYF-1_C-Ter_Fwd	GTCGACTGGCGCCATTTGAATATTTGGAAG
GYF-1_C-Ter_Rev	GCGGCCGCCTAACGGCGCGAAGGATT
GYF-1_Mid_Fwd	GTCGACCAGCTCCGATTGTAAAAG
GYF-1_Mid_Rev	GCGGCCGCTTATTCCAAATATTCAAATGGC

GYF domain mutant_Fwd	GAAGTGATTCATCCGTAGCAGCTGCCGCTTTGAACCATAC
GYF domain mutant_Rev	GTATGGTTCAAAGCGGCAGCTGCTACGGATGAATCACTTC
PATR-1_PPPGL_mutant_Fwd	GATAACAAATTCTCACATGCAGCTGCGGGAGCCAATCAAAATGTTCAACC
PATR-1_PPPGL_mutant_Rev	GGTTGAACATTTTGATTGGCTCCCGCAGCTGCATGTGAGAATTTGTTATC
Antibody generation	
GYF-1_Fwd	GAATCTGTCGACTACCTGCTGCAACTCGAAGCG
GYF-1_Rev	GAATCTGCGGCCGCTTACCGTCGAATCTTTTCTTCTGCC
IFE-4_Fwd	GCATCCGGATCCATGGAAGCTGAAACGTCAAC
IFE-4_Rev	GCATCCAAGCTTTCATTTGCAGATATTTTTAGTAG

Table A2-4. Related to Material and methods (Chapter 3). List of oligonucleotides used in this study.

APPENDIX 3: Supplemental information to Chapter 4

Enhancement of microRNA-mediated deadenylation by the TRIM-NHL protein NHL-2 and DEAD-box protein CGH-1

Vinay K. Mayya, Mathieu N. Flamand, Elva Vidya, Nahum Sonenberg, James A. Wohlschlegel , Christopher M. Hammell, Thomas F. Duchaine

Sequence ID	Protein	NHL-2 (1) NSAFE5	NHL-2 (2) NSAFE5	NHL-2 (3) NSAFE5	Average NSAFE5	Homology
B0464.7	BAF-1	376.647	720.5668	486.1756	527.7965	BANF1
T09B4.5a	T09B4.5	59.79895	114.4019	19.84845	64.68311	Unknown
K07H8.10	K07H8.10	70.01166	92.08371	24.40016	62.16518	Unknown
ZK105.1	ZK105.1	30.03726	64.64763	34.89486	43.19325	Unknown
F21C3.5	PFD-6	22.17036	31.81074	51.51146	35.16419	PFDN6
Y55F3AM.3c	RBM-39	25.68704	33.7852	39.78816	33.0868	RBM39
Y53G8AR.9	Y53G8AR.9	35.47258	46.65575	13.73639	31.95491	ZC3H10
F53B7.3	ISY-1	41.84967	35.02755	16.20585	31.02769	ISY1-RAB43
F58A4.8	TBG-1	28.31215	51.1551	9.745411	29.73755	TUBG1/2
M04B2.1	MEP-1	25.68704	52.21349	9.94704	29.28252	Unknown
F55F8.5	WDR-12	38.17948	39.56415	9.856407	29.20001	WDR12
F54B3.3	ATAD-3	23.4745	53.89113	7.272206	28.21261	ATAD3A
F26F12.7	LET-418	29.78271	35.06312	7.097259	23.98103	CHD3/4
Y47G6A.11	MSH-6	27.08672	39.42815	3.648366	23.38775	MSH6
C42D4.6	SKR-16	30.86702	14.763	23.90587	23.17863	SKP1
T17H7.4k	PAT-12	19.13332	8.134253	39.51564	22.26107	Unknown
F36F2.6	FCP-1	23.3142	30.41087	6.565952	20.09701	CTDP1
Y44E3A.6a	EDC-4	16.608	15.88646	20.58008	17.69151	EDC4
D2030.2b	D2030.2	5.943543	14.21331	32.22206	17.45964	CLPX
H04M03.3	H04M03.3	8.388785	8.024331	32.4847	16.29927	Unknown
Y57A10A.18e	PQN-87	13.18561	31.53188	2.917709	15.8784	Unknown
C28D4.3	GLN-6	11.38641	21.78344	11.75805	14.97597	GLUL
F42G9.1b	PPM-1.G	26.80297	8.546168	9.225933	14.85836	PPM1G
T21G5.3	GLH-1	10.98348	7.004199	25.51944	14.50237	DDX4
AH6.5	MEX-6	8.972587	17.16554	13.89817	13.34543	Unknown
B0495.8a	LUC-7L	8.924809	17.07413	13.82416	13.27437	LUC7L
B0432.4	MISC-1	9.128972	8.73236	21.2106	13.02398	SLC25A11
R07E5.3	SNFC-5	10.99789	14.02678	11.35686	12.12718	SMARCB1
Y37D8A.9a	MRG-1	8.338702	7.976424	19.37446	11.89653	MORF4L1/2
F57B9.7a	FLAP-1	11.87025	11.35454	12.25768	11.82749	LRRFIP2
Y57G11C.15b	SEC-61	9.480086	6.04548	19.57902	11.70153	SEC61A1/2
F20D12.1b	CSR-1	6.44398	15.41005	12.47682	11.44362	Unknown
H15N14.1e	ADR-1	18.76908	2.992276	12.11356	11.29164	ADAD1
C55B7.1	GLH-2	7.170085	8.230293	17.76987	11.05675	DDX4
C06G3.2	KLP-18	7.493201	14.33531	9.285327	10.37128	KIF15

F48F7.1a	ALG-1	9.757613	16.00061	4.318326	10.02552	AGO
F38A5.13	DNJ-11	7.114088	11.34169	11.01943	9.825068	DNAJC2
K10C3.6b	NHR-49	5.868625	5.61366	13.63539	8.372557	HNF4A/G
F22B7.5a	DNJ-10	9.18903	5.859873	9.488953	8.179285	DNAJA3
Y54F10BM.2	IFFB-1	11.70446	7.463972	4.028829	7.732422	EIF5B
C49H3.5c	NTL-4	7.036436	10.0961	5.449575	7.527371	CNOT4
F22G12.4a	F22G12.4	12.61728	2.413823	5.863093	6.964731	ANKFY1
C12D8.10a	AKT-1	5.163522	7.408785	7.998083	6.856796	AKT1/2/3
C07G1.5	HGRS-1	9.579785	3.665435	5.935477	6.393565	HGS
C18G1.4a	PGL-3	4.030974	5.78377	9.36572	6.393488	Unknown
F35G12.4b	WDR-48	6.162056	3.929562	6.36318	5.484933	WDR48
F10C2.4	F10C2.4	6.460373	2.47188	6.004111	4.978788	POLD1
T16G12.5	EKL-6	4.346678	5.54378	4.488551	4.793003	TANGO6
ZK520.4b	CUL-2	3.609128	3.452328	5.590391	4.217282	CUL2
F43G6.9	PATR-1	3.353499	3.207805	5.194432	3.918579	PATL1/2
D2085.1	PYR-1	1.906369	1.215697	6.890068	3.337378	CAD
K12H4.8	DCR-1	2.925095	1.399006	2.265425	2.196509	DICER1

Table A3-1. List of NHL-2 interactors (RNase A treated).

Proteins (52) identified by MuDPIT in three independent NHL-2 purifications are ordered based on normalized spectral counts (NSAFE5). Proteins found in the negative control (N2) strains were excluded. Homology data for each protein was obtained from Wormbase WS277.

Sequence ID	Protein	% Peptide Coverage	Homology
Y44E3A.6	EDC-4	49-62	EDC-4
ZC518.3	CCR-4	33-63	Ccr4/CNOT6, CNOT6L
F22G12.4	F22G12.4	34-58	ANKFY1
Y56A3A.20	CCF-1	48-53	Caf1/CNOT7
Y65B4BR.5	ICD-2	24-48	NACAD/NACA2/NACA
Y71G12B.12	ATG-5	38-48	Atg5p, ATG5
R05D11.8	EDC-3	35-47	Edc3
Y56A3A.1	NTL-3	18-45	CNOT3
F57B9.2	NTL-1	28-45	CNOT1
Y11D7A.12	FLH-1	32-43	Unknown
T20F5.6	T20F5.6	28-39	RNF225
K04G7.3	OGT-1	4-38	OGT
Y39A1A.3	Y39A1A.3	33-38	SSSCA1
C26E6.3	NTL-9	13-38	RQCD1
Y73F8A.25	NTL-11	6-35	CNOT11
Y73F8A.25	NTL-2	8-35	CNOT2
F22B5.2	EIF-3.G	19-35	EIF3G
ZK520.4	CUL-2	19-35	Cullin-2
C34G6.7	STAM-1	17-34	STAM
ZK112.2	NCL-1	25-31	TRIM2
W03F9.1	W03F9.1	20-30	Zpr-1
F44A2.1	TAG-153	18-30	CNOT2 homolog
Y92C3B.2	UAF-1	23-30	U2AF65
C37C3.2	C37C3.2	21-28	eIF5 - translation activator
Y55F3AM.15	CSN-4	18-27	CSN4
T22D1.10	RUVB-2	12-27	RUVBL2
ZK632.7	PANL-3	19-26	PAN3
E02D9.1	E02D9.1	10-25	QKI
T23G7.1	DPL-1	20-24	TFDP1
K02B12.7	K02B12.7	9-25	ArfGAP1
T23D8.4	EIF-3.C	8-24	eIF3C
R10E4.2	SUP-26	19-23	RBMS1
C27A12.8	ARI-1	25-27	ARIH1
C18D1.1	DIE-1	15-23	CG18265
R06F6.4	SET-14	15-22	SMYD1

C49H3.5	NTL-4	17-22	CNOT4
ZC518.2	SEC-24.2	9-22	SEC24B
Y17G7B.2	ASH-2	18-24	Set1/Ash2 isoform 1
Y54E5A.7	Y54E5A.7	6-23	RANBP10
K07C5.1	ARX-2	11-21	Arp-2
C06G1.4	AIN-1	8-21	GW182/TRNC6
C39E9.13	RFC-3	9-23	RfC3
Y108G3AL.1	CUL-3	8-21	Cullin-3
C26E6.2	FLH-2	10-20	Unknown
D2013.2	WDFY-2	14-20	WDFY2
Y55F3AM.12	DCAP-1	13-19	Dcp1
C30G12.7	PUF-8	10-13	PUM2
F31E3.4	PANL-2	12-14	PAN2
C18H9.3	GYF-1	3-8	GIGYF1/2
W06B11.2	PUF-9	8-10	PUM2
T21G5.3	GLH-1	0-21	DDX4
B0041.2	AIN-2	0-11	GW182/TRNC6

Table A3-2. List of NHL-2 interactors (RNase A untreated).

Proteins (51) identified by MuDPIT in at least two independent NHL-2 purifications are listed. Proteins found in the negative control at more than 1 peptide in the N2 (WT) strain were excluded. Homology data for each protein was obtained from Wormbase WS250.

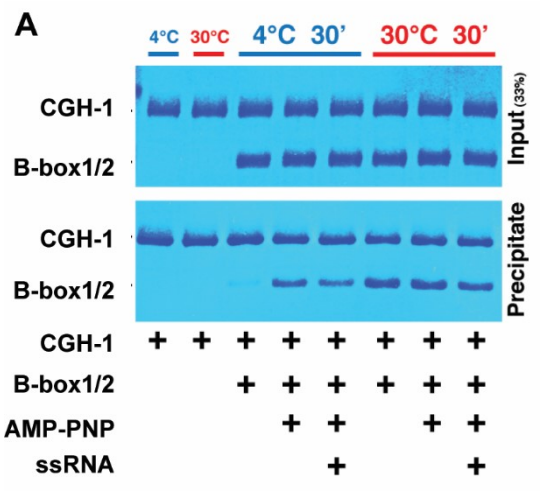

Figure A3-1. Refers to Figure 4-1. NHL-2 interacts with the DEAD-box helicase, CGH-1.
A pull-down assay showing the interaction between TAP-tagged CGH-1 and MBP-tagged B-Box1/2 domain of NHL-2. The inputs and precipitates were analyzed by SDS-PAGE and Coomassie staining.

APPENDIX 4: Development of a single-molecule imaging technique to study miRISC/target interactions

Vinay K. Mayya, Alice M Lambert, Ramunas Stanciauskas, Fabien Pinaud, and Thomas F. Duchaine

Work in progress

A4.1 Abstract

MicroRNAs are short RNA molecules that associate with Argonaute proteins to form the miRNA-Induced Silencing Complex (miRISC). The miRISC scan and bind complementary sequences embedded in 3`UTRs of mRNAs to silence gene expression. As much as it is known about the mechanism and the effector proteins involved in miRNA-mediate gene silencing, very few studies have carefully quantified miRISC target recognition kinetics. Moreover, how and when effector proteins assemble on target mRNA following miRISC target recognition is unclear. In this chapter, we describe a single-molecule imaging system that allows measurement of miRISC target recognition kinetics and can monitor the assembly of effector proteins on target RNAs in a cell-free *C. elegans* embryonic extract. Using CRISPR/Cas9 gene editing, functional tags that allow fluorescent labeling was introduced to *alg-1*, *ain-1*, and *ntl-1* locus. With fluorescent RNA bearing a miRNA-binding site as bait, the association of miRISC was detected using total internal reflection microscopy (TIRF). Our TIRF-microscopy system, combined with CRISPR-Cas9 gene editing of endogenous loci, provides a unique opportunity to visualize in real-time miRISC target recognition and recruitment of effector complexes in a near-physiological microenvironment.

Keywords: miRISC, single-molecule imaging, TIRF, deadenylase complex

A4.2 Introduction

MicroRNAs (miRNAs) are ~22 nucleotide-long RNA molecules that regulate a wide variety of biological processes by exerting a determining and widespread control over gene expression (Ameres and Zamore, 2013). When embedded into Argonaute proteins (ALG-1/2 in *C. elegans*) as part of the miRNA Induced Silencing Complex (miRISC), miRNAs direct mRNA target recognition through partial base-pairing with target sites most often located in 3′ untranslated regions (3`UTRs). This activates a cascade of events that culminate with the translational repression and the destabilization of target mRNAs. The underlying mechanism involves deadenylation through the CCR4-NOT deadenylase complex, de-capping, and other activities recruited onto miRISC via the GW182 proteins (AIN-1/2 in *C. elegans*) (Jonas and Izaurralde, 2015; Mayya and Duchaine, 2019).

Biochemical, structural, and bioinformatic analyses suggest that Argonaute proteins program miRNAs into distinct functional domains: the 5' anchor (guide nucleotide g1), the seed region (g2-g8), the central region (g9-12), supplementary region (g13-g16), and the 3` tail (g17-g22) (Friedman et al., 2009; Lewis et al., 2005; Schirle and MacRae, 2012; Wee et al., 2012). However, animal miRNAs predominantly bind their targets via the seed (g2-g8), and to a lesser extent, through the supplementary region (g13-g16) (Broughton et al., 2016; Grosswendt et al., 2014). Argonaute proteins pre-organize the seed into a conformation that enables efficient base pairing with target mRNAs (Schirle and MacRae, 2012; Wang et al., 2008). The initial pairing of g2-g5 to target mRNAs promotes conformational changes in the miRISC that exposes g2-g8 and g13-g16 for further target recognition (Schirle et al., 2014). Accordingly, miRISCs bind to targets matching the seed and supplementary regions at rates that approach macromolecular diffusion (3.6

x 10^7 M^{-1} s^{-1}), and mismatches in the two regions led to a 40-fold reduction in miRISC binding (Wee et al., 2012). While this data was obtained through ensemble-averaging techniques, recent advances in single-molecule fluorescence microscopy have enabled observation and precise examination of the individual domains of miRISC that contribute to target recognition (Chandradoss et al., 2015; Li and Zhang, 2012; Salomon et al., 2015). Within the seed region, g2-g5 base pairs contribute significantly to the binding of miRISC to target RNA, while g6-g8 base pairs mainly affect the dissociation rates of miRISC after successful target recognition. Although these studies provide a high spatio-temporal resolution on the kinetics of miRISC target recognition, these studies were performed using purified components or under over-expression and thus fail to fully represent the kinetics in a physiological setting.

Interactions between the Argonaute protein and GW182 on the one hand, and between GW182 and the effector machinery such as the CCR4-NOT complex, on the other hand, have been studied in several species primarily using recombinant or immunoprecipitation interaction assays (Braun et al., 2011; Jonas and Izaurralde, 2015). However, it remains unclear how and when these complexes are assembled and recruited to the target mRNA. Moreover, their role in target mRNA recognition by miRISC has not been studied. Here, we developed a single-molecule imaging technique to observe and quantitate miRISC assembly and mRNA association kinetics. Through transgenesis and CRISPR/Cas9 genome editing, functional tags that allow fluorescent labeling was introduced to Argonaute (ALG-1/2) and some of its interactors (AIN-2, NTL-1). miRISC association with target RNA was then monitored using total internal reflection microscopy (TIRF). In addition to monitoring the recruitment of the CCR4-NOT complex to target mRNAs by miRISC, we can study how cooperative miRISC interactions affect the assembly of various effector proteins involved in miRNA-mediated silencing.

A4.3 Results

A4.3.1 Development of a single-molecule strategy to monitor miRISC target recognition kinetics

To observe the assembly of miRISC on target mRNAs, we first generated transgenic animals that express SNAP-tagged ALG-2 protein. The SNAP-tag enables efficient, irreversible self-labeling with fluorescent dyes having O^6-benzylguanine (BG) derivatives (Keppler et al., 2004). To test whether introduction of SNAP-tag allows efficient labeling without altering the function of ALG-2, we performed pulldown assay on *C. elegans* embryonic extract expressing SNAP-ALG-2 and incubated with Vista green dye. Biotinylated 2'-*O*-Me oligonucleotides bearing a *miR-35* or *miR-16* (as a control) binding site was then pulled down using streptavidin-coupled magnetic beads. The captured miRISC was resolved by SDS-PAGE and in-gel fluorescence visualized (Figure A4-1B). The bait matching the *miR-35* miRNA captured fluorescently labeled SNAP-tagged ALG-2, while a non-specific bait for human *miR-16* did not. This validated that SNAP-tag in ALG-2 enables fluorescent labeling of the protein and does not affect the ability of ALG-2 to program *miR-35* miRNA and bind to target mRNAs.

We next designed a biotinylated Cy3-labeled RNA bearing a *miR-35* miRNA binding site. We examined its interaction with immunopurified SNAP-tagged ALG-2 through a non-denaturing gel-electrophoretic mobility shift assay (EMSA) and visualized by in-gel detection fluorescence imaging (Figure A4-1C). Upon addition of ALG-2, Cy3 RNA showed retarded mobility, and was relieved upon addition of a *miR-35* competitor RNA, indicating a specific interaction between ALG-2 and the Cy3 labeled target RNA. To confirm the interaction between ALG-2 and target RNA, we measure fluorescence resonance energy transfer (FRET) of SNAP-ALG-2 (Vista green) and towards the acceptor fluorophore in the RNA(Cy3) in the Protein:RNA duplex in gel.

Interaction between Vista green-labeled ALG-2 and Cy3-labeled *miR-35* target RNA led to FRET, while a background level of fluorescence was detected for an unlabeled *miR-35* target (as a control) (Figure A4-1D). Taken together, these results show that fluorescently labeled ALG-2 interacts with Cy3-labeled *miR-35* target RNA, and this interaction leads to FRET, and thus can be used to in single-molecule FRET assays.

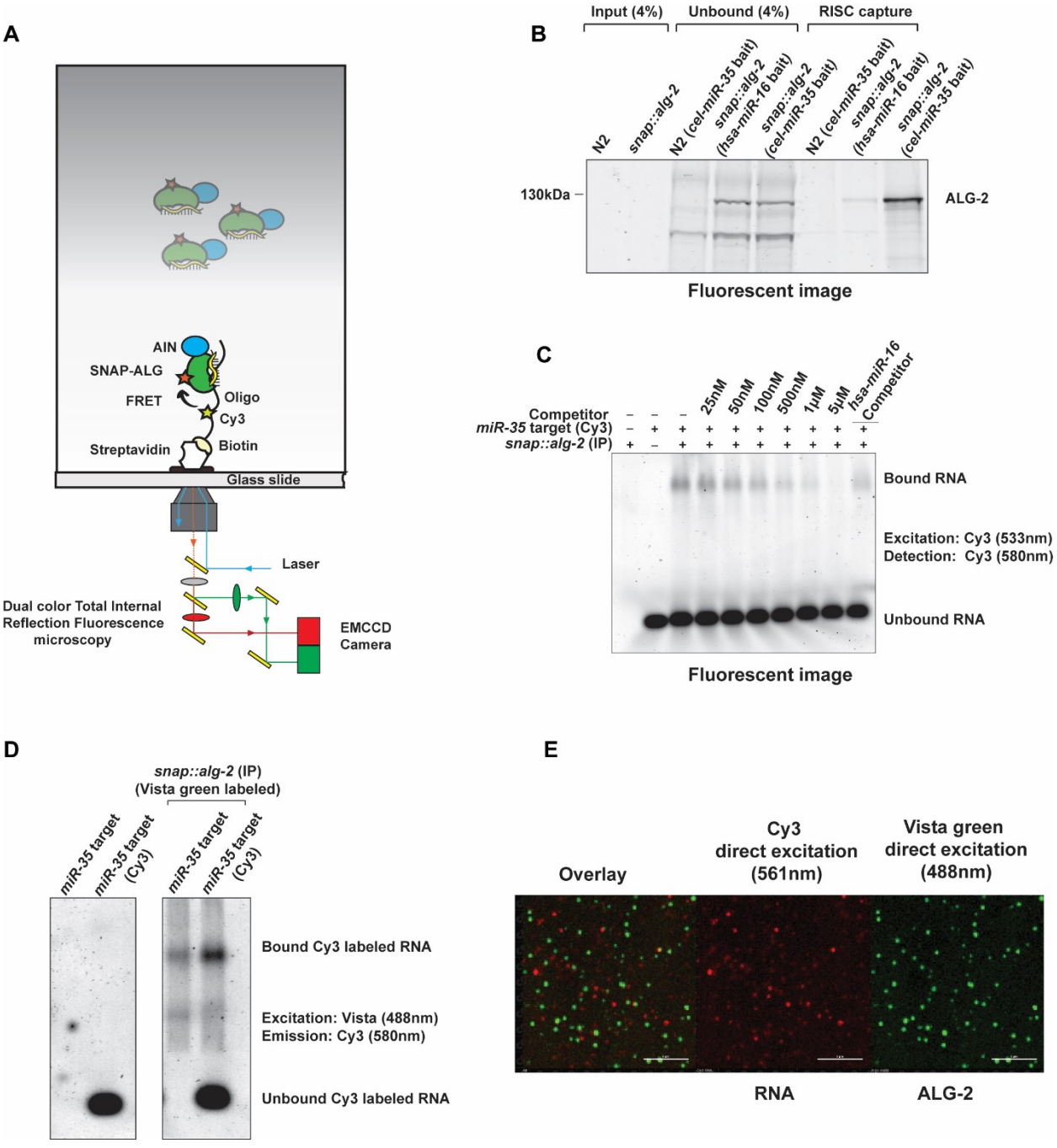

Figure A4-1. Development of a single-molecule strategy to monitor miRISC target recognition kinetics.

(A) A schematic representation of a single-molecule assay to monitor the miRISC interactions with target RNA. **(B)** Biotinylated 2'-O-Me oligonucleotides bearing binding-sites for *cel-miR-35* or *hsa-miR-16* (served as a control) were used in miRISC pull-down assays. Captured miRISC were detected through in-gel fluorescence method. **(C)** Gel-shift competition assay confirming

retardation of Cy3-labeled RNA is due to bound ALG-2. FLAG-SNAP-tagged ALG-2 was immunoprecipitated from *C. elegans* embryos. The eluate was then incubated 50nM of Cy3 target RNA and increasing concentrations of a competitor (a non-fluorescent 2'-O-Me-RNA harboring a perfect complementary binding site to *miR-35*. *hsa-miR-16* competitor at a concentration of 5uM was used as a negative control. The mixture was then resolved on an 0.8% TAE agarose gel and scanned using a typhoon scanner. **(D)** Gel-shift assay showing FRET between Vista Green-labeled ALG-2 to Cy3-labeled target RNA. **(E)** CCD images (overlay, and RNA, Protein channels) show Vista Green-labeled ALG-2 binding to Cy3-labeled target RNA. Individual spots represent single molecules.

To observe the assembly of miRISC on target mRNAs, we designed a dual-color total internal reflection fluorescence (TIRF) microscopy approach to excite only fluorescent molecules immediately above a glass-slide surface. Cy3-labeled RNA bearing a *miR-35* miRNA binding site was attached to a glass surface, then incubated with *C. elegans* embryonic extract expressing Vista green-labeled ALG-2 protein (Figure A4-1A). Colocalization of miRISC and target mRNA was observed through direct excitation of individual dyes or a donor fluorophore (on ALG-2) and detection of the acceptor (Cy3 labeled RNA). Excitation of both 488nm (ALG-2) and 561nm (RNA) lasers and imaging acquisitions show colocalization events occurring with a low frequency but clearly observable over the background signal (Figure A4-1E). Thus, our results show that TIRF microscopy can be used to observe target recognition by miRISC in *C. elegans* extracts.

A4.3.2 Single-molecule analyses of cooperative miRISC interactions

In *C. elegans* embryos, miRNA-binding sites in 3`UTRs of mRNAs functionally cooperate to silence gene expression (Wu et al., 2010). Here, cooperative miRISC interactions on multiple miRNA-binding sites promote the effector machinery assembly by recruiting the CCR4-NOT deadenylase complex to target mRNAs (Flamand et al., 2017; Wu et al., 2017). To better

understand cooperative miRISC interactions using single-molecule imaging, we constructed a 172-nt RNA target bearing the complete 3`UTR of *egl-1* mRNA along with 17 AlexaFluor555 dyes within a 148-nt 3' extension (Figure A4-2A). Multiple AlexaFluor555 dyes in the target RNA result in increased brightness, allowed us to reduce laser power and thereby decreased photobleaching rate (Salomon et al., 2015). *miR-35* and *miR-58* binding sites in *egl-1* 3`UTR functionally cooperate to silence its expression (Sherrard et al., 2017; Wu et al., 2010). Thus, to specifically observe cooperative miRISC interactions between these two miRNAs, we mutated the seed region for all other predicted miRNA-binding sites. AlexaFluor555-labeled RNA was then attached to a glass surface and observed using a TIRF-microscope. Bright and distinct spots were observed upon excitation in 555nm channel indicating individual RNAs bound to the glass surface (Figure A4-2C, left panel).

To enable fluorescent labeling of miRISC, we introduced a SNAP-tag to *alg-1* locus through CRISPR/Cas9 genome editing. As the *alg-2* paralog can confound the single-molecule colocalization signal with target RNA, we crossed SNAP-ALG-1 expressing animals with a null allele of *alg-2(ok304)*. Embryonic extracts were then prepared, labeled with AlexaFluor647 dye, and performed a miRISC capture experiment using either Cy3-labeled *miR-35* target RNA or AF555-labeled *egl-1* 3`UTR RNA, along with seed mutated controls. In-gel fluorescence detected SNAP-ALG-1 captured in both RNA baits that contained miRNA-binding sites and absent in baits wherein the miRNA seed regions were mutated, indicating a functional ALG-1 protein (Figure A4-2B). A strong signal was also observed upon the addition of AF647 labeled embryonic extracts onto a glass surface and excited in 647 channel, showing individual ALG-1 proteins (Figure A4-2C, right panel).

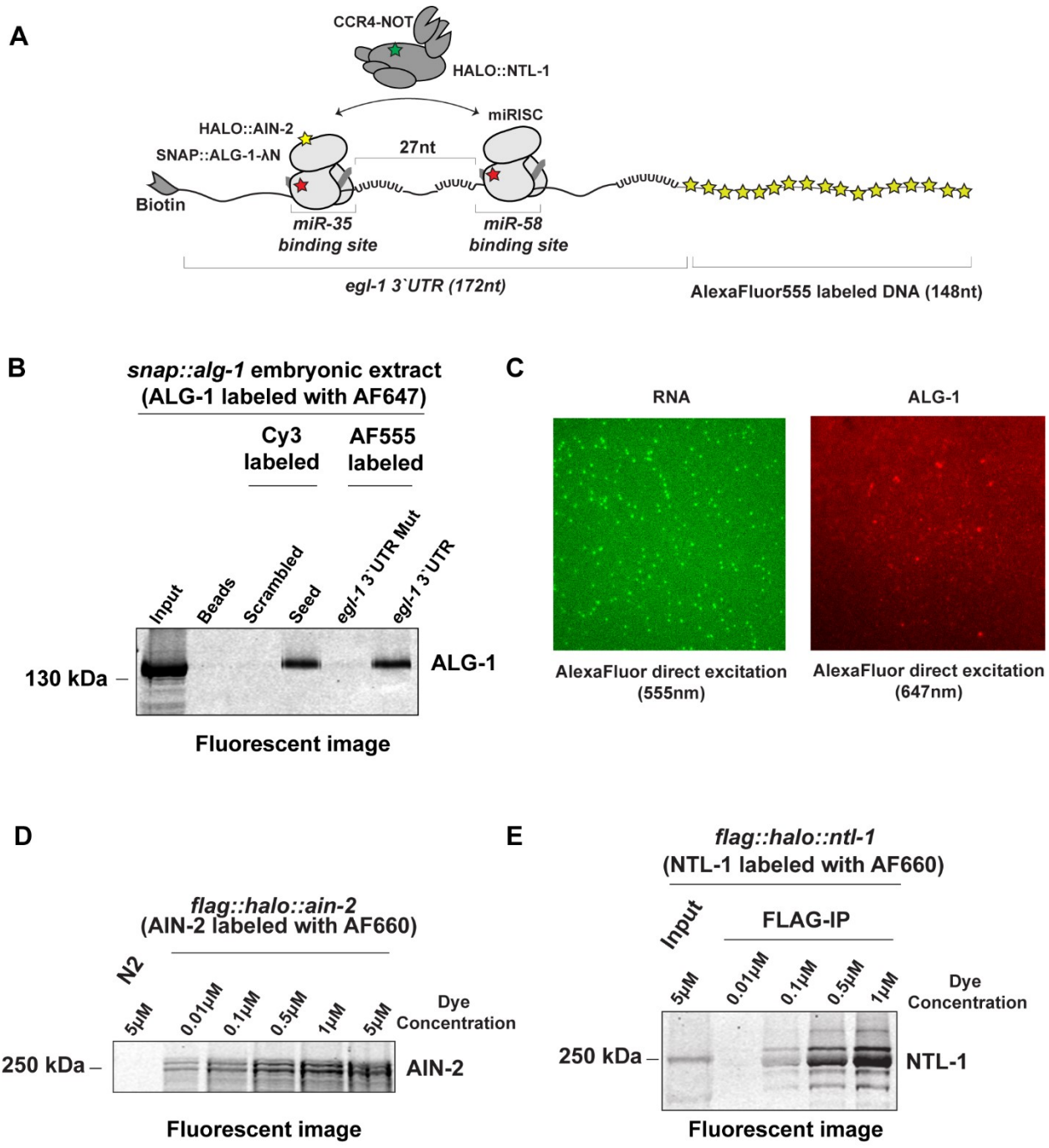

Figure A4-2. Single-molecule analysis of cooperative miRISC interactions.
(A) A strategy to monitor cooperative miRISC interactions and assembly of effector proteins such as AIN-2 and CCR4-NOT complex on target mRNA. **(B)** In-gel detection of fluorescently labeled ALG-1 captured from Cy3-labeled *miR-35* target RNA or AF555-labeled *egl-1* 3`UTR. Seed mutant target RNA served as a negative control. **(C)** CCD images (RNA and Protein channels) show AlexaFluor-555-labeled *egl-1* 3`UTR and AlexaFluor-647-labeled ALG-1. Individual spots

represent single molecules. **(D-E)** In-gel detection of fluorescently labeled AIN-2 and NTL-1. (D) *flag::halo::ain-2* and *flag::halo::ntl-1* animals were lysed and incubated in increasing concentrations of AF660 dye at 4 °C for 30 minutes. Protein lysates (60 µg) was then resolved in using SDS-PAGE. N2 (wild-type) animals served as a control. (E) Fluorescently labeled NTL-1 was immunoprecipitated using anti-FLAG M2 agarose beads, eluted, and resolved using SDS-PAGE.

Biochemical studies suggest that the CCR4-NOT complex is recruited to mRNA following target recognition by miRISC (Wu et al., 2017). To validate and observe these interactions at a single-molecule resolution, we introduced a Halo-tag to both *ain-2* and *ntl-1* locus using CRISPR-Cas9 gene-editing technique. Lysates from animals expressing Halo-tagged AIN-2 or FLAG-Halo-tagged NTL-1 were individually labeled with AF660. Crude lysates of fluorescently labeled AIN-2 or FLAG-immunoprecipitated NTL-1 samples were then resolved using an SDS-PAGE and detected through In-gel fluorescence. Strong fluorescent signals were observed for both AIN-2 and NTL-1, confirming the introduced Halo-tag functionality (Figure A4-2D-E).

A4.4 Discussion

Recent improvements in fluorescent protein photostability, the sensitivity of camera detectors, robust software algorithms that track fluorescently labeled proteins, and analytical tools to improve the signal-to-noise ratios have enabled researchers to understand several critical biological processes at a single-molecule resolution (Shashkova and Leake, 2017). With precise genome engineering, we developed a single-molecule imaging technique to monitor the kinetics of miRISC target recognition in *C. elegans* embryos. Furthermore, by using the complete 3`UTR of the *egl-1* gene and introducing fluorescent dyes to an effector complex (CCR4-NOT complex), we extended the single-molecule method to allow observation of effector assembly on target RNA.

Our transgenic *snap::alg-2* animals enabled us to develop the single-molecule system- from testing the ability of SNAP-tag to self-label fluorescent dyes to monitoring the miRISC target recognition under the microscope. In subsequent years, groups of Macrae and Zamore published single-molecule imaging studies showing target recognition by miRISC. While both groups use slightly different techniques (FRET- Macrae lab; dual-excitation -Zamore Lab), they reached similar conclusions. However, these studies were performed using purified miRISC, and they lacked physical constraints such as endogenous RNA and proteins that can affect the kinetics of target recognition. This allowed us to improve and extend our initial design to monitor target recognition by endogenously expressed miRISC. Unlike previous studies, we used *C. elegans* embryonic extract that recapitulates translation as well as miRNA-mediated silencing. While this approach is still performed under *in vitro* conditions, the transcriptome and RBPs are still maintained and intact, thus offering us a near-physiological measurement of miRISC target recognition kinetics.

Cooperative action of miRNAs had been evident since the early days of its discovery. For example, in *C. elegans,* heterochronic genes *lin-14* and *lin-41* contain multiple binding sites for *lin-4* and *let-7* miRNA, respectively (Lee et al., 1993; Reinhart et al., 2000; Vella et al., 2004; Wightman et al., 1991; Wightman et al., 1993). Each of these sites seems to be functionally important in regulating the development of the animal. Recent *in vitro* and *in vivo* work by the Conradt group, and us have demonstrated that *miR-35* and *miR-58* miRNAs cooperate in potentiating deadenylation and the silencing of *egl-1* mRNA (Flamand et al., 2017; Sherrard et al., 2017; Wu et al., 2010). While biochemical evidence indicates that the CCR4-NOT complex is recruited due to miRNAs' cooperative action (Wu et al., 2017), the mechanism and the kinetics of CCR4-Not complex recruitment are still poorly resolved. Our design of the fluorescently labeled RNA bearing the complete 3`UTR of *egl-1* mRNA and CRISPR-edited *ntl-1* animals allow us to precisely unravel the events of CCR4-NOT complex recruitment to target RNA. Double mutant animals (*snap::alg-1; halo::ntl-1)* can be labeled using fluorochromes of different excitation spectra. This allows us to measure the kinetics of (i) miRISC when two miRNA-binding sites are in proximity, (ii) the recruitment of the CCR4-NOT complex due to the cooperative action of miRISCs. Using a structural model of cooperating miRISCs, Flamand et al. proposed that conformational changes occurring between the miRISCs (in the Argonaute or GW182 proteins) might facilitate recruitment of the CCR4-NOT complex. Our single-molecule FRET strategy can precisely test this hypothesis. Any rearrangements in conformations of miRISCs upon target binding will be reflected in changes in fluorescence intensity due to FRET efficiencies. Our system can also be extended to study the interaction between Argonautes and GW182 proteins, and cooperativity between miRISC and RBPs.

A4.5 Acknowledgements

We would like to apologize to authors whose directly related work may not have been cited in this manuscript. We greatly thank Dr. Fabien Pinaud and Dr. Gary Brouhard's lab members for assisting us with fluorescence image acquisition and analysis.

A4.6. Funding

This work was supported by the Canadian Institutes of Health Research (CIHR) MOP-123352 (to T.F.D.); The Charlotte and Leo Karassik Foundation PhD fellowship award to V.K.M.

A4.7 Material and Methods

A4.7.1 Worm strains

N2 Bristol (WT), FD23(*qeIs27(Palg-2::snap::1x-flag::alg-2;rol-6(d);alg-2(ok304)*), FD101(*qe31(snap::1x-flag::alg-1;alg-2(ok304)*) *;alg-2(ok304)*), FD79(*qe29(halo::1x-flag::ntl-1)*), FD96(*qe30(snap::1x-flag::alg-2)*), FD102(*qe32(halo::1x-flag::ain-2)*). All strains were maintained at 16°C.

A4.7.2 Transgenics

The SNAP-tag vector was a gift from New England Biolabs & Ana Egana (Addgene plasmid # 101137). SNAP-tag was cloned into pBS vector flanking the promoter of *alg-2* and the *alg-2* CDS along with its 3`UTR. Transgenic animals were obtained by microinjection of *alg-2(ok304)* animals with *alg-2* constructs at 50ng/µL, 50ng/µL pBS construct (as a carrier), and 100ng/µL *rol-6* construct (as a selectable marker). Extrachromosomal arrays were then integrated into the genome after UV irradiation of transgenic animals.

A4.7.3 CRISPR

The different alleles of *alg-1, alg-2, ain-1,* and *ntl-1* were generated using a modified protocol (Paix et al., 2015). mRNP complex was assembled with rCas9 and *in vitro*-transcribed modified sgRNA(F+E) (Ward, 2015). Injection mixes contained 1.2µg/µL Cas9, 300mM KCl, 12.5mM HEPES pH7.4, 50ng/µL dpy-10 sgRNA, 200ng/µL gene-specific sgRNA, 13.75ng/µL dpy-10 repair ssODN and ~300ng/µL of PCR-generated gene-specific repair templates (Table A4-1). Approximately 15 germlines of N2 gravid adults grown on *cku-80* RNAi plates were injected. Roller (heterozygotes for *dpy-10*) or dumpy animals were screened for edits by PCR.

A4.7.4 Preparation of embryonic extracts and fluorescent labeling

C. elegans embryos expressing SNAP/HALO-tagged versions of ALG-1/ALG-2/AIN-2/NTL-1 were lysed in 10 mM HEPES-KOH pH 7.4, 15 mM Potassium chloride, 1.8 mM Magnesium acetate, and 2 mM DTT. The recovered supernatant following centrifugation of the embryonic slurry, was incubated at 4°C with the addition of 1 µM fluorescent dyes (AF488/AF546/AF647/Vista green/JF646). The extract was then fractionated by size-exclusion chromatography (Sephadex G-25 superfine beads). Using 30 mM HEPES-KOH pH 7.4, 100 mM Potassium acetate, 1.8 mM Magnesium acetate, and 2 mM DTT, the extract was filtered and eluted. The resultant eluates, free of un-incorporated fluorescent dyes were assayed for protein concentration and translation activity. To measure the translation activity, embryonic extracts were incubated with mRNA encoding *Renilla* luciferase (1 nM) at 16°C for 3 hours. Luciferase activities were measured using the Dual-Luciferase Reporter assay system (Promega). To confirm fluorescent labeling of proteins of interest, 5 µL aliquots were subjected to in-gel detection (see below).

A4.7.5 Preparation of fluorescent RNA

A gene-block encoding a T7-promoter and *egl-1* 3`UTR wherein all the predicted binding sites except for *miR-35* and *miR-58* mutated were synthesized and obtained from IDT. The gene-block was then cloned into a pSCA vector (Agilent), digested with DraI restriction enzyme, and used as template for *in vitro* transcription. Using MegaShort T7 transcription kit (Thermofisher), *egl-1* 3`UTR was transcribed with a 1.5-fold molar excess of 5'-Biotin-G-Monophosphate (TriLink Biotechnologies) over the theoretical amount GTP. Fluorescent DNA was added to the *in vitro*-transcribed (IVT) RNA using a Klenow extension method. In brief, a Klenow template of 148 nt in length containing 17 Adenosine was added in a 2-fold molar excess to IVT product in 10 mM

HEPES-KOH pH 7.4, 20 mM NaCl, and 0.1 nM EDTA. The mixture was incubated at 70 °C and slowly cooled to 30 °C over a course of 20 minutes. The mixture was then incubuated with dATP, dCTP, Klenow Fragment exo minus (5 U/μL) (NEB), 2-fold molar excess of Alexa Fluor 555-aminohexylacrylamido-dUTP (Life technologies) over the theoretical amount of dUTP required for Klenow extension in NEB buffer 2 at 37 °C for 1 hour. Using a trap-oligo (reverse complementary sequence of the Klenow template) was then added in a 10-fold molar excess to trap any Klenow template that has not annealed to the IVT product. The reaction was then resolved in a denaturing gel, size selected, and purified. Biotinylated Cy3-labeled RNA bearing a *miR-35* binding site was synthesized and obtained from IDT.

A4.7.7 Immunoprecipitation (IP), gel-shift assay, and in-gel detection

Embryonic pellets expressing either wild-type (N2) or FLAG-tagged ALG-2 were homogenized in lysis buffer (50 mM Tris-HCl pH 8, 150 mM NaCl, 1% Triton X-100 with Complete EDTA-free protease inhibitors [Roche]) and cleared by 17,500 × *g* centrifugation. The FLAG-tagged ALG-2 was purified using anti-FLAG M2 Affinity Gel (Sigma-Aldrich A2220). For each IP, 5 mg of proteins were used at a concentration of 2 mg/mL in lysis buffer. IP was carried out at 4°C for 2 hours with 50 μl of bead slurry per IP. Beads were washed four times in lysis buffer before eluting them using 3x-FLAG peptides (Sigma-Aldrich F4799). One tenth of the eluate was then incubated with 50 nM of Cy3-labeled target RNA harboring *miR-35* binding site. Unlabeled *miR-35* site bearing RNA served as a negative control. For competitor assay, increasing concentrations of 2'-O-Methyl RNA bearing perfect complementarity to *miR-35* was added to samples containing SNAP-ALG-2 and Cy3-labeled target RNA. RNA bearing a binding site for *hsa-miR-16* served as a negative control. Following incubation for 1 hour at 4°C, the mixture was resolved in 0.8 % TAE-agarose gel. The bound and unbound RNA was then detected using a typhoon scanner by

setting the excitation channel to 533 nm and the detection channel to 580 nm. FRET between ALG-2 and target RNA was observed by exciting ALG-2 proteins (Excitation channel at 480 nm) and detecting the RNA (detection channel at 580 nm).

A4.7.8 miRISC capture

Embryonic extracts or crude lysates expressing SNAP-tagged ALG-1/ALG-2 were fluorescently labeled and incubated with biotinylated Cy3-labeled target RNA bearing a binding site for *miR-35* or AF555-labeled *egl-1* 3`UTR at 4 °C for 1 hour. Using streptavidin coupled magnetic beads, ALG-1/ALG-2 was captured and eluted in 2x-SDS loading buffer. RNA containing a *hsa-miR-16* binding site or *egl-1* 3`UTR whose miRNA-binding had been mutated served as negative controls. The captured miRISC were then subjected to 8 % SDS-PAGE and detected using a typhoon scanner.

A4.7.9 Preparation of glass slides and coverslips for TIRF-microscopy

Cleaning of slides and coverslips. Glass slides and coverslips were rinsed three times in MilliQ water. The slides and coverslips are then placed in a beaker containing 1 M KOH and sonicated three times for 5 minutes. The slides were then rinsed with MilliQ water and dried using N2. In a chemical hood, with a 3:1 ratio between H_2O_2 and H_2SO_4, the glass slides and cover slips are etched in a glass beaker. The beaker was gently mixed and left undisturbed for 5 minutes. The glass slides and cover slips were then rinsed three times in MilliQ water and placed in a glass jar containing methanol.

Amino-salinization of slides and coverslips. The surface of the glass slides and coverslips were functionalized with amine group via the amino-salinization chemistry. The glass slides and coverslips were incubated in a glass jar containing 100 mL of methanol, 5 mL of acetic acid, and

3 mL of APTES (3-aminopropyl trimethoxysilane) for 20 minutes. Following a brief sonication (1 minute), the glass slides and coverslips were rinsed in methanol and dried using N2.

Surface passivation. 0.2 mg of biotinylated NHS-ester PEG (3400 Da) (Laysan Bio) and 8 mg of mPEG-SVA (2000 Da) (Laysan Bio) were mixed and dissolved in freshly prepared 0.1 M of sodium-bicarbonate (pH 8.5). The solution was centrifuged for a minute and ~75 µL of the PEGylation mixture was dropped onto the glass slide. Cover slips were then gently placed over the glass slide and incubated in a dark and humid environment, overnight.

Microfluidic chamber preparation. The glass slides and coverslips were rinsed in MilliQ water and dried using N_2 gas. With the PEGylated surface facing up, channels were created by squeezing high-vacuum silicone grease (Fisher scientific) through a 20 µL pipette tip. Coverslips were then then gently pressed over the glass slide. Freshly prepared or -20 °C frozen aliquots of 0.1 mg/mL of Streptavidin dissolved in wash buffer (10 mM Tris-HCl (pH 8.0), 50 mM NaCl) was pipetted along the sides of the microfluidic chamber. Following a minute of incubation, the channels were flushed with wash buffer.

A4.7.10 Microscopy

Prior to performing single-molecule imaging experiments, emission filters for all the channels were aligned using 0.1 µm fluorescent TetraSpeck microspheres (Thermo Fisher Scientific). 1:1000 dilutions of Tetraspeck microspheres in wash buffer was run through the microfluidic chamber. Following a minute of incubation, the channels were flushed with wash buffer and imaged. TIRF images were acquired on an inverted Nikon Eclipse Ti-E microscope, equipped with a 100× 1.49 NA objective (Nikon), an iXon EMCCD camera (Andor), perfect focus drift compensation optics, laser lines at 405, 488, 561, and 647 nm (Agilent), a quad-band

ZT405/488/561/647 dichroic mirror (Chroma), and appropriate emission filters for imaging of Cy3-target RNA and Vista green/AF660-labeled Argonaute.

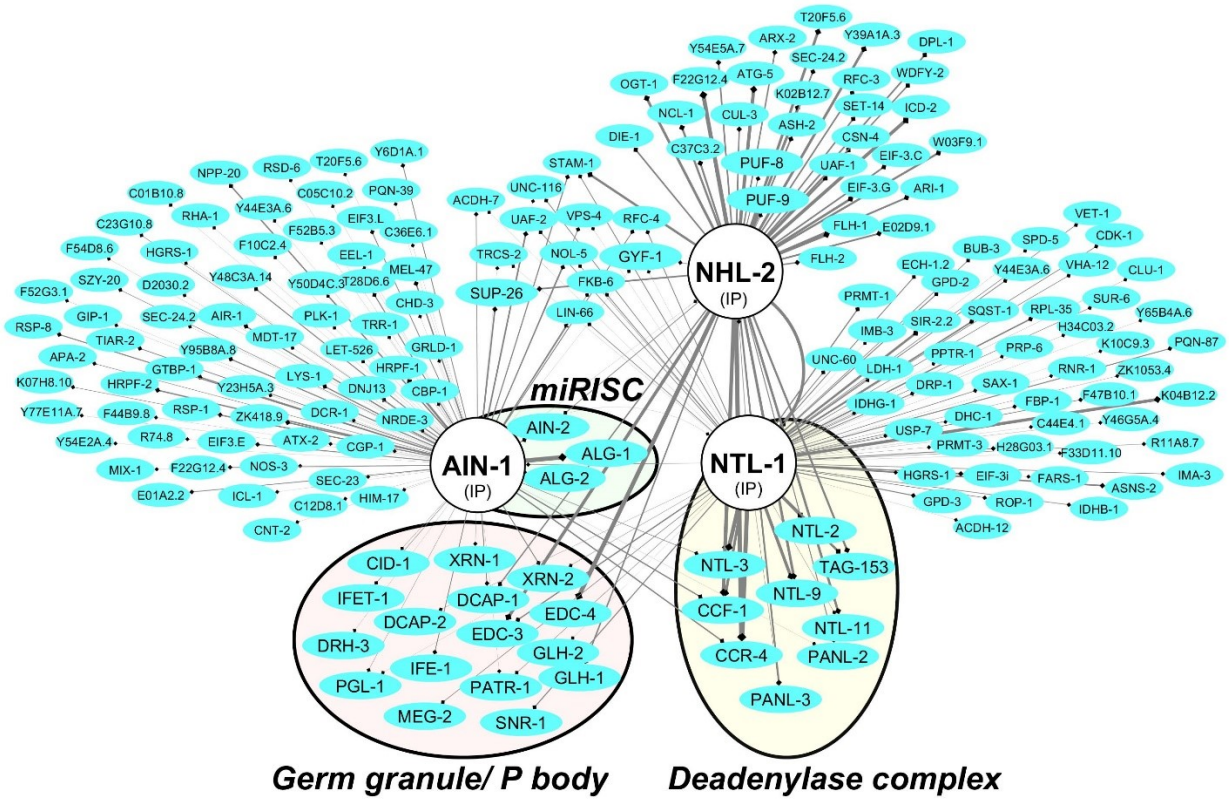

Figure A5.1. Overlapping proteins detected in FLAG immunoprecipitations if AIN-1, NTL-1, and NHL-2 are presented.

From (Wu et al., 2017) and Chapter 4 proteomic datasets. Homology data for each protein was obtained from Wormbase WS277.

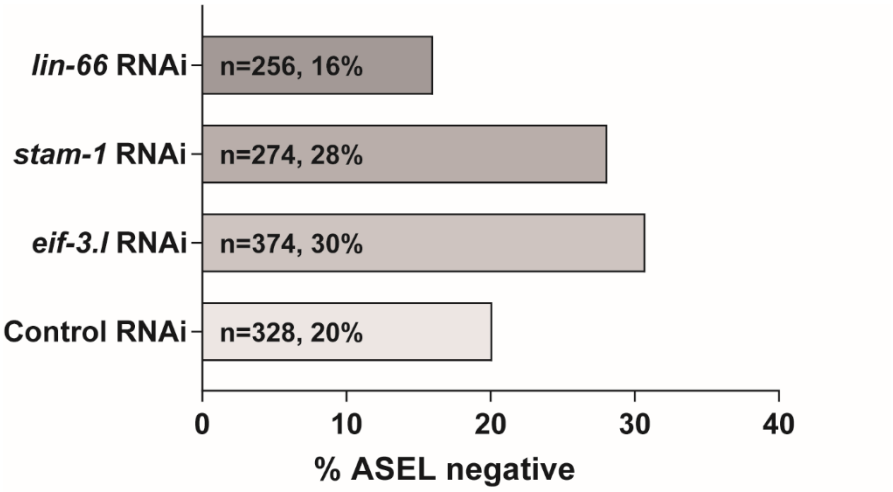

Figure A5.2. *stam-1* and *eif-3.i* genetically interact with *lsy-6* miRNA.
lsy-6 (ot150) animals (L4-stage) were injected with *dsRNA* against the indicated genes, and F1 animals were scored for expression of GFP in the ASEL